

**Foam Delivery of Hydrogen for Enhanced Aquifer Contacting
and Anaerobic Bioremediation of Chlorinated Solvents**

SERDP Contract
DACA72-01-C-0021

Project Number
CU-1203

George J. Hirasaki, *Department of Chemical Engineering*
Joseph B. Hughes, *Department of Civil and Environmental Engineering*
Clarence A. Miller, *Department of Chemical Engineering*
Rice University

SERDP Final Report
November, 2005

This report was prepared under contract to the Department of Defense Strategic Environmental Research and Development Program (SERDP). The publication of this report does not indicate endorsement by the Department of Defense, nor should the contents be construed as reflecting the official policy or position of the Department of Defense. Reference herein to any specific commercial product, process, or service by trade name, trademark, manufacturer, or otherwise, does not necessarily constitute or imply its endorsement, recommendation, or favoring by the Department of Defense.

REPORT DOCUMENTATION PAGE*Form Approved
OMB No. 0704-0188*

The public reporting burden for this collection of information is estimated to average 1 hour per response, including the time for reviewing instructions, searching existing data sources, gathering and maintaining the data needed, and completing and reviewing the collection of information. Send comments regarding this burden estimate or any other aspect of this collection of information, including suggestions for reducing the burden, to the Department of Defense, Executive Services and Communications Directorate (0704-0188). Respondents should be aware that notwithstanding any other provision of law, no person shall be subject to any penalty for failing to comply with a collection of information if it does not display a currently valid OMB control number.

PLEASE DO NOT RETURN YOUR FORM TO THE ABOVE ORGANIZATION.

1. REPORT DATE (DD-MM-YYYY)		2. REPORT TYPE		3. DATES COVERED (From - To)	
4. TITLE AND SUBTITLE				5a. CONTRACT NUMBER	
				5b. GRANT NUMBER	
				5c. PROGRAM ELEMENT NUMBER	
6. AUTHOR(S)				5d. PROJECT NUMBER	
				5e. TASK NUMBER	
				5f. WORK UNIT NUMBER	
7. PERFORMING ORGANIZATION NAME(S) AND ADDRESS(ES)				8. PERFORMING ORGANIZATION REPORT NUMBER	
9. SPONSORING/MONITORING AGENCY NAME(S) AND ADDRESS(ES)				10. SPONSOR/MONITOR'S ACRONYM(S)	
				11. SPONSOR/MONITOR'S REPORT NUMBER(S)	
12. DISTRIBUTION/AVAILABILITY STATEMENT					
13. SUPPLEMENTARY NOTES					
14. ABSTRACT					
15. SUBJECT TERMS					
16. SECURITY CLASSIFICATION OF:			17. LIMITATION OF ABSTRACT	18. NUMBER OF PAGES	19a. NAME OF RESPONSIBLE PERSON
a. REPORT	b. ABSTRACT	c. THIS PAGE			19b. TELEPHONE NUMBER (Include area code)

TABLE OF CONTENTS

EXECUTIVE SUMMARY	12
INTRODUCTION	14
Project Background.....	14
Technical Objectives.....	15
Technical Approach	15
PROJECT ACCOMPLISHMENTS	16
Task 1 - Screen surfactants for their foam properties in porous media.....	16
Task 2 - Evaluation of surfactants to verify that they are benign to the microbial process and are not rapidly degraded.....	20
2.1 - Effects of Surfactants on the Dechlorination of Chlorinated Ethenes.....	20
2.2 - Hydrogen Foam Generation and Hydrogen Consumption.....	20
2.3 - Culture Characterization	23
2.4 - Surfactant Effects on Mixed Dechlorinating Cultures.....	28
References	32
Tables	34
Figures.....	39
Task 3 - Evaluation of the acceleration of reductive dechlorination due to solubilization of DNAPL into micelles.....	60
Task 4 - Use sand columns and mechanistic models to quantify enhanced foam mobility in heterogeneous systems.....	60
4. Lateral Contacting of Aquifer---2-Dimensional preliminary sandpack experiments for proof of concept.....	60
4.1 Experimental	60
4.2 Preliminary experiments	62
4.2.1 Comparison of regular air foam and hydrogen foam	62
4.2.2 Proof of concept--- foam increased the lateral transport of gas.....	64
4.2.3 Effect of pressure drop across sand pack	66
4.2.4 Experiments in heterogeneous sandpack.....	68
4.3 Summary of Section 4.....	70
Task 5 - Validation of foam enhancement of reductive dechlorination by hydrogen sparging in a bench scale three-dimensional sand pack model.....	72

5.1	2x2x2 ft 3-D sand tank experiments.....	72
5.1.1	3-D tank set up and experimental procedures	72
5.1.2	Homogeneous sand pack experimental results	75
5.1.2.1	Comparison of air/water and foam experimental results	75
5.1.2.2	Different foam injection strategies.....	80
5.1.3	Heterogeneous sand pack results	84
5.1.3.1	Comparison of air/water and foam experimental results	85
5.1.3.2	Comparison between different injection strategies	90
5.1.3.3	Foam stability.....	94
5.2	Rice ECRS Tank experiments	95
5.2.1	Experimental.....	95
5.2.2	Experimental results	96
5.3	Summary for section 5.....	101
	Task 6 - Incorporation of the heterogeneity enhanced mechanisms in the UTCHEM numerical simulator.....	102
6.1	Introduction:	102
6.2	Foam simulation model description:.....	102
6.2.1	Change of k_{rg}^f	102
6.2.2	Change of μ_g^f	103
6.2.3	Model summary and discussion:.....	107
6.3	1-D Column Experiments: Parameter Determination:.....	107
6.3.1	Determine the gas residual saturation when foam is present	108
6.3.2	Determine the parameters for foam shear thinning effect (v_{ref}, n), saturation dependence (S_{gm}, m) and $C_{\mu f}$	109
6.3.2.1	v_{ref} and n determination	109
6.3.2.2	S_{gm}, m and $C_{\mu f}$ determination.....	112
6.3.2.2.1	40 darcy sand column experimental results	112
6.3.2.2.2	200 darcy sand column experimental results	116
6.3.3	Table of 1-D parameters:	118
6.4	Case Study: Foam simulations --- 1-D and 3-D comparison	118

6.4.1	1-D column foam simulation results	118
6.4.2	3-D tank foam simulation	121
6.4.2.1	Homogeneous sand tank simulation	121
6.4.2.2	F_g value obtained from the homogeneous sand tank	124
6.4.2.3	Heterogeneous sand tank experiments simulation	124
6.5	Summary of Section 6.....	129
	Task 7 - Design for a hypothetical field application.....	130
7.1	Introduction	130
7.2	Preparing for the field application---some preliminary experiments	130
7.2.1	The threshold surfactant concentration to generate strong foam	130
7.2.2	The effect of injection pressure on foam strength and simulation parameters.....	131
7.2.3	The minimum amount of surfactant solution needed.....	134
7.2.4	Scaling up in simulation--- making a connection between 1-D and 3-D	136
7.2.5	Modeling the shear thinning effect between the well bore and the grid block	139
7.3	A hypothetical aquifer for hydrogen biosparging	139
7.3.1	Description	139
7.3.2	Choice of the injection pressure in a field application	140
7.4	Case studies of two different hypothetical aquifer formations	141
7.4.1	40 darcy homogeneous sand aquifer.....	142
7.4.1.1	The spacing of the injection wells	142
7.4.1.2	Injection rate comparison between with and without foam cases.....	145
7.4.2	40 darcy and 200 darcy heterogeneous sand aquifer	145
7.4.2.1	The spacing of injection wells	145
7.4.2.2	Injection rate comparison between with and without foam cases.....	147
7.5	Discussion and summary of Section 7	148
7.5.1	A comparison with the results of Cape Canaveral aquifer	148
7.5.2	Summary.....	149
	References	150
	Action Item.....	152
	Effects of Surfactants on the Dechlorination of Chlorinated Ethenes.....	153

Table of Tables

Table 1.1 Surfactant properties.....	18
Table 2-I. Primers used for identifying organisms and reductive dehalogenase genes present in enrichment cultures.	34
Table 2-II. Real time PCR primers used for quantifying organism. Table 2-III. Enrichment culture description and time required during enrichment process for production of cis-dichloroethene, vinyl chloride, and ethene as major end product.....	36
Table 2-III. Enrichment culture description and time required during enrichment process for production of cis-dichloroethene, vinyl chloride, and ethene as major end product.....	37
Table 2-IV. Identification of dechlorination populations in enrichment cultures using 16S rRNA gene targeted primers. (D = direct PCR; N = nested PCR)	37
Table 2-V. Identification of reductive dehalogenase genes in enrichment cultures using gene targeted primers.	38
Table 2-VI. Dechlorination capabilities and membrane properties of dechlorinating organisms found in the mixed dechlorinating cultures.	38
Table 4-1 Comparison air foam and hydrogen foam.....	62
Table 6-1 Parameters determined from 1-D column experiments.....	118
Table 6-2 Comparison of simulated and experimental gas saturation	121
Table 6-3 Comparison of parameters for 1-D and 3-D simulation.....	125
Table 7-1 Simulation parameters under different injection pressure	133

Table of Figures

Fig. 1 Gas distribution in aquifer during sparging.....	14
Figure 1-1 1-D column experiment description	17
Figure. 1-2 Comparison of surfactant's foam ability (I).....	18
Figure. 1-3 Comparison of surfactant's foam ability (II).....	19
Figure 2-1. Schematic of column set-up.	39
Figure 2-2. Schematic of Experimental Set-up for measuring the gas saturation in the column.	40
Figure 2-3. Comparison of Foam Strength Formed Using 0.5% CS-330 with Hydrogen and Air in a 1-D Column (1.6 Pore Volumes Injected).....	41
Figure 2-4. Comparison of Foam Strength Formed Using 0.5% CS-330 with Hydrogen and Air in a 1-D Column (1.8 Pore Volumes Injected).....	42
Figure 2-5. Determination of foam strength by varying volume of surfactant (0.5% active CS-330 with 2.3 g/L NaCl and 0.025 g/L CaCl ₂) in a 1-D column. All data taken at 1.8 pore volumes of hydrogen injected.	43
Figure 2-6. Residual hydrogen saturation dependence on initial volume of surfactant (0.5% active CS-330 with 2.3 g/L NaCl and 0.025 g/L CaCl ₂) in a 1-D column.	44
Figure 2-7. Culture specific dechlorination with 3 mM MeOH and 0.25 mM PCE: A) Owls culture, B) Cornhusker culture, and C) Longhorns culture. Symbols: PCE; TCE; DCE; VC; ETH.....	45
Figure 2-8. Culture specific volatile fatty acid production with 3 mM MeOH and 0.25 mM PCE: A) Owls culture, B) Cornhusker culture, and C) Longhorns culture. This data taken at the same time as the dechlorination data in Figure 2-2. Symbols: succinate; formate; acetate; propionate; butyrate.	46
Figure 2-9. Quantification of <i>Dehalococcoides</i> spp. and <i>Dehalobacter</i> spp. in enrichment cultures using real time PCR.	47
Figure 2-10. Quantification of Archaea in enrichment cultures using real time PCR. ND = not detected	48
Figure 2-11. Culture specific volatile fatty acid production with 3 mM MeOH and no PCE: A) Owls culture, B) Cornhusker culture, and C) Longhorns culture. Symbols: formate; acetate; propionate; butyrate.	49
Figure 2-12. Owls culture A) positive control; B) 0.005% CS-330 and C) 0.01% CS-330. Symbols: PCE; TCE; DCE; VC; ETH.....	50
Figure 2-13. Cornhuskers culture A) positive control; B) 0.005% CS-330 and C) 0.01% CS-330. Symbols: PCE; TCE; DCE; VC; ETH.....	51

Figure 2-14. Longhorns culture A) positive control; B) 0.005% CS-330 and C) 0.01% CS-330. Symbols: PCE; TCE; DCE; VC; ETH.....	52
Figure 2-15. Owls culture A) positive control; B) 0.005% C13-4PO and C) 0.01% C13-4PO. Symbols: PCE; TCE; DCE; VC; ETH.	53
Figure 2-16. Effect of mixtures of CS-330 and C13-4PO with Owls Cultures. Data taken after 7 days of exposure.	54
Figure 2-17. Determination of CS-330 concentration that has no effect on dechlorination. A) Owls culture; B) Cornhusker culture.....	55
Figure 2-18. Effect on extent of dechlorination from adding (600 mg/L) gram negative A) <i>Escherichia coli</i> and gram positive B) <i>Bacillus subtilis</i> organisms with 0.005% CS-330.....	56
Figure 2-19. Owls culture exposed to A) no surfactant, PCE only; B) 0.01% CS-330, PCE and C) no surfactant, PCE and O ₂ . Symbols: PCE; TCE; DCE; VC; ETH.	57
Figure 2-20. Real time PCR monitoring of A) <i>Dehalobacter</i> spp. B) <i>pceA</i> gene from <i>Sulfurospirillum</i> spp. and C) <i>Dehalococcoides</i> spp. during 4 treatments. Symbols: positive control; 0.01% CS-330; O ₂ ; Culture only.	58
Figure 2-21. Resuspension of cells into fresh media from A) positive control and B) 0.01% CS-330. Symbols: PCE; TCE; DCE; VC; ETH. ...	59
Figure 4-1 2-D sandpack experiment description.....	61
Figure 4-2 Effect of foam on sweep and gas saturation	64
Figure 4-3 Gas Saturation after liquid flush that followed approximately 1 PV throughput at $\Delta p \sim 10\text{psi}$	65
Figure 4-4 Gas Saturation after liquid flush that followed approximately 1 PV throughput at $\Delta p \sim 2\text{psi}$	66
Figure 4-5 Gas Saturation after approximately 1 PV throughput at $\Delta p \sim 8\text{psi}$.	67
Figure 4.6 Gas Saturation profile of the homogeneous sandpack at $\Delta p \sim 8\text{psi}$	68
Figure 4.7 Gas Saturation after approximately 1PV air injected at $\Delta p \sim 2\text{psi}$..	69
Figure 4.8 Gas Saturation after approximately 1PV air injected at $\Delta p \sim 10\text{psi}$	69
Figure 4-9 Gas Saturation after approximately 10PV air injected at $\Delta p \sim 10\text{psi}$	70
Figure 4-10 Gas saturation in the heterogeneous sandpack with air injected at a target injection pressure of 10 psi.	70
Figure. 5-1 An overlook of the 3-D tank (before sand packing).....	72
Figure 5-2 Sketches of the side and top views of the tank.....	73
Figure 5-3 Homogeneous and Heterogeneous sand pack.....	73

Figure 5-4	Experimental outlines of the 3-D tank	75
Figure 5-5	Air/Water homogeneous sand tank, injection rate; Constant injection pressure ~0.8 psi, 6 PV gas injected	76
Figure 5-6	Air/Water homogeneous sand tank results; Constant injection pressure ~0.8 psi, 6 PV gas injected	76
Figure 5-7	Foam, homogeneous sand tank, injection rate; Constant injection pressure ~0.8 psi, 1 PV gas injected	77
Figure 5-8.A	Foam, Homogeneous sand tank, gas fraction flow contour plot; Constant injection pressure ~0.8 psi, ~0.37 PV gas injected	78
Figure 5-8.B	Foam, Homogeneous sand tank, gas fraction flow contour plot; Constant injection pressure ~0.8 psi, ~1 PV gas injected	78
Figure 5-9	Comparison of air/water and foam results along the diagonal cross section of the tank, Constant injection pressure ~0.8 psi	79
Figure 5-10	Foam, homogeneous sand tank, Injection rate; Intermittent gas injection, pressure ~0.8 psi 1 PV gas injected	80
Figure 5-11.A	Foam, Homogeneous sand tank, gas fraction flow contour plot; Intermittent gas injection, ~0.8 psi, ~0.37 PV gas injected	81
Figure 5-11.B	Foam, Homogeneous sand tank, gas fraction flow contour plot; Intermittent gas injection, ~0.8 psi, ~1 PV gas injected	81
Figure 5-12.A	Foam, Homogeneous sand tank, gas fraction flow contour plot; Constant rate gas injection, ~0.39 LPM, ~0.37 PV gas injected	82
Figure 5-12.B	Foam, Homogeneous sand tank, gas fraction flow contour plot; Constant rate gas injection, ~0.39 LPM, ~1 PV gas injected	82
Figure 5-13	Air/water, heterogeneous sand tank, Injection rate curve; Continuous gas injection, pressure ~0.8 psi 1 PV gas injected	84
Figure 5-14.A	Air/water, Heterogeneous sand tank, gas fraction flow contour plot; Constant injection pressure, ~0.8 psi, ~1 PV gas injected	85
Figure 5-14.B	Air/water, Heterogeneous sand tank, gas fraction flow contour plot; Constant injection pressure, ~0.8 psi, ~6 PV gas injected	85
Figure 5-15	Foam, heterogeneous sand tank, Injection rate curve; Continuous gas injection, pressure ~0.8 psi	86
Figure 5-16.A	Foam, Heterogeneous sand tank, gas fraction flow contour plot; Constant injection pressure, ~0.8 psi, ~0.37 PV gas injected	88
Figure 5-16.B	Foam, Heterogeneous sand tank, gas fraction flow contour plot; Constant injection pressure, ~0.8 psi, ~1 PV gas injected	88
Figure 5-17	Comparison of air/water and foam results along the diagonal cross section of the tank; Constant injection pressure ~0.8 psi	89

Figure 5-18	Foam, heterogeneous sand tank, Injection rate curve; Continuous gas injection, pressure ~0.4 psi	90
Figure 5-19.A	Foam, Heterogeneous sand tank, gas fraction flow contour plot; Constant injection pressure, ~0.4 psi, ~0.37 PV gas injected	91
Figure 5-19.B	Foam, Heterogeneous sand tank, gas fraction flow contour plot; Constant injection pressure, ~0.4 psi, ~1 PV gas injected	91
Figure 5-20	Foam, heterogeneous sand tank, Injection rate curve; Intermittent gas injection, pressure ~0.8 psi	92
Figure 5-21.A	Foam, Heterogeneous sand tank, gas fraction flow contour plot; Intermittent gas injection, ~0.8 psi, ~0.37 PV gas injected.....	93
Figure 5-21.B	Foam, Heterogeneous sand tank, gas fraction flow contour plot; Intermittent gas injection, ~0.8 psi, ~1 PV gas injected.....	93
Figure 5-22	Foam, heterogeneous sand tank, constant injection pressure ~0.8 psi ; After 1 PV gas injected, the change of gas saturation in the tank	94
Figure 5-23	Layout of the Rice ECRS tank	95
Figure 5-24	Gas distribution for the gas injection case, injection pressure 5 psig, 0.63 PV gas injected, average injection rate 1 ft ³ /min	96
Figure 5-25	Surfactant distribution before foam experiment; Injected surfactant solution concentration: 0.1% (wt).....	97
Figure 5-26	Gas distribution for the foam injection case, middle injection port, injection pressure 5 psig, 0.075 PV gas injected,	97
Figure 5-27.A	First day, Foam, left injection port, 5 psig, 0.03PV gas injected, Average injection rate 0.04ft ³ /min, Percent of trapped gas 84%	98
Figure 5-27.B	Second day, Foam, left injection port, 5 psig, 0.05PV more gas injected, Average injection rate 0.09 ft ³ /min, Percent of trapped gas 50%.....	98
Figure 5-28	Remaining gas distribution in the tank, after vibration	100
Figure 5-29	Gas distribution after gas reinjection from the middle injection point, Foam, 5 psig, 0.025PV gas injected, Average injection rate 0.08 ft ³ /min, Percent of trapped gas 60%	100
Figure 6-1	Relationship between S _g and n_f	104
Figure 6-2	Gas residual saturation measurement using 1-D column	108
Figure 6-3	Foam shear thinning effect at high velocity, 40 darcy sand	110
Figure 6-4	Foam shear thinning effect at high velocity, 200 darcy sand	110
Figure 6-5	Gas saturation vs. foam effective viscosity and gas superficial velocity; 40 darcy sand, 0.4 psi constant injection	112
Figure 6-6	Relationship between foam effect viscosity and gas saturation; 40 darcy sand, 0.4 psi constant injection	113

Figure 6-7 Gas saturation vs. foam effective viscosity and gas superficial velocity; 40 darcy sand, 0.2 psi constant injection	114
Figure 6-8 Relationship between foam effect viscosity and gas saturation; 40 darcy sand, 0.2 psi constant injection	115
Figure 6-9 Gas saturation vs. foam effective viscosity and gas superficial velocity; 200 darcy sand, 0.4 psi constant injection	115
Figure 6-10 Relationship between foam effect viscosity and gas saturation; 200 darcy sand, 0.4 psi constant injection	116
Figure 6-11 Gas saturation vs. foam effective viscosity and gas superficial velocity; 200 darcy sand, 0.2 psi constant injection	117
Figure 6-12 Relationship between foam effect viscosity and gas saturation; 200 darcy sand, 0.2 psi constant injection	118
Figure 6-13 1-D column simulation results vs. experimental data; 40 darcy sand, 0.4 psi constant injection pressure.....	119
Figure 6-14 1-D column simulation results vs. experimental data; 40 darcy sand, 0.2 psi constant injection pressure.....	119
Figure 6-15 1-D column simulation results vs. experimental data; 200 darcy sand, 0.4 psi constant injection pressure	120
Figure 6-16 1-D column simulation results vs. experimental data; 200 darcy sand, 0.2 psi constant injection pressure	120
Figure 6-17 Homogeneous 3-D sand tank; 40 darcy, 0.8 psi constant injection pressure	121
Figure 6-18 Gas fractional flow contour plots, diagonal cross section; 0.8 psi constant pressure injection, 1 PV gas injected	122
Figure 6-19 Homogeneous 3-D sand tank, foam, pressure profile; 0.8 psi constant injection pressure	123
Figure 6-20 Gas fractional flow contour plots, diagonal cross section; 0.39 LPM constant injection rate, 1 PV gas injected	123
Figure 6-21 Homogeneous Sand Tank, 0.39LPM constant injection; Pressure profile	124
Figure 6-22 Heterogeneous 3-D tank; 0.8 psi constant injection pressure.....	126
Figure 6-23 Gas fractional flow contour plots, diagonal cross section; 0.8 psi constant injection pressure, 1 PV gas injected	126
Figure 6-24 Heterogeneous 3-D tank, 0.8 psi constant injection pressure; Pressure profile.....	127
Figure 6-25 Heterogeneous 3-D tank, 0.4 psi; Injection rate.....	127
Figure 6-26 Gas fractional flow contour plots, diagonal cross section; 0.4 psi constant injection pressure, 1 PV gas injected	128

Figure 6-27 Heterogeneous 3-D tank, 0.4 psi constant injection pressure; Pressure profile.....	128
Figure 7-1 Surfactant concentration effect on steady state foam effective viscosity	131
Figure 7-2 The effect of injection pressure on steady state foam strength	132
Figure 7-3 The change of C_{nf} value with the change of pressure gradient	134
Figure 7-4 Effect of different surfactant amount on foam sweep efficiency; Comparison based on a homogeneous 3-D sand tank foam experiment; 0.8 psi over hydrostatic constant injection pressure, bottom sampling layer	135
Figure 7-5 A sketch of a field injection	137
Figure 7-6 Side view of the hypothetical contaminated aquifer	140
Figure 7-7 Top view of the hypothetical contaminated aquifer	140
Figure 7-8 Side views of the two hypothetical aquifers	141
Figure 7-9 Gas saturation contour plots for with and without foam cases; homogeneous aquifer	143
Figure 7-10 Gas injection rate, with foam in the aquifer.....	144
Figure 7-11 Gas injection rate, without foam in the aquifer.....	144
Figure 7-12 Gas saturation contour plots for with and without foam cases; heterogeneous aquifer	146
Figure 7-13 Gas injection rate, with foam in the heterogeneous aquifer	147
Figure 7-14 Gas injection rate, without foam in the heterogeneous aquifer....	148
Figure 7-15 Hydrogen sparging result from Cape Canaveral aquifer.....	149

EXECUTIVE SUMMARY

Hydrogen biosparging of aquifers contaminated with chlorinated solvents is promising as a method to enhance *in situ* microbial dechlorination. A major problem is the inability to distribute hydrogen throughout the contaminated interval such that complete dechlorination can occur. Foam is a dispersion of gas in water that is stabilized from coalescence by the presence of a low concentration of surfactants. A promising method to greatly extend the horizontal migration of hydrogen in the subsurface is to inject an aqueous surfactant solution followed by hydrogen, causing foam to be generated *in situ*.

Various surfactants were investigated to determine both their ability to generate foam in sand packs and their possible inhibiting effect on dechlorination of dissolved tetrachloroethene (PCE). Hydrogen is not useful in the immediate vicinity of liquid PCE (and presumably TCE) in the subsurface because biodegradation is inhibited by high concentrations of dissolved contaminant. Several surfactants were found which were good foamers and did not prevent dechlorination of dissolved PCE to trichloroethene (TCE) and dichloroethene (DCE). However, except at extremely low surfactant concentrations further dechlorination of DCE to vinyl chloride and ethene, the desired end product, did not occur.

Batch studies were performed with mixed dechlorinating cultures to determine which dechlorinating organisms were being affected by surfactants. These studies showed that *Sulfurospirillum* spp. and *Dehalobacter* spp., organisms capable of dechlorination of PCE to DCE, were not inhibited by the surfactant and that *Dehalococcoides* spp., organism capable of dechlorination of PCE to ethene, were inhibited. These studies also showed that the inhibition was not reversible and it appeared that the surfactants were lysing the cells.

In parallel with this work experiments on and simulation of foam flow in sandy materials were conducted to determine the effect foam would have on the distribution of hydrogen in an aquifer. The experiments used a mixture of anionic surfactants which is an excellent foamer and effective in hard water. Once it was shown that foams generated with hydrogen and with air behaved similarly, air was used in subsequent experiments. Initial experiments in one-foot sand columns and in a two-dimensional model demonstrated that gas could be distributed more uniformly and with higher average volume fraction when foam was generated than when gas was injected in the absence of surfactant.

Previous work has shown that it is more difficult to achieve uniform gas sweep in three dimensions than in one or two dimensions, but this phenomenon has not been well understood nor modeled quantitatively. Accordingly, an instrumented three-dimensional tank was built with dimensions 2x2x2 ft. It has glass walls permitting observation of foam location and 36 interior sampling ports allowing either local pressure or gas fractional flow to be measured at various

times during the course of an experiment. After it is packed with sand and filled with water or surfactant solution, gas is injected just above the bottom of the tank near one corner, while water is produced from the entire vertical length of wells in the other three corners. Both a homogeneous packing of sand and a heterogeneous packing with two layers of coarser (more permeable) sand were studied.

In the absence of surfactant, gas breakthrough at the top surface of the sand occurred quickly, and sweep was poor near the bottom of the tank for both homogeneous and heterogeneous packings. With foam, however, later gas breakthrough, much better lateral propagation of foam, and a higher gas content in the sand at the end of the experiment were seen. Results were slightly better with intermittent than with continuous injection of gas at constant pressure. Both cases were substantially better than injection at constant flow rate.

A model to describe foam flow in a three-dimensional porous medium was developed using parameters obtained from sand column experiments, which are much simpler to conduct than tank experiments. With these parameters and a single adjustable parameter with the same value for all experiments, simulations of the experiments with homogeneous packing yielded results in good agreement with those observed. An additional parameter is needed for the heterogeneous packing to account for additional foam generation at boundaries where gas flows from a lower to a higher permeability layer.

This model was also used to simulate hydrogen injection with foam formation in an aquifer similar to that at Cape Canaveral, where Groundwater Services conducted a field test of hydrogen injection without foam a few years ago. Good sweep of the bottom of the aquifer was predicted for a well spacing nearly twice that used in the field test.

Because biodegradation is inhibited both by dissolved contaminant concentrations near saturation and by surfactant concentrations well below those expected to be injected, use of hydrogen foam in a source zone where there is considerable liquid contaminant would be of limited value. However, it might prove useful as a barrier through which water with lower concentrations of dissolved TCE or PCE would be required to flow before exiting a contaminated region. As water flowed through such a barrier, it would gain dissolved hydrogen and some surfactant. The latter would be diluted by dispersion once water exited the barrier, allowing dechlorination to proceed. Moreover, surfactant concentration in the continuous aqueous phase of the foam would be quite low once a little water had passed through. There is some evidence from other work in our group that foam made with one of the commercial anionic surfactants emphasized in this project will maintain a stable foam in a sand column even after some of its more soluble components have desorbed. The less soluble components remain at the surfaces of the foam bubbles and hinder coalescence.

INTRODUCTION

Project Background

Hydrogen Biosparging

Hydrogen can be delivered to the aquifer for reductive dechlorination by sparging with an injection well as is done during biosparging. Thus the practice of hydrogen biosparging can build on air sparging technology. A review of this technology is the report, "Air Sparging Design Paradigm," (Leeson, et al, 1999). Similar to air sparging, the controlling factor in the success of hydrogen reductive dechlorination is the distribution of the gas in the aquifer. In the presence of NAPL, achieving good hydrogen distribution may be a greater challenge than for air sparging of LNAPL because chlorinated solvents are DNAPL and thus are present at the bottom of the aquifer as pools or ganglia rather than at the water table.

Gas distribution in aquifer. Hydrogen has low density and viscosity compared to water. Thus the buoyancy gradient rather than the viscous pressure gradient will dominate the flow of hydrogen. Hydrogen injected at the base of the aquifer will form fingers of hydrogen, which migrate upward while simultaneously deflecting laterally as they encounter heterogeneity. This is illustrated in Fig. 1 with a random-walk simulation of gas bubbles that makes a random transverse move for each step upward.

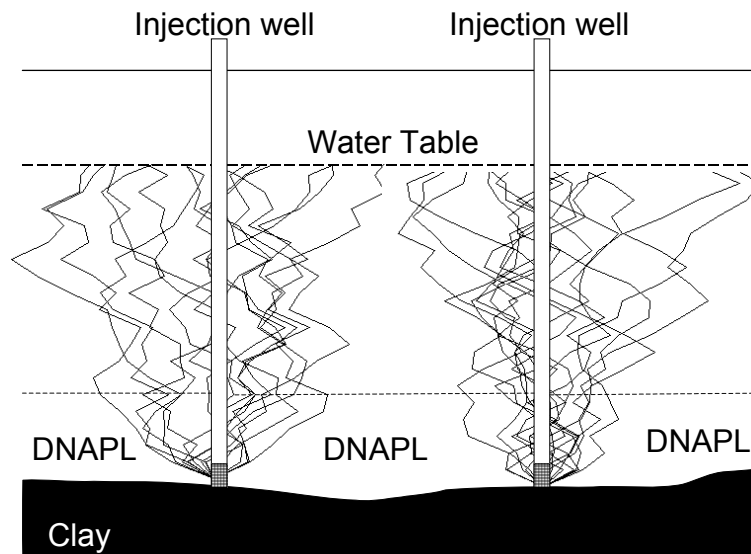


Fig. 1

This figure illustrates the key problem with biosparging when contaminants exist as a DNAPL. The gas tends to rise and does not contact much of the DNAPL at the base of the aquifer. As described later, one role of foam is to

promote the lateral transport of gas in the aquifer in order to contact the DNAPL at the base of the aquifer.

Potential application of H₂ foam in source zone or reactive barrier. Fig. 1 illustrates hydrogen distribution during biosparging in a DNAPL source zone. If a significant amount of DNAPL is present, it may be advantageous to first produce free-phase DNAPL and then inject surfactant solution to displace the residual DNAPL by solubilization and/or mobilization. In this case, air or hydrogen can first be used to generate foam to improve contacting of the aquifer with the surfactant solution as will be described later. Following displacement of most of the DNAPL with the surfactant, dilute surfactant solution and hydrogen can continue to be injected intermittently to degrade any remaining chlorinated hydrocarbons that may diffuse from unswept tight regions or fractures in the aquitard.

In addition to removal of DNAPL from source zones, reductive dechlorination by hydrogen biosparging can be used as a reactive barrier to degrade the dissolved chlorinated hydrocarbons in the plume down gradient from the source zone. Without foam, contaminants may pass undegraded between the injection wells in the region not contacted by gas as illustrated in Fig. 1. Foam will direct more hydrogen throughout the aquifer and thus form a more effective barrier.

Technical Objective

The objective of this project is to assess the potential for hydrogen - foams to more effectively contact contaminated aquifers with electron donor and support rapid reductive dechlorination processes, compared to conventional hydrogen sparging. Results will provide the basis to evaluate this delivery system for field applications. Specifically, studies will be conducted to investigate foam application in source zones or immediately down gradient of source zones where the volumes of contaminated aquifers to be contacted are not prohibitory.

Technical Approach

The individual tasks to be accomplished in this research project are as follows: (1) Screen surfactants for their foam properties in porous media. (2) Evaluation of surfactants to verify that they are benign to the microbial process and are not rapidly degraded. (3) Evaluation of the acceleration of reductive dechlorination due to solubilization of DNAPL into micelles. (4) Use sand columns and mechanistic models to quantify enhanced foam mobility in heterogeneous systems. (5) Validation of foam enhancement of reductive dechlorination by hydrogen sparging in a bench scale three-dimensional sand pack model. (6) Incorporation of the heterogeneity enhanced mechanisms in the UTCHEM numerical simulator. (7) Design for a hypothetical field application.

PROJECT ACCOMPLISHMENTS

Task 1 - Screen surfactants for their foam properties in porous media.

For a surfactant to be effective in improving hydrogen biosparging, it must be capable of reducing the mobility of gas flowing through water-saturated sand. By measuring the reduction of gas mobility in a sand column at a specified surfactant concentration for different surfactants, it will be possible to compare candidate surfactants for application to H₂ foam. The candidate surfactants we chose include those that have already been evaluated for mobility control, either in aquifer remediation or enhanced oil recovery. Only surfactants exhibiting desirable foam properties will be used in the dechlorination and solubilization tests.

1. 1-Dimensional column experiments for surfactant screening

1.1 Experimental

A series of experiments were performed in a glass column to screen the foam ability of surfactants. The column was 1 foot in length with 1 in. internal diameter. It was packed with 120 darcy F-32 sand obtained from US Silica (Berkeley Springs, WV). Diagram of the experimental apparatus is shown in Fig. 1-1

The sand column was pre-filled by surfactant solution first. Then air and surfactant solution are co-injected into the column at a ratio of air:surfactant solution=2:1 ($f_g=0.67$). A pressure transducer was connected to the inlet of the sand column and was used to control the pressure drop during the experiments. All the experiments were conducted at constant injection pressure 1 psig. From the flow rate at steady state of the column, the gas apparent viscosity for different surfactants or surfactant mixtures can be calculated, and used to compare the surfactants' ability to generate foam.

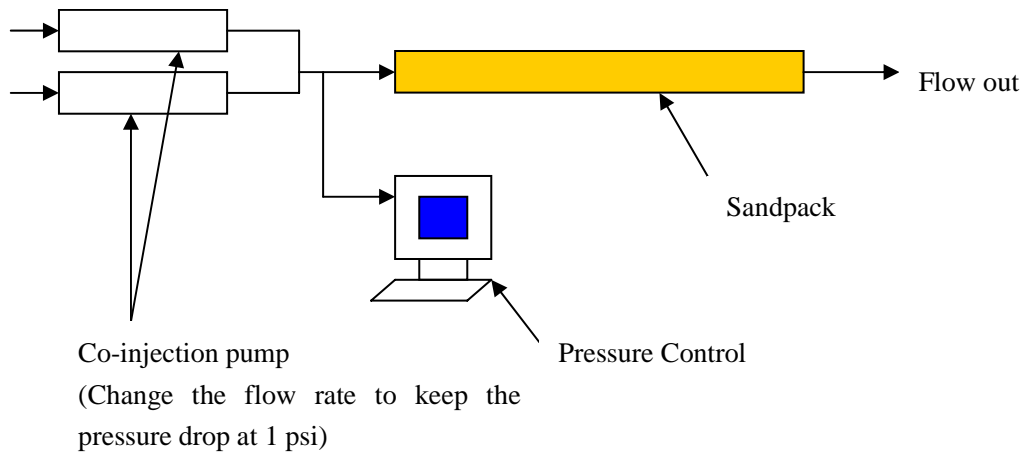


Figure 1-1 1-D column experiment description

1.2 Experimental Results

Table 1-1 lists the properties of the surfactants which were tested for their foam abilities. Among them, Neodol 25-7 and Tween 80 are nonionic surfactants. The others are anionic surfactants.

1.2.1 Comparison of Neodol 25-7, Tween 80, Aerosol MA80-1, AOS14-16, CS 230 and CS330

These surfactants were compared using a total concentration of 0.5%(wt) surfactant and 0.5%(wt) NaCl. Figure 1-2 shows the comparison results for these surfactants. According to Figure 1-2, AOS14-16 is a better foamer than CS-330 with the present of NaCl. However, it will precipitate with only 0.05% CaCl_2 , Thus it will not be considered further because we are planning to inject nutrient solution for the benign of microorganisms. In the nutrient solution, the concentration of CaCl_2 will be about 0.07%.

For the rest of these surfactants, Tween 80 and MA80-1 can only generate weak foam under the experimental condition, the gas apparent viscosity for these two surfactants were less than 10 cp. Among CS330, CS230 and Neodol 25-7, the strongest foam was obtained in CS330 case, the gas apparent viscosity in the CS330 case was around 200 cp, which is the highest among these surfactants.

Surfactant	Chemical Class	Chemical Formula ^a	MW g/mole	CMC ^b mg/L (%)	COD ^c g O ₂ /g
Neodol 25-7	Nonionic	CH ₃ (CH ₂) ₁₁₋₁₄ O(EO) ₇ H	515	9(0.0009)	1.98 ± 0.02
Tween 80	Nonionic	C ₁₈ S ₆ (EO) ₂₀	1308	33-45 (<0.005)	1.56 ± 0.02
Aerosol MA80-1	Anionic	[(C ₂ H ₅) ₂ CHCH ₂ COOCH] ₂ SO ₃ Na	388	7100 (0.71)	1.57 ± 0.05
AOS 14-16	Anionic	CH ₃ (CH ₂) ₁₀₋₁₂ CH=CHCH ₂ SO ₃ Na	315	1200 (0.12)	1.66 ± 0.04
Steol CS-330	Anionic	CH ₃ (CH ₂) ₁₁ (EO) ₃ OSO ₃ Na	422	449 (0.045)	1.65 ± 0.02
C12-3PO	Anionic	ALFOTERRAI12-3PO-SO ₄		<400	ND ^d
C14-4PO	Anionic	ISOFOL14T-4PO-SO ₄ ⁻ Na ⁺		<400	ND ^d
C13-4PO	Anionic	CH ₃ [CH ₃ (CH ₂) ₆]CH(CH ₂) ₄ -4PO-SO ₄ ⁻ NH ₄ ⁺		<400	ND ^d

^aEO=ethylene oxide, S₆=sorbitan ring, ^bCMC, critical micelle concentration
^cCOD, chemical oxygen demand, ^dND not determined

Table 1.1 Surfactant properties

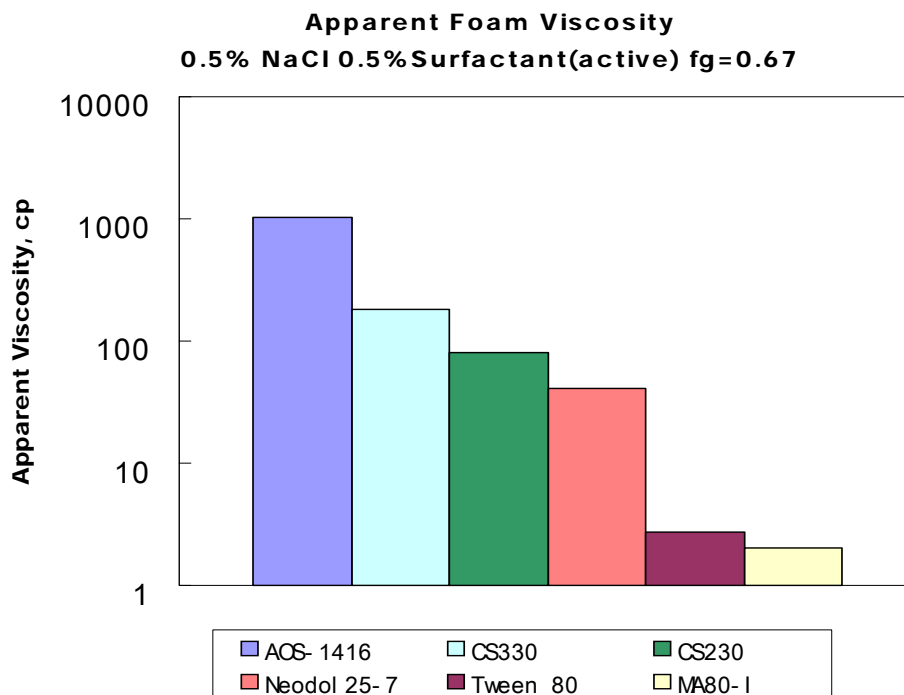


Figure. 1-2 Comparison of surfactant's foam ability (I)

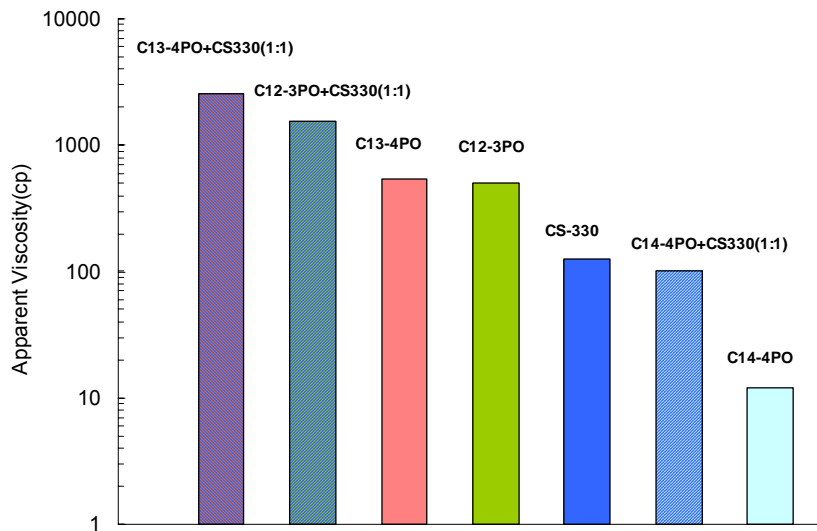


Figure. 1-3 Comparison of surfactant's foam ability (II)

1.2.2 Comparison of CS330, C12-3PO, C14-4PO and C13-4PO

Because the 0.5%(wt) surfactant concentration of CS330 is still too high to be benign to the microbial process in the biodegradation, we performed more experiments using lower surfactant concentration solutions (0.1%wt). Since CS330 has been proved to be the best choice in the former surfactant group, we just picked it out and compared it to several other surfactants. Also, a nutrition solution which contains 0.04%(wt) Mg^{2+} , 0.069%(wt) Ca^{2+} , 0.23%(wt) Na^{+} was added into the surfactant solution during these tests. This is to simulate a real environment of a remediation application during which the nutrition solution will be injected as a nutrition supply for the biodegradation process. So we just added it to the surfactant solution to be tested.

Figure 1-3 shows the experimental results for these surfactants and some of their mixtures. From this figure we can find that when these surfactants were used alone, C13-4PO can generate the strongest foam among them. The foam generated by C12-3PO or CS330 is weaker than that of C13-4PO. C14-4PO alone has the weakest foam ability, the gas apparent viscosity for C14-4PO foam was less than 20 cp. For surfactant mixtures, we found that the mixture of two different surfactants is much stronger than any one of them. Among them, the mixture of C13-4PO and CS330 (1:1) has the strongest foam ability, the gas apparent viscosity for the foam of this surfactant mixture was more than 2000 cp. This surfactant mixture is the best foamer among these surfactants we have tested and we will choose it in our 3-D experiments.

Task 2 - Evaluation of surfactants to verify that they are benign to the microbial process and are not rapidly degraded.

Subtask 2.1 - Effects of Surfactants on the Dechlorination of Chlorinated Ethenes

The influence of surfactants on a perchloroethene (PCE) dechlorinating mixed culture was investigated in laboratory experiments. Surfactants (Steol CS-330, Aerosol MA 80-I, alpha olefin sulfonate 14 to 16, Neodol 25-7, Tween 80, alkyl polyglycoside, C16TAB [trimethylammonium bromide], and sodium dodecyl sulfate) were evaluated for their effects on the rate and extent of PCE reductive dechlorination and their potential biodegradation by the mixed culture. Limited, if any, surfactant biodegradation was observed for the surfactants tested, and all surfactants impaired dechlorination in either the rate of PCE dechlorination or the terminal dechlorination products observed. Based on initial testing, a nonionic surfactant, Tween 80, and an anionic surfactant, Steol CS-330, were selected for additional investigation. Dechlorination of PCE to dichloroethene (DCE), vinyl chloride (VC), and ethene (ETH) occurred in all Tween 80-amended microcosms, with a depressed rate of ETH production as the only adverse effect. Steol CS-330, however, inhibited dechlorination beyond DCE at all surfactant concentrations exceeding 25 mg/L. Attempts to acclimate a culture to Steol CS-330 were unsuccessful. Inhibition of VC and ETH production was reversible on dilution of the surfactant to a concentration of 10 mg/L or less, indicating that surfactant interactions with the enzyme system responsible for reductive dechlorination of DCE may be the cause of inhibition.

This work has been published and is available in the appendix of this report as a PDF file of the publication manuscript.

Subtask 2.2 - Hydrogen Foam Generation and Hydrogen Consumption

Objective

The overall objective of these experiments was to determine the conditions that are necessary to generate a strong hydrogen foam in a 1-D glass column packed with sand and to assure the conditions are favorable for bacterial growth. Determination of these conditions will allow for the generation of a strong hydrogen foam in a column with actively dechlorinating bacteria, which will increase the residual hydrogen saturation in the column and decrease the frequency of hydrogen delivery.

Materials and Methods

Chemicals

Tetrachloroethene was obtained in neat liquid form (99+%, Acros). Steol CS-330 (27% active) was obtained from Stepan. Hydrogen (UHP) and CO₂ (anaerobic grade) was obtained from Matheson -Tri Gas.

Nutrient Media

The medium consisted of the following: 400 mg/L NH₄Cl, 400 mg/L KCl, 400 mg/L MgCl₂·6H₂O, 140 mg/L KH₂PO₄, 25 mg/L CaCl₂·2H₂O, 10 mg/L (NaPO₃)₁₆, 2.5 mg/L KI, 2.5 mg/L CoCl₂·6H₂O, 0.5 mg/L ZnCl₂, 0.5 mg/L MnCl₂·4H₂O, 0.5 mg/L H₃BO₃, 0.5 mg/L NiCl₂·6H₂O, 0.5 mg/L Na₂MoO₄·2H₂O, 0.5 mg/L NH₄VO₃, 200 mg/L yeast extract, and 3.5 g/L NaHCO₃.

Column Design

Experiments were carried out in columns shown in Figure 2-1. The columns were glass (30 cm x 2.5 cm ID, Spectrum Chromatography) with stainless steel endpieces that attached to each end with a threaded polymer collar and sealed with viton-o-rings (American Packing and Gasket Co.). Each endpiece was fitted with screen and the large end from a rubber stopper (size 4) to prevent any sand from exiting the column. Each endpiece also accepted Swagelok fittings to allow connection of both Teflon tubing and a glass sampling port with Teflon stopcock (Rice University Support Shop) to the column.

Three columns were packed with sand by adding approximately 200 ml of sand to the column while vibrating the column with a rubber mallet to assure the settling of the sand. This procedure yielded consistent porosities of 0.41 – 0.42.

Pressure Measurement

The measurement of the pressure drop across the column was performed with a Validyne DP15-38 pressure transducer. Data-collection software from Validyne Engineering Corporation was used to automatically record the pressure data with a personal computer. The pressure transducer was capable of measuring up to an 8 psi pressure drop.

Foam Strength and Gas Saturation

A column was saturated with 0.5% active CS-330 with 2.3 g/L NaCl and 0.025 g/L CaCl₂. Two pore volumes of either hydrogen or air were added with a plastic syringe (140 ml) and syringe pump (as shown in Figure 2-1) at various flow rates: 5 (1.02), 10 (2.04), 15 (3.06), 20 (4.07), 25 (5.09), 30 (6.11), and 35 (7.13) ml/min (cm/min). The pressure transducer was used to record real time pressure data while injecting hydrogen or air.

To determine the gas saturation in the column, the effluent from the column was collected into a graduated cylinder (100ml) as shown in Figure 2-2. The volume of liquid pushed out of the column by the gas was recorded. Then one pore volume of surfactant, for surfactant foam tests, or DI water, for non-

surfactant foam tests, was injected (5ml/min) into the column and the volume of liquid pushed out by the liquid was recorded.

Volume of Surfactant Necessary to Generate a Strong Foam

The same procedure for foam strength and gas saturation determination was followed except the column was not initially saturated with surfactant. Instead, the initial volume of surfactant in the column was varied: 20, 30, 40, 50, and 60 ml. The pressure data was recorded and the gas saturation measured for all volumes of surfactant used.

Inoculation of Columns and Hydrogen Utilization

Two columns, identical to those shown in Figure 2-1, were inoculated with dechlorinating bacteria. These columns had a constant flow (0.83 ml/hr) of media saturated with PCE and were sparged twice daily with 15 ml of hydrogen. There was a 30 day period between the inoculation of the columns and the hydrogen utilization test.

After the columns were sparged with hydrogen, the level of the liquid in the glass sampling chamber was marked. The columns were allowed to sit with no flow for approximately 9 hours and then a glass syringe (10 ml) was used to add DI water to the sampling chamber until the liquid level was back up to the mark on the glass sampling chamber. The volume of DI water added to the chamber was recorded. This test was performed once a day for six days.

Results and Discussion

Gas Saturation

The gas saturation in the 1-D glass columns was determined using a column saturated with a hydrogen foam and a column saturated with water. The column with a hydrogen foam had a gas saturation of $69 \pm 2\%$ and the column with no hydrogen foam had a gas saturation of $5 \pm 1\%$. Therefore, gas saturation in the column with the hydrogen foam is at least 7 times higher than the gas saturation in the column with no foam. This could translate into having to add hydrogen to the subsurface 7 times more often when there is no hydrogen foam present.

Hydrogen Foam versus Air Foam

It has been proven in our laboratories that air can generate a strong foam. Tests were performed to determine if hydrogen foam was different from an air foam. Foams were generated with both air and hydrogen under the same conditions (i.e., gas flow rate and activity of surfactant) in the 1-D glass columns. The pressure drops across the column were recorded and compared at different pore volumes. Figure 2-3 and Figure 2-4 show the pressure drops for various gas velocities of air or hydrogen injected at 1.6 pore volumes and 1.8 pore volume, respectively. Also shown on these figures are the pressure drops obtained when no surfactant is present in the column. Without surfactant in the column the pressure drop across the column was about 0.29 psi. When surfactant is added to the column the pressure drop increases considerably.

Figures 2-3 and 2-4 also show that there is no significant difference between the strength of the foam formed for air and hydrogen.

In order to generate foam in the column, the column must first be saturated with surfactant. This requires the addition of a pore volume of surfactant to the column. There is concern that this addition of surfactant could push-out the bacteria in the column. Therefore, tests were performed with smaller volumes of surfactant in the column to determine if a strong foam could be generated without the initial saturation of the column with surfactant. Figure 2-5 shows the pressure drop across the column as a function of the volume of surfactant added to the column. All of this pressure data is after 1.8 pore volumes of hydrogen has been injected into the column. The figure also compares the results of 2 gas velocities 6.11 and 7.13 cm/min. When 60 ml (1 pore volume) of surfactant is added to the column the pressure drop across the column is approximately 6 psi; this is considered a strong foam. If less than a pore volume of surfactant is added to the column, the foam strength varies greatly. This proves that using less than a pore volume of surfactant in the column makes generating a strong foam unpredictable. However, Figure 2-6 shows that the hydrogen gas saturation in the column is not dependent on the strength of the foam. Even with high hydrogen gas saturations, the inability to predict the foam strength when less than one pore volume of surfactant is used leads to the conclusion that pregenerating the foam and then injecting it into the column is the best way to assure foam strength and microbial viability.

Hydrogen Utilization

The hydrogen utilization test was performed to determine the rate in which the bacteria in the column were consuming the hydrogen injected into the column when no surfactant foam is present. The tests showed that the bacteria had hydrogen utilization rates of 15 ± 4 ml/day. If there is only a 5% residual hydrogen saturation when no foam is in the column the bacteria are capable of consuming all of the hydrogen in 5 hours, which indicates the columns would have to be sparged 5 times a day to assure that hydrogen was not the limiting factor in the dechlorination of PCE.

Subtask 2.3 - Culture Characterization

Objective

The focus of this work was to enrich three mixed dechlorinating cultures; two from tetrachloroethene contaminated sites and one from an enrichment culture that had been operating in the laboratories at Rice University for approximately 9 years. After culture enrichment, characterization of the cultures with 16 S rRNA gene targeted primers and reductive dehalogenase targeted primers was done. The goal was to enrich cultures with different dechlorinating populations to test the effects of surfactants on these organisms.

Materials and Methods

Chemicals

The following chemicals were obtained in neat liquid form: tetrachloroethene (PCE) (99+% Acros), trichloroethene (TCE) (99.5%, Acros), *cis*-dichloroethene (DCE) (97% Acros), and methanol (MeOH) (HPLC grade Fisher). Sodium hydroxide (NaOH, 1N) was obtained from Fisher Scientific. Gaseous chemicals obtained from Trigas included vinyl chloride (VC) (8%, balance N₂) and nitrogen (Ultra High Purity). Ethene (ETH) (99.5%) and Methane (99%) were obtained from Scott Specialty Gases.

Nutrient Medium

Reagent-grade chemicals and deionized water were used in the preparation of nutrient medium. The medium consisted of the following: 400 mg/L NH₄Cl, 400 mg/L KCl, 400 mg/L MgCl₂·6H₂O, 140 mg/L KH₂PO₄, 25 mg/L CaCl₂·2H₂O, 10 mg/L (NaPO₃)₁₆, 2.5 mg/L KI, 2.5 mg/L CoCl₂·6H₂O, 0.5 mg/L ZnCl₂, 0.5 mg/L MnCl₂·4H₂O, 0.5 mg/L H₃BO₃, 0.5 mg/L NiCl₂·6H₂O, 0.5 mg/L Na₂MoO₄·2H₂O, 0.5 mg/L NH₄VO₃, 300 mg/L Na₂S·9H₂O, and 40 mg/L FeCl₂·4H₂O.

Analytical Methods

Gas chromatography was used to determine the aqueous and gaseous concentrations of all chlorinated ethenes, ethene and methane. Headspace samples (100 µL) were directly injected onto a GC (Hewlett-Packard 5890) equipped with a flame ionization detector (FID) and a packed column (6 ft x 1/8 in. OD) containing 60/80 Carbopack B/1% SP-1000 (Supelco). The operating parameters were as follows: 40 °C, hold 2 min, ramp at 20° C/min to 150° C, ramp at 10° C/min, to 200° C, hold 10 min. The detector temperature was set at 275 ° C and the injection port at 200° C. The flow rates for the gases were: helium (12 mL/min), hydrogen (40 mL/min), zero air (460 mL/min). Standards were prepared by adding PCE, TCE and *cis*-DCE dissolved in methanol, and VC, ETH and methane gases at known volumes, to a serum bottle (70 ml) containing deionized water (50 mL).

Cultures

Bioreactor Design

Three bioreactors were constructed using Nalgene low-density polyethylene carboys (2-25 L and 1-30 L, Fisher Scientific). These reactors were fitted with polypropylene closures, which allowed for headspace sampling, liquid sampling, and addition of nutrient media, PCE, and sodium hydroxide.

Bioreactors were filled with 10 L of nutrient media and then the source for each culture was added. For the Owls culture, the reactor was connected to the effluent of an up flow anaerobic blanket reactor, which was enriched with an actively dechlorinating culture that had been fed PCE for approximately 9 years. This column has been previously described by [1]. The Cornhuskers and Longhorns culture were started from contaminated groundwater samples from Nebraska and Texas, respectively, and were obtained from Groundwater Services Inc. (Houston, TX). The groundwater (15 L for the Cornhuskers and 10 L for the Longhorns) was pumped in the reactors using a peristaltic pump. All cultures were operated with an 80-day retention time and were fed 3 mmol/L-d of MeOH. The addition of PCE was initially low (0.05 mM) and increased as the dechlorination rate increased. After complete dechlorination occurred cultures were fed 0.25 mmol/L-d PCE. Sodium hydroxide (1 N) was added as necessary to adjust the pH.

Bioreactor Microcosms

Microcosm studies (48 hrs) were performed periodically to determine the extent of dechlorination accomplished by each culture. Serum vials (70 mL) were sealed with a with Teflon lined butyl rubber stoppers (Supelco) and aluminum crimp caps (Supelco) with stir bar enclosed. The bottles were purged with ultra high purity N₂ gas (12 min) to remove oxygen. The culture (50 mL) was added to the serum bottles and then sparged with N₂ (12 min) to remove any residual volatile contaminants. After sparging, PCE (0.25 mM) and MeOH (3mM) were added. The microcosms were allowed to run for 48 hours and then headspace samples were analyzed by GC/FID.

DNA Extraction and PCR

Culture fluid (30 ml) was placed in two aliquots into 15 ml flacon tubes and centrifuged at 3900 RPM (? g) for 1 hour at 4 °C. The resulting pellet was used for DNA extraction with Ultraclean™ Soil DNA Isolation Kit (Mo Bio Laboratories, Inc., Solana Beach, CA). The manufacturer's protocol was followed, except that a mini-bead beater was used instead of a vortex for cell lysis. The DNA was quantified spectrophotometrically and the quality was verified on a 1% agarose gel.

PCR was performed in 20 µl reactions with 2.5x Eppendorf PCR Mastermix (Brinkman), which contains 1.25 U Taq polymerase and 200 µM of each deoxynucleoside triphosphate for each reaction. For each reaction, 30 – 50 ng of template was used. For each target organism and enzyme, the primer sequence is listed in Table DI. Nested PCR was also performed with the Unibac 8F and 1541 R primers. The PCR products were visualized on a 1% agarose gel in Tris-acetate-EDTA buffer and stained in an ethidium bromide solution.

Real-time PCR (RTm PCR)

The numbers of important organisms in the cultures were estimated using a RTm PCR approach. The primers used for this are listed in Table 2-II. The *pceA* primers listed in this table were initially developed by Benjamin K. Amos and Dr. Frank E. Löffler as a part of SERDP project CU-1293 (Development of Assessment Tools for Evaluation of the Benefits of DNAPL Source Zone Treatment). The PCR reaction (25 μ l) for the bacterial and archaeal primers contained 0.9 μ M of each primer (0.45 μ M of the forward and reverse for the archaeal primers), 0.25 μ M of the probe, 1 X TaqMan Universal PCR Mastermix (Applied Biosystems), and DNA template. An ABI Prism 7000 sequence detection system (Applied Biosystems) was used with the following PCR conditions: 2 min at 50 °C, 10 min at 95 °C, followed by 40 cycles of 15 sec at 95 °C and 1 min at 60 °C. The remaining primers were used with a SYBR green approach. The PCR reaction (30 μ l) contained 1X SYBR[®] Green PCR Master Mix (Applied Biosystems), forward primer and reverse primer (300 nM), and DNA template. PCR conditions were as follows: 2 min at 50 °C, 15 min at 95 °C, followed by 40 cycles of 15 sec at 94 °C and 1 min at 58 °C (for *Dehalobacter* spp.), 60 °C (for *Dehalococcoides* spp.) and 52 °C for the *pceA* gene and 30 sec at 72 °C. The PCR was carried out in a spectrofluorimetric thermal cycler (ABI Prism 7500 sequence detection system, Applied Biosystems).

Results

Culture Enrichment

Table 2-III describes the culture enrichments. Two of the cultures were obtained from contaminated sites and one from an industrial wastewater treatment plant. All three cultures are capable of complete dechlorination to ethene, but during the enrichment process each culture took a different amount of time to reach this end point. The Owls culture was the first culture to start producing 100% ethene from PCE, which is most likely due to the fact that this culture had been enriched in the laboratory for approximately 9 years in an up flow anaerobic sludge reactor before it was changed to the semi-batch configuration. The Cornhuskers and Owls culture remained at approximately 80% VC and 20% ethene for about 2 years before finally switching over to 100% production of ethene from PCE.

Figure 2-7 shows the dechlorination capability of all three cultures with 3 mM MeOH and 0.25 mM PCE. All three cultures completely dechlorinate PCE to ethene in less than 4 days. The Cornhuskers culture completely dechlorinates PCE in 24 hours. Figure 2-8 shows the volatile fatty acid (VFA) production during the dechlorination shown in Figure 2-7. During dechlorination none of the VFAs produced changed in concentration appreciably.

Each culture was analyzed for known dechlorinating populations using published primers specific for the 16S rRNA genes of these organisms. Both direct and nested PCR was performed for the 16S rRNA genes and the results

are listed in Table 2-IV. All three cultures contain *Dehalococcoides* spp. and *Dehalobacter* spp., which were detected by direct PCR. Nested PCR detected two species of *Sulfurospirillum* spp. capable of dechlorination. The Owls culture also contains the newly discovered *Geobacter* sp strain SZ, which is capable of dechlorinating PCE to *cis*-DCE. The cultures were also analyzed for known reductive dehalogenase genes and these results are shown in Table 2-V. All three cultures contained the *tceA* gene, responsible for dechlorination of TCE to ethene and the *pceA* gene, responsible for the dechlorination of PCE to *cis*-DCE. None of the cultures contain the *bvcA* gene, but two cultures contained the *vcrA* gene, which leaves one culture, Cornhuskers, with no known VC reductase.

RTm PCR was used to quantify the numbers of the major dechlorinating species present in the cultures. Figure 2-9 shows that the 3 enrichment cultures contain roughly the same number of *Dehalobacter* spp., but that the Cornhuskers culture contains almost an order of magnitude more *Dehalococcoides* spp. The number of archaeal organisms present in each culture was also determined with RTm PCR. Figure 2-10 shows that the Owls culture contains the most archaeal cells, and that the Cornhuskers culture contains no archaeal cells. This matches with the methane production from each culture because the Owls culture produces the most methane and the Cornhuskers culture produces no methane (data not shown).

Short term studies of the VFA production showed no change in the concentration of most VFA produced. So, long term experiments were set up to determine if the VFAs produced were dead end products or if they were utilized by organisms in the cultures. These experiments were set up in the same manner as all other experiments, but only MeOH was added and no PCE. Figure 2-11 shows that after 112 days of incubation, on the Owls culture used all of the VFAs produced and the Longhorns and Cornhuskers culture used only the formate that was produced. This means that the acetate, propionate and butyrate produced are dead end products for these cultures.

Discussion

The objective of this work was to obtain three different communities of dechlorinating organisms to test surfactant effects on different dechlorinating species. After enrichment for 3 years, the cultures merged to almost identical endpoints in terms of dechlorinating populations. Where the cultures differed was in their method of energy generation from MeOH. There are only a few organisms that can convert MeOH to acetate, formate, or carbon dioxide and methane. It is obvious that there are organism in all three cultures that are capable of producing acetate and formate, but only the Owls culture can utilize the acetate. This implies that the Owls culture contains acetoclastic methanogens, which utilize acetate and produce methane. Syntrophic organisms are ones that can oxidize fatty acids and produce hydrogen. These are most likely the hydrogen producers in these cultures.

Subtask 2.4 - Surfactant Effects on Mixed Dechlorinating Cultures

A surfactant screening study was first performed to determine the effect of different types of surfactants on the rate and extent of dechlorination. This work has been published in a Master's thesis [2] and in the journal Environmental Toxicology and Chemistry [3]. Both of these documents are in the appendix of this document.

Objective

This section focuses on the effect of surfactants on mixed dechlorinating cultures. It was shown in previous work [3] that many surfactants cause dechlorination to stop at an intermediate step in dechlorination such as TCE or *cis*-DCE. The objective of this work is to determine the conditions in which complete dechlorination will occur in the presence of surfactant, and to determine which organisms in the mixed dechlorinating cultures are negatively affected by surfactants.

Materials and Methods

Chemicals

The following chemicals were obtained in neat liquid form: tetrachloroethene (PCE) (99+% Acros), trichloroethene (TCE) (99.5%, Acros), *cis*-dichloroethene (DCE) (97% Acros), and methanol (MeOH) (HPLC grade Fisher). Sodium hydroxide (NaOH, 1N) was obtained from Fisher Scientific. Gaseous chemicals obtained from Trigas included vinyl chloride (VC) (8%, balance N₂) and nitrogen (Ultra High Purity). Ethene (ETH) (99.5%) and Methane (99%) were obtained from Scott Specialty Gases. Steol CS-330 (27% active) was obtained from Stepan. Tridecyl alcohol, propoxylated, sulfated, ammonium salt (C13-4PO; 18% active) was obtained from Stepan Chemical Co.

Nutrient Medium

Reagent-grade chemicals and deionized water were used in the preparation of nutrient medium. The medium consisted of the following: 400 mg/L NH₄Cl, 400 mg/L KCl, 400 mg/L MgCl₂·6H₂O, 140 mg/L KH₂PO₄, 25 mg/L CaCl₂·2H₂O, 10 mg/L (NaPO₃)₁₆, 2.5 mg/L KI, 2.5 mg/L CoCl₂·6H₂O, 0.5 mg/L ZnCl₂, 0.5 mg/L MnCl₂·4H₂O, 0.5 mg/L H₃BO₃, 0.5 mg/L NiCl₂·6H₂O, 0.5 mg/L Na₂MoO₄·2H₂O, 0.5 mg/L NH₄VO₃, 300 mg/L Na₂S·9H₂O, and 40 mg/L FeCl₂·4H₂O.

Analytical Methods

Gas chromatography was used to determine the aqueous and gaseous concentrations of all chlorinated ethenes, ethene and methane. Headspace

samples (100 μ L) were directly injected onto a GC (Hewlett-Packard 5890) equipped with a flame ionization detector (FID) and a packed column (6 ft x 1/8 in. OD) containing 60/80 Carbopack B/1% SP-1000 (Supelco). The operating parameters were as follows: 40 °C, hold 2 min, ramp at 20 °C/min to 150 °C, ramp at 10 °C/min, to 200 °C, hold 10 min. The detector temperature was set at 275 °C and the injection port at 200 °C. The flow rates for the gases were: helium (12 mL/min), hydrogen (40 mL/min), zero air (460 mL/min). Standards were prepared by adding PCE, TCE and *cis*-DCE dissolved in methanol, and VC, ETH and methane gases at known volumes, to a serum bottle (70 ml) containing deionized water (50 mL).

Surfactant Studies

Microcosm studies were used to determine surfactant effects on the extent of dechlorination. Serum vials (70 mL) were sealed with Teflon lined butyl rubber stoppers (Supelco) and aluminum crimp caps (Supelco) with stir bar enclosed. The bottles were purged with ultra high purity N₂ gas (12 min) to remove oxygen. The culture (50 mL) was added to the serum bottles and then sparged with H₂/CO₂ (12 min) as the source of electron donor. Surfactant was added using a stock solution made in media and allowed to stir for 10 minutes. Neat PCE was added (0.25 mM). H₂/CO₂ was added as needed and headspace samples were analyzed by GC/FID.

DNA Extraction and PCR

Culture fluid (5 ml) was taken from microcosm studies, added to 15 ml flacon tubes and centrifuged at 3900 RPM (? g) for 1 hour at 4 °C. The resulting pellet was frozen at -20 °C until all samples were ready to be extracted. The DNA was extracted with an Ultraclean™ Soil DNA Isolation Kit (Mo Bio Laboratories, Inc., Solana Beach, CA). The manufacturer's protocol was followed, except that a mini-bead beater was used instead of a vortex for cell lysis. The DNA was quantified spectrophotometrically and the quality was verified on a 1% agarose gel.

Real-time PCR (RTm PCR)

The quantity of *Dehalococcoides* spp., *Dehalobacter* spp. and the *pceA* gene from *Sulfurospirillum* spp. were determined using RTm PCR. The primers listed in Table ## were used and conditions described in section ## were employed.

Results and Discussion

This work began by focusing on the surfactant Steol CS-330, which is an anionic surfactant. CS-330 was chosen because it is an excellent surfactant for

generating surfactant foam. Figures 2-12 – 2-14 show the extent of dechlorination of PCE in the presence of 0% (control), 0.005% and 0.01% CS-330. These CS-330 concentrations were chosen because they were the lowest concentrations at which foam generation was possible. For both the Owls and the Cornhuskers cultures complete dechlorination to ethene occurred in the controls, but in the presence of CS-330 dechlorination stopped at *cis*-DCE. CS-330 had a slightly different effect on the Longhorns culture. When exposed to CS-330 dechlorination was stopped at a combination of TCE and *cis*-DCE, complete conversion to *cis*-DCE never occurred.

The next surfactant tested was an experimental surfactant: C134PO. This surfactant was only tested with the Owls culture at 0%, 0.005% and 0.01%. Figure 2-15 shows the effect of C134PO on the extent of dechlorination in the Owls culture. The control dechlorinated PCE to ethene and in the presence of C134PO the culture dechlorinated PCE to a mixture of *cis*-DCE and vinyl chloride. Unfortunately, this surfactant is not capable of generating a foam as strong as CS-330, but the combination of C134PO and CS-330 did allow for strong foam generation, so a combination of CS-330 and C134PO was tested to determine if dechlorination would proceed past *cis*-DCE.

Figure 2-16 shows the result of combining 0.005% of CS-330 and C134PO (0.01% surfactant) and 0.01% CS-330 and C134PO (0.02% surfactant). With both surfactant concentrations, dechlorination still stopped at *cis*-DCE thus combining surfactants did not improve the extent of dechlorination of PCE.

With the Owls and Cornhuskers culture the surfactant concentration where there was no effect of the surfactant on dechlorination was determined and is shown in Figure 2-17. The Owls culture shows a definite surfactant concentration where the dechlorination is affected: at 0.003% CS-330 there is no effect, at 0.0035% dechlorination stopped at vinyl chloride and at 0.004% dechlorination stopped at *cis*-DCE. With the Cornhuskers culture, at CS-330 concentrations as low as 0.0006% dechlorination was still incomplete.

Anionic surfactants have been used in the removal of hydrocarbon contamination from sediments; therefore, the effect of surfactants on organisms capable of degrading hydrocarbons has been extensively studied. From these studies researchers have proposed two mechanisms in which surfactants can interact with microorganisms 1) they can interact with peripheral or membrane bound proteins or 2) they can interact directly with the membrane and destroy membrane integrity (Berg and Zimmer 1987). In these studies, they have shown that anionic surfactants have little or no interaction with gram negative organisms. They attribute this fact to the gram negative organism's membrane structure, which includes an outer membrane and a thin layer of peptidoglycan which is above the cytoplasmic membrane. Researchers hypothesize this membrane structure prevents the surfactant from embedding in the membrane. To test this hypothesis, an experiment was done where an excess source of gram negative (*Escherichia coli*) and gram positive (*Bacillus subtilis*) bacteria were added to actively dechlorinating mixed cultures in the presence of surfactant to see if dechlorination would proceed past *cis*-DCE. Figure 2-18 shows that when *E. coli* are added, dechlorination still stops at *cis*-DCE and

when *B. subtilis* is added, dechlorination can proceed past *cis*-DCE to vinyl chloride and ethene.

It appears that the first hypothesis above does not apply to the dechlorinating systems. *Dehalococcoides ethenogenes* has a two enzyme pathway, the first PCE-rdase converts PCE to TCE and the second TCE-rdase converts TCE to ethene (vinyl chloride to ethene is cometabolic). If the surfactant was interacting with the enzyme, dechlorination would stop at TCE or not proceed at all. So, therefore, it appears that the second hypothesis could apply to the dechlorinating system, where one organism that converts PCE to *cis*-DCE is not affected by the surfactant, but the second organism that converts *cis*-DCE to ethene is affected by the surfactant. Table ## shows some of the membrane structures of the dechlorinating organisms that have been identified in the cultures. Both *Dehalobacter* spp. and *Sulfurospirillum* spp. are gram negative organisms and both are capable of dechlorinating PCE to *cis*-DCE. The organism in all three cultures responsible for *cis*-DCE to ethene dechlorination is *Dehalococcoides* spp. and its membrane structure is unique and does not fit into the gram negative or gram positive category, but resembles more of an archaeal membrane. From this, it seems that *Dehalococcoides* spp. are being affected by CS-330.

To test this hypothesis, a 10% inoculum of the Owls culture was added to fresh media with four different conditions: 1) PCE with no surfactant (positive control), 2) PCE with 0.01% CS-330, 3) no surfactant, PCE and O₂, and 4) no PCE, no surfactant. These conditions show 1) normal growth, 2) growth effected by the surfactant, 3) killed cells and 4) cells that are starved. Figure 2-19 shows the dechlorination for all the conditions except the fourth where no PCE was added. As expected, the positive control completely dechlorinated the PCE, the culture exposed to CS-330 stopped dechlorinating at *cis*-DCE, and the culture exposed to oxygen did not dechlorinate the PCE.

RTm PCR was used to quantify the dechlorinating populations over time as the dechlorination occurred. Figure 2-20 A and B show that both *Dehalobacter* spp. and *Sulfurospirillum* spp. stay a relative constant concentration, except for an initial increase for all the conditions. Figure 2-20 C shows the same trend for all conditions, but that the *Dehalococcoides* spp. that are exposed to CS-330 decrease over time. This proves that the *Dehalococcoides* spp. are the organisms being affected by the CS-330.

To determine if this affect is reversible, at day 15 (end of experiment) the cells from the positive control and the surfactant exposed culture were washed and resuspended into fresh surfactant free media. Figure 2-21 A shows the positive control dechlorinates PCE to ethene in approximately 60 days. Figure 2-21 B shows that the culture exposed to CS-330, even when resuspended, does not regain activity.

This work has shown that the surfactant CS-330 has a negative impact on *Dehalococcoides* spp. in actively dechlorinating cultures and that the effect is not reversible. It has been shown that this surfactant does interact with gram positive organisms and in the subsurface there will be more microbial diversity than what is present in the dechlorinating enrichment cultures, so there is a

chance for the *Dehalococcoides* to survive in a subsurface environment. Also, CS-330 was only tested in this work in the dissolved phase and not in the foam form. There is a possibility that CS-330 in the foam form would interact with the *Dehalococcoides* spp. differently.

References

1. Carr, C.S. and J.B. Hughes, *Enrichment of high rate PCE dechlorination and comparative study of lactate, methanol, and hydrogen as electron donors to sustain activity*. Environmental Science & Technology, 1998. **32**(12): p. 1817-1824.
2. McGuire, T., *Effects of surfactants on a PCE dechlorinating mixed culture*, in *Department of Civil and Environmental Engineering*. 2002, Rice University: Houston.
3. McGuire, T. and J.B. Hughes, *Effects of surfactants on the dechlorination of chlorinated ethenes*. Environmental Toxicology and Chemistry, 2003. **22**(11): p. 2630-2638.
4. Löffler, F.E., et al., *16S rRNA gene-based detection of tetrachloroethene-dechlorinating *Desulfuromonas* and *Dehalococcoides* species*. Applied and Environmental Microbiology, 2000. **66**(4): p. 1369-1374.
5. Schlotelburg, C., et al., *Microbial structure of an anaerobic bioreactor population that continuously dechlorinates 1,2-dichloropropane*. Fems Microbiology Ecology, 2002. **39**(3): p. 229-237.
6. Hendrickson, E.R., et al., *Molecular Analysis of *Dehalococcoides* 16S Ribosomal DNA from Chloroethene-contaminated Sites Throughout North America and Europe*. Applied and Environmental Microbiology, 2002. **68**(2): p. 485-495.
7. Pietari, J.M.H., *Characterization of Tetrachloroethene dechlorinating cultures and isolation of a novel tetrachloroethene to cis-1,2-dichloroethene halorespiring bacterium*, in *Department of Civil and Environmental Engineering*. 2002, University of Washington: Seattle.
8. Ebersole, R.C. and E.R. Hendrickson, *Nucleic acid fragments for identification of dechlorinating bacteria*. 2005: USA.
9. El Fantroussi, S., et al., *Introduction and PCR detection of *Desulfomonile tiedjei* in soil slurry microcosms*. Biodegradation, 1997. **8**(2): p. 125-133.
10. Sung, Y., *Isolation and ecology of bacterial populations involved in reductive dechlorination of chlorinated solvents*, in *Civil and Environmental Engineering*. 2005, Georgia Institute of Technology: Atlanta.
11. Magnuson, J.K., et al., *Trichloroethene reductive dehalogenase from *Dehalococcoides ethenogenes*: Sequence of *tceA* and substrate range characterization*. Applied and Environmental Microbiology, 2000. **66**(12): p. 5141-5147.

12. Krajmalnik-Brown, R., et al., *Genetic identification of a putative vinyl chloride reductase in Dehalococcoides sp strain BAV1*. Applied and Environmental Microbiology, 2004. **70**(10): p. 6347-6351.
13. Müller, J.A., et al., *Molecular Identification of the Catabolic Vinyl Chloride Reductase from Dehalococcoides sp. Strain VS and Its Environmental Distribution*. Applied and Environmental Microbiology, 2004. **70**(8): p. 4880-4888.
14. Suzuki, M.T., L.T. Taylor, and E.F. DeLong, *Quantitative analysis of small-subunit rRNA genes in mixed microbial populations via 5'-nuclease assays*. Applied and Environmental Microbiology, 2000. **66**(11): p. 4605-4614.
15. Smits, T.H.M., et al., *Development of a real-time PCR method for quantification of the three genera Dehalobacter, Dehalococcoides, and Desulfitobacterium in microbial communities*. Journal of Microbiological Methods, 2004. **57**(3): p. 369-378.
16. Regard, C., J. Maillard, and C. Holliger, *Development of degenerate and specific PCR primers for the detection and isolation of known and putative chloroethene reductive dehalogenase genes*. Journal of Microbiological Methods, 2004. **56**(1): p. 107-118.

Table 2-I. Primers used for identifying organisms and reductive dehalogenase genes present in enrichment cultures.

Target Group	Primer Name	Sequence	Reference
Bacteria	Unibac 8F Unibac 1541R	5'-AGAGTTTGATCCTGGCTCAG-3' 5'-AAGGAGGTGATCCAGCCGCA-3'	[4]
<i>Dehalobacter restrictus</i>	Deb179F Deb1007R	5'-TGTATTGTCCGAGAGGCA-3' 5'-ACTCCCATATCTCTACGG-3'	[5]
<i>Dehalococcoides</i> spp.	FpDHC1 RpDHC1212	5'-GATGAACGCTAGCGGCG-3' 5'-GGATTAGCTGTTCACT-3'	[6]
<i>Sulfurospirillum</i> sp. strain JPD-1	JPDF JPDR	5'-CCCCATACTCCAATTAT C-3' 5'-TTCTAGGTGACCAGTTTCG-3'	[7]
<i>Sulfurospirillum multivorans</i>	Fp DHSPM 576 Rp DHSPM 1210	5'-GCTCTCGAACTGGTTACCTA-3' 5'-GTATCGCGTCTCTTTGTCCTA-3'	[8]
<i>Desulfuromonas</i> spp.	Desulf for Desulf rev	5'-AACCTTCGGGTCCTACTGTC-3' 5'-CGGCAACTGACCCCTATGTT-3'	[4]
<i>Desulfitobacterium</i> spp.	Dd1 Dd2	5'-AATACCGNATAAGCTTATCCC-3' 5'-TAGCGATTCCGACTTCATGTTTC-3'	[9]

Table 2-I. Primers used for identifying organisms and reductive dehalogenase genes present in enrichment cultures.

Target Group	Primer Name	Sequence	Reference
<i>Desulfomonile</i> spp.	Dt1	5'-CAAGTCGTACGAGAAACATATC-3'	[9]
	Dt2	5'-GAAGAGGATCGTCTTTCCACGA-3'	
<i>Geobacter</i> sp. strain SZ	GeoF	5'-GAATATGCTCCTGATTC-3'	[10]
	GeoR	5'-ACCCTCTACTTTCATAG-3'	
<i>tceA</i>	797F	5'-ACGCCAAAGTGCGAAAAGC-3'	[11]
	2490R	5'-GAGAAAGGATGGAATAGATTA-3'	
<i>bvcA</i>	bvcAF	5'-TGCCTCAAGTACAGGTGGT-3'	[12]
	bvcAR	5'-ATTGTGGAGGACCTACCT-3'	
<i>vcrA</i>	vcrAF	5' – CTATGAAGGCCCTCCAGATGC – 3'	[13]
	vcrAR	5' – GTAACAGCCCCAATATGCAAGTA - 3'	

Table 2-II. Real time PCR primers used for quantifying organism.

Target Group	Primer Name	Sequence	Reference
Bacteria	BACT1369F	5'-CGGTGAATACGTTTCYCGG-3'	[14]
	PROK1492R	5'- GGWTACCTTGTTACGACTT-3'	
	TM1389F	Fam-5'-CTTGTACACACCGCCCGTC-3'BHQ1	
Archaeal	Arch1-1369F	5'-CGGTGAATACGTCCCTGC-3'	[14]
	Arch2-1369F	5'-CGGTGAATATGCCCCTGC-3'	
	PROK1541R	5'-AAGGAGGTGATCCTGCCGCA-3'	
	TM1389F	Fam-5'-CTTGTACACACCGCCCGTC-3'BHQ1	
<i>Dehalobacter restrictus</i>	Dre441F Dre645R	5'-GTTAGGGAAGAACGGCATCTGT-3' 5'-CCTCTCCTGTCCTCAAGCCATA -3'	[15]
<i>Dehalococcoides</i> spp.	dhcRTfor dhcRTrev	5'-CTGGAGCTAATCCCCAAAGCT-3' 5'-CAACTTCATGCAGGCGGG-3'	[6]
<i>pceA</i>	Spsm1f Spsm1r	5' – TCGTTGCAGGTATCGCTATG – 3' 5' – TTCAACAGCAAAGGCAACTG – 3'	[16]

Table 2-III. Enrichment culture description and time required during enrichment process for production of cis-dichloroethene, vinyl chloride, and ethene as major end product.

Culture	Origin	Time in Operation	Time to Production as Major End Product		
			<i>cis</i> -DCE	VC	Ethene
Owls	Industrial plant	3 yrs 1 month	N/A	0 months	6 months
Cornhuskers	Contaminated site - NE	3 yrs	1 month	2 months	2 yrs
Longhorns	Contaminated site - TX	2 yrs 9 months	6 months	9 months	2 yrs 1 months

Table 2-IV. Identification of dechlorination populations in enrichment cultures using 16S rRNA gene targeted primers. (D = direct PCR; N = nested PCR)

Target Population	Owls	Cornhusker	Longhorns
<i>Dehalobacter</i> spp.	+ (D)	+ (D)	+ (D)
<i>Dehalococcoides</i> spp.	+ (D)	+ (D)	+ (D)
<i>Sulfurospirillum</i> sp. strain JPD-1	+ (N)	+ (N)	+ (N)
<i>Sulfurospirillum multivorans</i>	+ (N)	+ (N)	-
<i>Desulfuromonas</i> spp.	-	-	-
<i>Desulfitobacterium</i> spp.	-	-	-
<i>Desulfomonile tiedjei</i>	-	-	-
<i>Geobacter</i> sp. strain SZ	+ (N)	-	-

Table 2-V. Identification of reductive dehalogenase genes in enrichment cultures using gene targeted primers.

Target Gene	Owls	Cornhuskers	Longhorns
<i>tceA</i> TCE → ETH (<i>Dehalococcoides</i> spp.)	+	+	+
<i>bvcA</i> DCEs → ETH (<i>Dehalococcoides</i> sp. strain BAV 1)	-	-	-
<i>vcrA</i> DCEs → ETH (<i>Dehalococcoides</i> sp. strain VS or strain H10)	+	-	+
<i>pceA</i> PCE → DCE (<i>Sulfurospirillum multivorans</i>)	+	+	+

Table 2-VI. Dechlorination capabilities and membrane properties of dechlorinating organisms found in the mixed dechlorinating cultures.

Organism	Dechlorination Capability	Gram Stain
<i>Dehalobacter restrictus</i>	PCE → DCE	Gram-negative
<i>Sulfurospirillum multivorans</i>	PCE → DCE	Gram-negative
<i>Dehalococcoides ethenogenes</i> 195	PCE → ETH	unknown
<i>Dehalococcoides</i> sp. strain VS	DCEs → ETH	unknown

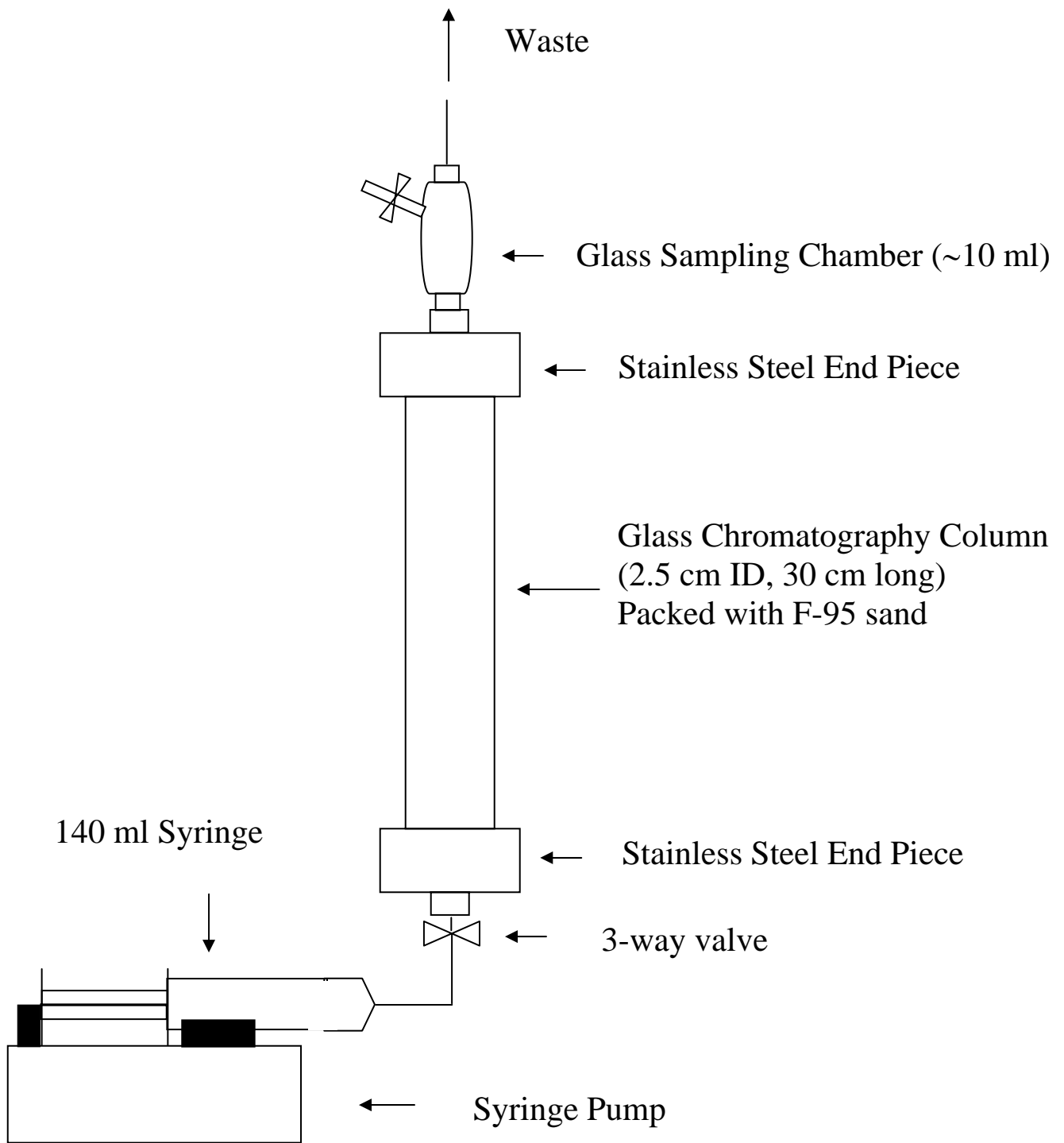


Figure 2-1. Schematic of column set-up.

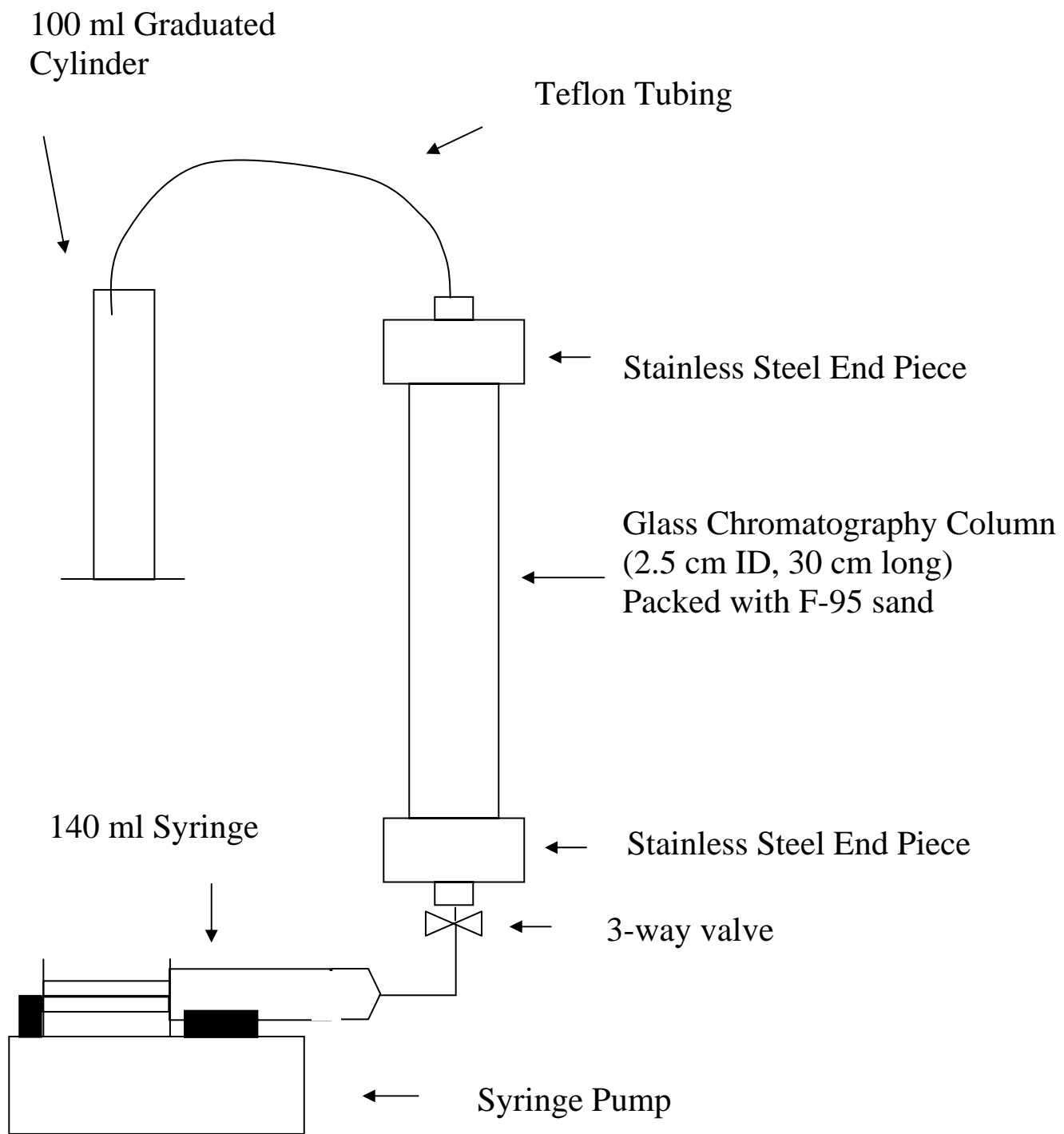


Figure 2-2. Schematic of Experimental Set-up for measuring the gas saturation in the column.

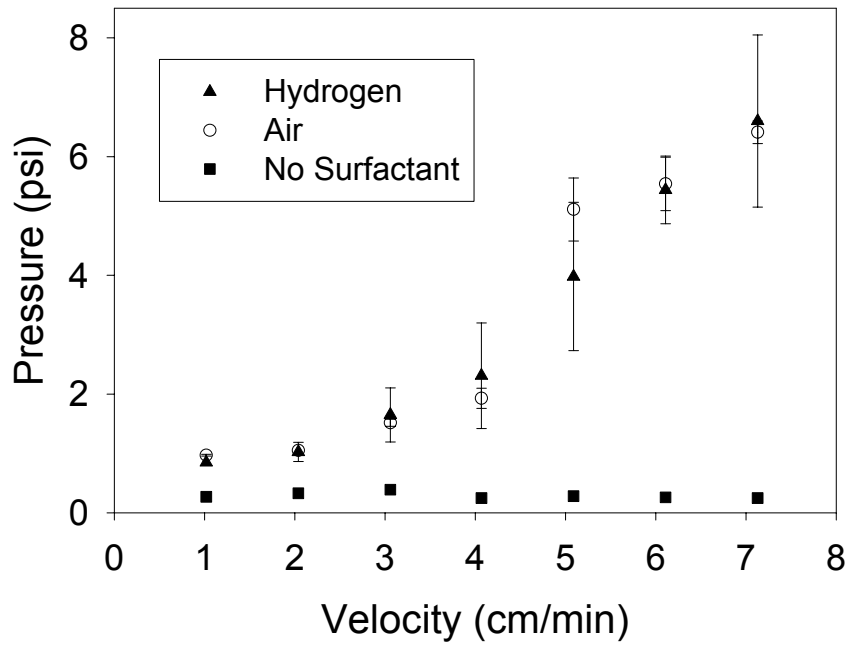


Figure 2-3. Comparison of Foam Strength Formed Using 0.5% CS-330 with Hydrogen and Air in a 1-D Column (1.6 Pore Volumes Injected).

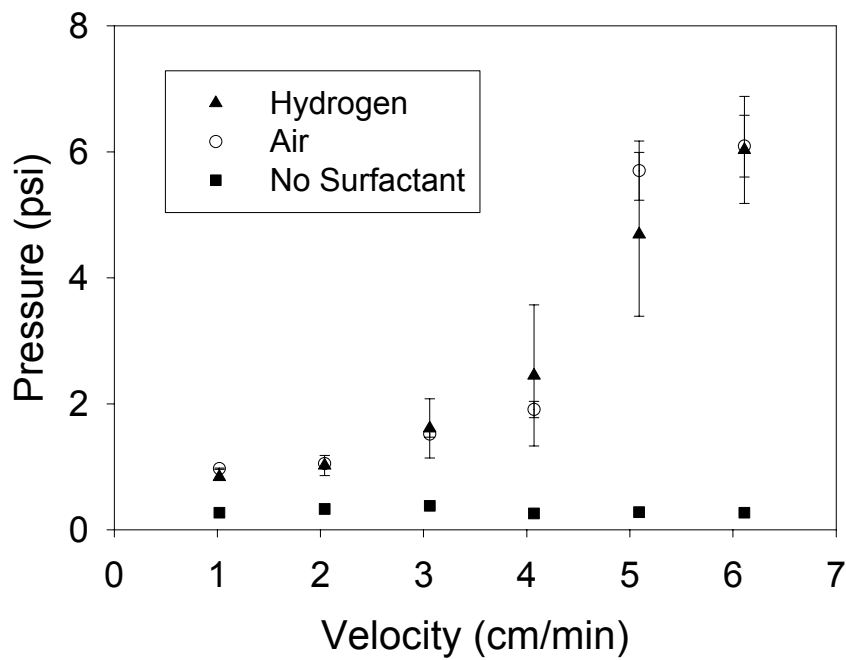


Figure 2-4. Comparison of Foam Strength Formed Using 0.5% CS-330 with Hydrogen and Air in a 1-D Column (1.8 Pore Volumes Injected).

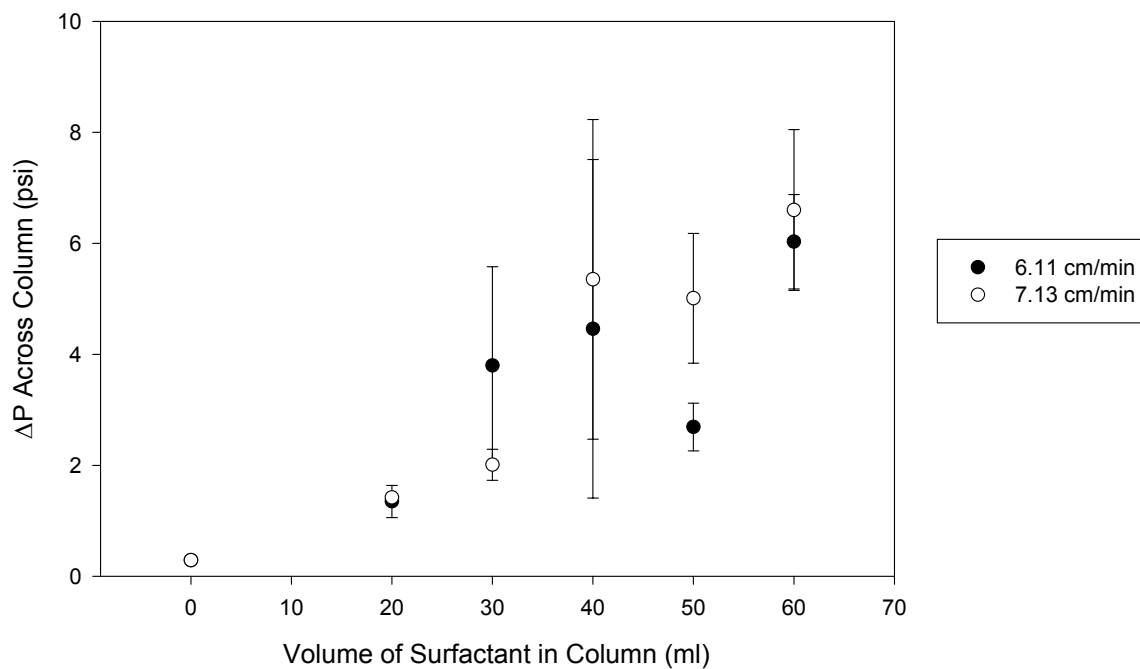


Figure 2-5. Determination of foam strength by varying volume of surfactant (0.5% active CS-330 with 2.3 g/L NaCl and 0.025 g/L CaCl₂) in a 1-D column. All data taken at 1.8 pore volumes of hydrogen injected.

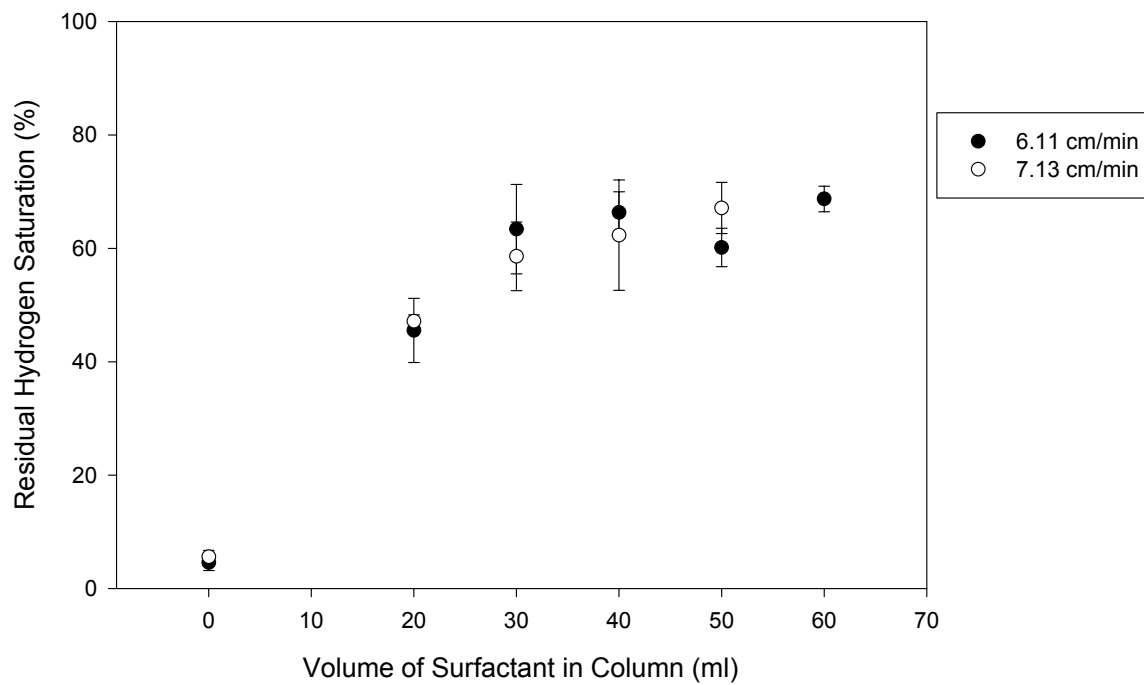


Figure 2-6. Residual hydrogen saturation dependence on initial volume of surfactant (0.5% active CS-330 with 2.3 g/L NaCl and 0.025 g/L CaCl₂) in a 1-D column.

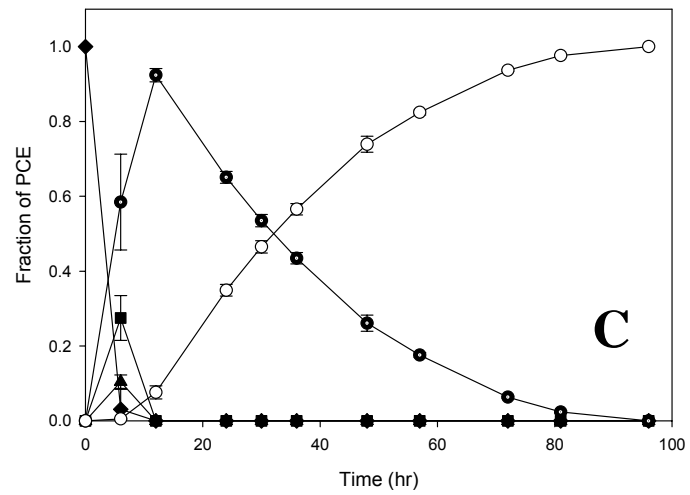
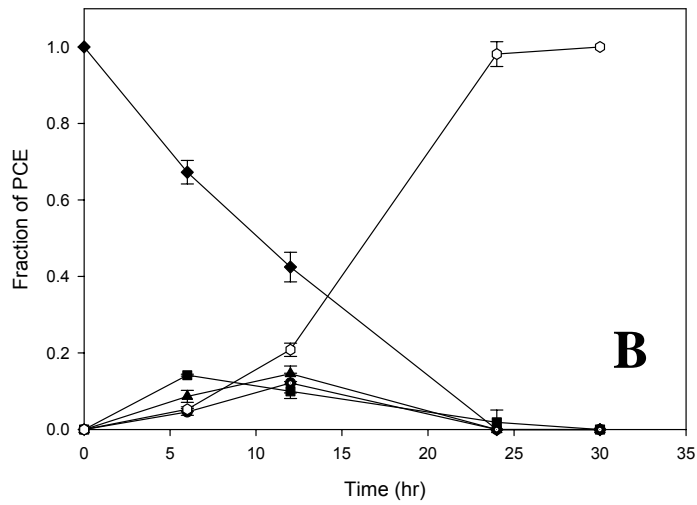
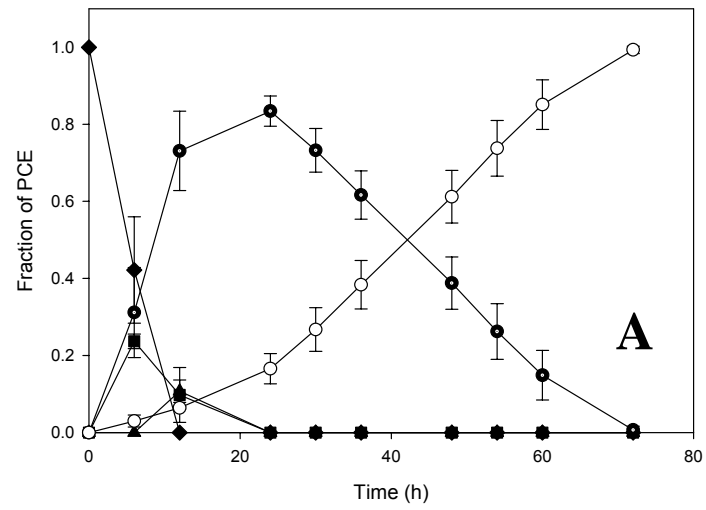


Figure 2-7. Culture specific dechlorination with 3 mM MeOH and 0.25 mM PCE: A) Owls culture, B) Cornhusker culture, and C) Longhorns culture. Symbols: ◆ PCE; ■ TCE; ▲ DCE; ● VC; ○ ETH.

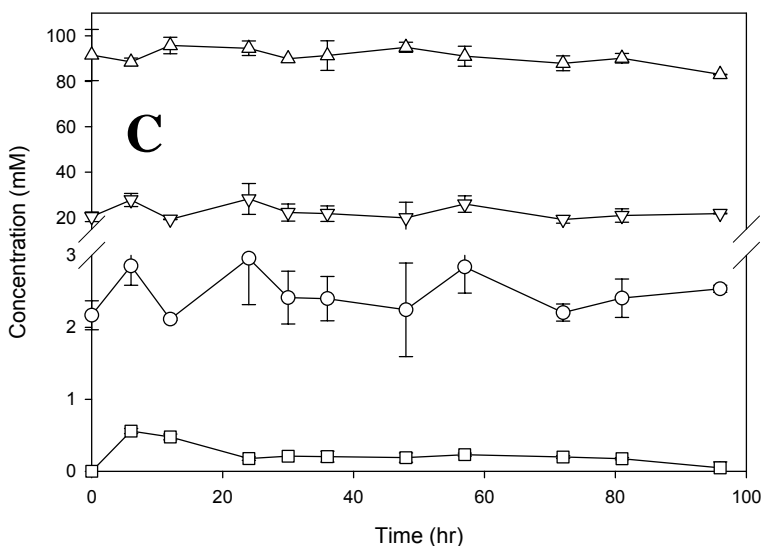
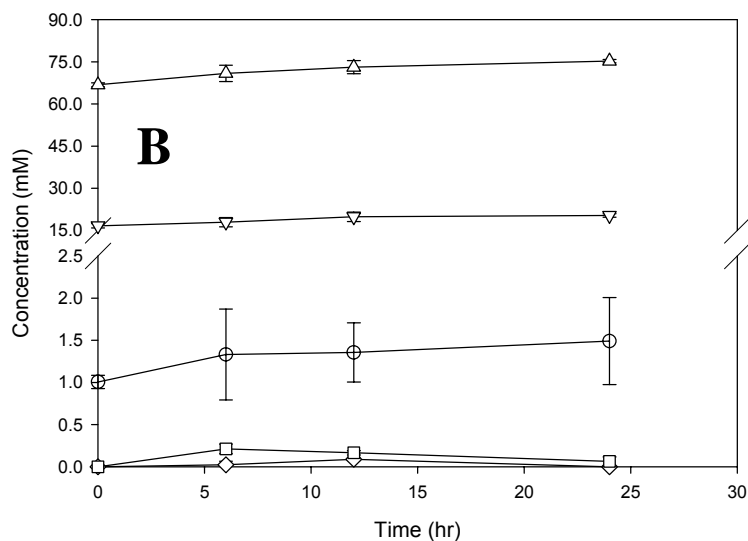
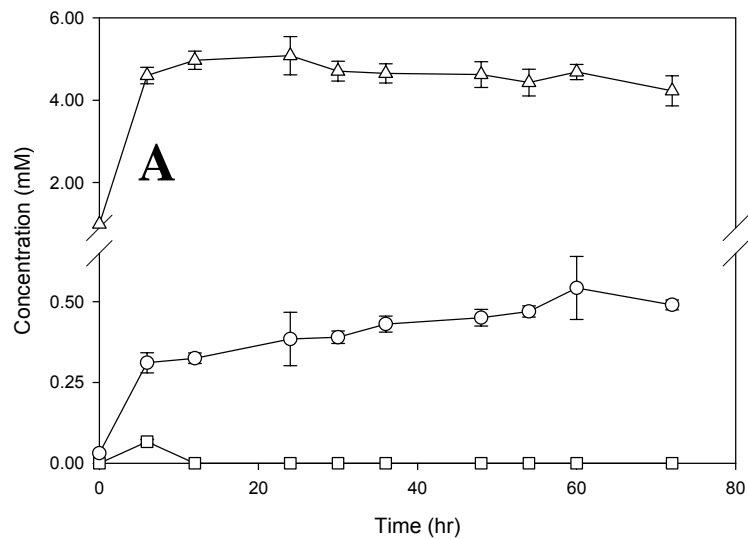


Figure 2-8. Culture specific volatile fatty acid production with 3 mM MeOH and 0.25 mM PCE: A) Owls culture, B) Cornhusker culture, and C) Longhorns culture. This data taken at the same time as the dechlorination data in Figure 2-2. Symbols: \diamond succinate; \square formate; \triangle acetate; \circ propionate; ∇ butyrate.

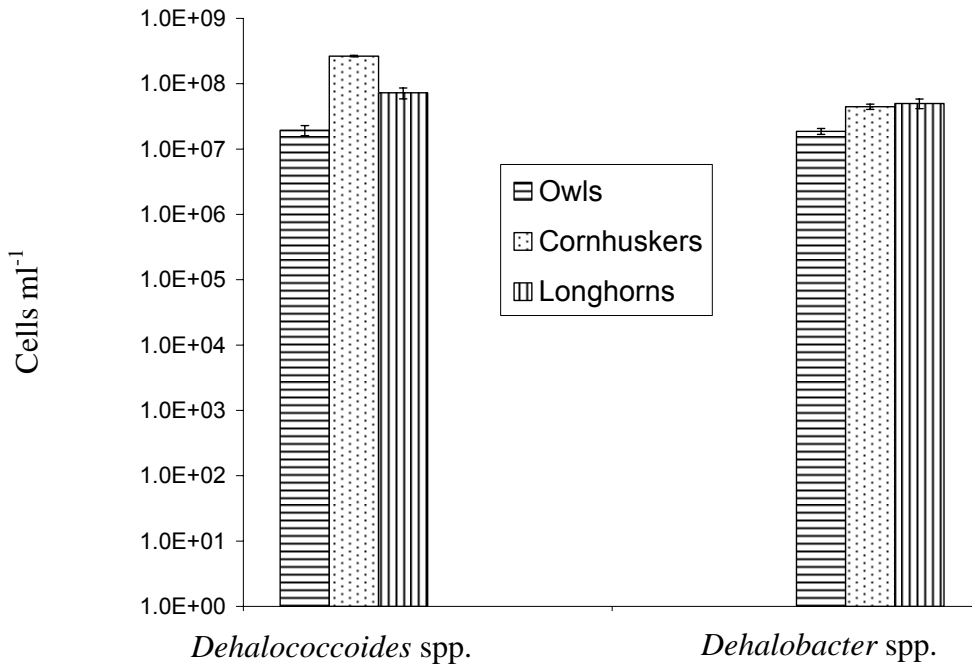


Figure 2-9. Quantification of *Dehalococcoides* spp. and *Dehalobacter* spp. in enrichment cultures using real time PCR.

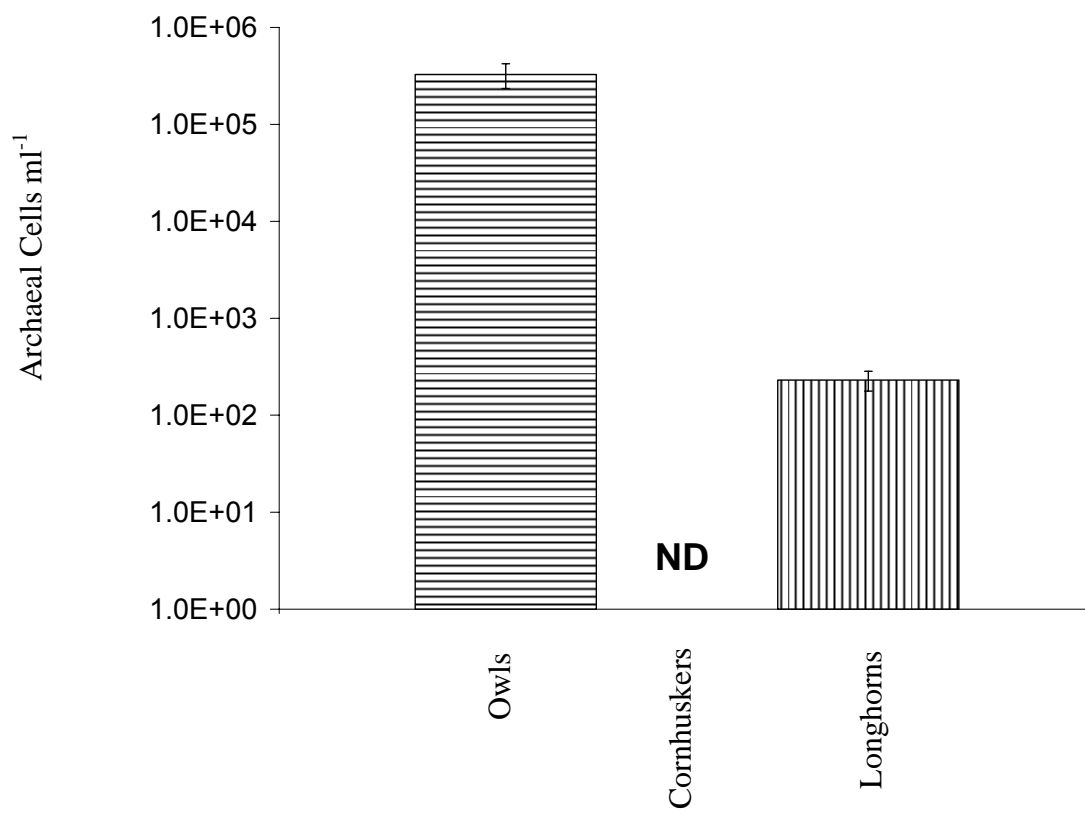


Figure 2-10. Quantification of Archaea in enrichment cultures using real time PCR. ND = not detected

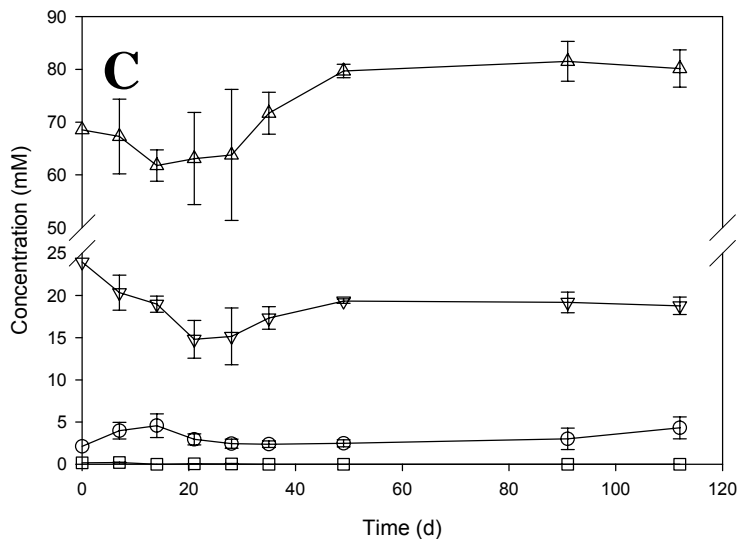
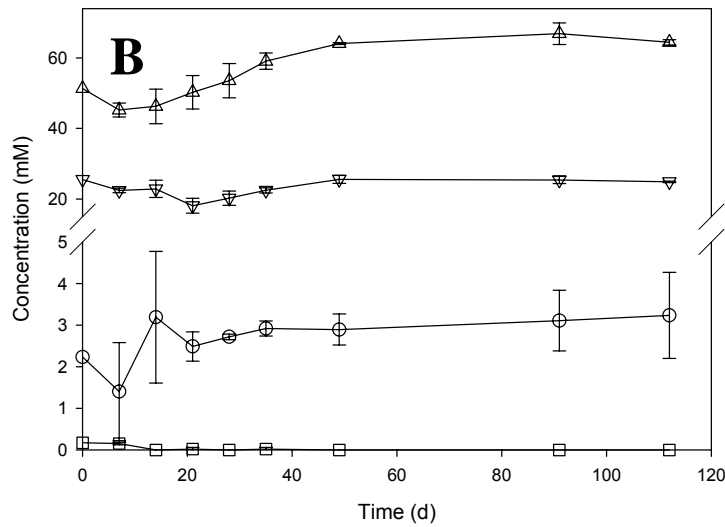
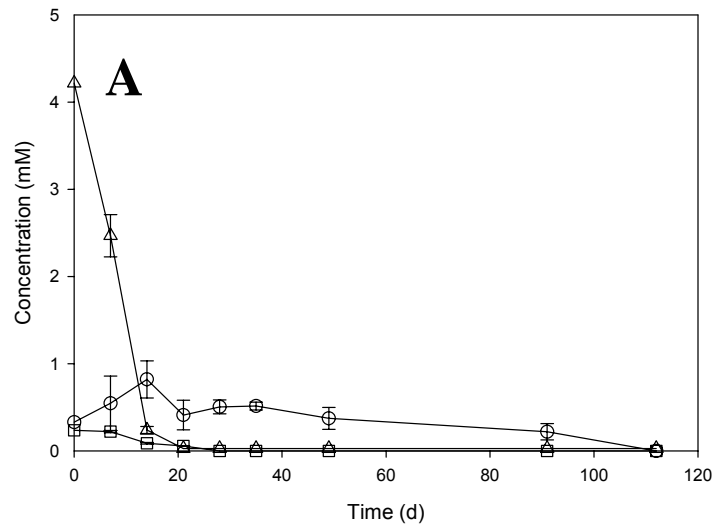


Figure 2-11. Culture specific volatile fatty acid production with 3 mM MeOH and no PCE: A) Owls culture, B) Cornhusker culture, and C) Longhorns culture. Symbols: \square formate; \triangle acetate; \circ propionate; ∇ butyrate. 49

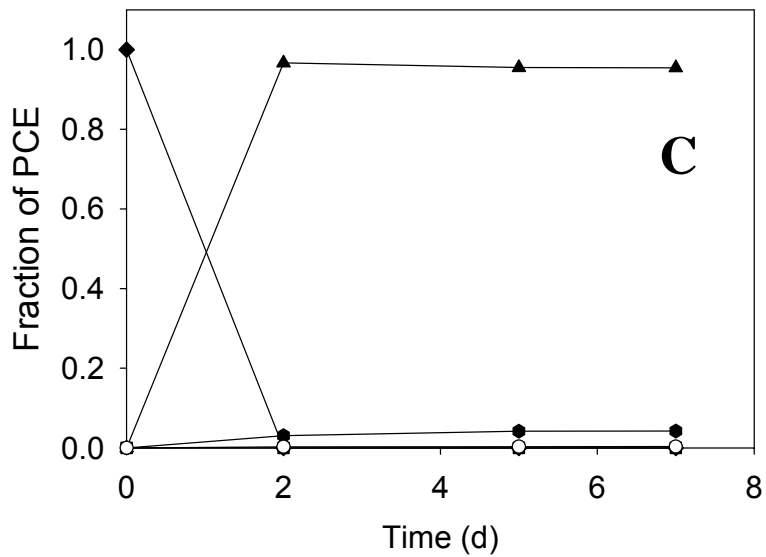
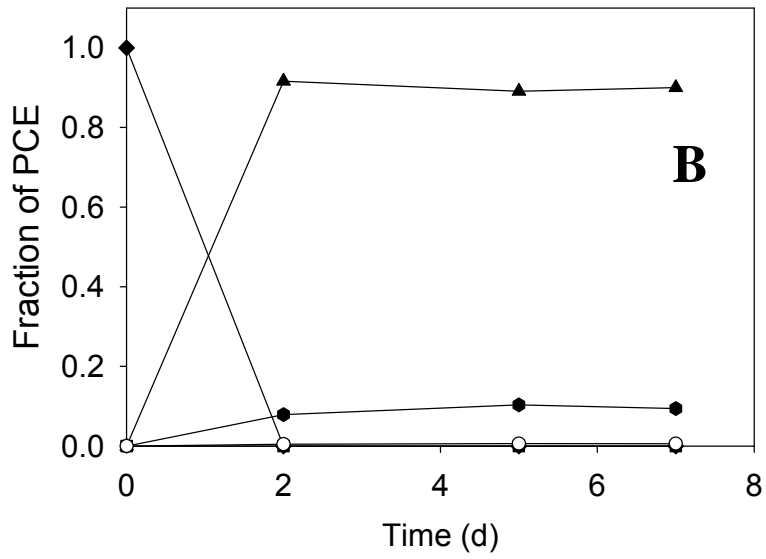
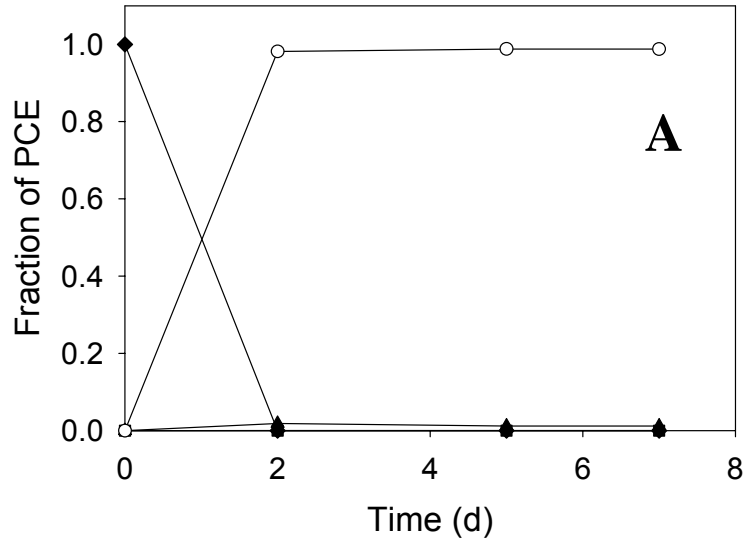


Figure 2-12. Owls culture A) positive control; B) 0.005% CS-330 and C) 0.01% CS-330. Symbols: ◆ PCE; ■ TCE; ▲ DCE; ● VC; ○ ETH.

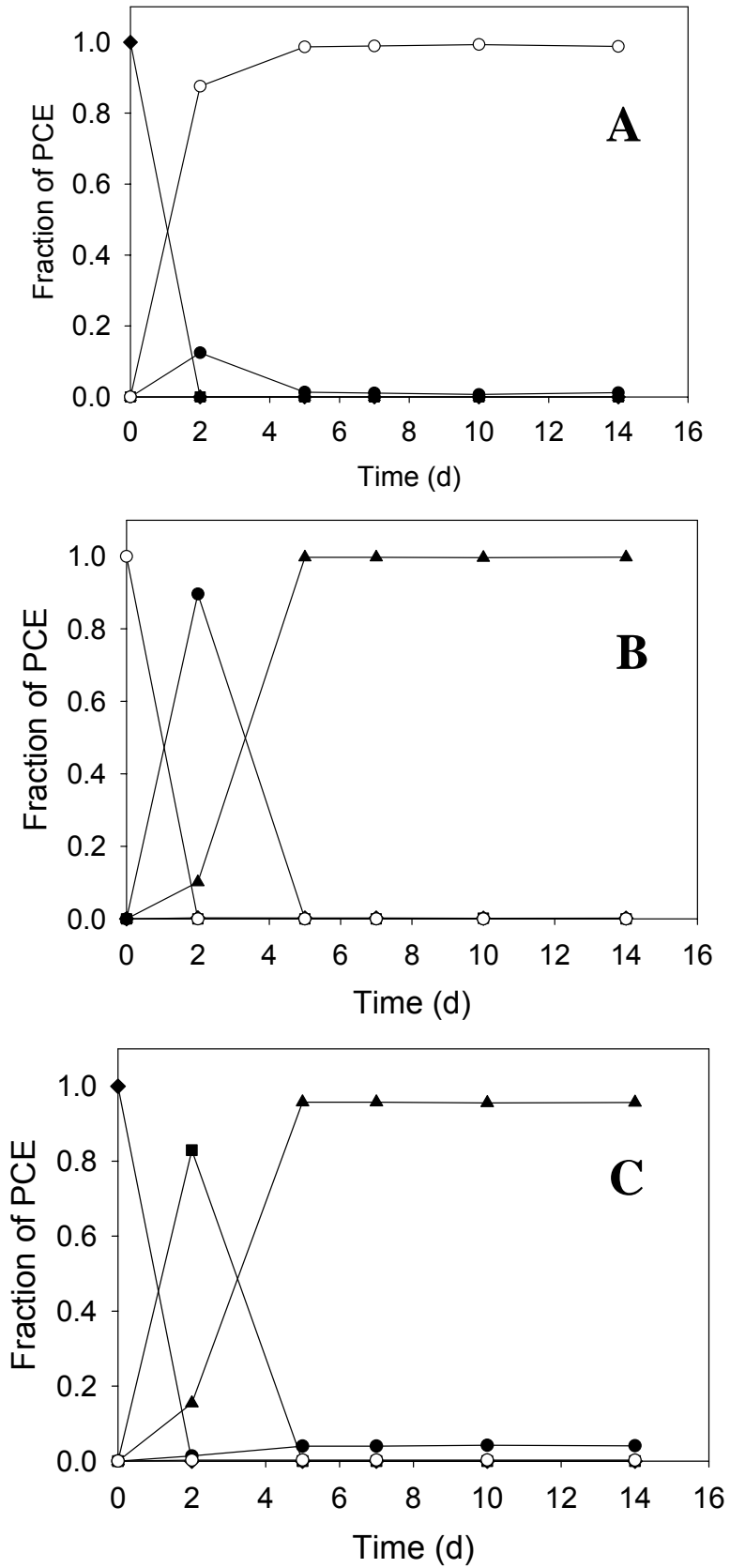


Figure 2-13. Cornhuskers culture A) positive control; B) 0.005% CS-330 and C) 0.01% CS-330. Symbols: ◆ PCE; ■ TCE; ▲ DCE₅₁; ● VC; ○ ETH.

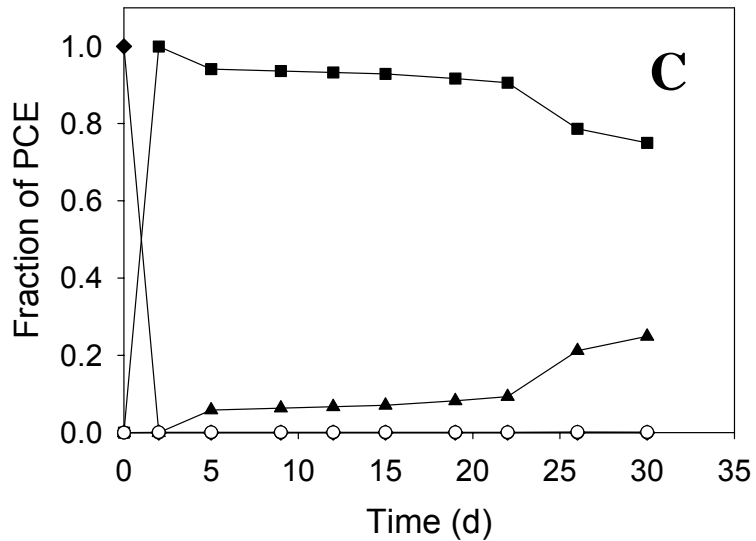
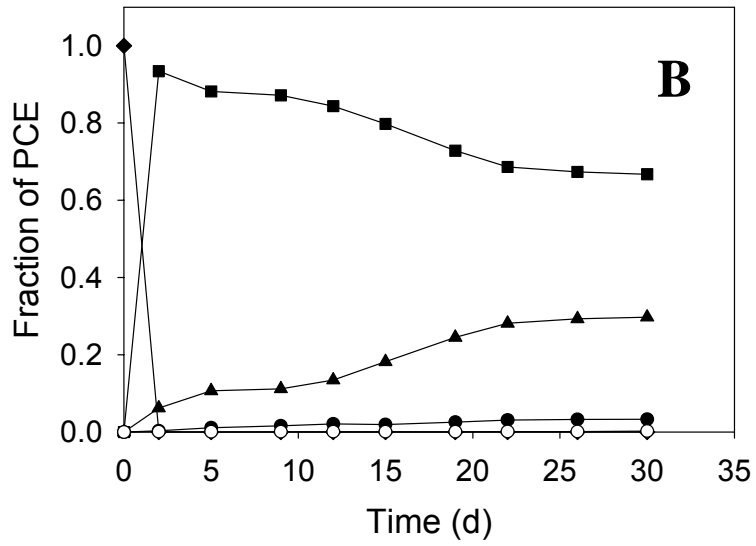
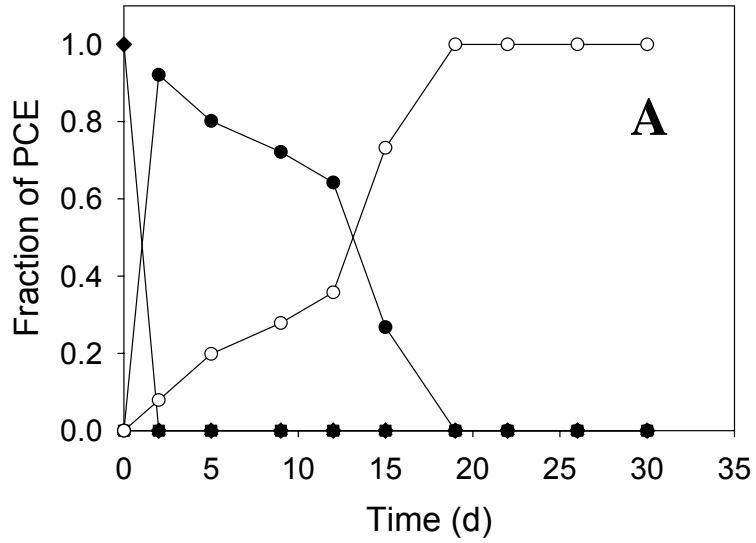


Figure 2-14. Longhorns culture A) positive control; B) 0.005% CS-330 and C) 0.01% CS-330. Symbols: ◆ PCE; ■ TCE; ▲ DCE, ● VC; ○ ETH.

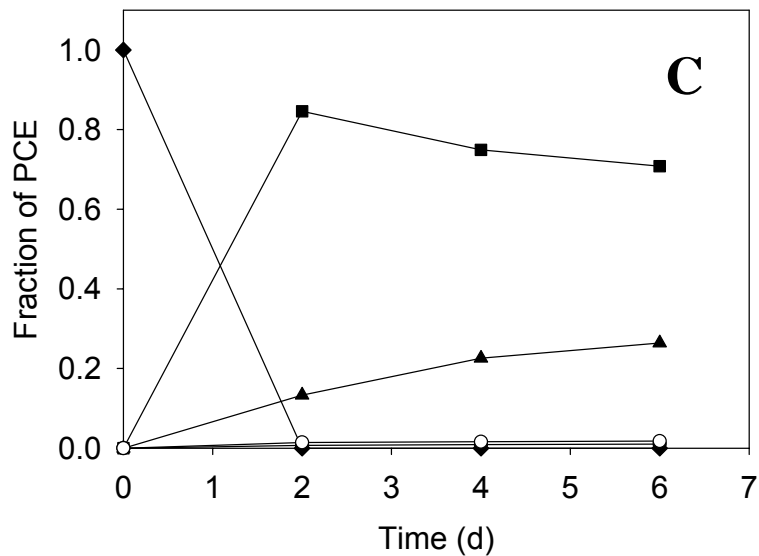
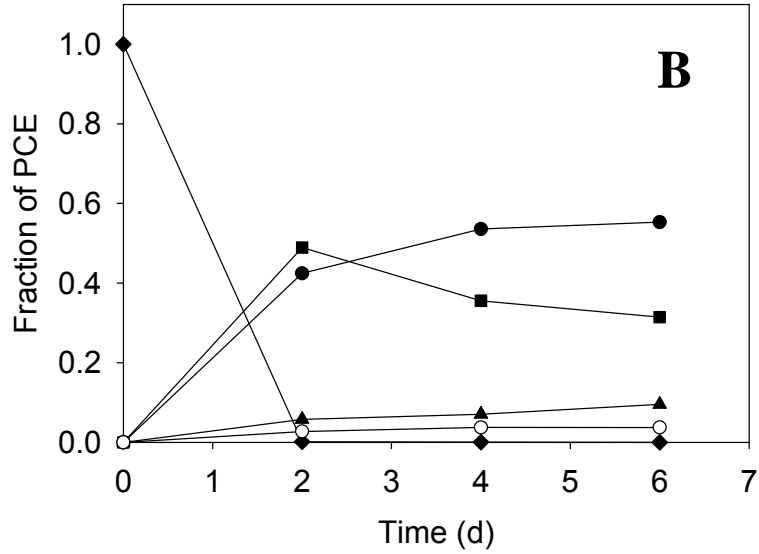
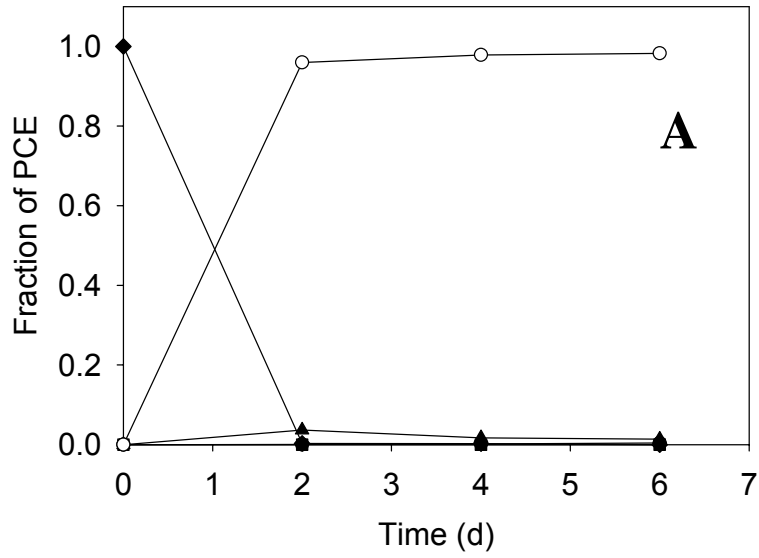


Figure 2-15. Owls culture A) positive control; B) 0.005% C13-4PO and C) 0.01% C13-4PO. Symbols: ◆ PCE; ■ TCE; ▲ DCE; ● VC; ○ ETH.

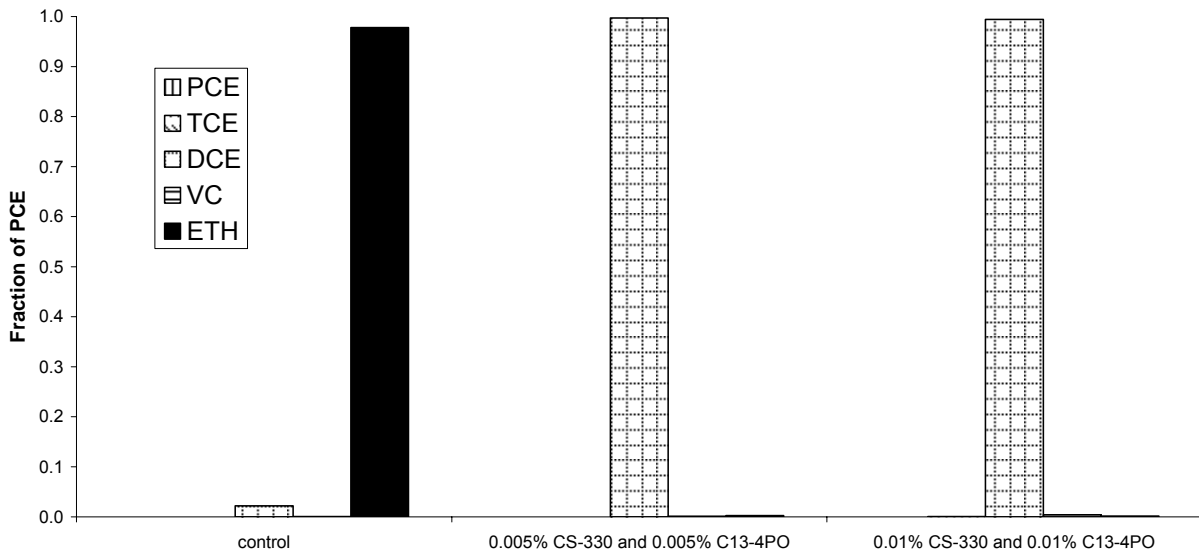


Figure 2-16. Effect of mixtures of CS-330 and C13-4PO with Owls Cultures. Data taken after 7 days of exposure.

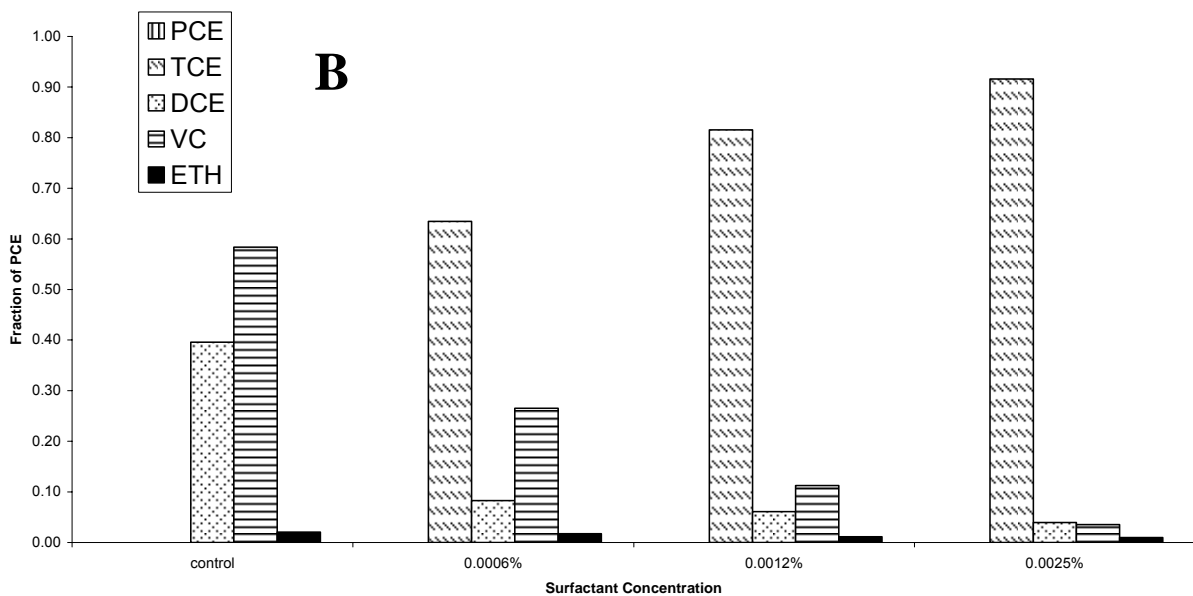
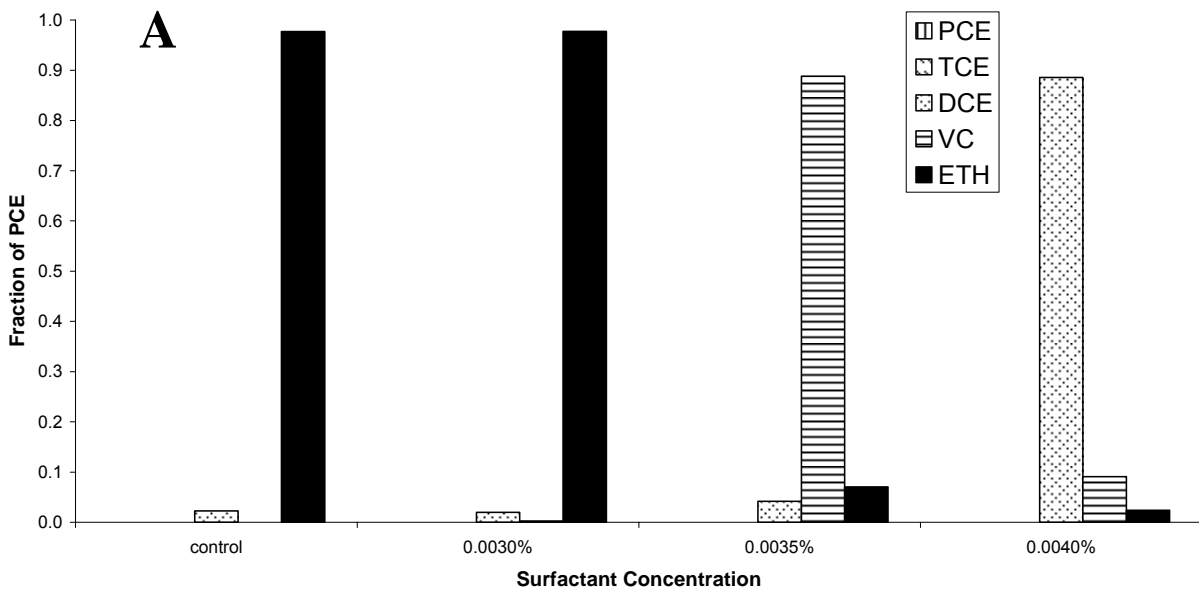


Figure 2-17. Determination of CS-330 concentration that has no effect on dechlorination. A) Owls culture; B) Cornhusker culture.

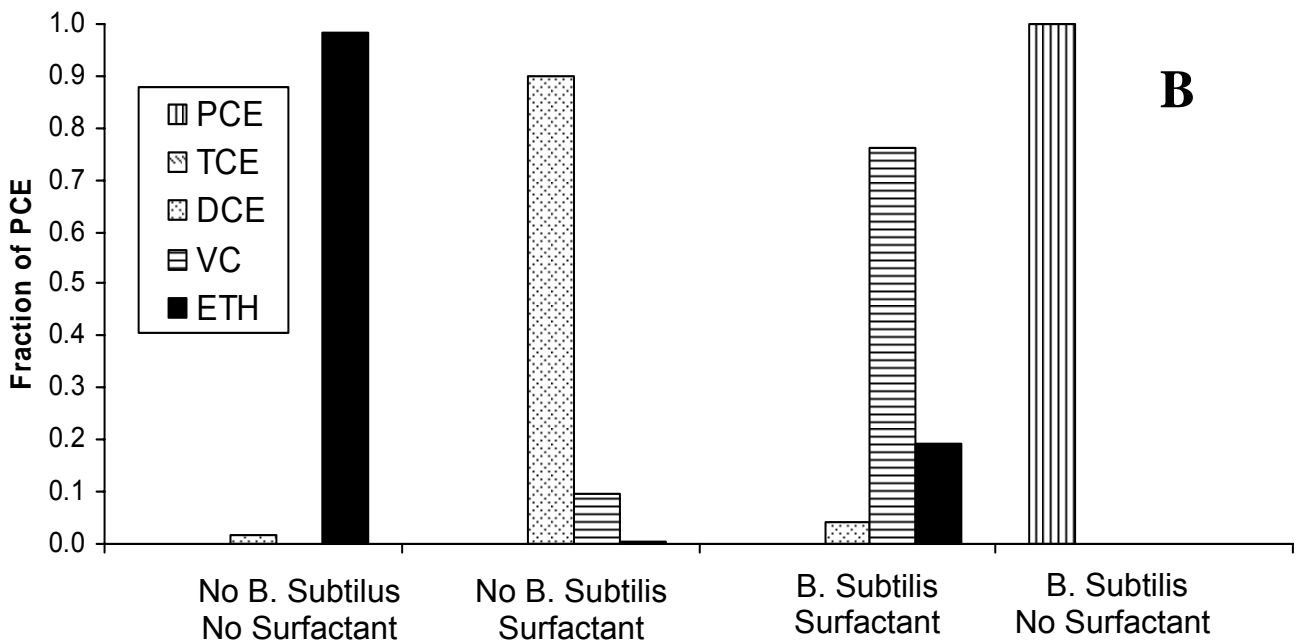
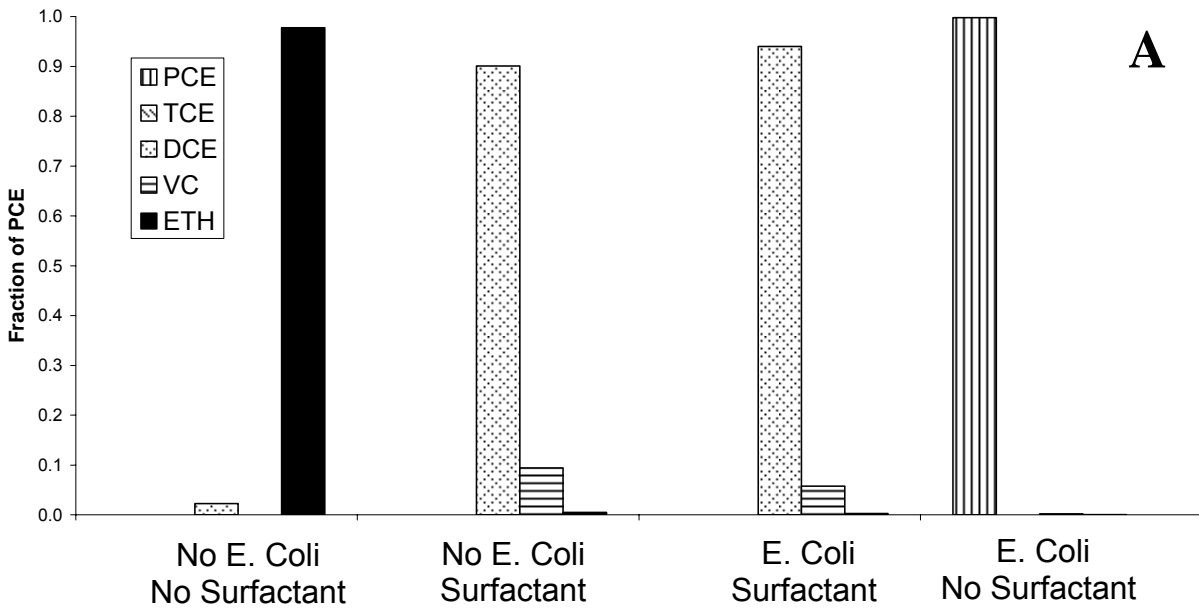


Figure 2-18. Effect on extent of dechlorination from adding (600 mg/L) gram negative A) *Escherichia coli* and gram positive B) *Bacillus subtilis* organisms with 0.005% CS-330.

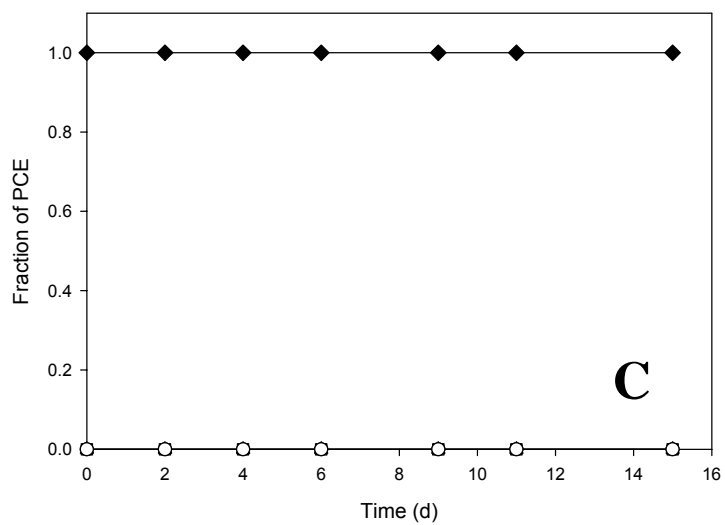
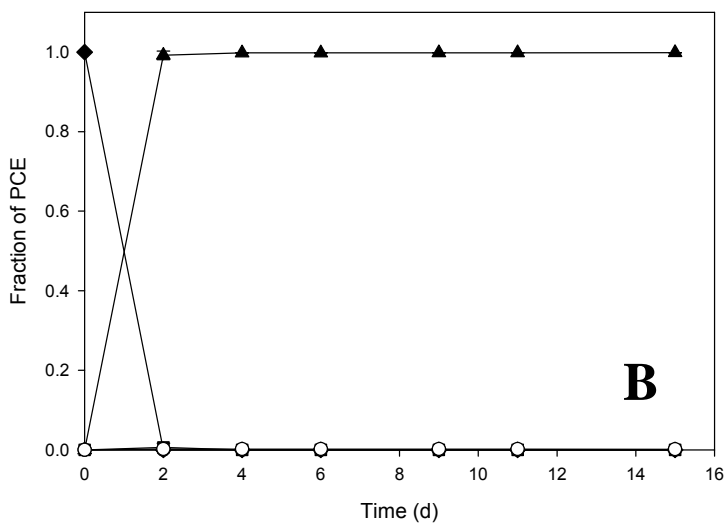
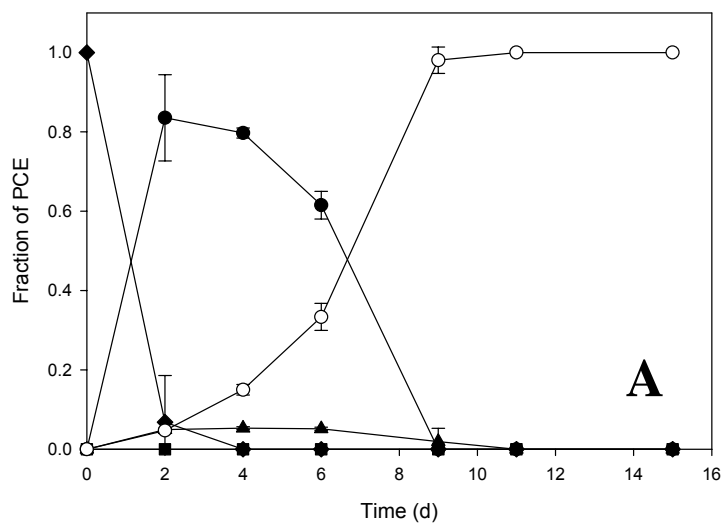


Figure 2-19. Owls culture exposed to A) no surfactant, PCE only; B) 0.01% CS-330, PCE and C) no surfactant, PCE and O₂. Symbols: ◆ PCE; ■ TCE; ▲ DCE; ● VC; ○ ETH.

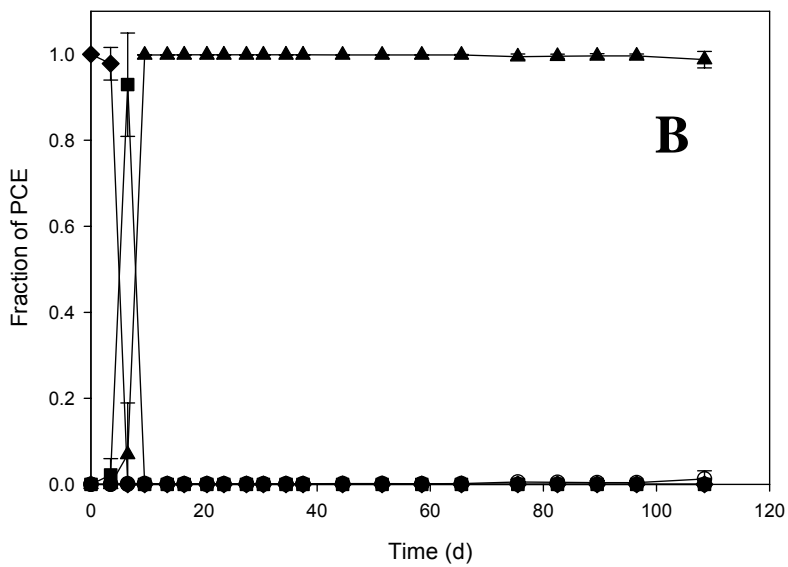
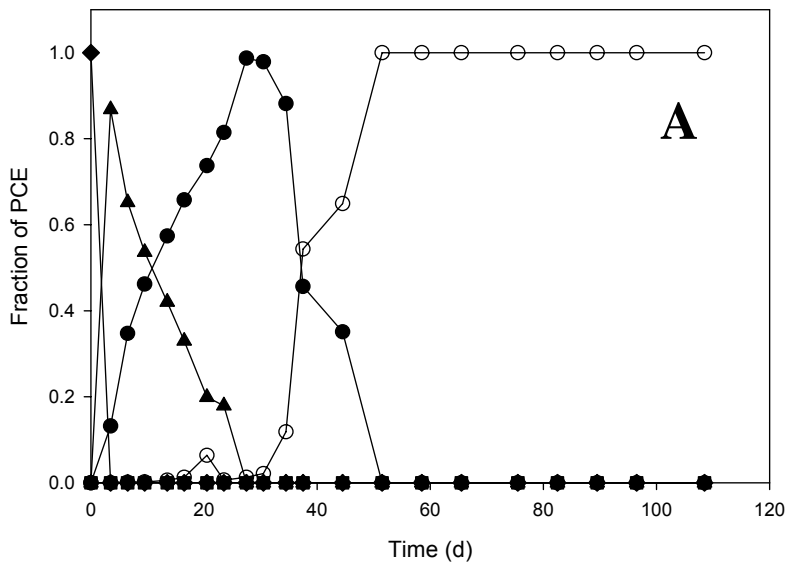


Figure 2-21. Resuspension of cells into fresh media from A) positive control and B) 0.01% CS-330. Symbols: ◆ PCE; ■ TCE; ▲ DCE; ● VC; ○ ETH.

Task 3 - Evaluation of the acceleration of reductive dechlorination due to solubilization of DNAPL into micelles.

Task 3 was not carried out because of the observation that complete dechlorination does not occur either in the presence of high concentrations of either surfactant or perchloroethene. Thus hydrogen biosparging of PCE DNAPL is not practical even if perfect contacting of the aquifer was possible. A better approach would be to first use surfactant with air-foam for mobility control to solubilize and displace the DNAPL to a very low saturation. Then foam assisted hydrogen biosparging can be used to remediate the low concentration of chlorinated solvents and degradation products that may remain after the surfactant flood.

Task 4 - Use sand columns and mechanistic models to quantify enhanced foam mobility in heterogeneous systems.

4. Lateral Contacting of Aquifer---2-Dimensional preliminary sandpack experiments for proof of concept

The purpose of 2-Dimensional sand-pack experiments is to demonstrate the effectiveness of foam in increasing the lateral transport of hydrogen across the aquifer. Also, comparisons between regular air foam and hydrogen foam were made using the results from this 2-D sand-pack.

4.1 Experimental

Two similarly-constructed flow models were used for the lateral contacting experiments. The first is a plastic-cased two-dimensional model that holds a 20"x3 $\frac{3}{4}$ "x $\frac{3}{4}$ " sandpack (the "plastic sandpack"). The pressure in this plastic sandpack is limited to about 6 psig. The second is a steel-cased two-dimensional model that holds a 20"x3 $\frac{1}{4}$ "x $\frac{3}{4}$ " sandpack (the "steel sandpack") which could operate at much higher pressures. Both models were obtained as gifts from Shell Oil Company (Houston, TX). The plastic model was constructed of $\frac{3}{4}$ "-thick clear PVC. It has three inlet/outlet ports at each end. A perforated plate and a 60-mesh screen were placed at the inside of each end to hold the sand in place and to distribute flow. The model is sealed with a Viton rubber sheet and metal piece at the top. Additionally, the model is clamped to prevent leakage.

The steel model was constructed of stainless steel with a 1 $\frac{1}{4}$ "-thick glass window in the front of the model that allows visual observations. It was previously used by Szafranski [1997] to demonstrate the effectiveness of the surfactant/foam process for aquifer remediation. Sand is packed in the interior of the model. Similar to the plastic model, the steel model has three inlet/outlet ports at each end. However, a pair of 200- and 60-mesh screens was placed over each port rather than throughout the entirety of each end. At the back of the

Dimension $3.8 \times 0.8 \times 21$ inch Permeability 120 darcy

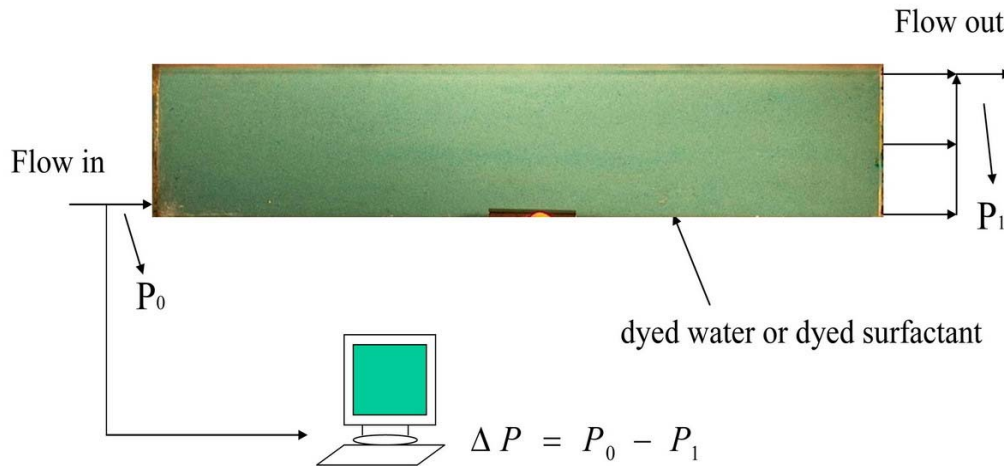


Figure 4-1 2-D sandpack experiment description

model, there are fifteen similarly-screened internal pressure ports that can also be used for fluid injection/sampling. The interior space above the sandpack was filled with plaster of Paris enfolded in polyethylene wrap (Saran Wrap) that acted as a non-permeable barrier. A Viton rubber sheet was placed on top of the plaster of Paris and the small air space between the rubber sheet and the top steel cover was pressurized with approximately 70 psig of overburden pressure.

The models were packed following the procedure developed by Szafranski [1997]. Clean silica sand obtained from U.S. Silica (Berkeley Springs, WV) was used for the packing. Most experiments were performed with the models packed homogeneously with coarse F-32 sand. The permeability of this sandpack was determined to be about 120 darcy. Although this is more permeable than typically encountered in an aquifer, the coarse sand was selected to enhance the effect of gravity in the laboratory-scale sandpicks. The porosity obtained with the packing procedure is usually around 40%, which was confirmed from the volume of water displaced during packing.

Some experiments were also performed with the steel model packed heterogeneously with two layers of sand: fine F-95 sand in the lower half and coarse F-32 sand in the upper half of the pack. The permeability contrast was estimated by injecting dyed solution into the heterogeneous sandpack. The ratio of the propagation velocities in the coarse and fine sands reflects the permeability ratio, and it was determined to be about 13. The upper layer had a permeability of about 130 darcy, and the lower layer about 10 darcy.

Preliminary experiments were performed in both the plastic and steel models. Figure 4-1 shows the layout of the 2-D sandpack experiments. Gas,

2-D Plastic Sandpack Experiments		Average gas saturation inside the sandpack	
		Air injection	Hydrogen injection
0.8~1.0 psi	1PV injected	69%	61%
	Re-inject fluid (After Steady State)	54%	40%
1.8~2.0 psi	1PV injected	77%	72%
	Re-inject fluid (After Steady State)	64%	56%

Surfactant solution: (0.5% CS-330 0.04%Mg 0.23%Na 0.069%Ca)

Table 4-1 Comparison air foam and hydrogen foam

either hydrogen or air, was hand-injected using a syringe while trying to maintain a specified target injection pressure. About 1/3 PV of gas was injected with each syringe, with a little down time between each injection. The injection pressure was measured using a transducer from Validyne (Northridge, CA) that was connected to the inlet port. Gas saturation in the sandpack was calculated at standard pressure from the volumes of gas injected and liquid produced. Small 1/16"-ID tubing was used for the flow lines outside the sandpack. Remaining gas saturation was measured by injecting liquid (either water or surfactant) following the end of gas injection until no more gas was produced in the effluent. The injection pressure during this liquid flush was maintained either at about or less than the injection pressure during gas injection.

4.2 Preliminary experiments

4.2.1 Comparison of regular air foam and hydrogen foam

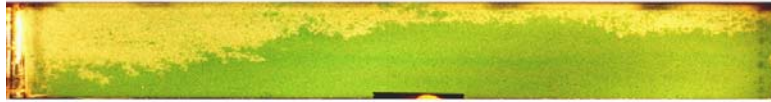
Hydrogen is explosive when mixed with air. It should be good for us to perform our experiments using regular air instead of hydrogen to avoid any possible dangers. But hydrogen has a smaller molecule size compared to regular air, so it is necessary for us to perform some experiments to investigate if there is any difference between regular air foam and hydrogen foam.

Two kinds of different injection pressure experiments were performed in the plastic sandpack. One is around 1 psig and the other one is about 2 psig. One pore volume (PV) of air or hydrogen is injected followed by liquid injection at the same injection pressure until steady state is obtained. The gas saturation inside the tank was calculated using material balance. The results of hydrogen and regular air are listed in Table 4-1. From Table 4-1 we can see for both of these two injection pressures, the average gas saturation difference between regular air foam and hydrogen foam is very small. For example, in the ~2 psig injection pressure case, for regular air foam, after 1PV air injected, the average

gas saturation inside the sandpank was about 77%. For hydrogen foam, this value was about 72%, which is very close to 77%. After liquid flush to steady state, in the regular air case, the remaining gas saturation in the sandpack was about 64% and in the hydrogen case, the remaining gas saturation was about 56%, which was also very close to 64%.

From these comparisons, we can see there is almost no difference between regular air foam and hydrogen foam. So in general, we can use regular air in our lab when performing our foam experiments. In this way, we can avoid the danger of explosion but obtain reliable results at the same time.

(A) Without surfactant, $S_g=33\%$

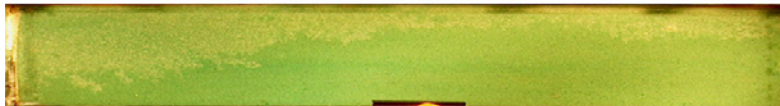


(B) With surfactant, $S_g = 73\%$



Gas Saturation after approximately 1 PV throughput at $\Delta p \sim 5\text{ psi}$

(A) Without surfactant, $S_g = 11\%$



(B) With surfactant, $S_g = 54\%$



Gas Saturation after liquid flush that followed hydrogen injection at
 $\Delta p \sim 5\text{ psi}$

Figure 4-2 Effect of foam on sweep and gas saturation

4.2.2 Proof of concept---- foam increased the lateral transport of gas

Figure 4-2 illustrates the effects of foam on increasing gas sweep and saturation in the sandpack. The experiment was performed under a constant injection pressure of about 5 psig. When 1 PV hydrogen was injected, the hydrogen saturation in the foam case was about 73% but in the no foam case it was only about 33%. The hydrogen saturation in the foam case is more than two times greater than in the no foam case. After liquid flush, in the foam case, there still remained about 54% gas in the sandpack, but in the no foam case, only 11% gas remained in the sand pack.

At this time the contrast in trapped hydrogen saturation is about a factor of 5. Also, without surfactant, only about 50% of the sand is contacted by hydrogen while with surfactant, about 90% of the sand is contacted.

(A) Without surfactant, $\overline{S}_g = 32\%$



(B) With surfactant, $\overline{S}_g = 79\%$



Gas Saturation after approximately 1 PV throughput at $\Delta p \sim 10\text{psi}$

(A) Without surfactant, $\overline{S}_g = 18\%$



(B) With surfactant, $\overline{S}_g = 63\%$



Figure 4-3 Gas Saturation after liquid flush that followed approximately 1 PV throughput at $\Delta p \sim 10\text{psi}$

A similar experiment was performed using a higher injection pressure of 10 psig. Figure 4-3 compares the experimental results without and with surfactant cases. After 1 PV of gas was injected into the sand pack, for the without surfactant case, gravity override was quite pronounced and very little of the base of the sandpack was swept by gas. With surfactant, the generated foam swept about 2/3 of the base of the sandpack. The average gas saturation S_g without surfactant was only 32%, as opposed to 79% with surfactant. Liquid was injected after 1 PV of hydrogen was injected in both cases. Without surfactant, the liquid flush reduced the gas saturation to $S_g = 18\%$. With surfactant, most of the gas remained immobilized and the average gas saturation was reduced only to $S_g = 63\%$.

The above preliminary experiments illustrated the benefit of in-situ generated foam in improving gas sweep. More of the sandpack was swept by gas and more of the gas remained in the sandpack after liquid flush in the presence of surfactant

(A) Without surfactant, $\bar{S}_g = 43\%$



(B) With surfactant, $\bar{S}_g = 60\%$



Gas Saturation after approximately 1 PV throughput at $\Delta p \sim 2 \text{ psi}$

(A) Without surfactant, $\bar{S}_g = 10\%$



(B) With surfactant, $\bar{S}_g = 36\%$



Figure 4-4 Gas Saturation after liquid flush that followed approximately 1 PV throughput at $\Delta p \sim 2 \text{ psi}$

4.2.3 Effect of pressure drop across sand pack

Several pairs of experiments were performed in different pressure, i.e. 2 psi, 8 psi and 10 psi. All these experiments were stopped after about 1 PV of gas was injected into the sand pack. Higher pressure drop may improve gas sweep both with and without surfactant. The improvement may be slight or unnoticeable in the absence of surfactant. In those above experiments, gas saturation at the end of the hydrogen injection in the surfactant-free cases was even slightly higher at $\Delta P \sim 2 \text{ psi}$ than at $\Delta P \sim 8 \text{ psi}$ (Figures 4-4 and 4-5). The higher gas saturation with the lower pressure drop is due most likely to experimental variations. Nevertheless, hydrogen reached more of the lower parts of the sandpack at the higher pressure drop. Improvement due to the higher pressure was more pronounced in experiments with surfactant (Comparing Figures 4-4 and 4-5). After 1 PV throughput, the average gas saturation was 75% at the higher pressure drop, compared to 60% at the lower pressure drop. Although the higher pressure drop led only to a 15 percentage-point increase in gas saturation, foam

(A) Without surfactant, $\bar{S}_g = 34\%$



(B) With surfactant, $\bar{S}_g = 75\%$



Gas Saturation after approximately 1 PV throughput at $\Delta p \sim 8\text{psi}$

(A) Without surfactant, $\bar{S}_g = 12\%$



(B) With surfactant, $\bar{S}_g = 73\%$

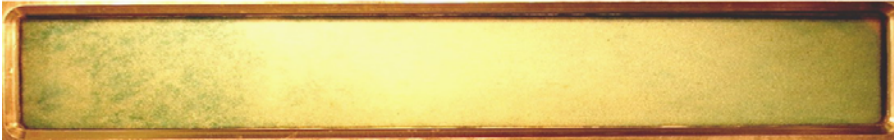


Figure 4-5 Gas Saturation after approximately 1 PV throughput at $\Delta p \sim 8\text{psi}$

generated at the higher pressure drop was much stronger. This is evident from the fact that most of the foam generated at the higher pressure drop remained immobile during liquid flush. An average gas saturation of 73% remained in the sandpack for the foam generated at $\Delta P \sim 8\text{ psi}$, compared to 36% at $\Delta P \sim 2\text{ psi}$.

The presence of strong foam in the $\Delta P \sim 8\text{ psi}$ experiment was also evident from the propagation profiles illustrated in Figure 4-6. Hydrogen traveled in a piston-like displacement front until about 1/3 PV throughput (Figure 4-6.A), indicating very strong, low-mobility foam. The piston-like front remained at 2/3PV throughput (Figure 4-6.B). A gas-override front, however, developed ahead of the piston-like front as some of the foam had broken, allowing weaker, more-mobile foam to flow ahead of the strong foam. Nevertheless, the whole sandpack was swept at 1 PV throughput (Figure 4-6.C), indicating a nearly 100% sweep efficiency.

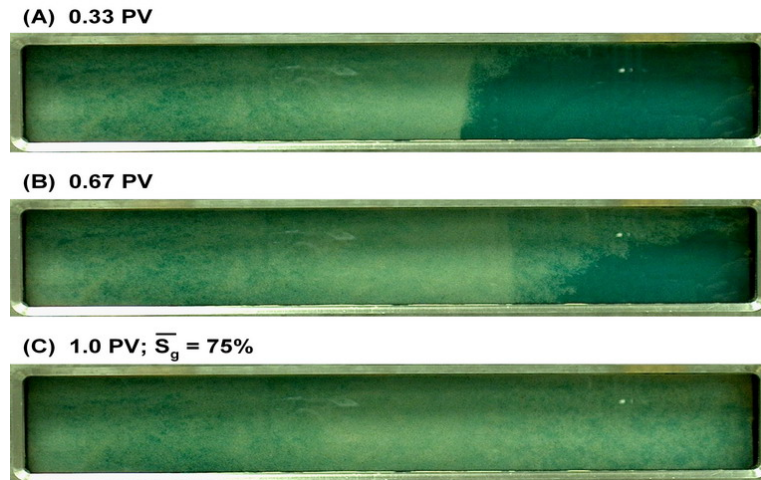


Figure 4.6 Gas Saturation profile of the homogeneous sandpack at $\Delta p \sim 8 \text{ psi}$

The piston-like front observed with $\Delta P \sim 8 \text{ psi}$ indicated the generation of very-strong, low-mobility foam. This behavior was not observed in the experiment with $\Delta P \sim 2 \text{ psi}$.

High pressure drop is indeed a necessary condition for the generation of strong foam. Ransohoff and Radke [1989] found the existence of a critical pressure drop for the generation of strong foam. Below this critical pressure drop, only weak foam with relatively high mobility could be generated. Tanzil [2001] confirmed the existence of the critical pressure drop and determined the necessary pressure drop for the generation of strong foam in 1-ft-long one-dimensional sandpacks. We will have more discuss on how the critical pressure drop scales with sandpack length and other dimensions in Section D of this report.

4.2.4 Experiments in heterogeneous sandpack

The heterogeneous sandpack configuration presents a greater challenge for gas sweep efficiency. This is especially true with the more permeable layer at the top of the sandpack. Most of the injected gas flows in this thief zone, especially in the absence of foam. Two pairs of experiments were performed in the heterogeneous sandpack, each pair consisting of experiments with and without surfactant. These experiments are preliminary, following the same procedure used for the preliminary experiments in the homogeneous sandpacks. The first pair of experiments in the heterogeneous sandpack was performed with a target injection pressure of 2 psig. The second pair was performed with a higher target injection pressure of 10 psig. Air was used as the injected gas. Even at the lower injection pressure, the benefit of foam was apparent. Figure 4-7 compares the propagation profiles after 1 PV of air was injected with the 2-psig target injection pressure. Without surfactant (Figure 4.7.A), most of the gas

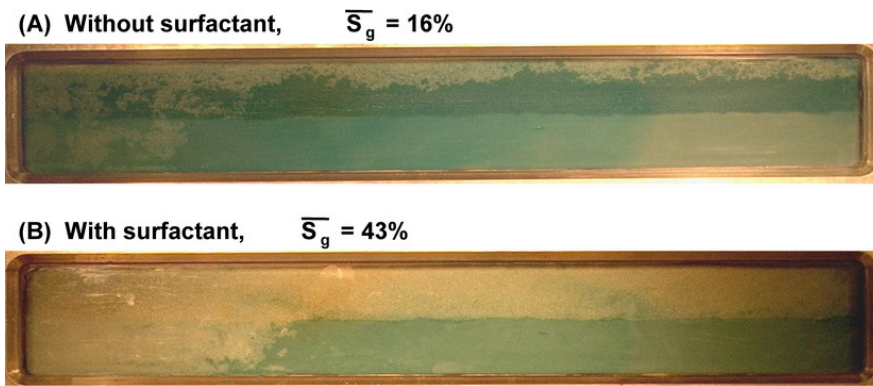


Figure 4.7 Gas Saturation after approximately 1PV air injected at $\Delta p \sim 2\text{ psi}$

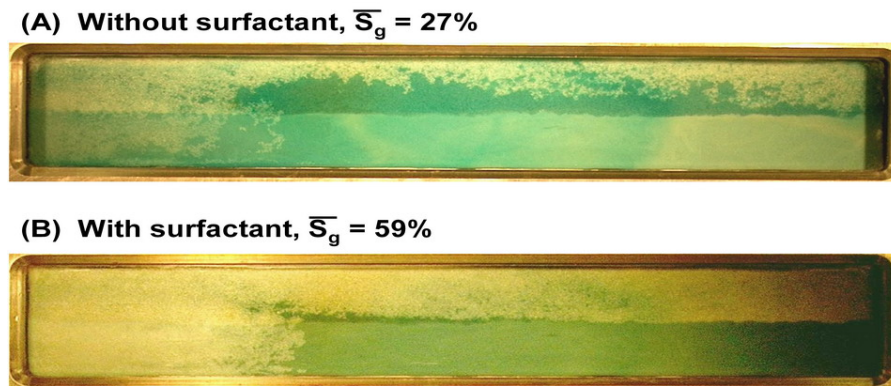


Figure 4.8 Gas Saturation after approximately 1PV air injected at $\Delta p \sim 10\text{ psi}$

flowed along the top of the sandpack in the high-permeability layer. The average gas saturation S_g at 1 PV with no surfactant was only 16%. With surfactant (Figure 4.7.B), more gas entered both layers and S_g was considerably higher, at 43%.

At the higher injection pressure, gas sweep was improved for both without and with surfactant. Figure 4.8 displays photographs of the sandpack taken after 1 PV of air was injected at 10-psig target injection pressure. Without surfactant, S_g reached 27%. With surfactant, S_g reached 59%. The benefit of foam was more apparent after about 10 PV of air was injected in both cases (Figure 4.9). Without surfactant, gas flowed mostly in the upper high-permeability region and only about $\frac{1}{4}$ of the low-permeability layer was swept by gas.

In contrast, gas swept the entire sandpack in the surfactant case. Average gas saturation at about 10 PV was $S_g = 48\%$ when without surfactant, and $S_g = 98\%$ when with surfactant.

(A) Without surfactant, $\bar{S}_g = 48\%$



(B) With surfactant, $\bar{S}_g = 98\%$



Figure 4-9 Gas Saturation after approximately 10PV air injected at $\Delta p \sim 10\text{psi}$

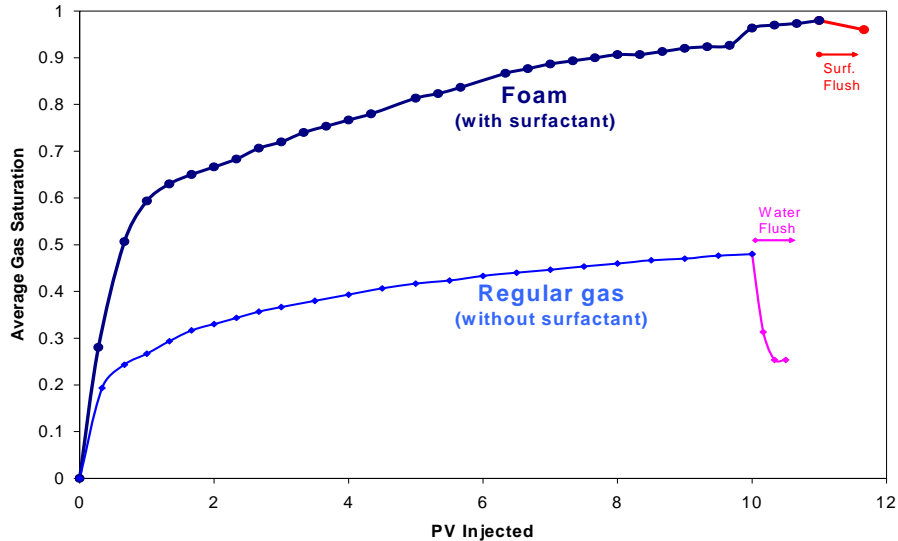


Figure 4-10 Gas saturation in the heterogeneous sandpack with air injected at a target injection pressure of 10 psi.

Figure 4-10 plots the gas saturation history for the 10-psig experiments in the heterogeneous sandpack. The benefit of foam was also very apparent after liquid (either water or surfactant solution) was injected following the end of gas injection. Without surfactant, S_g dropped from 48% to about 20% as the injected water mobilized most of the gas. With surfactant, however, very small fraction of the gas was mobilized when the surfactant solution was injected and S_g remained above 90%.

4.3 Summary of Section 4

Surfactant screening experiments were performed using 1-D sand column. The foam abilities of some surfactants were tested. Among these surfactants, we found that the mixture of C13-4PO and CS330 (1:1) has the strongest foam ability with the presence of the nutrition solution. Also, since the surfactant concentration cannot be too high and inhibit the biodegradation process, we will choose the total concentration of surfactant solution to be 0.1%(wt) in our 3-D experiments.

Some preliminary 2-D foam experiments were performed. Foam was proved to be able to increase both the gas sweep and the average gas saturation in the sand pack, either homogeneous or heterogeneous. Injection pressure can affect the experimental results. In our 2-D sand pack experiments, higher sweep efficiency and gas saturation can be obtained under higher injection pressure.

Task 5 - Validation of foam enhancement of reductive dechlorination by hydrogen sparging in a bench scale three-dimensional sand pack model.

According to some experimental results from Tanzil, foam strength declines with the flow dimension increases, i.e. 1-D foam is stronger than 2-D and 2-D foam is stronger than 3-D. So although we performed some preliminary 2-D experiments which proved the enhancement of foam on gas sweep and trapped gas saturation, it is necessary for us to perform some foam experiments in 3 dimensional experimental equipments to verify the effect of foam. Also, to build a foam simulation model to simulate 3-D foam flow, the 3-D foam experiments are indispensable because nobody else did this kind of experiments before.

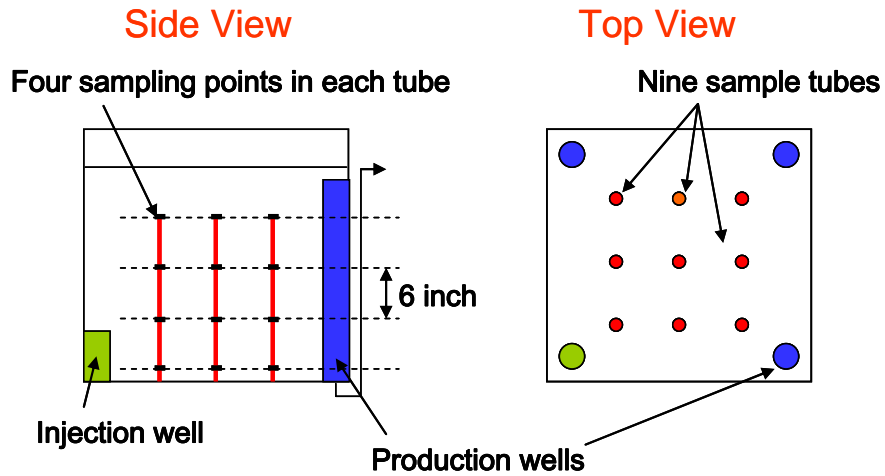
5.1 2x2x2 ft 3-D sand tank experiments

5.1.1 3-D tank set up and experimental procedures

A 3-D sandpack was designed and constructed for the 3-Dimensional foam experiments. Figure.5-1 shows an overlook of the tank. The tank is set on a wood table frame. It has glass walls for its four sides. Steel frame is used in the corners and edges to make the tank strong enough to hold the experimental pressure. The actual scale of the tank is 2ftx2ftx2.5ft with a height 2.5ft. But we still call it '2x2x2 ft tank' because the extra 0.5 ft in its height was not packed by sand in our 3-D experiments. The term '2x2x2 ft' here only means the porous media size inside the tank.



Figure. 5-1 An overlook of the 3-D tank (before sand packing)



A snapshot of the injection well and some sampling tubes

Figure 5-2 Sketches of the side and top views of the tank

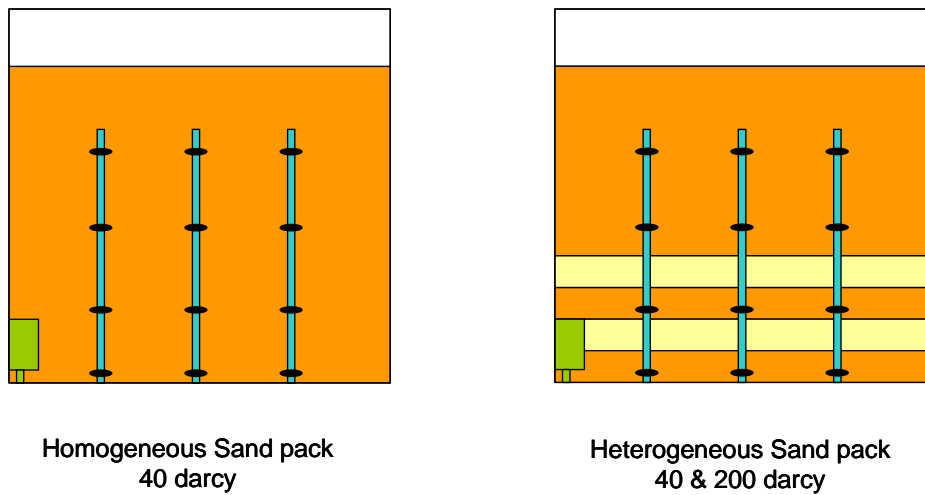


Figure 5-3 Homogeneous and Heterogeneous sand pack

There are nine sampling tubes and four injection/production wells in the tank. Figure 5-2 gives the sketches of the side and top views of the sand tank. The sampling tubes are placed in lines and in each line, they are 0.5 ft far from

each other. The distance from line to line is also 0.5 ft. These tubes are made by ¼" inch stainless steel tube. In each of these sampling tubes, there are four sample openings. The heights of these openings are 0, 0.5, 1 and 1.5 ft from the bottom of the tank. Four individual plastic tubing connect these openings to the outside of the tank. During experiments, these sampling tubes can be used to get the information such as gas distribution, surfactant distribution inside the tank.

The tank has one injection well, three production wells as shown in Figure 5-3. These wells are made by perforated PVC tubes. The diameter of these tubes is 1.75 inch. To keep sands out of these wells, these tubes are wined by 200 mesh stainless steel screen. The injection well is 3.5 inch high and the other three production wells are 2 ft high from the bottom. All these production wells have their outlets at the bottom of the tank but use a ¼" inch stainless steel tube to make the flow outlet to be at the same level as the height of the sand pack. This is just to keep the pressure potential inside these production wells to be a constant and simulate an unconfined aquifer. Figure 5-2 also gives a snapshot of the injection well and several sampling tubes.

A 150 mesh screen and a ~200 lbs overburden are put on the top of the sand pack, which is to keep the sand from flowing upwards during gas injection at high pressure. The ~200 lbs overburden can increase the maximum possible injection pressure of the sand pack without fluidize the sand.

Two different sand pack formats were used. The sand used was from U.S. Silica. Figure 5-3 shows a drawing of these two different formats. One is a homogeneous sand pack using F-42 sand which has a permeability of about 40 darcy. The other one is a heterogeneous sand pack. In this heterogeneous pack, two layers of high perm sand (200 darcy) were packed in the lower part of the tank. Both of these two layers are 2.5 inch thick. One is 2.5 inch and the other one is 7.5 inch high from the bottom of the tank. The rest part of the tank is packed by 40 darcy sand.

Figure 5-4 shows the experimental procedure for these 3-D tank experiments. A pressure transducer was connected to the injection line to measure the injection pressure. A water monometer was installed at the injection line to monitor the air injection pressure. This monometer can hold 2 psig pressure. When injection pressure exceeds 2 psig, water will be blow out to avoid fluidizing the sand in the tank. Two air flow controller were installed in the injection line. The flow rate range of them are 0.1~10LPM and 1~100LPM. A three way valve was installed in the injection line which can switch between these two controllers during the experiments to get desired flow rate. Three pressure transducers were installed along the diagonal cross section of the tank. The height of the measure point is 0.5 foot from the bottom of the tank. P1, P2 and P3 of Figure 5-4 indicate the location of these transducers.

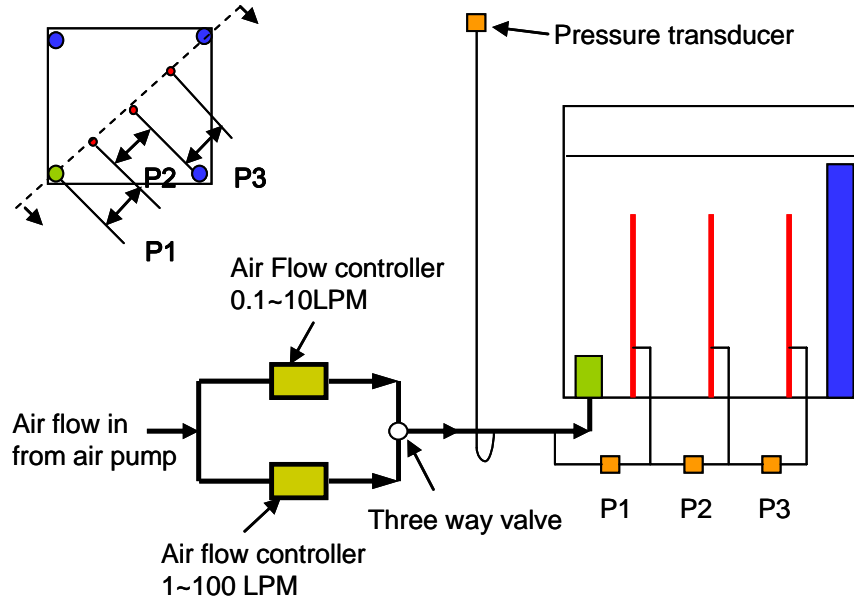


Figure 5-4 Experimental outlines of the 3-D tank

Both air/water and foam experiments were performed in the sand tank. Tank was filled with surfactant free water or surfactant solution before any of these experiments. Just as we discussed in Section A, the surfactants solution was a 1:1 mixture of: 0.05%(wt)CS-330 and 0.05%(wt)C13-4PO. Nutrition salts were also added into the solution, their concentrations were: 0.04%(wt)Mg, 0.23%(wt)Na, 0.069%(wt)Ca.

Air was injected into the tank either continuously or intermittently. In most of our experiments, we kept the injection pressure to be a constant by adjusting the air injection flow rate.

5.1.2 Homogeneous sand pack experimental results

Though homogeneous sand formation is not natural, it is necessary for us to start from a homogeneous system to investigate the 3-D flow properties of foam. In a homogeneous system, the snap-off foam generation mechanism, which mainly happens when there is a permeability contrast of more than 4, is not the main mechanism to generation foam. Instead, lamella division is the basic foam generation mechanism in a homogeneous porous media.

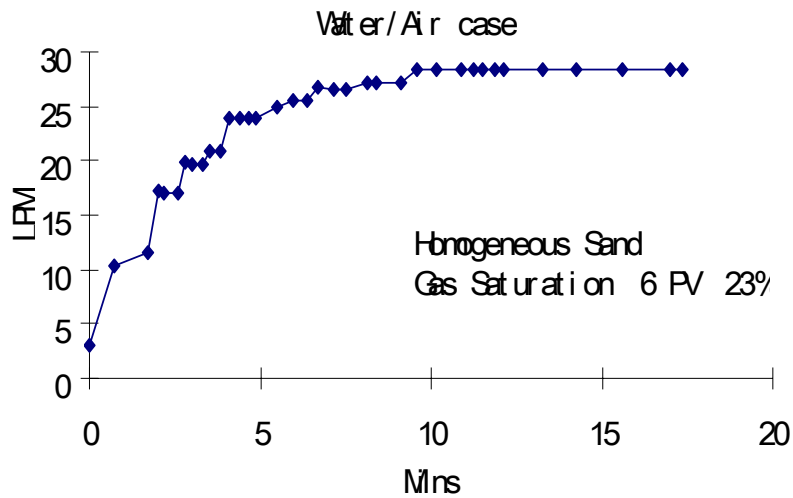


**Figure 5-5 Air/Water homogeneous sand tank, injection rate
Constant injection pressure ~0.8 psi, 6 PV gas injected**

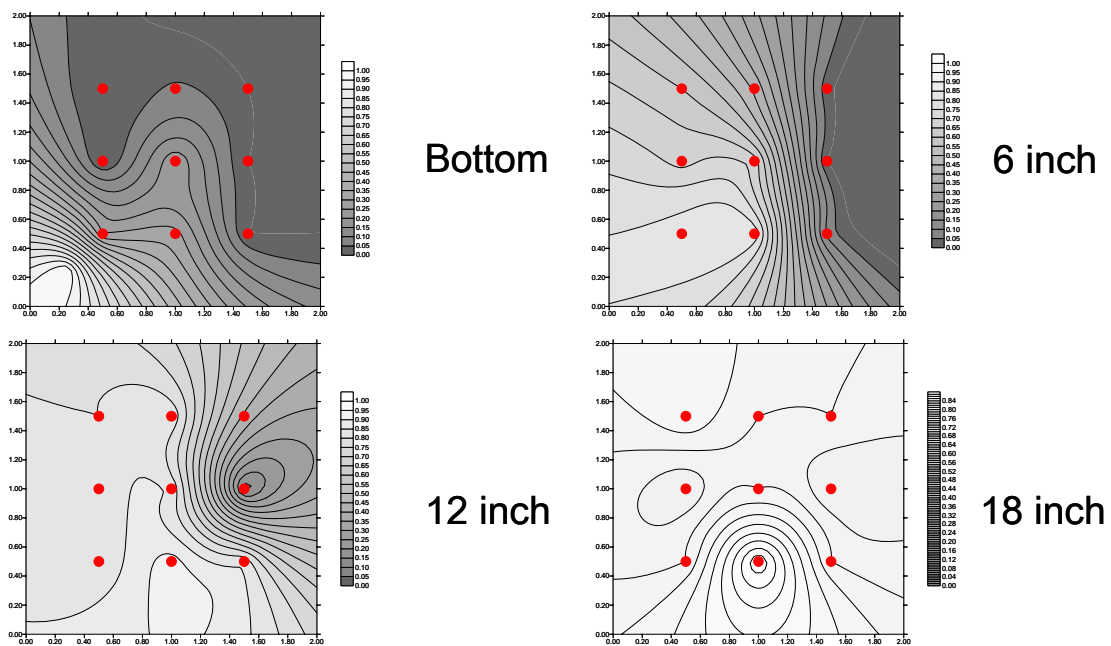


**Figure 5-6 Air/Water homogeneous sand tank results
Constant injection pressure ~0.8 psi, 6 PV gas injected**

5.1.2.1 Comparison of air/water and foam experimental results

Before a foam experiment was performed, an air/water experiment was performed in the sand tank. The air/water experiment was performed in a constant injection pressure ~0.8 psig over hydrostatic pressure. Figure 5-5 plots the figure of gas injection time vs. gas injection rate for the air/water experiment.

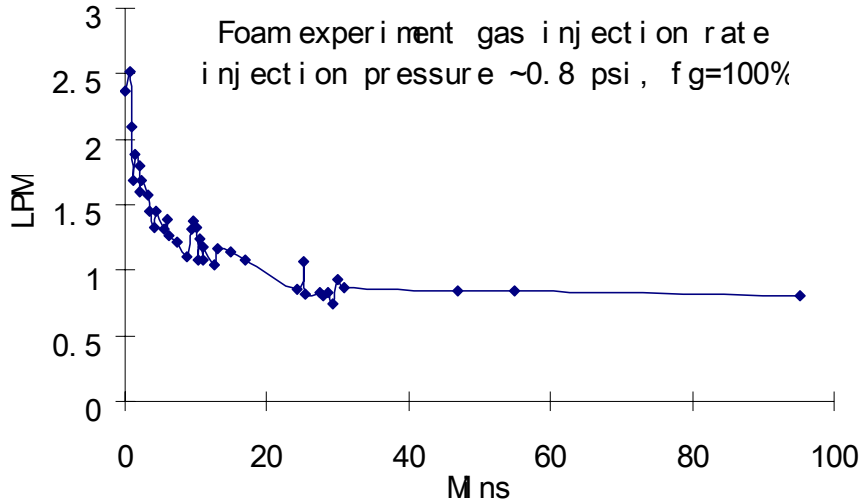


**Figure 5-7 Foam, homogeneous sand tank, injection rate
Constant injection pressure ~0.8 psi, 1 PV gas injected**

From the curve we can see after about 7 minutes' injection, the injection rate reached a steady state. At steady state, the injection rate was about 28 LPM (Liter Per Minute). The total injection time was about 17 minutes and about 6 PV air was injected into the tank in this period. By measuring the produced water volume, we calculated the total gas saturation in the tank at the end of the experiment, which was about 23%.

Figure 5-6 shows the gas fractional flow contour plots after ~6 PV gas injected. The red dots in these figures represent the sampling ports in the tank. Gas fractional flow plots for the four sampling layers are plotted. Each corresponds to 0.05, 0.5, 1, 1.5 foot from the bottom of the tank. From these plots we can see gas contacted about half of the tank at the bottom layer (0.05 foot from bottom). In the layer of 0.5 foot from the bottom, gas contacted about 80% of the tank. For the upper two layers (1 and 1.5 foot from bottom), gas contacted almost all the sample layer.

A foam experiment was performed using the same injection pressure as in the air/water experiment. Figure 5-7 shows the curve of the gas injection rate vs. gas injection time. After about 25 minutes' injection, the injection rate reached a steady state. At steady state, it was around 0.8 LPM. The total injection time for 1 PV gas was about 80 minutes. After 1 PV gas injected, the total gas saturation in the tank was about 66%.

From the sample tubes we obtained the gas fraction flow information in the sand tank. Figure 5-8.A shows the contour plots after 0.37 PV gas injected. By that time, gas contacted about 1/2 of the tank in the lower three sampling layers (0.05, 0.5, 1 foot from the bottom). For the layer of 1.5 foot from the

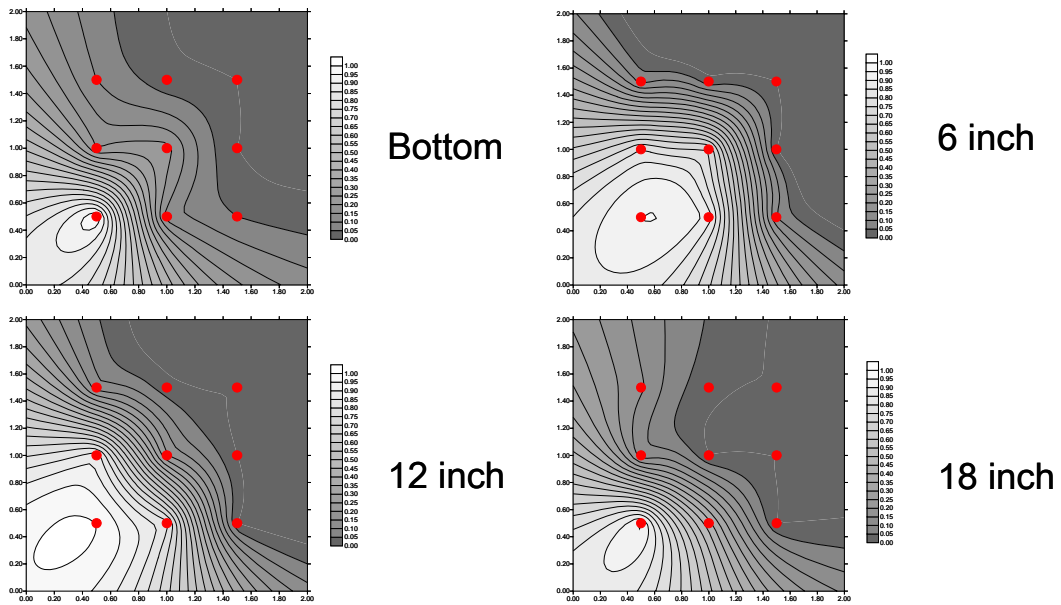


**Figure 5-8.A Foam, Homogeneous sand tank, gas fraction flow contour plot
Constant injection pressure ~ 0.8 psi, ~ 0.37 PV gas injected**

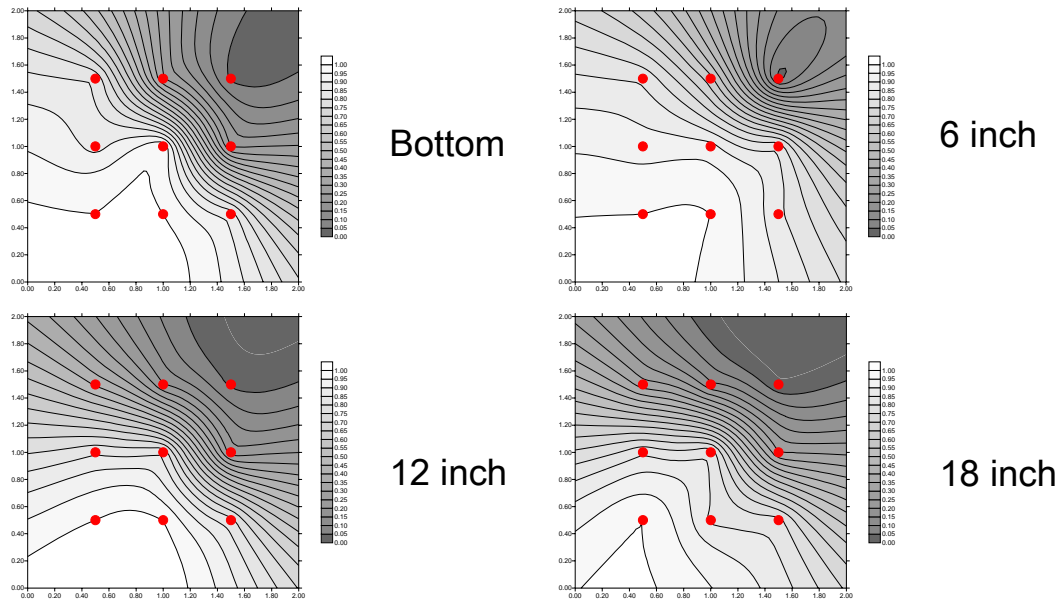


**Figure 5-8.B Foam, Homogeneous sand tank, gas fraction flow contour plot
Constant injection pressure ~ 0.8 psi, ~ 1 PV gas injected**

bottom, gas contacted only about 1/3 of it. Figure 5-8.B shows the results after about 1PV gas injected, gas contacted more than about 4/5 area of the tank in the lower three sampling layers. At the top layer (1.5 feet from the bottom), gas contacted about 2/3 area of it. This phenomena shows that more gas was conducted horizontally than vertically in the tank during the foam injection.

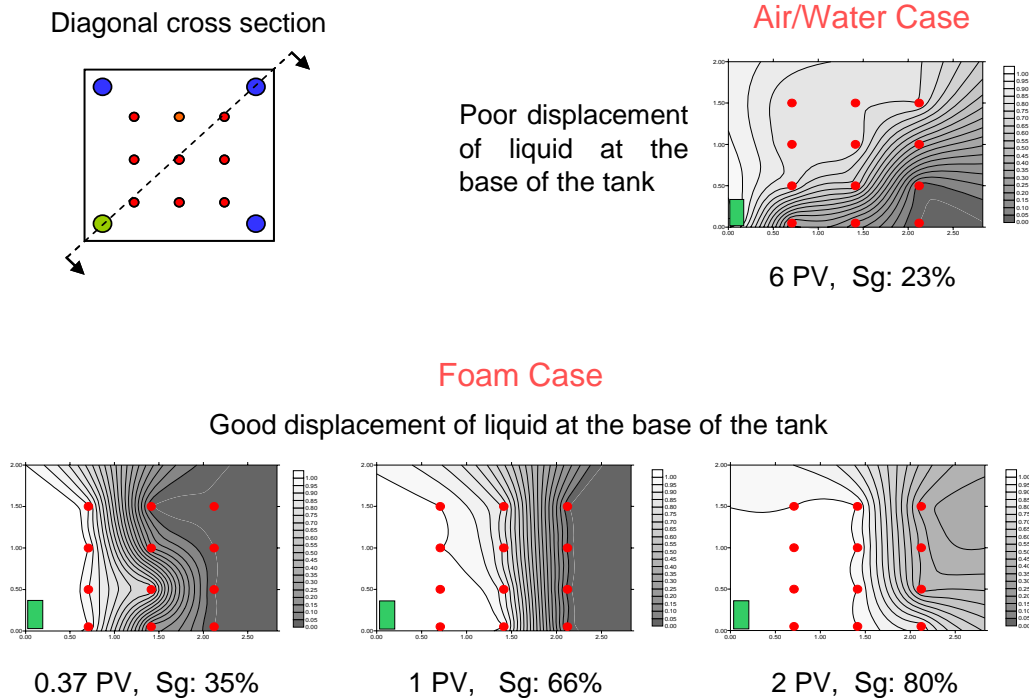


Figure 5-9 Comparison of air/water and foam results along the diagonal cross section of the tank, Constant injection pressure ~0.8 psi

From Figure 5-5, 5-6, 5-7, 5-8, we can find the main differences between air/water and foam experiments are the gas distribution, the gas injection rate and the total gas saturation in the tank. Figure 5-9 gives the diagonal cross section gas fraction flow contour plots for both of these two experiments. The difference between air/water and foam is more phenomenal in these diagonal plots. From the plots we can see, in the air/water case, after 6 PV gas injected, there still quite a lot of the bottom of the tank left uncontacted by gas. In this case, most of the injected gas tended to flow upwards and then out of the top of the tank. In the foam case, after only about 0.37 PV gas injected, in the bottom of the tank, the gas contacted area was already almost as large as in the air/water case after 6 PV injected. Gas continued to propagate horizontally along the bottom of the tank with the injection of more gas. After 2 PV gas injected, almost all the bottom of the tank was contacted by gas.

The total gas saturation in the foam case is also much higher than in the air/water case. In the foam case, after only 1PV gas injected, the gas saturation was about 66% and after 2 PV gas injected, this value reached about 80%. But for air/water case, after 6PV injected, the gas saturation was only about 23%. For the injectivity, in the air/water case, the injection rate reached a steady state after about 7 minutes of injection (about 3 PV injected). At steady state, the injection rate was about 28 LPM, which means V_g was about 2200 ft/day in the injection well. In the foam experiment, the injection rate reached a steady state after about 25 minutes injection (about 0.5 PV injected). At steady state, the

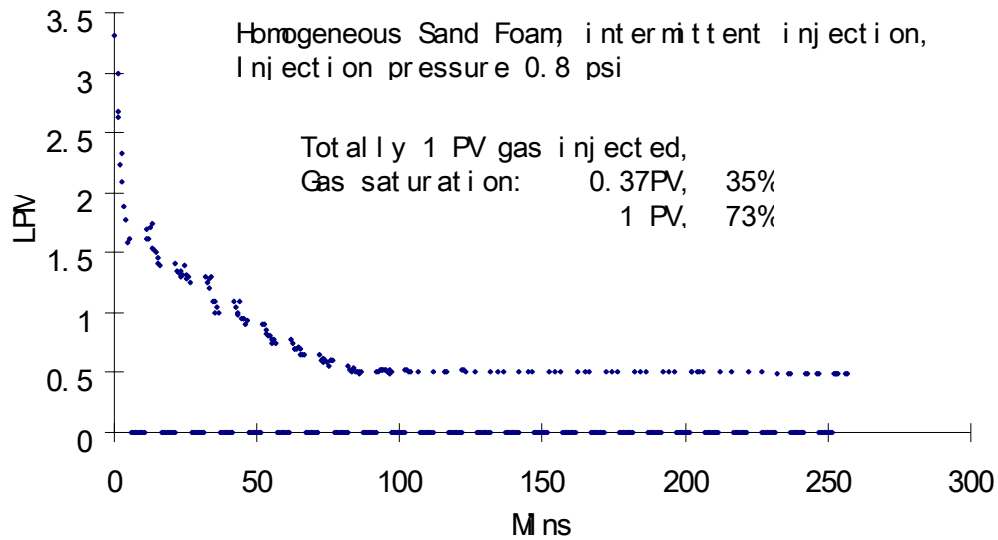


Figure 5-10 Foam, homogeneous sand tank, Injection rate Intermittent gas injection, pressure ~0.8 psi 1 PV gas injected

injection rate was about 0.8 LPM, which means V_g was about 70 ft/day in the injection well. Comparing these two cases, we can see for foam injection, the steady state of the injection rate can be reached with less PV gas injected. In foam case, to reach the steady state, the needed gas is about 6 times less than in air/water case. Also, in foam case, the injection rate at steady state is much lower than in air/water case. It is about 30 times less than in the air/water case. From these comparisons, it is apparent that foam can greatly increase the gas distribution and saturation in the sand tank. For our hydrogen biosparging process, the increased gas contacting and saturation is favorable. Also, foam will result in a lower inject rate compared to the air/water case, the ratio between foam and air/water is about 1/30.

5.1.2.2 Different foam injection strategies

Two other foam experiments were performed in the homogeneous 3-D tank to test the effect of different injection strategies. One is performed using an intermittent gas injection method: gas was injected into the tank in a 5 minutes on and 5 minutes off cycle. The other one was performed using a constant gas injection rate at about 0.4 LPM, which is about the half of the steady state injection rate in our former 0.8 psi constant injection pressure foam experiment. Figure 5-10 shows the curve of the injection rate for the intermittent injection foam experiment. The rate began from about 3.5 LPM at the beginning of the gas injection. With the injection time went on, it declined and reached its steady state after about 100 minutes operation time. Because it was an intermittent injection, the actual gas injection time was about 50 minutes. At steady state, the injection rate was about 0.5 LPM, which was lower than in the continuous gas injection foam experiment.

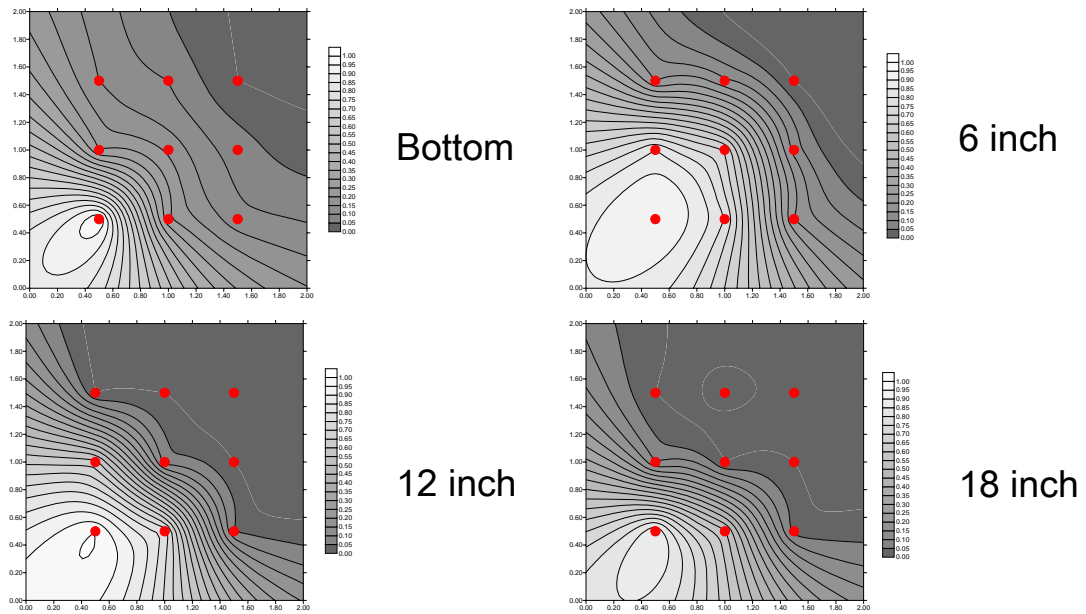


Figure 5-11.A Foam, Homogeneous sand tank, gas fraction flow contour plot Intermittent gas injection, ~0.8 psi, ~0.37 PV gas injected

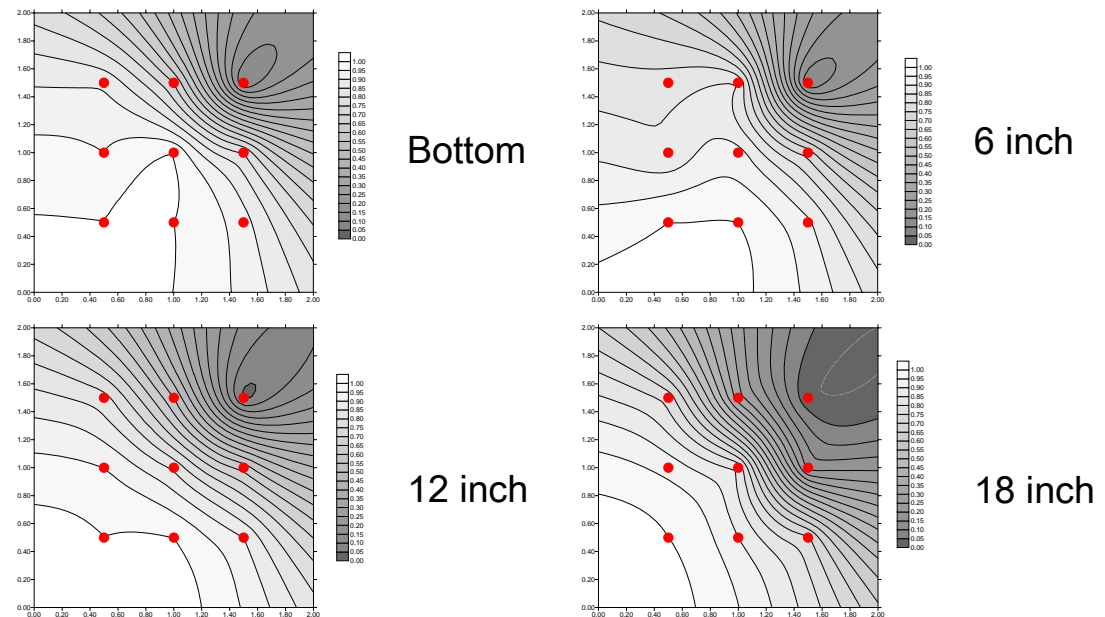
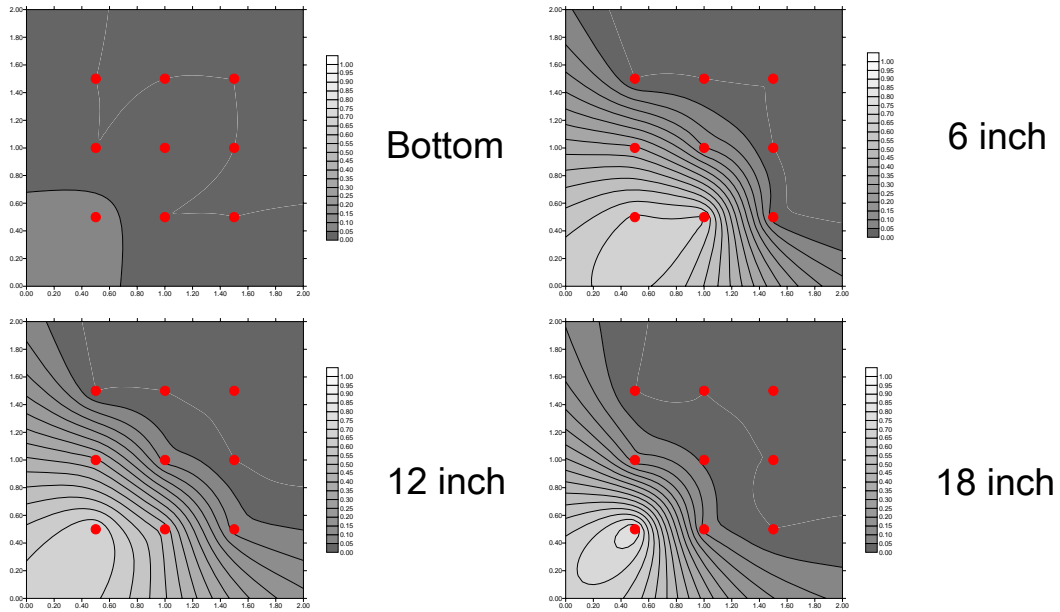
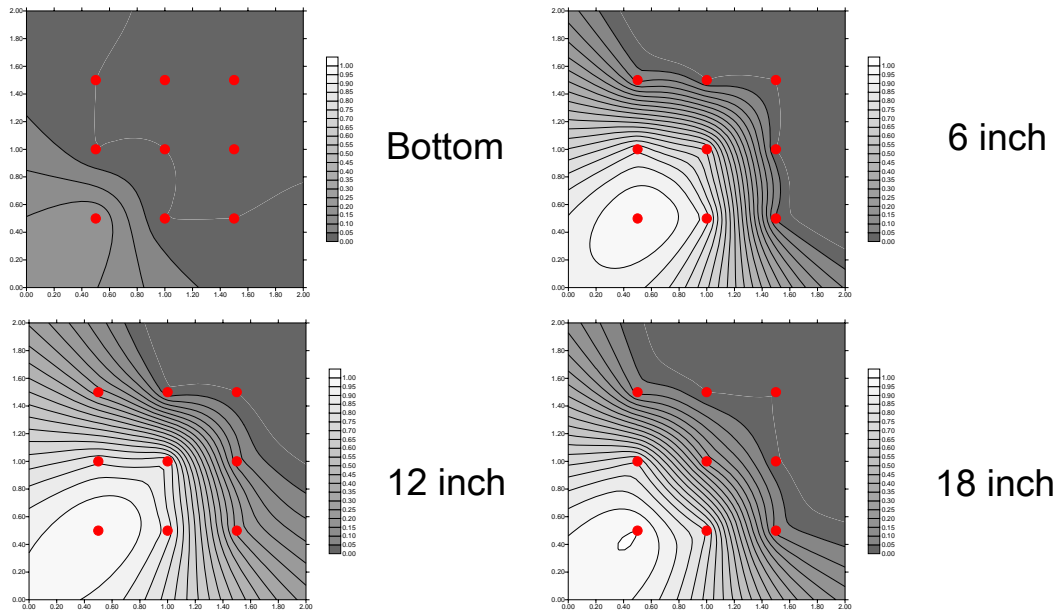


Figure 5-11.B Foam, Homogeneous sand tank, gas fraction flow contour plot Intermittent gas injection, ~0.8 psi, ~1 PV gas injected

Figure 5-11.A and B show the gas fractional flow contour plots after 0.37 PV and 1 PV gas was injected in this intermittent injection experiment. After 0.37 PV gas injected, around 80% of the bottom layer was already contacted by gas. There was almost no gas flowed out of the tank at after the injection of 0.37PV. The gas saturation in the tank was about 35% at that time. After 1 PV gas



**Figure 5-12.A Foam, Homogeneous sand tank, gas fraction flow contour plot
Constant rate gas injection, ~0.39 LPM, ~0.37 PV gas injected**



**Figure 5-12.B Foam, Homogeneous sand tank, gas fraction flow contour plot
Constant rate gas injection, ~0.39 LPM, ~1 PV gas injected**

injected, almost all the bottom of the tank was contacted by gas. For the higher level layers, gas also contacted more than 90% area of them. At that time, the gas saturation was about 73%, which was obviously higher than in the continuous air injection foam case, in that case, this value was about 66%

Figure 5-12.A and B show the gas fractional flow contour plots for the constant injection rate foam experiment. Though it was a constant injection rate experiment, in this experiment, the injection pressure reached steady state very quickly and stayed at about 0.4 psi. So, it was also a low injection pressure (0.4 psig) foam experiment.

From Figure 5-12 we can see the constant injection rate (low injection pressure) do not have a good gas sweep. After 0.37 PV gas injected, in the bottom of the tank, only a small area around the injection well was contacted by gas. After 1 PV gas injected, there still about 80% of the bottom did not contacted by gas. For the other upper layers, the gas sweep was also not good, gas can not propagate far horizontally and most of the injected gas flowed out from the top of the tank. One can also tell this from the gas saturation in the tank, after 1 PV gas injected, the gas saturation in the tank was only 37%, which was much less than that in the other foam experiments.

In the homogeneous sand tank, we preformed three kinds of foam experiments: continuous air injection at constant injection pressure, intermittent air injection at constant injection pressure, constant air injection rate (low injection pressure). Among all these three experiments, we obtained the best gas distribution and the highest gas saturation in the intermittent gas injection experiment.

Just take the bottom layer as an example of comparison, in the constant injection pressure, continuous air injection case, after 0.37PV gas injected, gas contacted about 1/2 of the tank in the bottom layer, after 1PV gas injected, gas contacted about 4/5 of the tank in the bottom layer. In the constant injection pressure, intermittent air injection case, after 0.37PV gas injected, gas contacted about 3/4 of the tank in the bottom layer, after 1PV gas injected, gas contacted almost all of the tank in the bottom layer. In the constant gas injection rate case, after 0.37PV gas injected, gas contacted about 1/16 of the tank in the bottom layer, after 1PV gas injected, gas contacted only about 1/5 of tank in the bottom layer.

We can see that the intermittent injection method can increase the latterly transport of the gas in the tank. The shut in interval during the experiment will make the sands been re-saturated and this can keep the generated foam from drying and then from breaking. The worst case in gas distribution was the constant injection rate case. The reason for this is because in the constant injection rate case, the actually total injection pressure was only about 0.4 psi above hydrostatic pressure, which was only about one half of the pressure in other foam experiments. Because of the lower pressure, the pressure gradient was lower and there was no strong foam generated. So the gas follow was dominated by gravity force and most of the gas flowed upwards and did not contact much of the bottom of the tank. To obtain best results, it is important to inject gas using a high enough injection pressure,

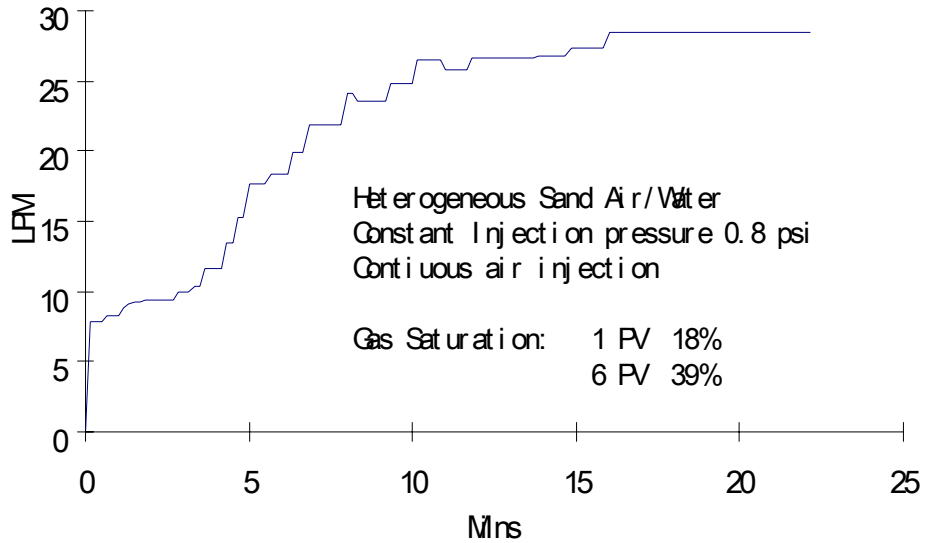


**Figure 5-13 Air/water, heterogeneous sand tank, Injection rate curve
Continuous gas injection, pressure ~0.8 psi 1 PV gas injected**

For the gas saturation in the tank, because in the intermittent air injection case, gas contacted more area in the tank and foam is stronger compared to the continuous air injection case, we obtained higher gas saturation in the intermittent air injection case.

From these comparisons, we can see constant injection pressure method provides better gas sweep efficiency than constant injection rate method, in which pressure is too low to generate strong foam. And for a constant injection pressure experiment, the intermittent injection method provides better gas sweep efficiency and higher total gas saturation than the continuous injection method.

5.1.3 Heterogeneous sand pack results

In a heterogeneous system, besides lamella division, lamella snap-off will also play an important role in determine the strength of generated foam. When gas flows from a low permeability region to a high permeability region, because of the difference of the capillary pressure in these two regions, lamella snap-off will occur. More lamella will be generated along the boundary of the low and high permeability sand, block the flow path of gas and hence increase the apparent viscosity of gas. In a regular air/water injection, the high permeability will act as a shortcut for the gas flow and the low perm region will left uncontacted. With the effect of foam, gas apparent viscosity will be greatly reduced in these high permeability regions and more gas can then flow into the low permeability region. So in a heterogeneous system, the effect of foam will be more apparent compared to regular air/water injection.

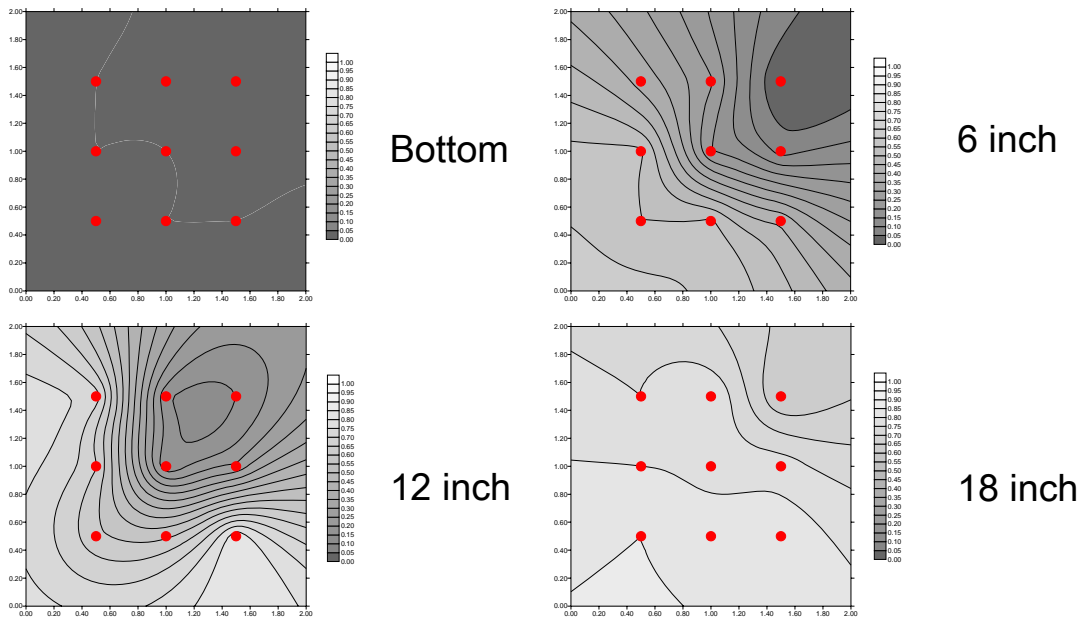


**Figure 5-14.A Air/water, Heterogeneous sand tank, gas fraction flow contour plot
Constant injection pressure, ~ 0.8 psi, ~ 1 PV gas injected**

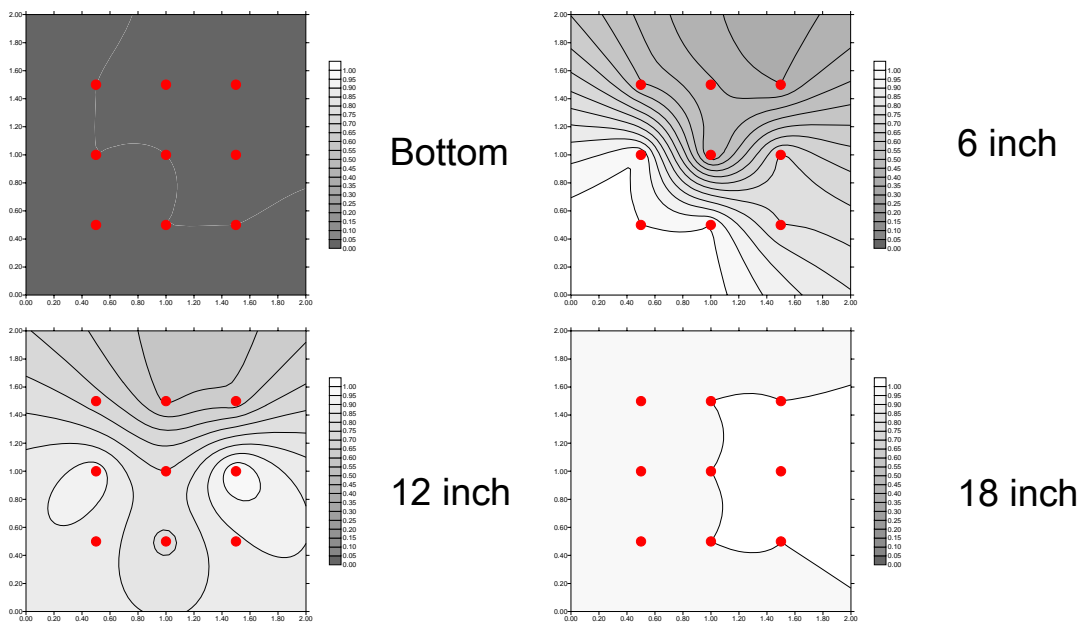


**Figure 5-14.B Air/water, Heterogeneous sand tank, gas fraction flow contour plot
Constant injection pressure, ~ 0.8 psi, ~ 6 PV gas injected**

5.1.3.1 Comparison of air/water and foam experimental results

Figure 5-13 shows the curve of the injection rate for the air/water case in the heterogeneous pack. Gas was injected into the tank at a constant injection

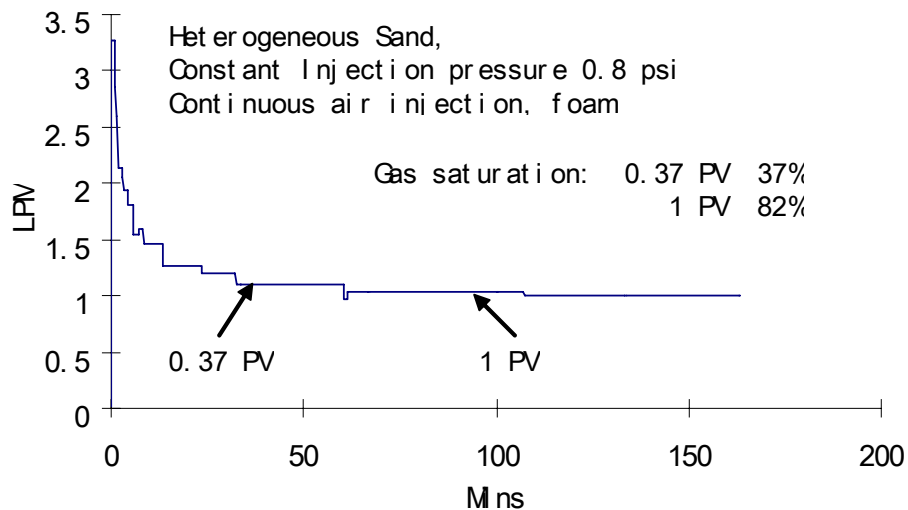


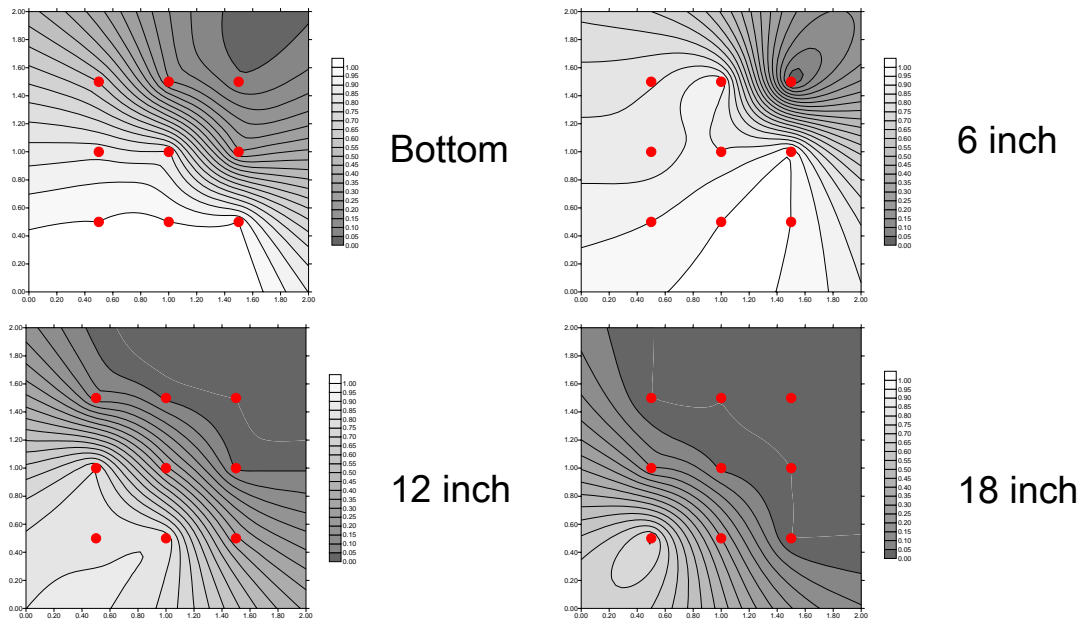
**Figure 5-15 Foam, heterogeneous sand tank, Injection rate curve
Continuous gas injection, pressure ~0.8 psi**

pressure of 0.8 psig over the hydrostatic pressure. From Figure 5-13 we can see the shape of the curve is similar to the curve of the air/water case in the homogeneous pack. The injection rate increased from the beginning of gas injection and after about 15 minutes' injection, it reached a steady state. At steady state the injection rate was about ~30 LPM. After about 23 minutes' injection, 6 PV gas was injected into the tank. The gas saturation after 1 PV and 6 PV gas injected was measured. After 1 PV gas injected, the total gas saturation in the tank was about 18%. After 6 PV gas injected, the total gas saturation increased to about 39%.

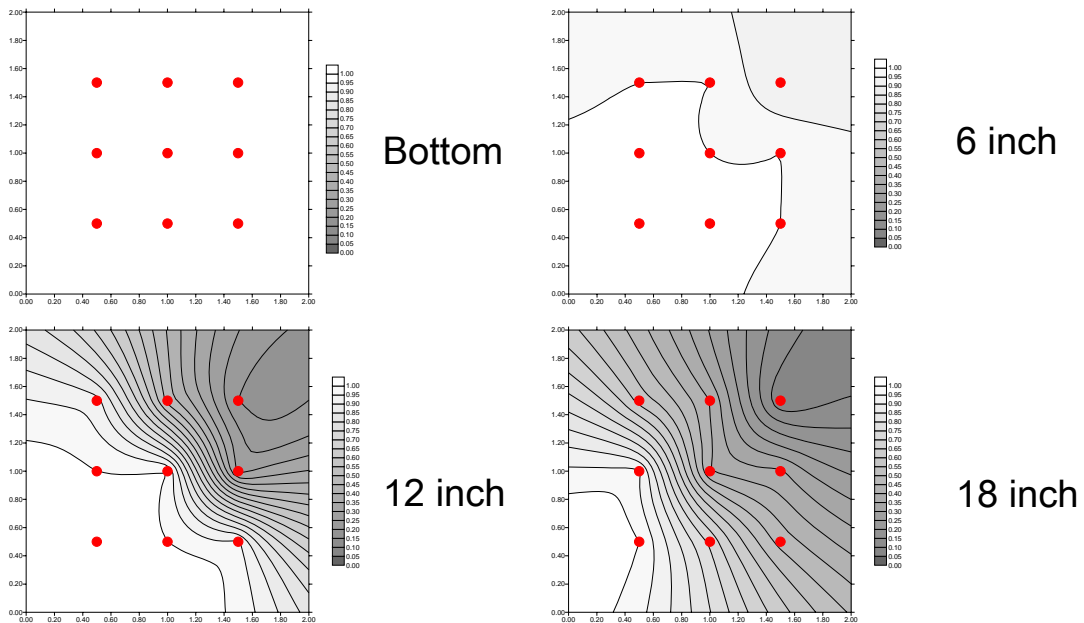
Figure 5-14 A and B are the gas fractional contour plots for the air/water case after 1 PV and 6 PV gas injected. From the plots we can find that the gas sweep at the bottom of the tank is bad. After 6 PV gas injected, all the bottom of the tank still left uncontacted by gas. Most of the injected gas flowed through the high permeability layer and then flowed upwards out of the tank. It was hard for gas to flow into the low permeability layer in the bottom of the tank.

Figure 5-15 gives the curve of the injection rate for the foam experiment. More than 1 PV gas was injected into the tank in this case. The injection rate reached its steady state after about 45 minutes injection. At that time around 0.37 PV gas was injected. At steady state, the injection rate was about 1 LPM which was a little bit higher than in the homogeneous foam case. The gas saturation after 0.37 PV gas injected was 37%, which means gas did not breakthrough to the top of the tank and all the injected gas was trapped in the tank at that time. This was because of the increased horizontal transport of gas by heterogeneity, more gas was traveling horizontally so it took a longer time for the injected gas to breakthrough. After 1 PV gas injected, the gas saturation in the tank was about 82%. Compared to the 66% gas saturation in the homogeneous tank under the

same experimental condition, the gas saturation in the heterogeneous sand pack increased 16% just because of the effect of heterogeneity.



**Figure 5-16.A Foam, Heterogeneous sand tank, gas fraction flow contour plot
Constant injection pressure, ~ 0.8 psi, ~ 0.37 PV gas injected**



**Figure 5-16.B Foam, Heterogeneous sand tank, gas fraction flow contour plot
Constant injection pressure, ~ 0.8 psi, ~ 1 PV gas injected**

Figure 5-16 A and B give the gas fractional flow contour plots for the heterogeneous foam experiment. We can see because of the two high permeability layers in the lower part of the tank, the gas sweep efficiency was greatly increased, especially near the bottom of the tank. After only 0.37 PV gas

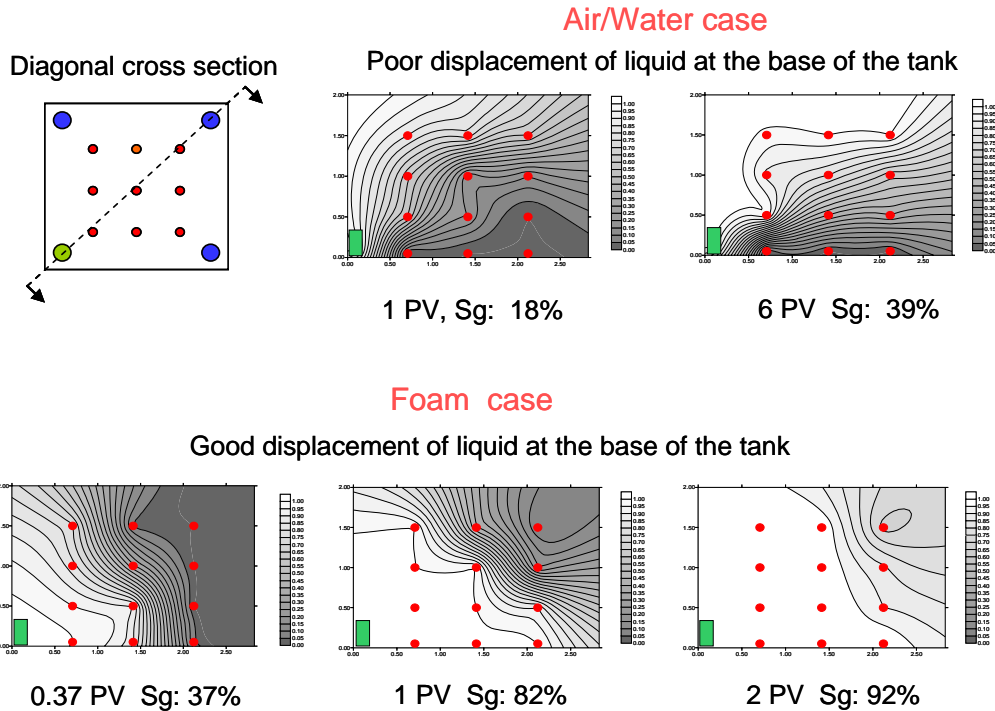


Figure 5-17 Comparison of air/water and foam results along the diagonal cross section of the tank, Constant injection pressure ~0.8 psi

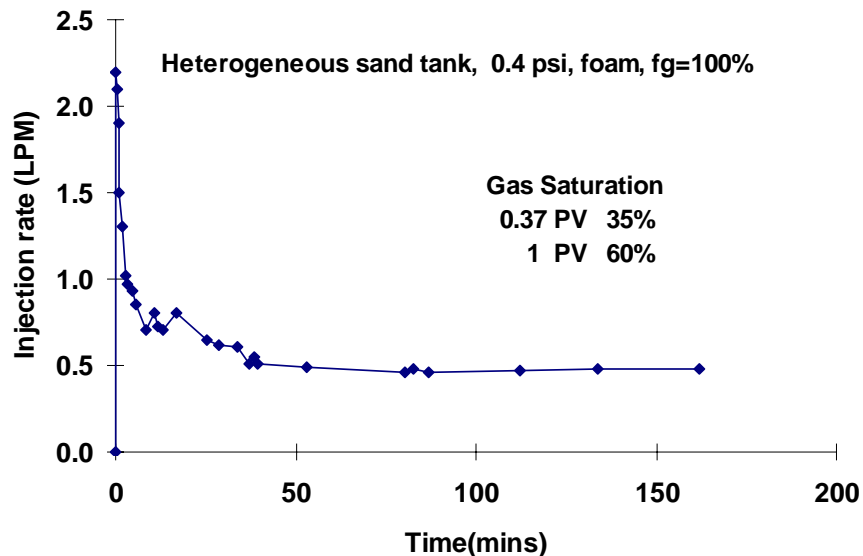
injected, more than 90% percent of the bottom of the tank was already contacted by gas. Also, gas contacted almost all the layer of 0.5 foot from the bottom. After 1 PV gas injected, all the bottom layer was contacted by gas (the gas fractional flow was 100% from all these 9 sampling points in the bottom). Gas also contacted almost all of the area of the other three upper layers. Figure 5-17 shows a comparison between air/water and foam cases in the heterogeneous tank. The plots there are the diagonal cross section gas fractional flow contour plots. The difference of air/water and foam is very apparent in these plots. In the air/water case, gas flow direction was mainly upwards and the shape of the flow area is more like a cone. But in the foam case, gas flow is more like a special flow. In the air/water case, after even 6 PV gas injected, most of the lower part of the tank were still not contacted by gas and gas saturation was still low (about 39%). In the foam case, after 2 PV gas injected, almost all the tank was contacted by gas and the gas saturation increased to about 92%. After 1 PV gas injected, in air/water case, gas saturation was only 18% and most of the lower part of the tank was not contacted by gas. On the contrary, in foam case, gas saturation was as high as 82%, most of the lower part of the tank was contacted by gas. From these comparisons we can see in the heterogeneous system, the effect of foam is more apparent. Foam greatly increased the gas sweep efficiency and the total gas saturation. Without foam, it is very difficult to sweep the whole tank, especially in those low permeability regions.

5.1.3.2 Comparison between different injection strategies

In our homogeneous pack experiments, we compared different injection strategies and found that by using the intermittent injection method, we can obtain the best foam experimental results. For the heterogeneous system, we also tested some different injection conditions and compared the results.

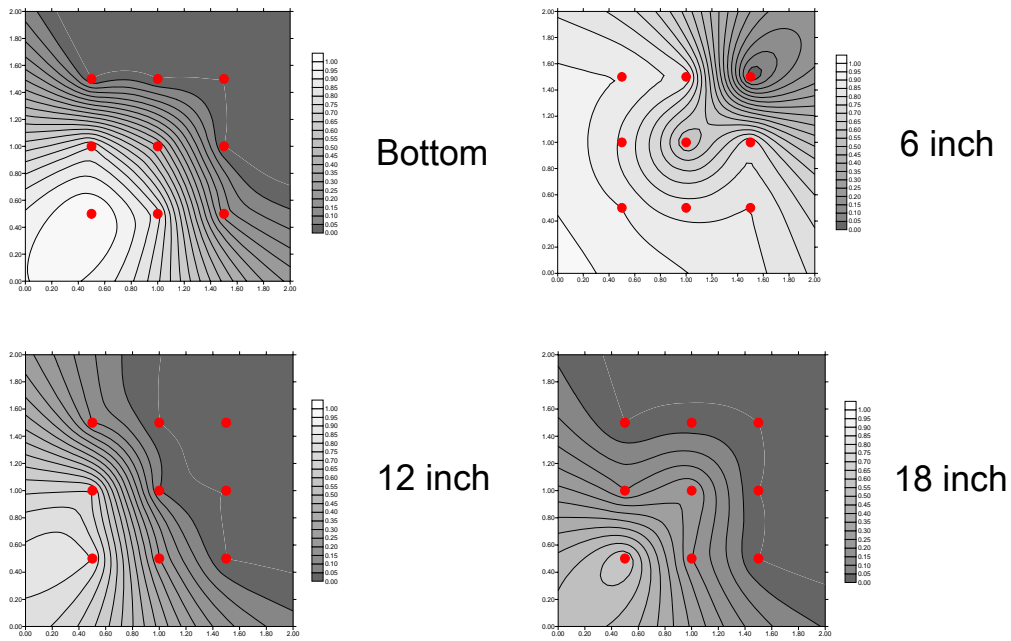
One experiment was performed using a lower injection pressure. This experiment was performed using 0.4 psi over hydrostatic pressure, which is half of the injection pressure we used in our former heterogeneous foam experiment.

Figure 5-18 gives the curve of the gas injection rate for this experiment. The injection reached a steady after about 45 minutes injection. At steady state, the gas injection rate was about 0.5 LPM. The steady state injection rate is about half of the steady state rate in the 0.8 psi injection pressure experiment. It took about 150 minutes to inject 1 PV gas into the tank. The gas saturation was lower than in the 0.8 psi foam experiment. After 1 PV gas injected, the gas saturation in the tank was only about 60%, which was 22% lower than in the 0.8 psi foam experiment.



**Figure 5-18 Foam, heterogeneous sand tank, Injection rate curve
Continuous gas injection, pressure ~0.4 psi**

Figure 5-19 A and B show the gas fractional flow contour plots when 0.37 and 1 PV gas was injected into the tank. From these plots we can see though the gas contacted area is still large in this 0.4 psi foam experiment, the gas sweep efficiency is obviously worse than in the 0.8 psi foam experiment (Figure 16 A



**Figure 5-19.A Foam, Heterogeneous sand tank, gas fraction flow contour plot
Constant injection pressure, ~0.4 psi, ~0.37 PV gas injected**

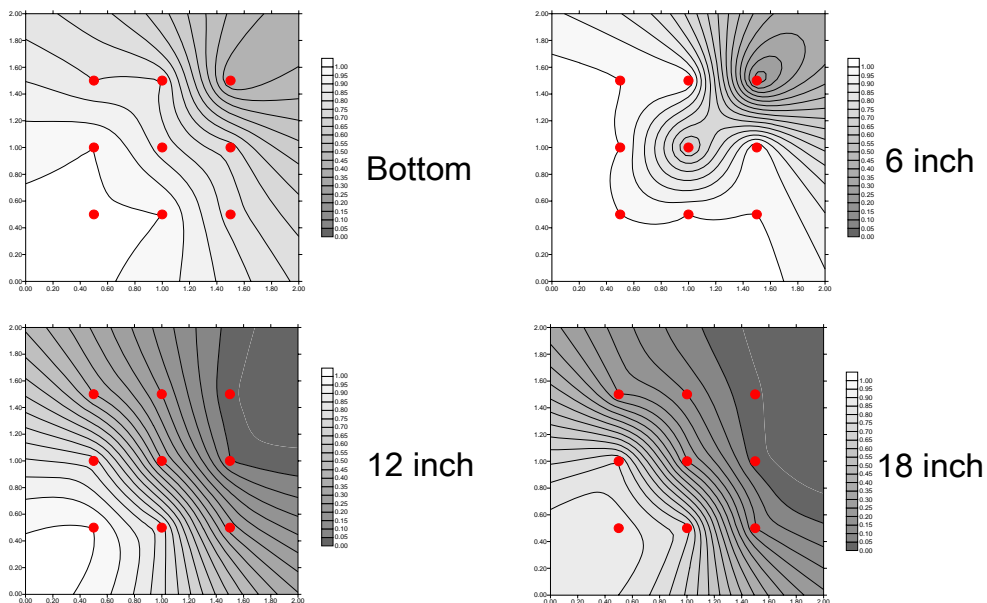


**Figure 5-19.B Foam, Heterogeneous sand tank, gas fraction flow contour plot
Constant injection pressure, ~0.4 psi, ~1 PV gas injected**

and B). After 0.37 PV gas injected, in the 0.4 psi foam experiment case, only about 75% area of the bottom was contacted by gas. But in the 0.8 psi foam experiment case, more than 90% was contacted by gas. After 1 PV gas injected, in the 0.4 psi case, there still quite a lot area in the lower two layers which did not

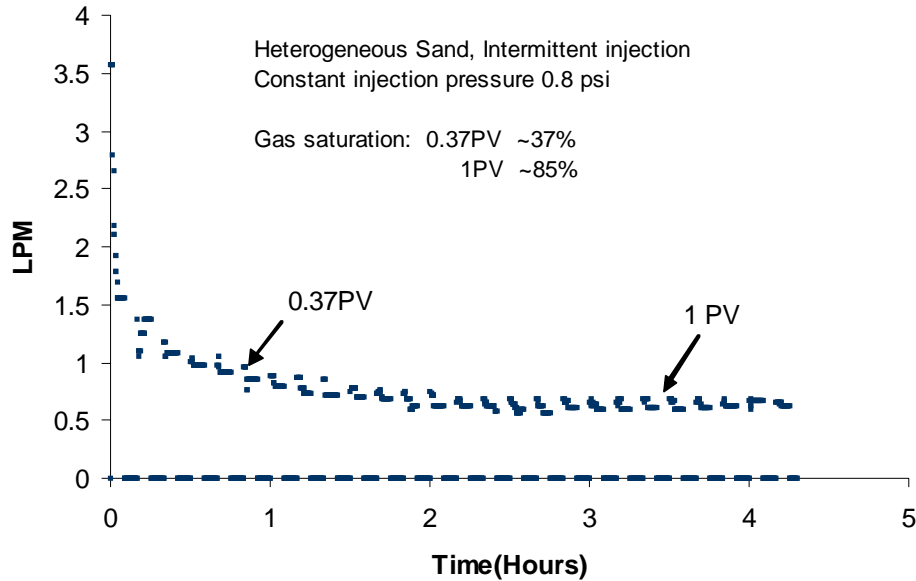


**Figure 5-20 Foam, heterogeneous sand tank, Injection rate curve
Intermittent gas injection, pressure ~0.8 psi**

contacted by gas. In the 0.8 psi case, almost all of the lower part of the tank was contacted by gas. This can be easily identified from the color of the contour plots, in the 0.4 psi case, there still a large area in the bottom remained dark which means low gas fractional flow there. But in the 0.8 psi case, almost all the bottom of the tank were white which means a very high value of gas fractional flow. From these comparisons we can see in the heterogeneous sand pack, the injection pressure is also very important to obtain a good sweep and high gas saturation. Just as in the homogeneous sand pack, the injection pressure should be high enough to generate strong foam and drive gas to flow further horizontally.

One intermittent injection experiment was performed in this heterogeneous sand tank. This experiment was performed using the same injection pressure as in the continuous gas injection experiment: 0.8 psi over hydrostatic pressure. Gas was injected into the tank using a 5 minutes on and 5 minutes off strategy. Figure 5-20 shows the curve of the injection rate. After about 1 hour's intermittent injection (30 minutes actual injection time), the injection rate reached a steady state. At steady state, the injection rate was about 0.6 LPM, which is lower than the steady state injection rate in the continuous injection case. The lower steady state gas injection rate indicates that stronger foam was generated in the tank than in the continuous injection case. One explanation for this phenomena is due to the intermittent injection method. During the 5 minutes gas turned off period, surfactant solution may flow back and increase the water saturation in the region where foam has been generated. This will keep the generated lamella from breaking and then make the generated foam

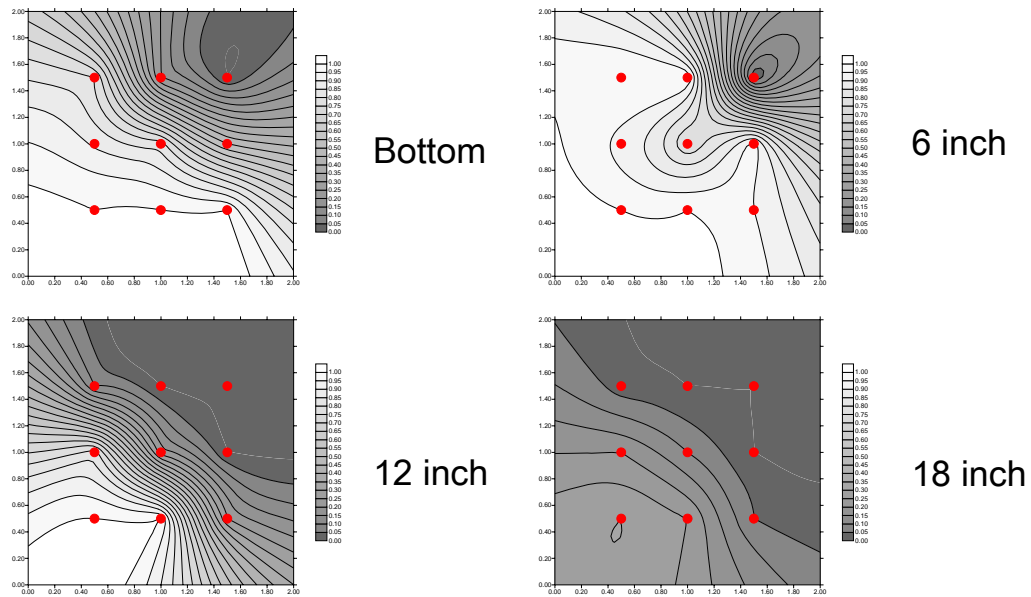


**Figure 5-21.A Foam, Heterogeneous sand tank, gas fraction flow contour plot
Intermittent gas injection, ~ 0.8 psi, ~ 0.37 PV gas injected**

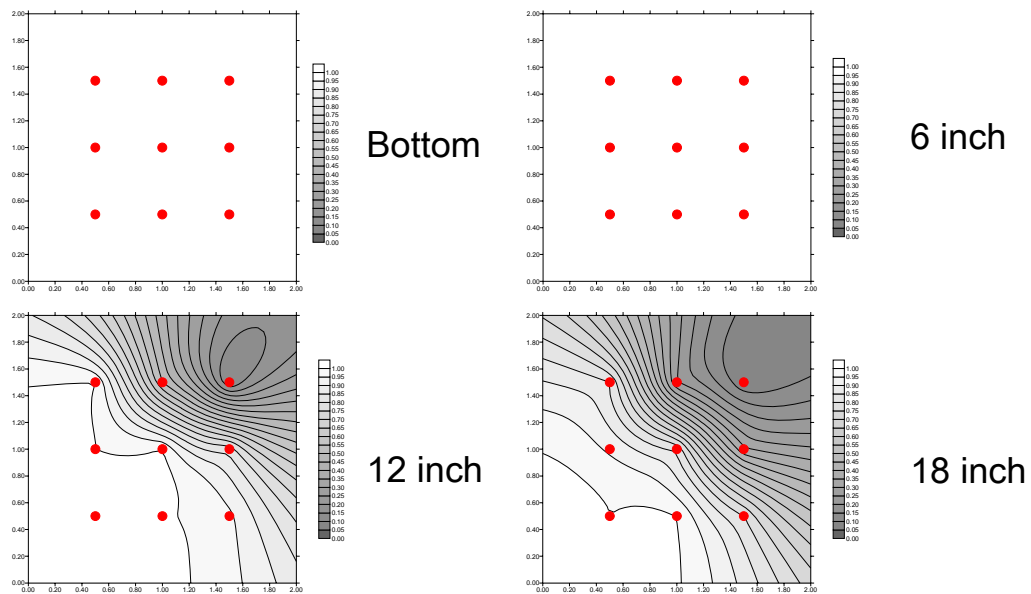


**Figure 5-21.B Foam, Heterogeneous sand tank, gas fraction flow contour plot
Intermittent gas injection, ~ 0.8 psi, ~ 1 PV gas injected**

stronger. In this intermittent experiment, after about 0.37 PV gas injected, the gas saturation inside the tank was about 37%. Gas did not break through at that moment. After 1 PV gas injected, the gas saturation in the tank reached about 85%, which was about 3% higher than in the continuous gas injection foam case.

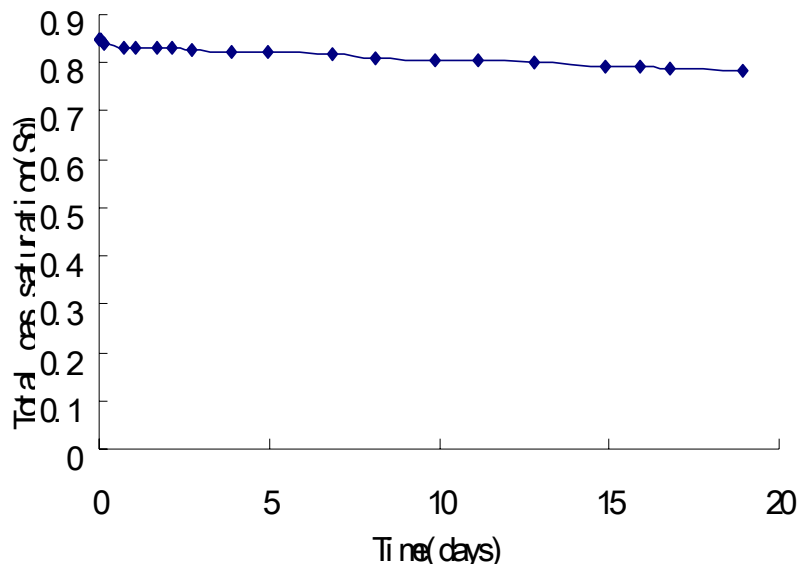


**Figure 5-22 Foam, heterogeneous sand tank, constant injection pressure ~0.8 psi
After 1 PV gas injected, the change of gas saturation in the tank**

Figure 5-21 A and B show the gas fractional flow contour plots for this intermittent injection foam experiment. By comparing to Figure 5-16 A and B, we can find that the gas sweep results of the intermittent injection case were very similar to the results of the continuous injection case. Both of these two cases had good gas sweep efficiency in the lower part of the tank. But strictly saying, the intermittent injection case had a better sweep efficiency than the continuous case, though the difference between them may be slight. For example, after 1 PV gas injected, in the intermittent case, the layer of 0.5 ft from the bottom was all contacted by gas. But in the continuous injection case, there still some area where the gas fractional flow value was not 100%.

From these comparisons we can see, in the heterogeneous pack, the effect of intermittent injection method is not as that apparent as in the homogeneous pack. But nevertheless, the intermittent injection method can still benefit the gas sweep efficiency and the total gas saturation in the tank, either in the homogeneous pack or the heterogeneous pack.

5.1.3.3 Foam stability

In the biodegradation process, hydrogen acts as an electron donor and halogenated compounds such as chlorinated solvents act as electron acceptors that are reduced in the reductive dechlorination process. So the foam stability is another important thing in the hydrogen biosparging process. If foam is stable, hydrogen can be trapped in the aquifer for a longer time, this will definitely benefit the biodegradation process. A foam stability experiment was performed after the

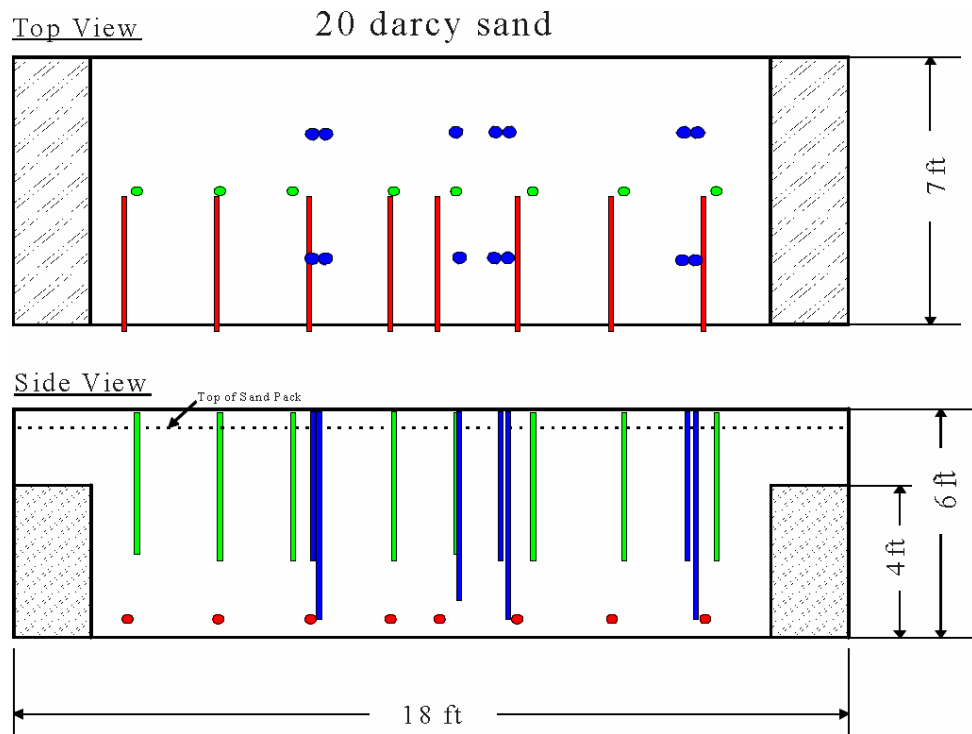


Figure 5-23 Layout of the Rice ECRS tank

0.8 psi continuous gas injection foam experiment. After 1 PV gas was injected into the tank, the gas injection was turned off and a water table was added on the top of the sand pack. By measuring the change of the water level on the top of the sand and doing a material balance, we can calculate the gas saturation inside the tank. Figure 5-22 shows the change of the gas saturation with time. From this plot we can see the generated foam is quite stable. After about 20 days, the gas saturation in the tank only changed about 5 percent. It dropped from about 85% to 80%.

5.2 Rice ECRS Tank experiments

Besides the 3-D tank experiments, we performed some other 3-D foam experiments in a larger scale. These experiments were performed in the Rice ECRS tank. The scale of the tank is intermediate between the laboratory bench-scale and full-scale field implementation. By doing these experiments, we can obtain more information on how foam affect the gas flow in a larger scale, i.e. a field application.

5.2.1 Experimental

Figure 5-23 shows the layout of the Rice ECRS tank. It is a 756 cubic feet rectangular container with dimensions 18 feet long, 7 feet wide and 6 feet deep. It is constructed by Galbreath Inc (Model OS1872). The tank is filled with 20 darcy sand. At each end of the tank, there is a pea gravel layer which is about

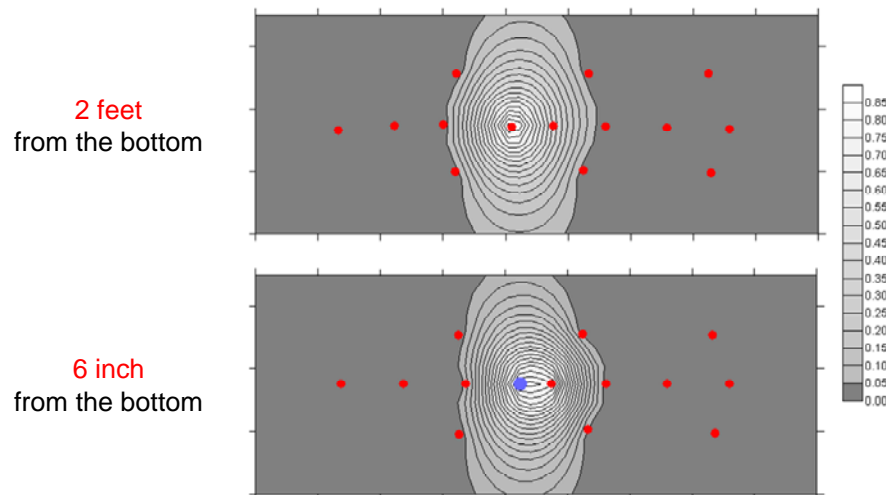


Figure 5-24 Gas distribution for the gas injection case, injection pressure 5 psig, 0.63 PV gas injected, average injection rate 1 ft³/min

1feet thick and 4 feet high. The permeability of the pea gravel layer is much higher than 20 darcy. There are two sampling layers in the tank, one is 6 inches from the bottom of the tank and the other one is about 2 feet from the bottom. Just as shown in Figure 5-24, the red dots and some of the blue dots are the sampling points of 6 inches layer. The green dots and the rest of the blue dots are the sampling points in the 2 feet layer. During the experiments, samples can be obtained through these tubes, and information such as gas or surfactant distribution can be obtained. The surfactant solution we chose was the same as in our 3-D tank experiment, a ratio of 1:1 mixture of 0.05% (wt) CS-330 and 0.05% (wt) C13-4PO.

Before an experiment, the ECRS tank was filled with water or surfactant solution first, and then gas was injected into the tank from the injection ports, which were located six inches from the bottom of the tank. In the foam experiments, we did not fill the whole tank with surfactant solution. Instead, we injected 1/3 PV water into the tank first and then injected 2/3 PV surfactant solution to fill the tank. This was because we were short of surfactant solution and cannot fill the whole tank with it. In the later part of this report (Section 6, field application design), we will prove that the 2/3 PV surfactant is enough to generate strong foam and can obtain similar results as in a surfactant full tank. During all these experiments, we kept the injection pressure at 5 psig over hydrostatic pressure, which was the maximum pressure we can have considering the condition of the tank. If the injection pressure was higher than 5 psig, the sand in the tank would be fluidized and then no useful results can be obtained.

5.2.2 Experimental results

Figure 5-25 shows the gas distribution for the air injection case. About 0.63 PV gas was injected into the tank. The average injection rate was about 1

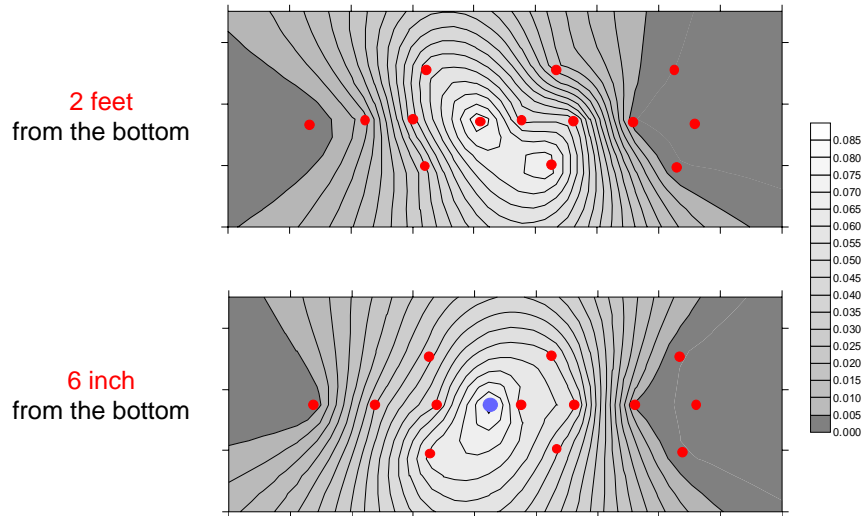


Figure 5-25 Surfactant distribution before foam experiment
Injected surfactant solution concentration: 0.1% (wt)

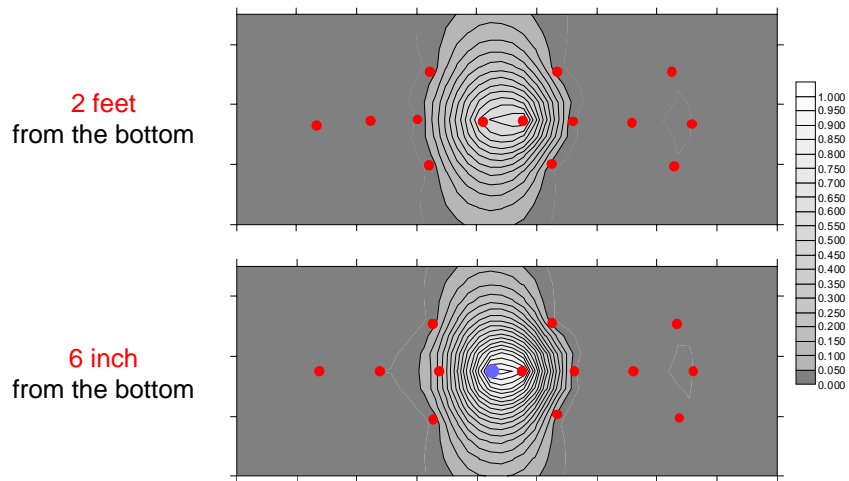


Figure 5-26 Gas distribution for the foam injection case, middle injection port,
injection pressure 5 psig, 0.075 PV gas injected,

ft³/min. In this air injection experiment, the water level change at the top of the tank was not measurable which indicated that only a small amount of the injected air was trapped in the sand tank.

After the air injection experiment, we washed the tank and injected the surfactant solution. Figure 5-25 shows the surfactant distribution in the tank before the foam experiment. Surfactant solution was injected from the middle injection port of the tank, which is the red dot in Figure 5-25. The injection port was 6 inch higher from the bottom. From the plots we can see we obtained the maximum surfactant concentration around the injection port. After the injection of the surfactant solution, we injected gas into the tank to generate foam. The gas

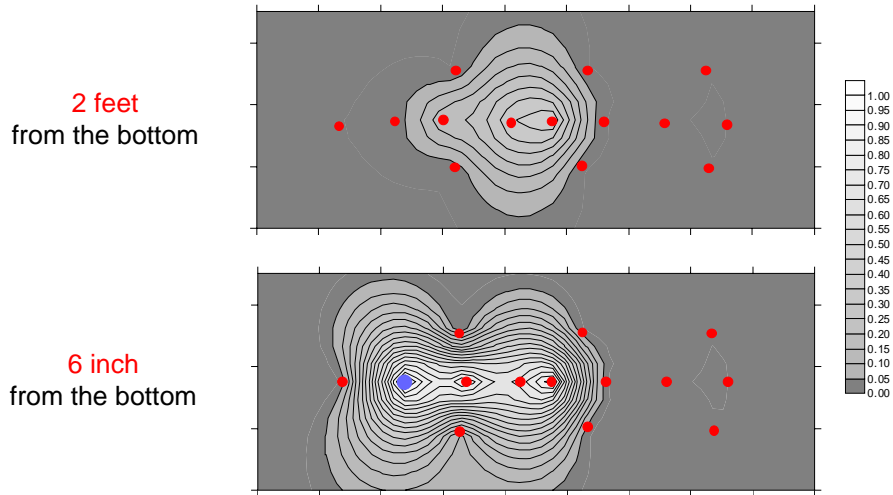


Figure 5-27.A First day, Foam, left injection port, 5 psig, 0.03PV gas injected, Average injection rate 0.04ft³/min, Percent of trapped gas 84%

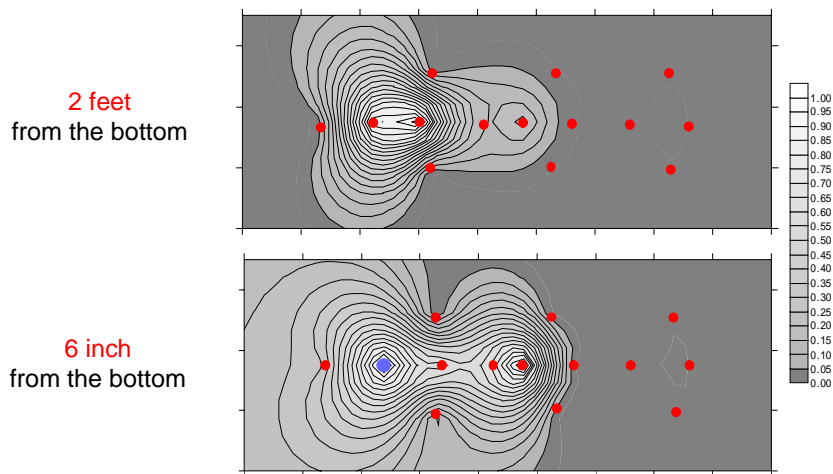


Figure 5-27.B Second day, Foam, left injection port, 5 psig, 0.05PV more gas injected, Average injection rate 0.09 ft³/min, Percent of trapped gas 50%

injection port was the same injection port as in the air/water experiment and in the surfactant solution injection process. The injection pressure was also kept at 5 psig. Figure 5-26 shows the gas distribution in the tank for the foam experiment after 0.075 PV gas injected. The average injection rate we obtained was about 0.22 ft³/min. Compared to the air/water experiment, the average gas injection rate for the foam case was about 1/5 of the gas injection rate in the air/water case. From these contour plots we can see, after only 0.075 PV gas injected, the gas distribution profile was already similar to the gas distribution in the air injection case. But in that case, 0.63 PV gas was injected, which was about 9 times more than in the foam case.

After injected 0.075 PV gas into the tank from the middle injection point, we changed our injection point to another location, which was at the same level of the original injection point but was on the left side of it. One reason for this injection location change was because we were suspecting that during the air injection, there may have formed some channels and holes which were just above the middle injection port. Then when we injected foam later from this point, foam may tend to flow into these channels and holes and cannot spread much laterally. If it was this case, we may not obtain the real image of the foam flow in a tight porous media.

Considering this, we changed the location of our injection port and injected gas from the new port in two separate days. Figure 5-27.A shows the gas distribution profile after the first day's experiment. About 0.03 PV gas was injected into the tank during this day and the average injection rate was about 0.04 ft³/min. Most of the injected gas, around 84%, was trapped in the tank. Only a few of them broke through to the top of the tank. From Figure 5-27.A we can also see most of the injected gas flowed along the bottom of the tank, the 6 inch from the bottom layer has an apparently higher gas saturation than in the 2 ft from the bottom layer.

After the first day's experiment, the gas injection was shut off and the tank was left there overnight and gas injection was continued in the second day. Figure 5-27.B shows the gas distribution profile after the gas injection of the second day experiment. In this injection period, we injected about 0.051PV gas into the tank and the average injection rate was about 0.09 ft³/min. The percent of the trapped injected gas was about 50%. From Figure 5-27.B we can see the gas contacted area increased and was larger than in the first day's experiment. Around the injection point, almost all the 6 inch from the bottom layer was contacted by gas. Though the gas contacted area in the 2 ft from the bottom layer also increased, the gas contacted area in the 6 inch from bottom layer is still larger than in the 2 ft from bottom layer. This indicates that under the effects of foam, the horizontal transport of gas in the porous media is greatly increased. Compared to air/water injection, more of the injected gas can flow along the horizontal direction and hence increased the gas sweep in the bottom of the tank. The time of gas breakthrough was also belayed by the presence of foam and then the trapped gas percentage in the tank be increased.

After finishing the left injection point experiments, we used a vibrator to vibrate the middle part sand of the tank, in an attempt to fix the possible holes and channels above the middle injection port. Then we re-injected foam from the middle injection port. During the vibration, most of the trapped gas flowed out of the tank but some gas still remained in the tank. Figure 5-28 shows the remaining gas distribution after we vibrated the tank. Figure 5-29 shows the gas distribution after we re-injected foam from the middle injection port. About 0.025 PV gas was injected. The average injection rate was about 0.08 ft³/min. Compared to the first time we injected foam from this injection port, the injection

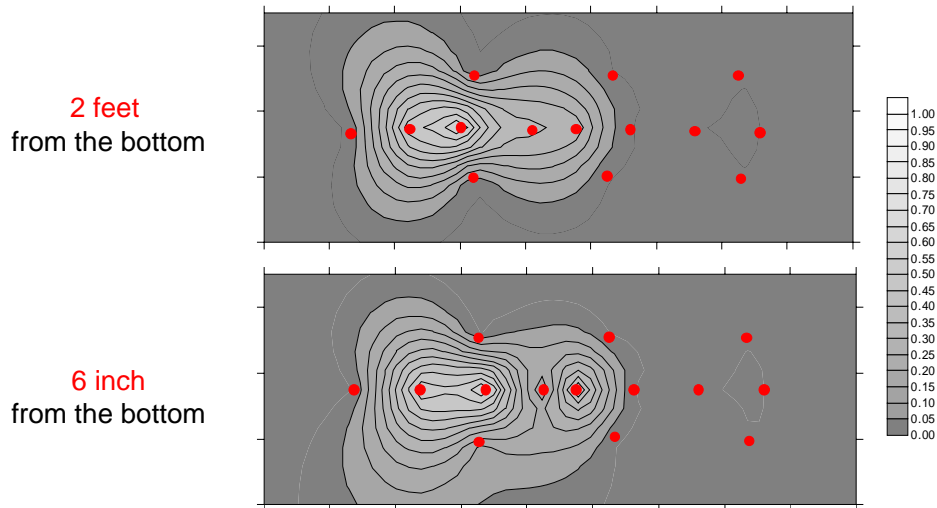


Figure 5-28 Remaining gas distribution in the tank, after vibration

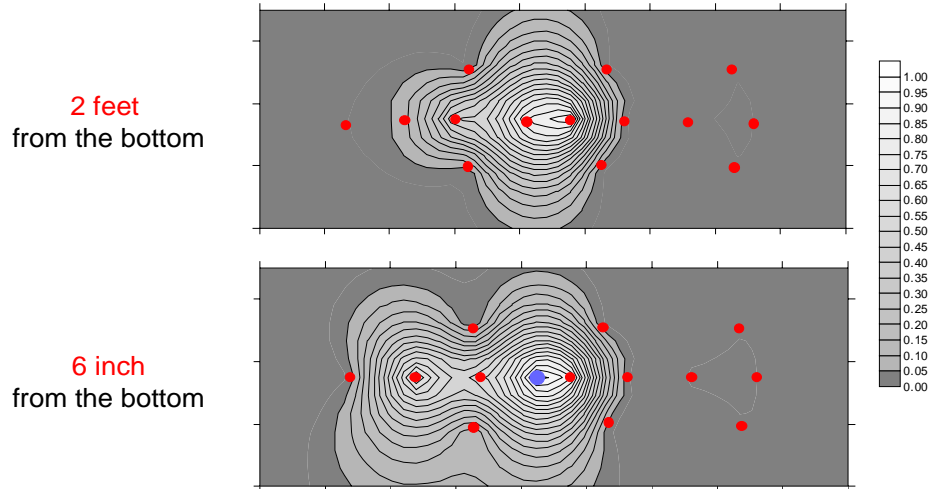


Figure 5-29 Gas distribution after gas reinjection from the middle injection point, Foam, 5 psig, 0.025PV gas injected, Average injection rate 0.08 ft³/min, Percent of trapped gas 60%

rate decreased from 0.22 ft³/min to 0.08 ft³/min. The decreasing of the injection rate proved that there were some channels or holes above the middle injection point when we first inject foam. These channels and holes were fixed by the vibration and we obtained a lower average injection rate compared to the first time we injected foam there. In this re-injection experiment, about 60% percent injected gas was trapped in the tank. We can also find from these plots that gas contacted more area in the bottom layer than in the 2 ft from the bottom layer.

These ECRS tank experiments proved that in a larger scale, i.e. a quasi-field scale, foam can still affect the flow of gas and increase the lateral gas distribution along the bottom. It can also increase the total gas saturation in the

porous media. In a porous media which has channels or big holes, foam effects will be weakened because gas will tend to flow into these fractures and form some flow shortcuts. Also, we found that in the ECRS tank, when foam is present and the porous media is tight, the injection rate was about 1/25 compared to the air/water injection rate. In our 3-D tank experiments, this ratio was about 1/30. The difference of these two ratios was caused more likely by the experimental variations. In general, in the 3-D foam flow under our experimental conditions, either in the 3-D sand tank or in the larger ECRS tank, the air/water injection rate vs. foam injection rate was around 1/30.

5.3 Summary for section 5

3-D foam experiments were performed to validate the effects of foam on the enhancement of gas/hydrogen sparging. Those foam experiments were performed both in a 2x2x2 ft tank and a 18x7x6 ft tank. Some conclusions can be made from the experimental results:

1. In both of these two kind of tanks, either homogeneous or heterogeneous, foam can greatly increase the lateral transport of gas and increase the gas sweep efficiency.
2. Foam can greatly increase the gas saturation in the tank.
3. The best injection strategy for a foam experiment, either in homogeneous pack or heterogeneous pack, is intermittent injection. Higher gas saturation and better gas sweep can be obtained by using this injection method.
4. If the porous media is not packed tightly, i.e. some channels and holes exist inside it, the effect of foam will not be as good as in a tightly packed porous media. Gas will flow into these channels and holes and is hard to be trapped in the porous media by foam.
5. In both of our 3-D tank and Rice ECRS tank experiments, the injection rate ratio between air/water case and foam case was about 1/30.
6. The generated foam is stable. Gas saturation in the tank is high and remains almost the same 20 days after stopping gas flow.

Task 6 - Incorporation of the heterogeneity enhanced mechanisms in the UTCHEM numerical simulator.

Simulation model for foam in porous media and simulation of 3-D foam form parameters obtained from 1-D experiments.

Besides the experimental validation of the effects of foam in porous media, we need to build a foam simulation model to simulate foam flow. By having a foam simulation model, we can use a simulator to simulate and predict 3-D foam behavior. It will save our time and labor because it takes too much time and effort to perform a single 3-D tank experiment.

6.1 Introduction:

Foam in porous media is defined as a dispersion of gas in a liquid such that the liquid phase is continuous, and at least some part of the gas is made discontinuous by thin liquid films called lamellae.

The transport of foam in porous media is governed by Darcy's Law:

$$u_g = \frac{kk_{rg}^f}{\mu_g^f} \nabla p \quad (1)$$

Flowing foams occur when snap-off or lamella division produces discrete bubbles. When foam is present, both the gas relative permeability k_{rg}^f and the gas apparent viscosity μ_g^f are affected. Its relative permeability will be smaller and its viscosity larger because the resistance to movement of lamellae.

The changing of gas relative permeability curve arises because only a fraction of the gas phase is actually flowing when foam is present. The increased gas trapping in the porous media will decrease the effect gas relative permeability value. The changing of apparent gas viscosity comes from the flow of foam bubbles. The generated lamellae will create resistance to mobile bubbles and then increase the apparent gas viscosity.

6.2 Foam simulation model description:

6.2.1 Change of k_{rg}^f

In the simulation, the relative permeability k_{rl} for liquid and gas phase is calculated using the Corey model as follows:

$$k_{rl} = k_{rl}^0 \left(\frac{S_l - S_{rl}}{1 - S_{rl}} \right)^{e_l} \quad (2)$$

From literature survey we know that liquid relative permeability stays the same either for with foam or without foam case. Gas relative permeability, k_{rg}^f , is changed from its original value k_{rg} when foam is present.

Some investigator, Falls *et al*, suggested that the effective foam permeability k_{rg}^f is reduced proportionally to the flowing gas fraction x_f :

$$k_{rg}^f(S_g) = x_f k_{rg}(S_g) \quad (3)$$

However, the fraction of gas that is flowing is a complex function of velocity, saturation, and capillary pressure. It is not easy to determine this function by simple experiments.

Since the reason for the changing of gas relative permeability is the increased gas trapping inside the porous media. Here we tried a simpler way to account for this: We just simply increase the gas residual saturation when calculating the gas relative permeability:

$$k_{rg}^f = k_{rg}^0 \left(\frac{S_g - S_{rg}^f}{1 - S_{rg}^f} \right)^{e_l} \quad (4)$$

When foam is weak, which means the flowing gas fraction is high, the value of S_{rg}^f should be lower compared to the value of S_{rg}^f in strong foam. The value of S_{rg}^f can be determined by doing sand pack experiments.

6.2.2 Change of μ_g^f

Friedmann *et al* used the following expression for gas apparent viscosity when foam is present:

$$\mu_g^f = \mu_g F_g k^{3/2} n_f (v_g / v_{ref})^{n-1} \quad \text{for } \mu_g^f > \mu_g \quad (5)$$

and $\mu_g^f = \mu_g$ for $\mu_g^f \leq \mu_g$

where μ_g is gas viscosity without foam, F_g is a geometric factor and the last term accounts for the shear-thinning nature of the foam. In their simulation approach, n_f is calculated by population-balance equations.

However, to solve a population-balance equation, many parameters need to be determined. These parameters are not easy to determine and so it is not very convenient to apply it to field application. Here, based on their thoughts, instead of solving the population-balance equation, we are trying to find some population correlation equation to calculate μ_g^f .

Bertin *et al* suggested a bubble-population correlation model to calculate foam texture n_f :

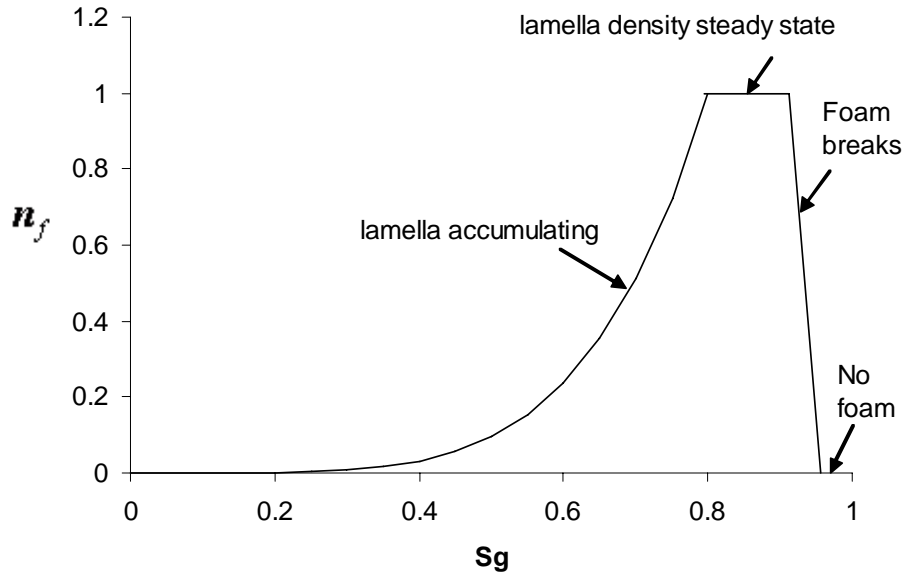


Figure 6-1 Relationship between S_g and n_f

$$n_f = \left(\frac{180(1-\phi)^2}{\phi^3} k \right)^{-3/2} S_g x_f \left(\frac{P_c^* - P_c(S_w)}{P_c(S_w)} \right) \quad (6)$$

He considered the limiting capillary effect in his model: the lamellae become more fragile when capillary pressure increases and are destroyed when P_c reaches its limiting value. Capillary pressure is also a function of gas saturation. So in general, we can simplify Eq (6) into the following way:

$$n_f = C_{nf} F(S_g) \quad (7)$$

Where C_{nf} is a constant coefficient and $F(S_g)$ is a function of S_g .

Now we need to find a detailed expression for $F(S_g)$ and then for n_f . Let's consider a foam generation process when gas invades into the porous media. Figure 6-1 shows a sketch of how the value of n_f changes with the changing of S_g .

When $S_g = 0$, which means there is no gas inside the porous media, of course there will be no foam texture, then we can get $F(S_g) = 0$ and $n_f = 0$.

With the increasing of gas saturation, lamellas are generated in the porous media. During this period, the foam generation rate is greater than the foam coalescence rate. We can call it the lamella density accumulating region. The lamella density value, n_f , increases in this region.

With the lamella density continuous accumulating, more and more lamellas are generated inside the porous media and the lamella coalescence rate will increase. When the gas saturation is greater than some particular value, S_{gm} , the foam generation rate and coalescence rate will be equal to each other. For simplicity of the model, we just assume they remain equal until at last the gas saturation is greater than a limiting gas saturation S_g^* at which foam breaks. During this period, n_f reaches its maximum value and remains a constant. We can call it lamella density steady state region.

When $S_g \geq S_g^*$ where S_g^* is the saturation at which $P_c(S_g^*) = P_c^*$, the capillary pressure in the porous media is greater than the limiting capillary pressure. According to the limiting capillary pressure theory, foam bubbles will break under this condition. After foam breaks, we will get $n_f = 0$ and $F(S_g) = 0$ again.

Following all of these analysis, we can define a correlation equation for n_f as a function of S_g and derive a expression of μ_g^f in the following format:

When $S_g < S_{gm}$, it is the lamella density accumulating region,

$$F(S_g) = \left(\frac{S_g}{S_{gm}} \right)^m, \text{ and } n_f = C_{nf} \left(\frac{S_g}{S_{gm}} \right)^m \quad (8)$$

Substitute Eq.(8) into Eq.(5) and combine the coefficients $k^{3/2}C_{nf}$ into a new coefficient $C_{\mu f}$, we can get the expression of μ_g^f in this region:

$$\mu_g^f = \mu_g F_g C_{\mu f} \left(\frac{S_g}{S_{gm}} \right)^m (v_g / v_{ref})^{n-1} \quad (9)$$

When $S_{gm} < S_g \leq (S_g^* - \varepsilon)$, it is the lamella density steady state region, in this region,

$$F(S_g) = 1, \text{ and } n_f = C_{nf} \quad (10)$$

The expression of μ_g^f in this region will be:

$$\mu_g^f = \mu_g F_g C_{\mu f} (v_g / v_{ref})^{n-1} \quad (11)$$

When $(S_g^* - \varepsilon) < S_g \leq (S_g^* + \varepsilon)$, foam breaks in this transient region,

$$F(S_g) = \left(\frac{S_g^* + \varepsilon - S_g}{2\varepsilon} \right), \text{ and } n_f = C_{nf} \left(\frac{S_g^* + \varepsilon - S_g}{2\varepsilon} \right) \quad (12)$$

In this transient region,

$$\mu_g^f = \mu_g F_g C_{\mu f} \left(\frac{S_g^* + \varepsilon - S_g}{2\varepsilon} \right) (v_g / v_{ref})^{n-1} \quad (13)$$

When $S_g > (S_g^* + \varepsilon)$, the capillary pressure is larger than the limiting capillary pressure and no foam exists,

$$F(S_g) = 0 \text{ and } n_f = 0 \quad (14)$$

In this no foam region,

$$\mu_g^f = \mu_g \quad (15)$$

Here we defined four foam regions. 1. lamella density accumulating, 2. lamella density steady state, 3. foam breaks transient region, 4. no foam region. Actually in our 1-D column and 3-D sand tank experiments, we only observed the first two regions. In other words, the generated foam is stable enough and didn't break under our experimental conditions. Our investigation and simulation are basically in these first two regions. But we still list the proposed equations for the last two foam regions here for the completion of the foam model.

6.2.3 Model summary and discussion:

This model modifies both of the gas relative permeability curve and the apparent gas viscosity to simulate foam flow in porous media.

In this model, there are 9 parameters from these equations: S_{rg}^f , S_{gm} , $C_{\mu f}$, v_{ref} ,

m , n , F_g , S_g^* and \mathcal{E}

Among these parameters, S_g^* and \mathcal{E} are parameters for the foam breaking transient region and the no foam region. Because in our experiments we did not observe these two regions, we did not try to determine these two parameters in our experiments and just focused our efforts on determining the parameters in the first two foam regions.

Among the remaining parameters, S_{rg}^f , S_{gm} , v_{ref} , m and n can be determined by performing column foam experiments. $C_{\mu f}$ is a coefficient which combines the effects of pressure gradient, permeability and surfactant concentration. The value of it represents the strength of the generated foam at steady state and can also be determined by 1-D column experiments. F_g is a geometry factor which represents the effects of flow dimensions on foam strength. For simplicity, we just define F_g equals to be one in 1-D foam flow. From our experimental observation among 1-D and 3-D experiments, the value of F_g is different for 1-D or 3-D foam flow. The F_g value for 3-D foam flow can be estimated by doing history match simulations.

6.3 1-D Column Experiments: Parameter Determination:

Some 1-D column foam experiments were performed to determine the simulation parameters for the simulation model. The experimental set up is similar to that in the surfactant screening experiment (Figure 1-1). The column is 1 ft long and packed with 40 darcy or 200 darcy sand. Gas or surfactant solution

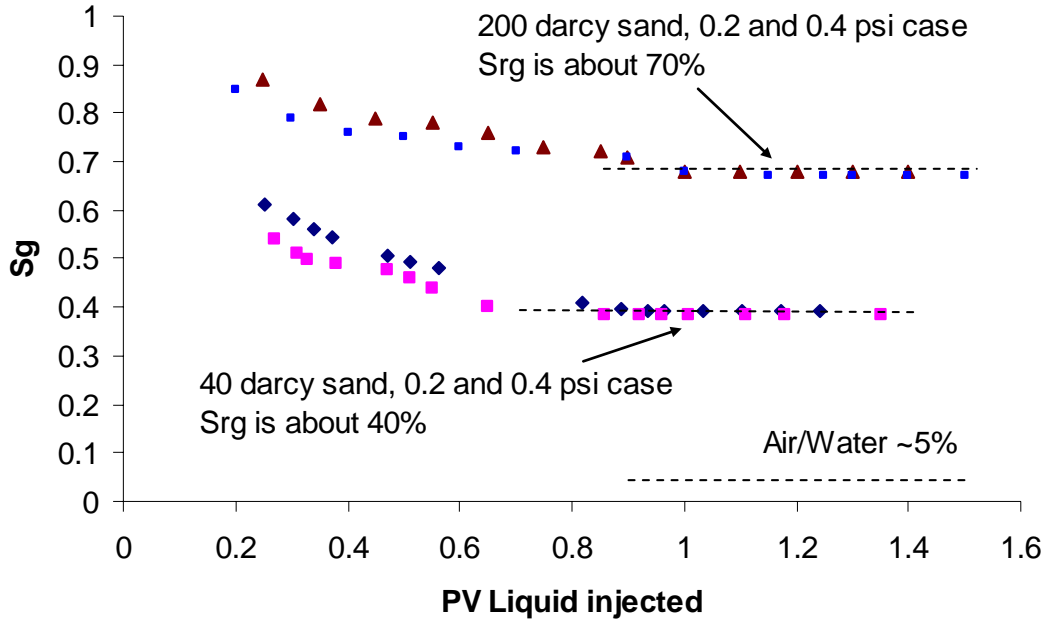


Figure 6-2 Gas residual saturation measurement using 1-D column

can be injected from one end of the column and fluids produced from the other end. A pressure transducer is used to record the injection pressure when needed. The only difference from Figure 1-1 is we were not using co-injection in these parameter determining experiments. Instead, f_g equaled to 100% in these experiments.

6.3.1 Determine the gas residual saturation when foam is present

To determine the residual gas saturation inside the column when foam is present, the column was pre-filled with 0.05% CS330+0.05% C13-4PO surfactant solution. Gas was injected into the column at a constant injection pressure. After all of the column was swept by foam and the injection rate reached its steady state, gas injection was turned off and surfactant solution was re-injected into the column under the same constant injection pressure of gas injection. When the injected liquid volume equals to the produced liquid volume in some time interval, by doing a material balance of the total injected and produced liquid volume, we can calculate the residual gas saturation inside the column. The gas residual saturation for both of the 40 darcy and 200 darcy sand were measured. For each of these sand, two different injection pressure, (0.2 psi and 0.4 psi) experiments were performed. Figure 6-2 shows the measured gas saturation vs. injected

liquid PV. From the results we can see for 40 darcy sand, the gas residual saturation when foam was present was about 40%, which did not change much with the change of injection pressure. For 200 darcy sand, the gas residual saturation when foam was present was about 70% and it also did not change much with the change of injection pressure.

6.3.2 Determine the parameters for foam shear thinning effect (v_{ref}, n), saturation dependence (S_{gm}, m) and $C_{\mu f}$.

From Eq.(9), we can get the following relationship:

$$\ln(\mu_g^f) - (n-1)\ln(v_g / v_{ref}) = \ln(\mu_g F_g C_{\mu f}) - m \ln S_{gm} + m \ln S_g \quad (16)$$

From this equation, we can find that when the value of S_g is a constant, the right side of the equation will be a constant and there will exist a linear relationship between $\ln(\mu_g^f)$ and $\ln(v_g)$, from the slope of the plot we can get the value of n.

The determination of m value depends on which kinds of experiment will be performed. If the experiment is performed under constant injection rate, which means v_g is a constant, then there will be a linear relationship between $\ln(\mu_g^f)$ and $\ln S_g$. The slope of the plots will be m. For constant injection pressure experiments, we can record every corresponding v_g for every measured S_g , then the linear relationship will exist between $\ln(\mu_g^f) - (n-1)\ln(v_g / v_{ref})$ and $\ln S_g$. The slope of the plots will also be m.

6.3.2.1 v_{ref} and n determination

To determine v_{ref} and n , the column was filled by surfactant solution first and then gas was injected into the column in a high injection pressure, i.e. 7 psi. After all of the column was swept by strong foam and the average gas saturation in the column did not change any more, the gas injection was turned off for several minutes to let the inside pressure of the column drops to zero. Then gas was re-injected into the column under different injection rates, the pressure drop for different injection rate was recorded to calculate the corresponding effective gas viscosity at that time using Eq. (1) and (2).

Both of the 40 darcy and 200 darcy sand were tested to measure the shear thinning effect parameters.

Figure 6-3 shows the plot of gas superficial velocity vs. μ_g^f for 40 darcy sand column. From this figure we can see when gas superficial velocity is less

than about 2 ft/day, there is no shear thinning effect. When the velocity becomes greater than 2 ft/day, the shear thinning effect reduces the value of μ_g^f and the

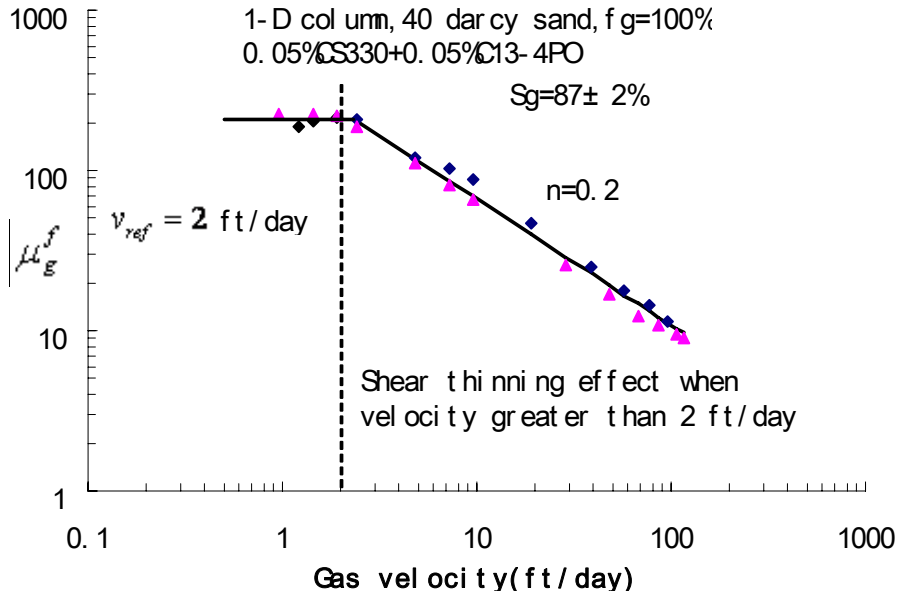


Figure 6-3 Foam shear thinning effect at high velocity, 40 darcy sand

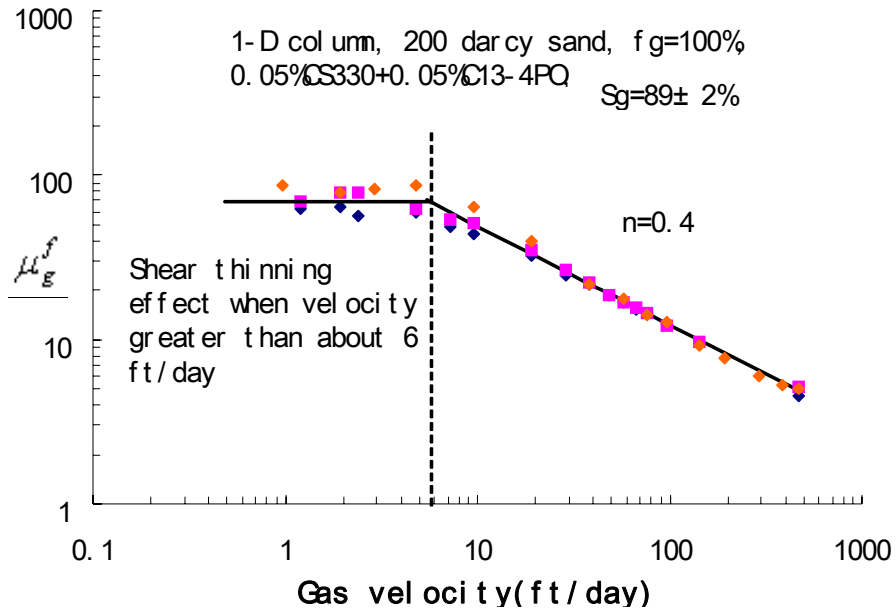


Figure 6-4 Foam shear thinning effect at high velocity, 200 darcy sand

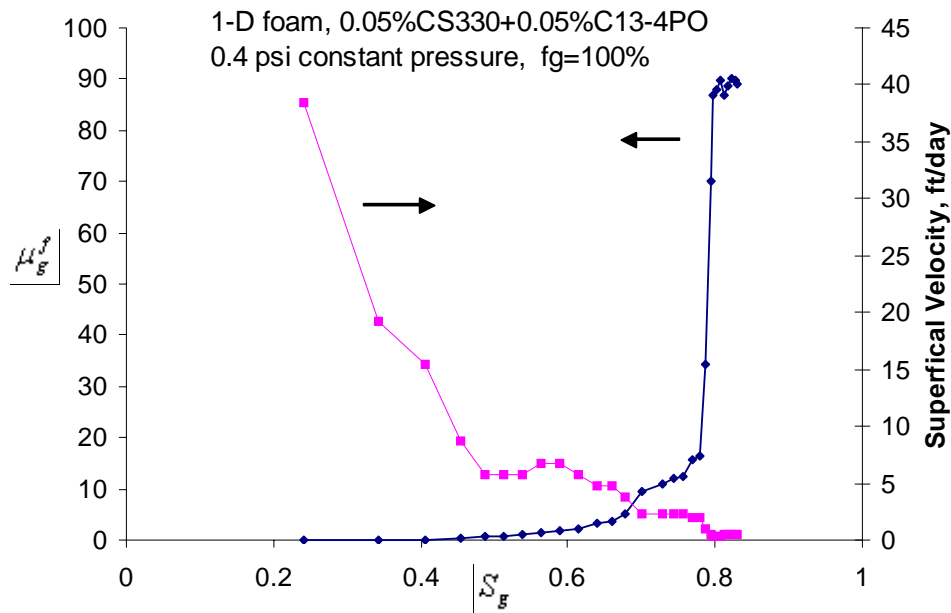
value of the power law exponent, n , is about 0.2. So for 40 darcy sand, we get $v_{ref} = 2$ ft/day and $n = 0.2$

Figure 6-4 shows the results for 200 darcy sand column. The reference velocity for 200 darcy sand is greater than that for 40 darcy sand. From this figure we can see when gas superficial velocity is greater than about 6 ft/day, the shear thinning effect reduces the value of μ_g^f . The value of the power law exponent, n , is about 0.4 which is also greater than that for the 40 darcy sand. The values of v_{ref} and n for 200 darcy sand are 6 ft/day and 0.4 correspondingly.

6.3.2.2 S_{gm} , m and $C_{\mu f}$ determination

These three parameters can be determined by doing constant injection pressure foam experiments. The injection pressure was kept a constant during the experiment. The average gas saturation in the column and the injection rate were recorded and the corresponding μ_g^f was calculated from these records.

6.3.2.2.1 40 darcy sand column experimental results



**Figure 6-5 Gas saturation vs. foam effective viscosity and gas superficial velocity.
40 darcy sand, 0.4 psi constant injection**

- 0.4 psi constant injection pressure

Figure 6-5 shows the relationship between μ_g^f and S_g in a 0.4 psi constant injection pressure foam experiment for 40 darcy sand column. From this figure we can see that with the increasing of gas saturation, foam effective viscosity also increased. The value of μ_g^f kept increasing when S_g was less than 0.8 and increased dramatically when S_g was between 0.75 and 0.8. But when S_g was greater than 0.8, the value of μ_g^f did not change much with the increasing of S_g and was approximately a constant value. So for this experiment, the S_{gm} value should be around 0.8. When $S_g < S_{gm}$, foam generation rate is greater than foam

coalescence rate and the value of μ_g^f increases. When $S_g > S_{gm}$, these two rate equals to each other and μ_g^f is approximately a constant value.

Also, from Figure 6-5, we can find that at steady state, the gas saturation is more than 80% and the gas superficial velocity is less the reference velocity 2 ft/day. So, there was no velocity effect at steady state. From Eq.11, we can get:

$$\mu_g^f = \mu_g F_g C_{\mu f} \tag{17}$$

Since we define F_g to be one in 1-D foam flow and the value of the steady state effective viscosity was about 90 cp, if we use 0.02 cp as the μ_g value, we will be able to calculate the value of $C_{\mu f}$. From the calculation, $C_{\mu f}$'s value is around 4500

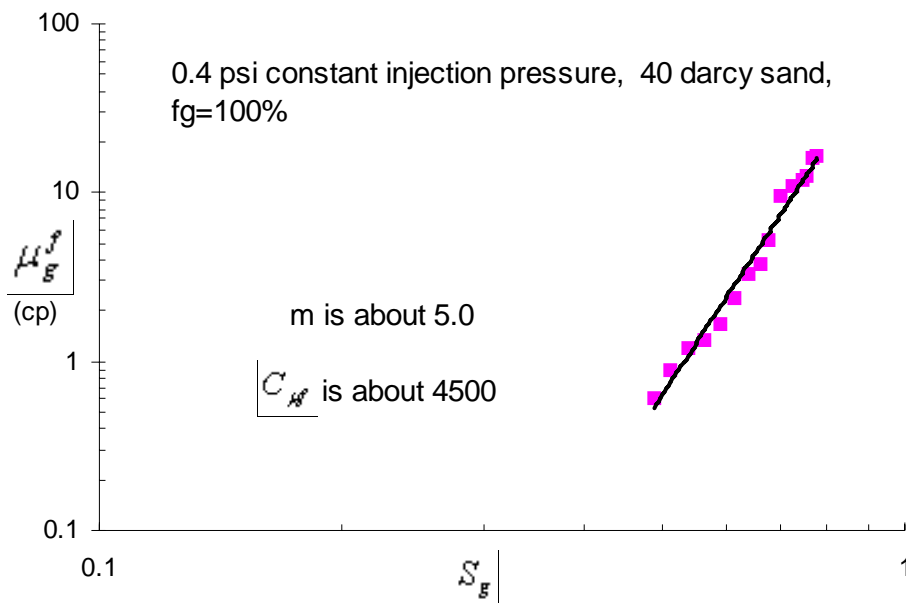


**Figure 6-6 Relationship between foam effect viscosity and gas saturation
40 darcy sand, 0.4 psi constant injection**

Figure 6-6 shows the log-log plots of μ_g^f vs. S_g . According to Eq.(16), for constant injection pressure experiments, there should be a linear relationship between $\{\ln(\mu_g^f) - (n-1)\ln(v_g / v_{ref})\}$ and $\{\ln S_g\}$. The slope of it will be the value of m . From the plots we can see the linear relationship exists and the value of m is around 5.0

- 0.2 psi constant injection pressure

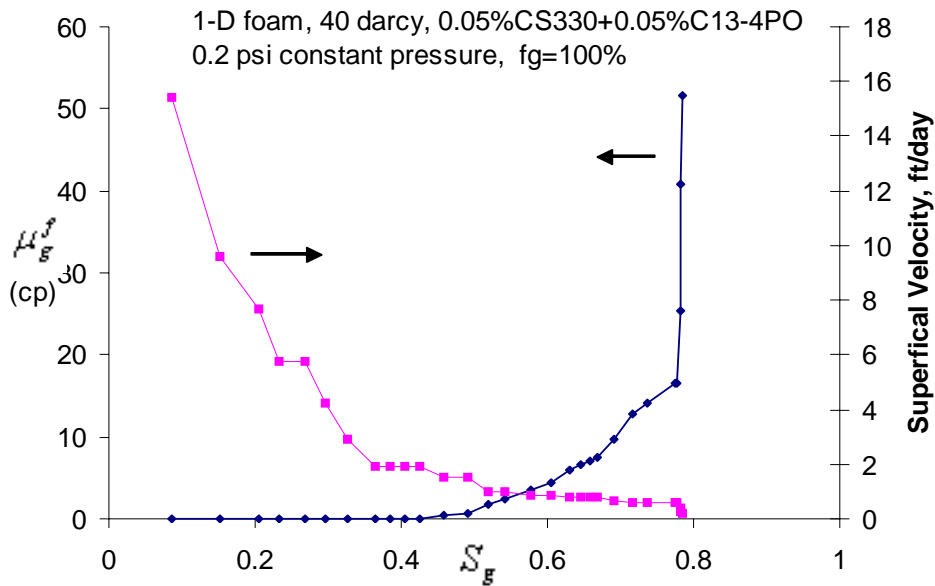
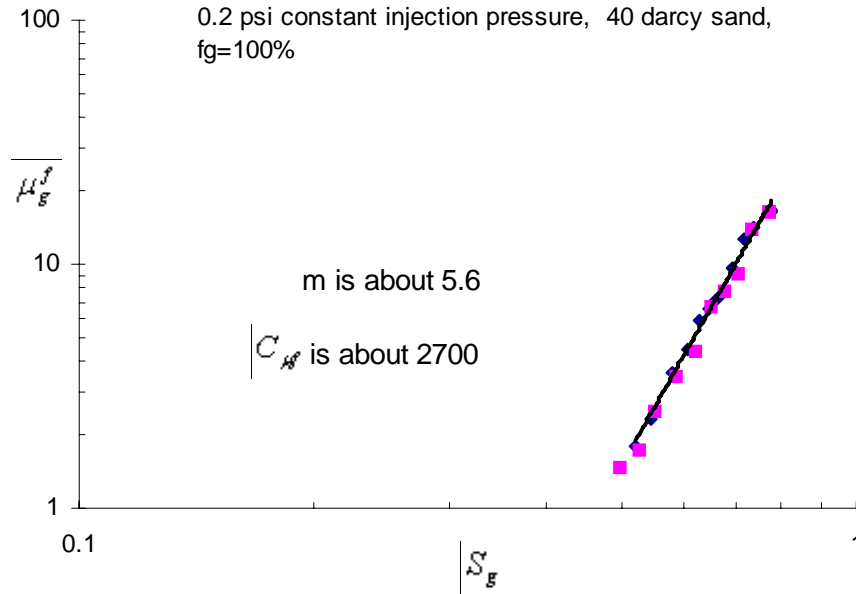


**Figure 6-7 Gas saturation vs. foam effective viscosity and gas superficial velocity.
40 darcy sand, 0.2 psi constant injection**

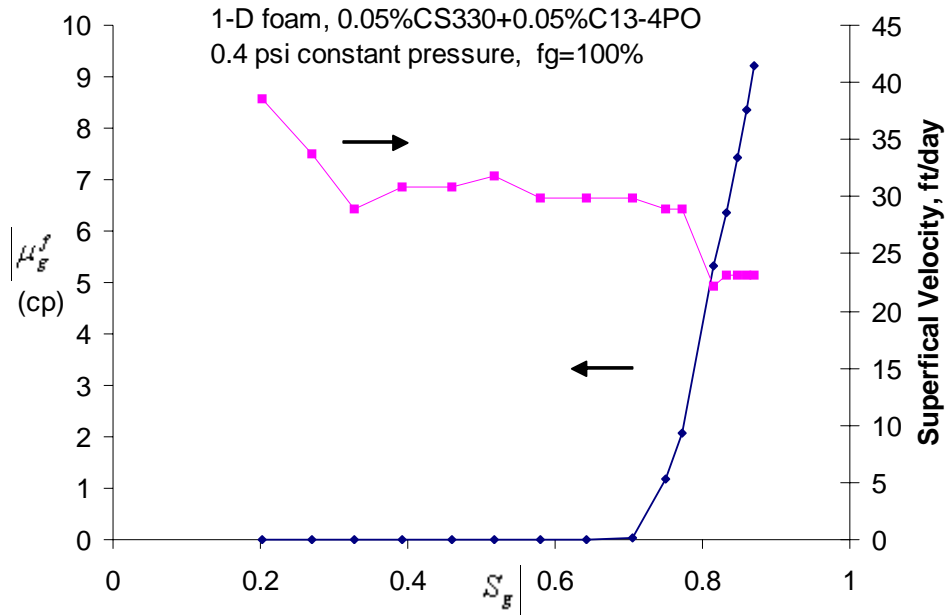
A 0.2 psi constant injection pressure experiment was performed in this 40 darcy column also. Figure 6-7 shows the relationship among S_g , μ_g^f and gas superficial velocity. The curves have a similar shape as in the 0.4 psi experimental results. Foam effective viscosity increased with the increasing of gas saturation and increased dramatically when S_g was between 0.77 and 0.78. The highest S_g which was reached in the 0.2 psi experiment was less than 0.8. It is lower than the highest S_g value got in the 0.4 psi experiment. This is because in the 0.2 psi experiment, the injection pressure was lower and the generated foam was weaker. Less gas can invade the small pores of the porous media which then results in a lower gas saturation. In the 0.2 psi constant injection pressure experiment, since the highest gas saturation is lower than 0.8, we can still take the reference S_{gm} value to be 0.8 in the simulation model. From Figure 6-7 we can also find out that at the steady state, there was no velocity effect on foam effective viscosity value. Then from Eq.(17), we can determine the value of $C_{\mu f}$, which is about 2700 for this experiment.

Figure 6-8 shows the linear relationship between $\ln(\mu_g^f)$ and $\ln(S_g)$. From the slope of the plot we get the value of m , which is around 5.6. Compared to the m value, 5.0, in the 0.4 psi experiment, the value of m did not change much with the change of injection pressure. It is reasonable that the m value is a little bit larger in the 0.2 psi injection pressure experiment than in the 0.4 psi injection

pressure experiment. It is because in the 0.2 psi injection pressure experiment,



**Figure 6-8 Relationship between foam effect viscosity and gas saturation
40 darcy sand, 0.2 psi constant injection**



**Figure 6-9 Gas saturation vs. foam effective viscosity and gas superficial
velocity.
200 darcy sand, 0.4 psi constant injection**

the pressure gradient is lower and then it will take a longer time to reach the same foam strength compared to the 0.4 psi injection pressure experiment. But

since these two m value did not change much in these two experiments, for simplicity, we just take m value to be 5.0 in both of the 0.4 and 0.2 experiments in our simulation.

6.3.2.2.2 200 darcy sand column experimental results

- 0.4 psi constant injection pressure

Figure 6-9 shows the relationship among S_g , μ_g^f and gas superficial velocity for the 200 darcy sand column under 0.4 psi constant injection pressure. The value of μ_g^f increased with the increasing of S_g . The highest gas saturation we got in this experiment was about 0.85. However, we did not observe a platform in this plot where μ_g^f did not change much with changing of S_g . The platform may exist in some higher gas saturation value but in this experimental condition, it didn't been reached. The value of S_{gm} should be between 0.85 and the water residual saturation. Since the value of 0.85 is already very high and

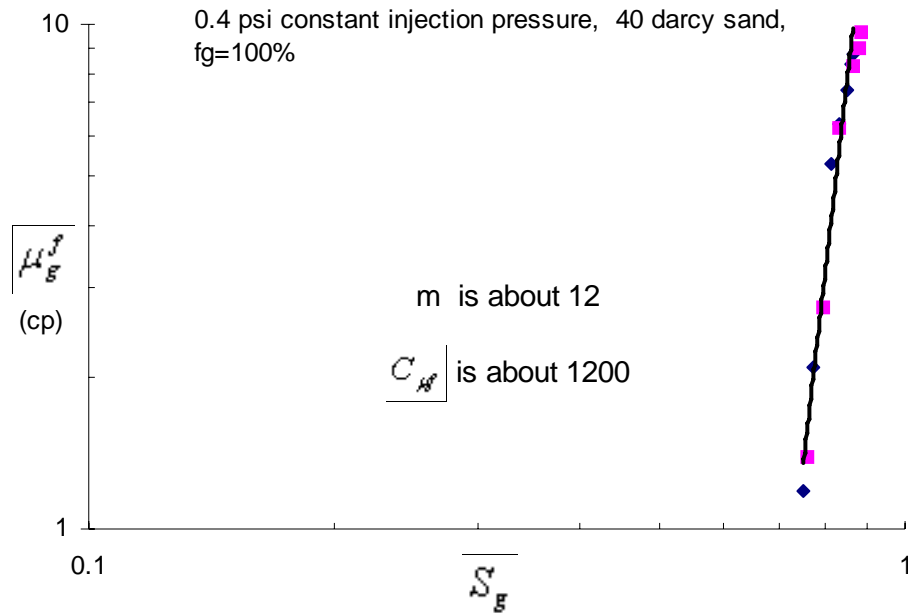


**Figure 6-10 Relationship between foam effect viscosity and gas saturation
200 darcy sand, 0.4 psi constant injection**

very close to the water residual saturation, though the actual value of S_{gm} may be a little bit higher than 0.85, we can just choose 0.85 as the value of S_{gm} . The simulated results will not change much by doing this simplification.

At steady state, the value of μ_g^f reached its highest value which was about 9 cp. But velocity effect still existed at the steady state. The

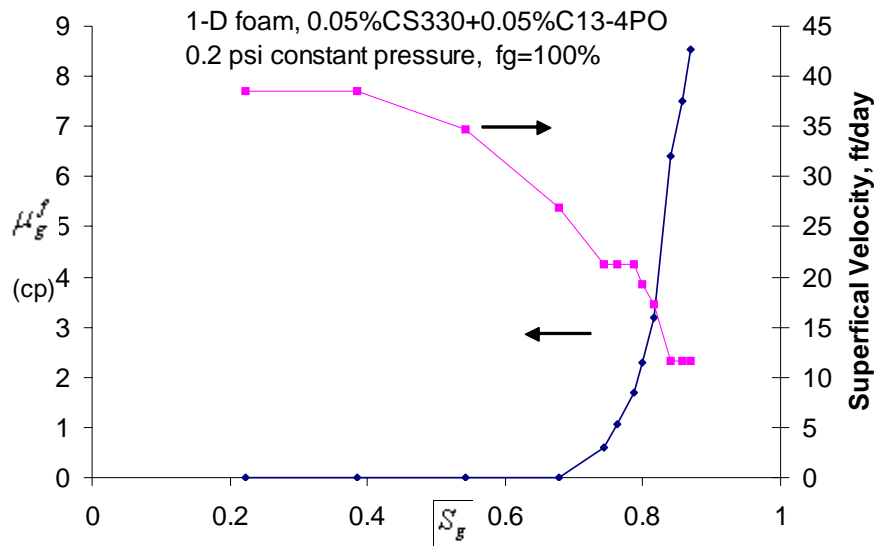


**Figure 6-11 Gas saturation vs. foam effective viscosity and gas superficial velocity.
200 darcy sand, 0.2 psi constant injection**

superficial gas velocity at steady state was about 23 ft/day, which was higher than the reference gas velocity (6 ft/day) we determined in our shear thinning effect experiment. From Eq.11, we can calculate the value of $C_{\mu f}$ for this experiment, which was about 1200.

Figure 6-10 shows the linear relationship between $\ln(\mu_g^f)$ and $\ln(S_g)$. From this plot we can determine the value of m , which was about 12 for this experiment.

- 0.2 psi constant injection pressure

A low injection pressure experiment, 0.2 psi constant injection pressure, was also performed in this 200 darcy sand column. Figure 6-11 shows the relationship among S_g , μ_g^f and gas superficial velocity. At steady state, the highest gas saturation value in the experiment was also about 85% and we did not observe a plateau in the μ_g^f curve also. Following the discussion in the 0.4 psi constant injection pressure experiment, we can also take the S_{gm} value to be the steady state S_g value, 0.85. In this experiment, as steady state, the highest value of μ_g^f was about 8 cp. The superficial gas velocity at steady state was about 13 ft/day which is still larger than the reference gas velocity. Again, from Eq.11, we can calculate the value of $C_{\mu f}$ for this experiment, which was about 650.

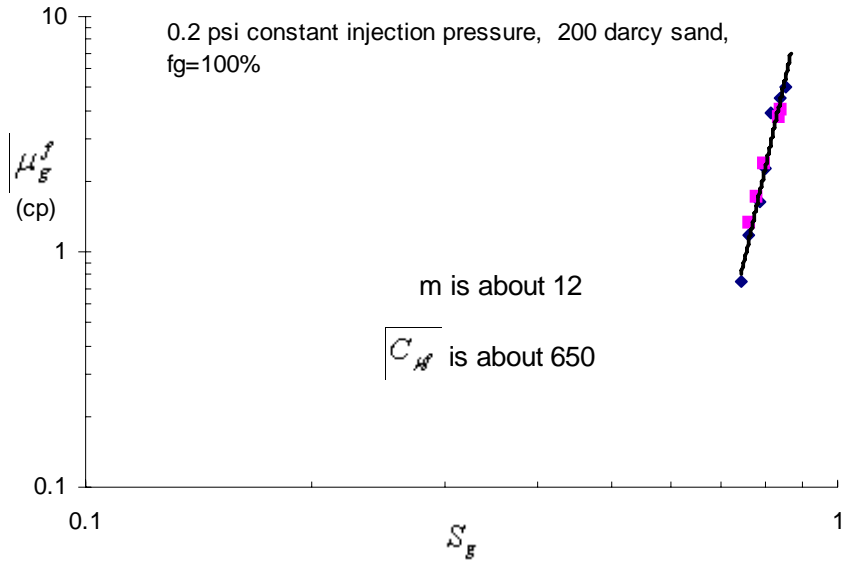


**Figure 6-12 Relationship between foam effect viscosity and gas saturation
200 darcy sand, 0.2 psi constant injection**

Figure 6-12 shows the linear relationship between $\ln(\mu_g^f)$ and $\ln(S_g)$. We found the value of m still be about 12 which did not change from the 0.4 psi constant pressure injection experiment.

6.3.3 Table of 1-D parameters:

Table 6-1 lists the parameters we determined from the 1-D column experiments for 40 darcy and 200 darcy under 0.4 psi and 0.2 psi constant injection pressure.

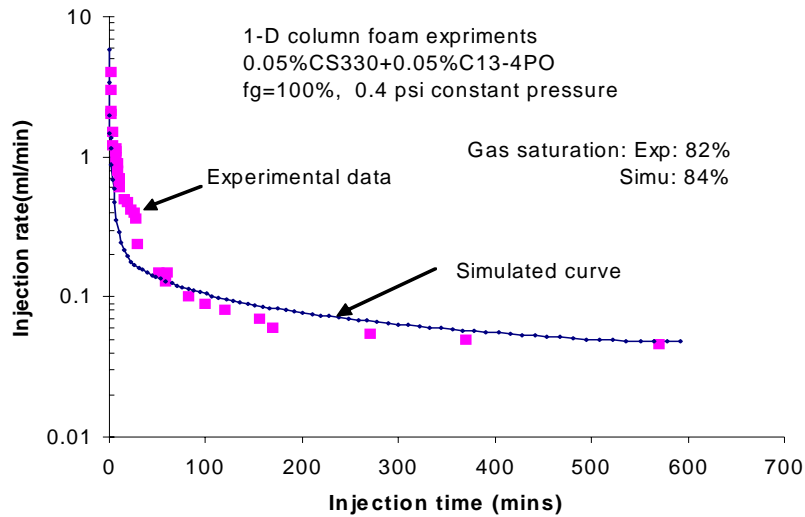
1-D column	Injection pressure	S_{rg}^f	v_{ref}	n	S_{gm}	m	$C_{\mu f}$
40 darcy	0.4 psi	0.4	2 ft/day	0.2	0.80	5	4,500
	0.2 psi	0.4	2 ft/day	0.2	0.80	5	2,700
200 darcy	0.4 psi	0.7	6 ft/day	0.4	0.85	12	1,200
	0.2 psi	0.7	6 ft/day	0.4	0.85	12	650

Table 6-1 Parameters determined from 1-D column experiments

6.4 Case Study: Foam simulations --- 1-D and 3-D comparison

6.4.1 1-D column foam simulation results

The determined parameters were used to simulate the corresponding 1-D column foam experiments. Figure 6-13,6-14,6-15,6-16 show the simulated injection rate compared to the experimental result for 40 darcy and 200 darcy sand under 0.4 and 0.2 constant injection pressure correspondingly. The simulated results matched the experimental results. Table 6-2 lists the comparison of simulated and experimental average gas saturation. The simulated gas saturation matched the experimental results also. From these comparisons we can see the 1-D column experimental results can be simulated and matched by using the proposed foam model and determined parameters.



**Figure 6-13 1-D column simulation results vs. experimental data
40 darcy sand, 0.4 psi constant injection pressure**

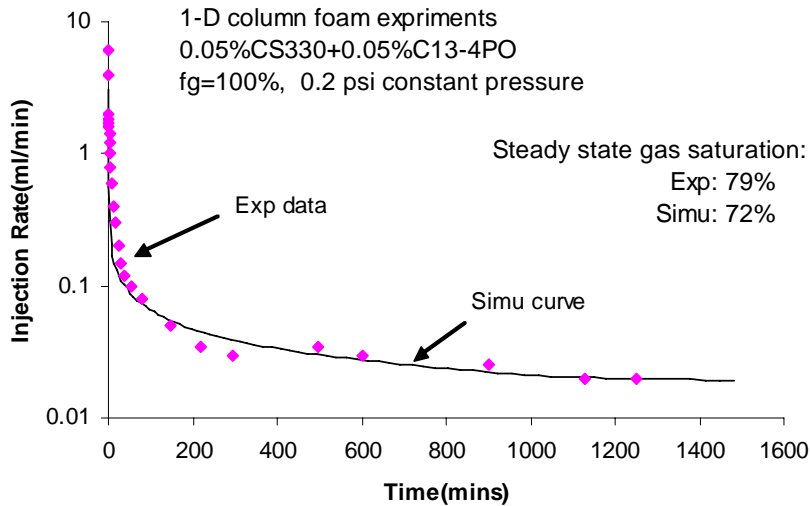


**Figure 6-14 1-D column simulation results vs. experimental data
40 darcy sand, 0.2 psi constant injection pressure**

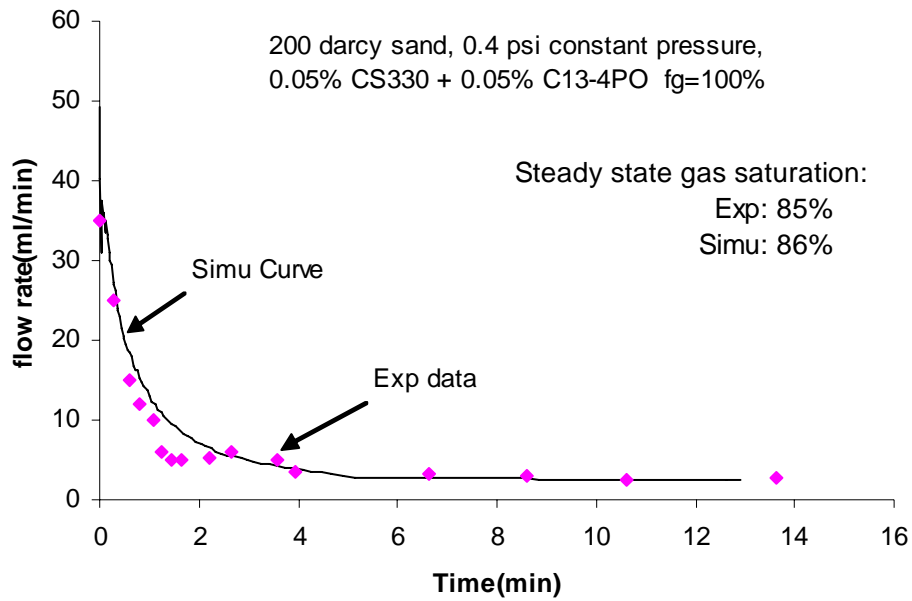


**Figure 6-15 1-D column simulation results vs. experimental data
200 darcy sand, 0.4 psi constant injection pressure**

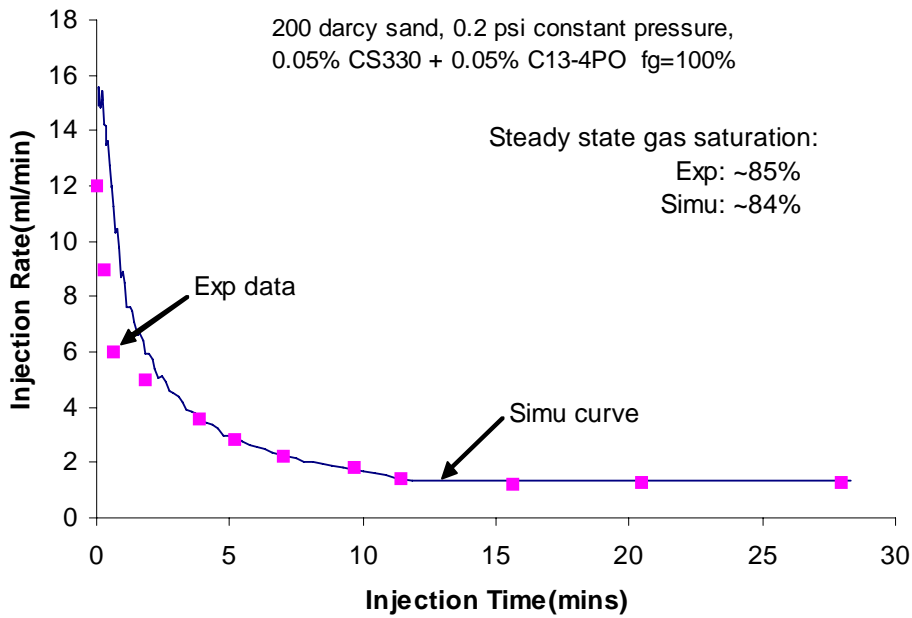


**Figure 6-16 1-D column simulation results vs. experimental data
200 darcy sand, 0.2 psi constant injection pressure**

0.05%CS-330		40 darcy sand column		200 darcy sand column	
0.05%C13-4PO fg=100%		0.4 psi	0.2 psi	0.4 psi	0.2 psi
Sg	Experimental	82%	79%	85%	85%
	Simulated	84%	72%	86%	84%

Table 6-2 Comparison of simulated and experimental gas saturation

6.4.2 3-D tank foam simulation

6.4.2.1 Homogeneous sand tank simulation

After the 1-D column simulations, we tried 3-D sand tank history match simulations using the same parameters from 1-D simulation. The homogeneous tank was packed using the same homogeneous 40 darcy sand we used in the column experiment. The dimension of the 3-D tank is 2x2x2 ft. Two experiments were performed in this sand pack, one was performed 0.8 psi constant injection pressure, the other one was performed under 0.39LPM constant injection rate(about 0.4 psi injection pressure). Compare to the column experiments, the overall pressure gradient in the tank experiments are equal to the pressure gradient of corresponding 1-D column experiments, i.e, in the 0.8 psi constant

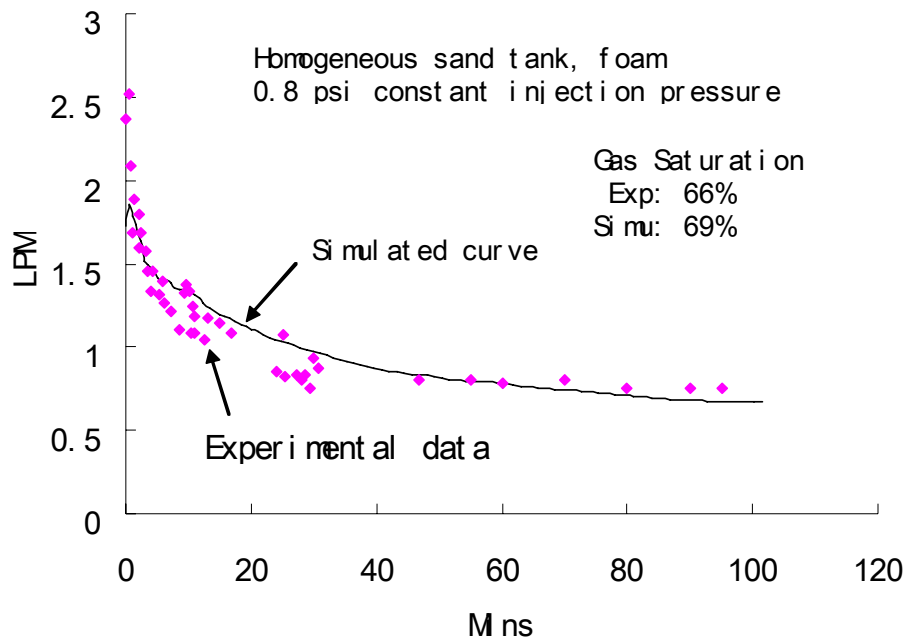


Figure 6-17 Homogeneous 3-D sand tank, 40 darcy, 0.8 psi constant injection pressure

injection pressure tank experiment, the overall pressure gradient is about 0.4 psi/ft which is equal to the pressure gradient in the 0.4 psi constant pressure 1-D column experiment. For the 0.39 LPM constant injection rate experiment, since the measured injection pressure reached and remained 0.4 psi almost from the beginning of the experiment, we just use the 0.2 psi constant injection pressure 1-D column experiment results as its comparison standards, both of these two experiments have a constant overall pressure gradient of about 0.2 psi/ft. In these experiments, the only difference is the flow dimension, 1-D column is 1-dimension flow and the 3-D tank is 3-dimension flow.

In our 3-D sand tank simulation, we kept all the parameters the same as in the 1-D column simulations except for the value of F_g . This value represents the effects of flow dimensions on foam strength. To get the best match simulation results, we needed to choose a smaller F_g value compared to the 1-D column simulation. In 1-D foam flow, for convenient, we defined this value to be one. In 3-D simulation, we found this value must be set to be around 0.21 to get the best match results

For the 0.8 psi constant injection pressure 3-D foam experiment, Figure 6-17 shows the simulated injection rate compared to the experimental data. The average gas saturation is also matched. After around 1 PV gas injected, the simulated average gas saturation inside the tank is about 69% and the experimental data is 66%. Figure 6-18 shows the simulated gas fractional flow contour plots compared to the experimental data. After about 1 PV gas injected, gas contacted more than 75% of the cross section area of the tank. Figure 6-19 shows the simulated inside pressure profile compared to the experimental data. From the pressure profile we can see that the highest pressure drop is around the middle part of the tank. The region near the injection well (p1) has lower

Homogeneous Sand Tank

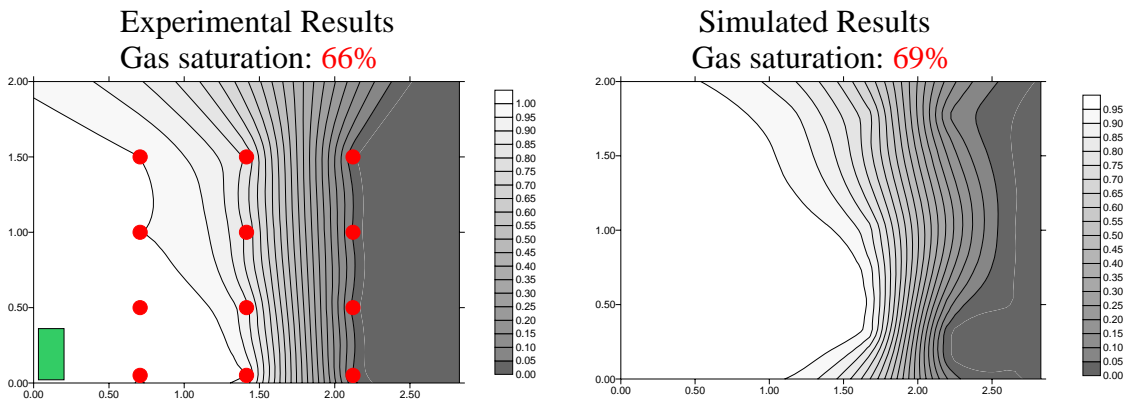


**Figure 6-18 Gas fractional flow contour plots, diagonal cross section
0.8 psi constant pressure injection, 1 PV gas injected**

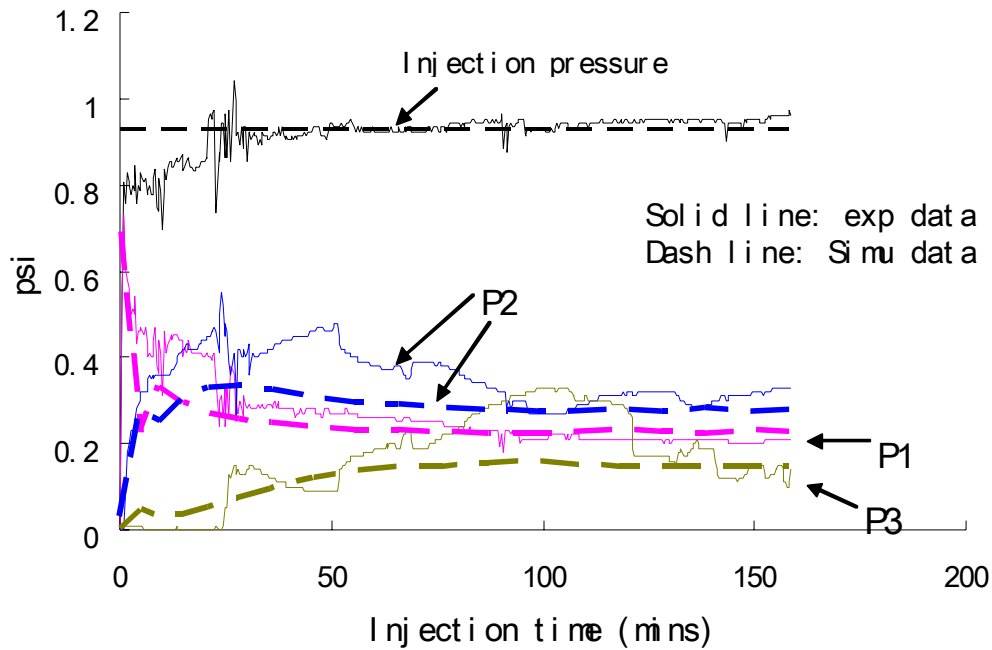


**Figure 6-19 Homogeneous 3-D sand tank, foam, pressure profile
0.8 psi constant injection pressure**

Homogeneous Sand Tank

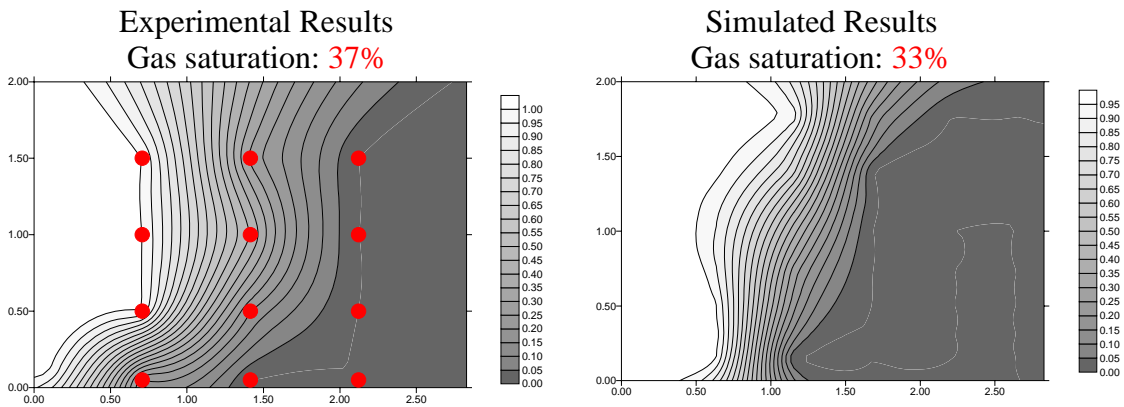


**Figure 6-20 Gas fractional flow contour plots, diagonal cross section
0.39 LPM constant injection rate, 1 PV gas injected**

pressure drop compared to the middle region (p2).

For the 0.4 psi constant injection pressure 3-D foam experiment, Figure 6-20 shows the simulated gas fraction flow contour plots compared to the experimental data. The simulated contour plots matched the experimental data. And the average gas saturation is also matched. In this experiment, the average

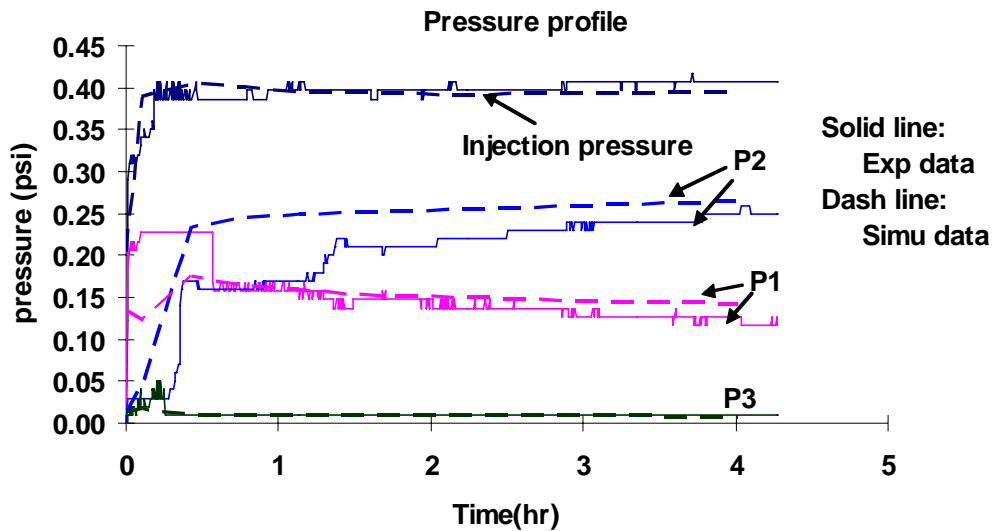


Figure 6-21 Homogeneous Sand Tank, 0.39LPM constant injection Pressure profile

gas saturation after about 1 PV gas injected was about 37% and the simulated result was about 33%. Figure 6-21 shows the comparison between the simulated pressure profile and the experimental data. Just like the 0.8 psi foam experiment, the pressure drop near the injection well (p1) is lower than the pressure drop in the farther region of the tank (p2).

6.4.2.2 F_g value obtained from the homogeneous sand tank

Experiments show that foam flow in 1-D is stronger than in 3-D. The reason for this phenomena is not known yet. In this foam model, we defined a dimensional parameter F_g to represent the phenomena. From the comparison of the case study simulations between 1-D and 3-D foam in homogeneous sand, we found that the value of this factor is about 0.21, which means if under the same conditions in our experiments, the 3-D foam flow is 5 times weaker than the 1-D foam flow.

6.4.2.3 Heterogeneous sand tank experiments simulation

The 3-D sand tank was repacked into a heterogeneous formation for more foam experiments. The formation of the heterogeneous has been described in earlier part of this report. One foam experiment was preformed under 0.8 psi constant injection pressure. In the history match simulation, for both of the 40 darcy sand and the 200 darcy sand, we kept most of the parameters from 1-

		S_{rg}^f	v_{ref}	n	S_{gm}	m	$C_{\mu f}$	F_g	
Homogeneous Sand									
0.4 psi constant injection pressure (1-D column, 1 ft)		0.4	2	0.2	0.80	5	4,500	1.00	
0.8 psi constant injection pressure (3-D tank, 2x2x2 ft)		0.4	2	0.2	0.80	5	4,500	0.21	
0.2 psi constant injection pressure (1-D column, 1 ft)		0.4	2	0.2	0.80	5	2,700	1.00	
0.39LPM constant rate (~0.4 psi injection pressure) (3-D tank, 2x2x2 ft)		0.4	2	0.2	0.80	5	2,700	0.21	
Heterogeneous Sand									
Case 1: 0.8psi constant injection pressure	High perm (200 darcy)	0.4 psi (1-D column)	0.7	6	0.4	0.85	12	1,200	1.00
		3-D sand tank	0.7	6	0.4	0.85	12	3,100	0.21
	Low perm (40 darcy)	0.4	2	0.2	0.80	5	4,500	0.21	
Case 2: 0.4psi constant injection pressure	High perm (200 darcy)	0.2 psi (1-D column)	0.7	6	0.4	0.85	12	650	1.00
		3-D sand tank	0.7	6	0.4	0.85	12	2,140	0.21
	Low perm (40 darcy)	0.4	2	0.2	0.80	5	4,000	0.21	

Table 6-3 Comparison of parameters for 1-D and 3-D simulation

D column experiments the same. We only changed the value of $C_{\mu f}$ to get the best match results. Table 6-3 lists the parameters which were chosen for the best match simulations. From this table we can see if we keep the F_g value the same as what we found from the homogeneous sand tank simulations, to get the best match results, the value of $C_{\mu f}$ in the high permeability layer needs to be higher than it is in the 1-D column experiments. For example, in the 200 darcy column experiment, the $C_{\mu f}$ is found to be about 1200, but in the 3-D heterogeneous simulation, keeping F_g as 0.21, a higher $C_{\mu f}$ value (3100) is needed which is about 3 times larger than the 1-D column value. This can be explained by the foam generation mechanism of snap-off: when gas flow from low perm region to the high perm region, because of the change of capillary pressure, foam can be

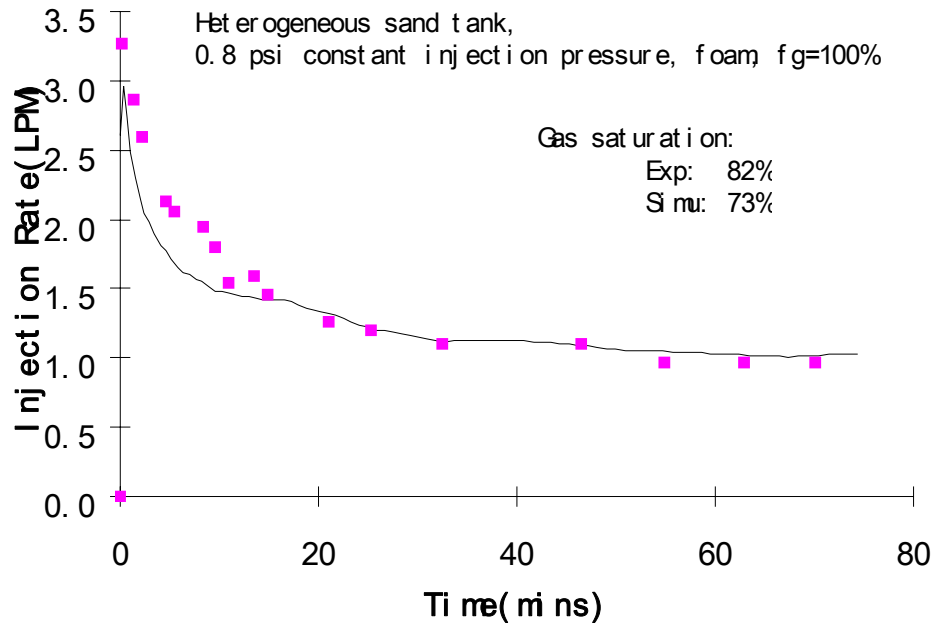


**Figure 6-22 Heterogeneous 3-D tank,
0.8 psi constant injection pressure**

Heterogeneous Sand Tank

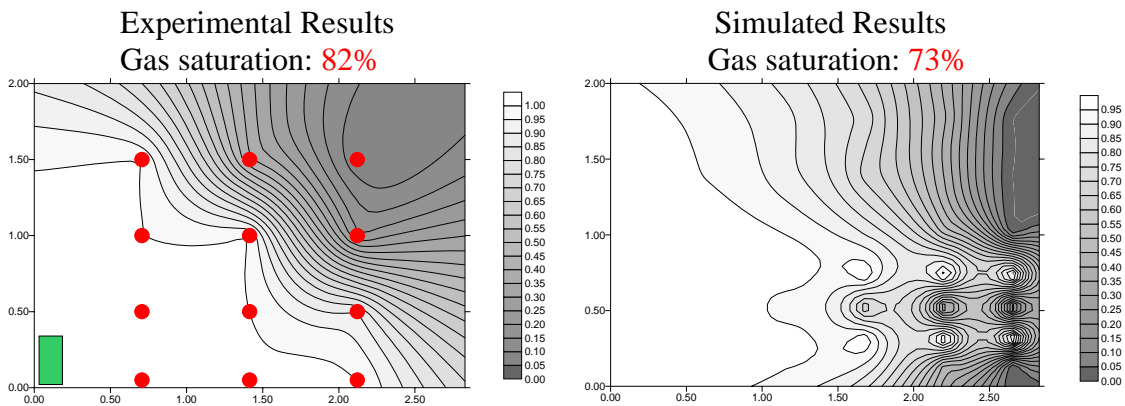


**Figure 6-23 Gas fractional flow contour plots, diagonal cross section
0.8 psi constant injection pressure, 1 PV gas injected**

generated along the boundary of the two regions by snap-off and hence the effective foam viscosity will be increased.

Figure 6-22 shows the comparison of simulated and experimental injection rate for the 0.8 psi constant injection pressure experiment. The simulated average gas saturation after 1 PV gas injected was about 74% and the experimental data was about 82%. Figure 6-23 shows the gas fractional flow contour plots after 1 PV gas injected. We can see most of the bottom of the tank

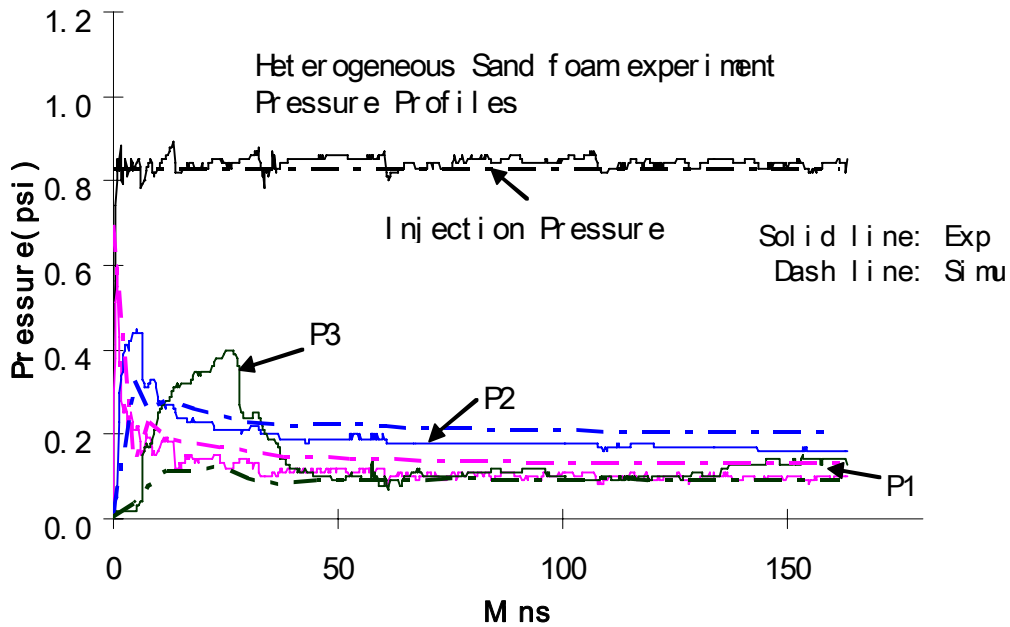


Figure 6-24 Heterogeneous 3-D tank, 0.8 psi constant injection pressure Pressure profile

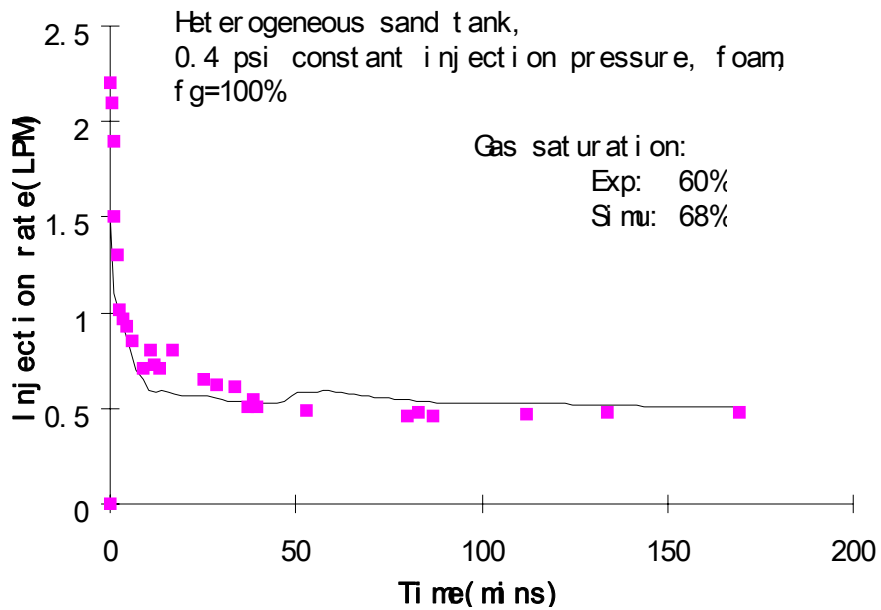
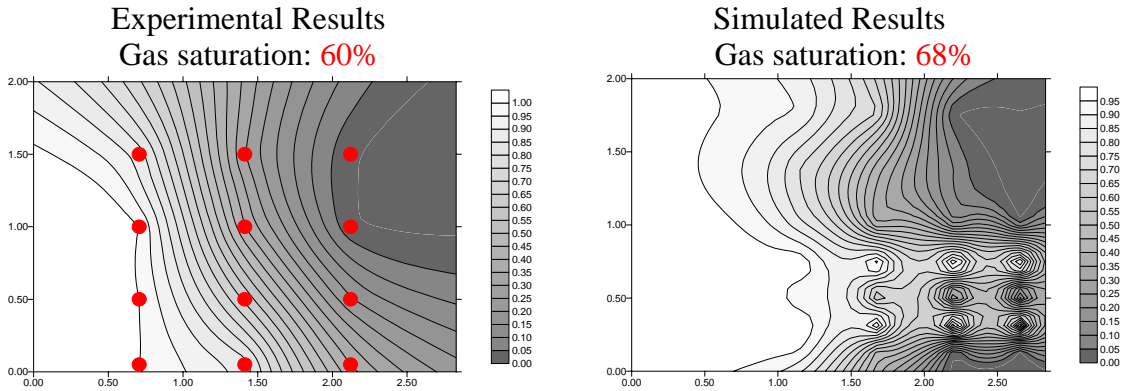


Figure 6-25 Heterogeneous 3-D tank, 0.4 psi Injection rate

was contacted by gas. Compared to Figure 6-20 of the homogeneous case, the lateral gas transport along the bottom of the tank was increased by the heterogeneous sand formation. Figure 6-24 shows the simulated pressure profile

Heterogeneous Sand Tank



**Figure 6-26 Gas fractional flow contour plots, diagonal cross section
0.4 psi constant injection pressure, 1 PV gas injected**

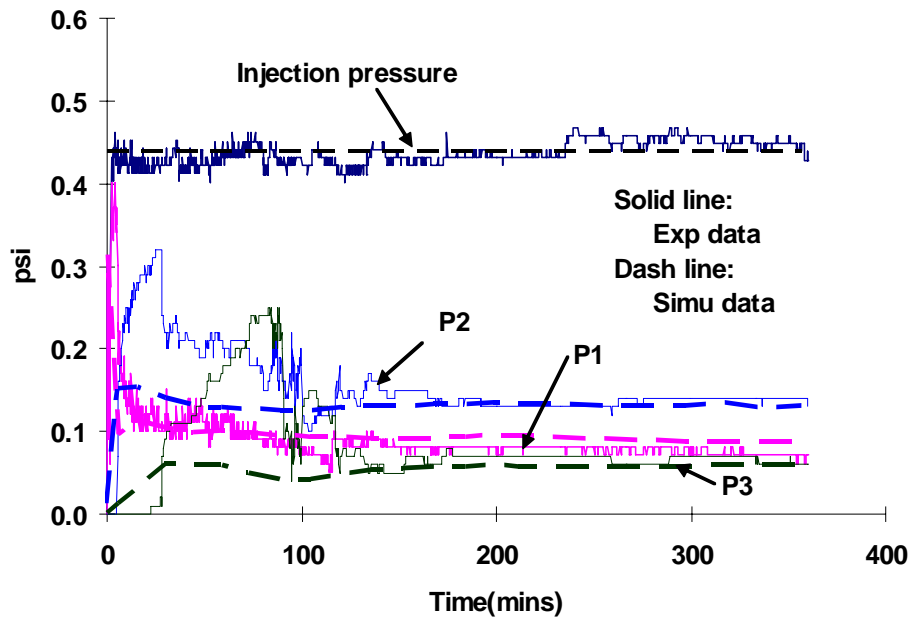


**Figure 6-27 Heterogeneous 3-D tank, 0.4 psi constant injection pressure
Pressure profile**

compared to the experimental data. The strongest foam region is also in the middle part of the tank.

Another foam experiment was performed under 0.4 psi constant injection pressure. Table 6-3 also lists the simulation parameters for this experiment. Because the injection pressure is lower than in the 0.8 psi case, the value of $C_{\mu f}$ was lower than the values in the simulation for 0.8 psi case. From the best

history match results, we can still find that the value of $C_{\mu f}$ in 3-D is larger than in 1-D column experiments. For the high permeability layer, the value of $C_{\mu f}$ increased more than 3 times and in the low permeability region, the value of $C_{\mu f}$ also increased, which means the heterogeneity not only increased the foam strength in the high perm region but also increased the foam strength in the low perm region. Figure 6-25 shows the comparison of simulated and experimental injection rate for the 0.4 psi constant injection pressure experiment. Figure 6-26 shows the comparison of gas fractional plots after 1 PV gas injected. The simulated average gas saturation after 1 PV gas injected was about 66% and the experimental data was about 60%. Figure 6-27 shows the simulated and experimental pressure profile.

6.5 Summary of Section 6

Foam generation is a complex process. For different experimental condition, i.e. different surfactant concentration, different injection pressure or injection rate, the generated foam strength may vary. A foam simulation model is present in this report trying to simulate 3-D foam by just doing 1-D experiments. In this model, when foam is present, both of the gas relative permeability curve and the apparent viscosity value are changed. The gas relative permeability curve changed because of the increased trapped gas saturation. The apparent viscosity is defined as a function of gas saturation, gas velocity and flow dimension. Most of its parameters can be determined by 1-D column experiments. Homogeneous 3-D foam simulations were performed using the parameters determined from the 1-D column experiments. A F_g value of about 0.21 is found to be needed to history match these 3-D homogeneous sand tank results. Taking the F_g value got from the homogeneous 3-D tank simulation, some more simulations were performed to simulate a heterogeneous sand pack foam experimental results. From the history match simulation results, we found that foam strength can be increased because of heterogeneity. In the high perm layer region, the value of $C_{\mu f}$ increased about 3 times. In the low perm region, the value of $C_{\mu f}$ also increased. In all these simulations, the F_g value was set to be 0.21

Task 7 - Design for a hypothetical field application.

7.1 Introduction

As our 2-D&3-D foam experiments have demonstrated, foam can improve the gas sweep efficiency and gas saturation in porous media. A new application of foam is in the area of aquifer remediation. In aquifer remediation process, foam was used for mobility control to displace DNAPL from low permeability sands that are often unswept during the remediation process. The first field demonstration of the surfactant/foam process for removal of DNAPL from a heterogeneous alluvial was conducted at Hill Air Force Base in Utah [Hirasaki *et al* 1997]. The process was successful in reducing the average DNAPL saturation of the swept pore volume to 0.03%.

Following the surfactant/foam process, a bioremediation process can be applied to the aquifer to dechlorinate the chlorinated compounds. Direct hydrogen addition, where hydrogen is delivered without the use of fermentation substrates or carbon sources is an in-situ bioremediation technology [Newell *et al*, 2001]. In this process, hydrogen acts as an electron donor and halogenated compounds such as chlorinated solvents act as electron acceptors that are reduced in the reductive dechlorination process.

Hydrogen can be delivered to the aquifer by sparging with an injection well as is done during biosparging. The practice of hydrogen biosparging can be built on air sparging technology. The controlling factor in the success of hydrogen reductive dechlorination is the distribution of the gas in the aquifer. Hydrogen has low density and viscosity compared to water. The buoyancy gradient rather than the viscous pressure gradient will dominate the flow of hydrogen. Hydrogen injected at the base of the aquifer tends to flow upwards and cannot contact much of the bottom of the aquifer laterally [Newell *et al*, 2000, 2001]. The role of foam in hydrogen biosparging is to promote the lateral transport of gas in the aquifer to contact the contaminants in the bottom of the aquifer, especially when the contaminants are DNAPL.

7.2 Preparing for the field application---some preliminary experiments

Before designing a hypothetical field application, some experiments and simulations are needed to answer several questions which will be encountered in a field application.

7.2.1 The threshold surfactant concentration to generate strong foam

In our previous 1-D or 3-D sand pack experiment, the surfactant concentration was high enough to generate foam wherever gas was present. But in a field application, the smaller pore volume of surfactant injected prior to foam and the lack of confinement allow gas to overtake the surfactant front. There may

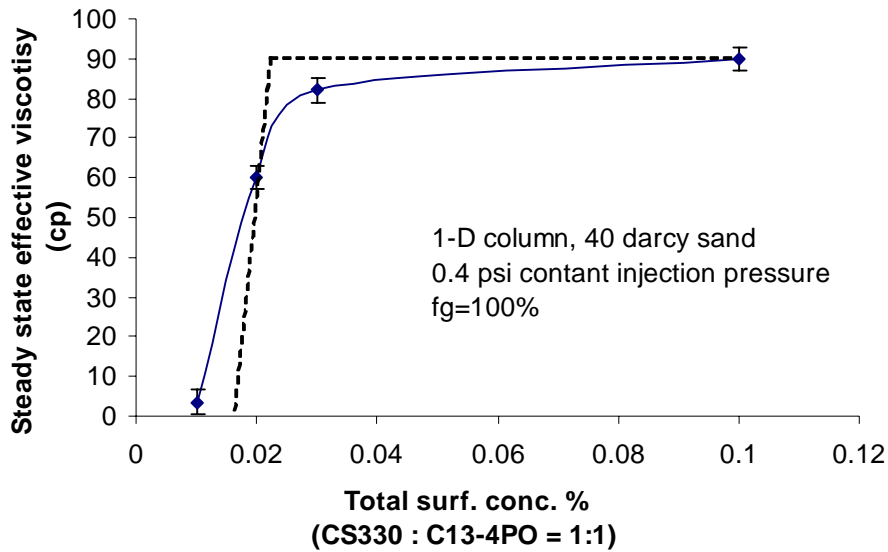


Figure 7-1 Surfactant concentration effect on steady state foam effective viscosity

be some place where surfactant concentration is not high enough to generate strong foam. It is important to know the threshold surfactant concentration under which strong foam cannot be generated.

Some 1-D foam experiments were performed using solutions of different surfactant concentrations to test the foam abilities of these surfactants. The experiments were performed in a 40 darcy sand column and the surfactant chosen was still the surfactant mixture of CS-330 and C13-4PO with an active weight ratio of 1:1. Different total concentrations were tested. Figure 7-1 shows the experimental results. Note that the effective foam viscosity drops dramatically when the total surfactant concentration is lower than 0.02%. So, in our simulation, we just set the threshold surfactant concentration to be 0.02% and set $0.02\% \pm 0.002\%$ to be the transient region. When the total surfactant concentration is greater than 0.022%, the surfactant solution has the ability to generate strong foam. And just for simplicity, when surfactant solution concentration is higher than 0.022%, we will take the steady state foam effective viscosity to be a same value and equal to the effective viscosity of the 0.1% surfactant solution. When the total surfactant concentration is less than 0.018%, the surfactant solution is too dilute to generate any foam. When the total surfactant concentration is between 0.018% and 0.022%, it is in a transient region and foam strength drops linearly. The dash line in Figure 7-1 shows the simplified curve we used in our simulation.

7.2.2 The effect of injection pressure on foam strength and simulation parameters

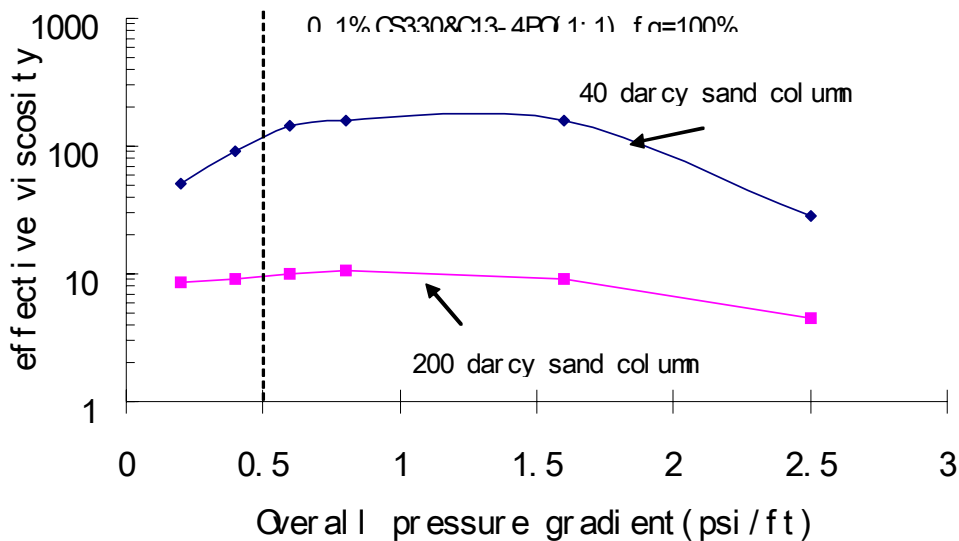


Figure 7-2 The effect of injection pressure on steady state foam strength

In our previous 3-D sand tank foam experiments, the highest injection pressure we tested was only 0.8 psi over hydrostatic pressure. In a field application, a higher injection pressure may be used to increase the injection efficiency. So it is necessary to find out how the foam strength and the simulation parameters change with the changing of different injection pressure.

Figure 7-2 shows the value of the steady state effective foam viscosity under different injection pressure for the 40 darcy and 200 darcy sand column. The length of the column is 1 ft long. From this figure we can see that when the injection pressure is low, the generated foam is not strong and the steady state effective foam viscosity is also low. With the increasing of the injection pressure, the effective foam viscosity also increases and reaches its highest value when the overall pressure gradient is about 0.8 psi/ft. It becomes lower when the overall pressure gradient is over 0.8 psi/ft. Note that when the overall pressure gradient is 2.5 psi/ft, for the 40 darcy sand, the steady state effective foam viscosity drops to about 20 cp and for the 200 darcy sand, it also drops to about half of the highest value. This phenomena is caused by the shear thinning effect of foam. The shear thinning effect is a beneficial effect that allows strong foam without excess pressure limitation near the injection well where the velocity is high. From these curves we can see that there exists a minimum overall pressure gradient when we apply a foam process. The overall pressure gradient cannot be too low to not be able to generate strong enough foam. For the surfactant mixture we are testing and for these two kinds of sands, the minimum overall pressure gradient which is required is roughly about 0.5 psi/ft, we can get relatively strong foam by applying an overall pressure gradient above this value.

Injection pressure		S_{rg}^f	v_{ref} ft/day	n	S_{gm}	m	$C_{\mu f}$	F_g
40 darcy sand column	0.2 psi	0.4	2	0.2	0.8	5.60	2,700	1
	0.4 psi	0.4	2	0.2	0.8	5.04	4,500	1
	0.8 psi	0.4	2	0.2	0.8	5.08	8,010	1
	1.6 psi	0.4	2	0.2	0.8	4.92	8,080	1
200 darcy sand column	0.2 psi	0.7	6	0.4	0.84	12.10	650	1
	0.4 psi	0.7	6	0.4	0.84	11.77	1,200	1
	0.8 psi	0.7	6	0.4	0.84	11.65	2,140	1
	1.6 psi	0.7	6	0.4	0.84	11.40	3,150	1

Table 7-1 Simulation parameters under different injection pressure

Table 7-1 lists the simulation parameters found for these different injection pressure experiments. From the table we can see that these five parameters: S_{rg}^f , v_{ref} , n , S_{gm} , m do not change much with the changing of the injection pressure, where S_{rg}^f is the gas residual saturation when foam is present, v_{ref} , n are the parameters representing the shear thinning effect on the strength of foam and S_{gm} , m are the parameters representing the saturation effect on the strength of foam. The only parameter which is changing is the value of $C_{\mu f}$, which represents the steady state foam strength. Figure 7-3 shows a plot of the changing of $C_{\mu f}$ with the change of overall pressure gradient. From this plots we can find that there exists a threshold pressure gradient at which the $C_{\mu f}$ value reaches its maximum value. For the 40 darcy sand, this threshold pressure gradient is between 0.6~0.8 psi/ft. For the 200 darcy sand, this value is about 1.5 psi/ft. When the overall pressure gradient is greater than this threshold value, $C_{\mu f}$ does not change with the increasing of the overall pressure gradient. So, during a foam process, in the regions where the pressure gradient is equal or higher than the threshold pressure gradient, all of the simulation parameters will be the same including the $C_{\mu f}$ value (it reaches its maximum value). In the regions where the pressure gradient is lower than the threshold pressure gradient, generally to say, the value of $C_{\mu f}$ will be lower than its maximum value

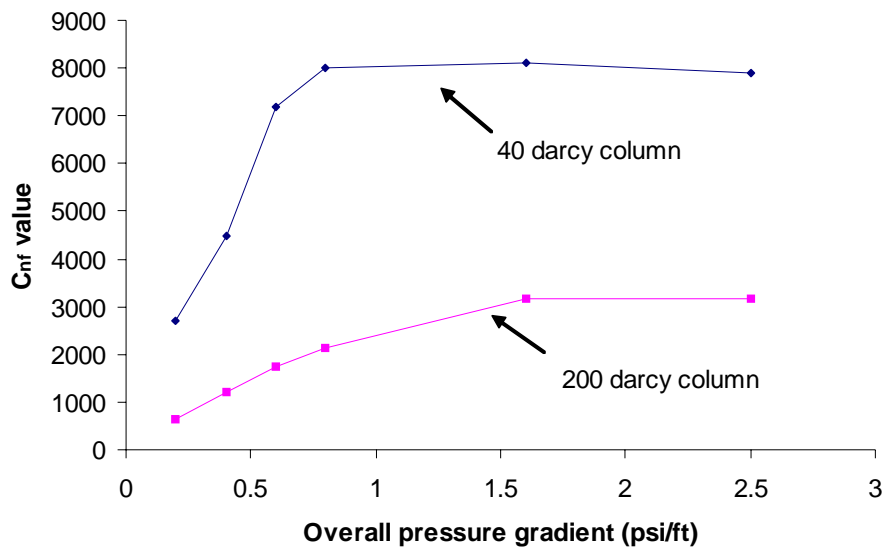


Figure 7-3 The change of C_{nf} value with the change of pressure gradient

since the pressure gradient is less than the threshold value and weaker foam will be generated at steady state, just as shown in the curves of Figure 7-3.

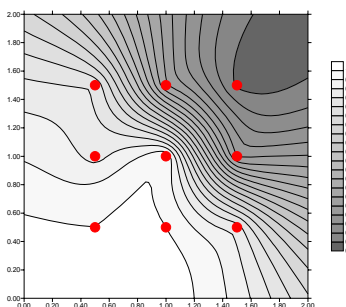
The parameters we determined here are just for the surfactant mixture at 0.1% total active concentration. The parameters will surely vary to some extent with the change of the surfactant composition and concentration (which means the foam ability of the solution changes). For different surfactant solutions, one may need to do corresponding experiments to determine the corresponding simulation parameters for that surfactant system. But in general, the surfactant mixture used here should be representative for good foamers and the conclusions from this mixture can be applied to other good foaming surfactants.

7.2.3 The minimum amount of surfactant solution needed

After we determined the threshold surfactant concentration and the minimum overall pressure gradient requirement, the next step is to determine the amount of surfactant solution needed for the field application. In our 3-D tank experiments, the tank was filled with surfactant solution before any gas was injected. In fact, in a field application, one cannot inject such amount of surfactant because it is not efficient and also not possible to fill the aquifer with surfactant solution. Here we will perform some simulations to determine the minimum amount of surfactant solution required.

By using a normal air sparging technology, there will be much of the bottom volume in an aquifer that cannot be contacted by hydrogen. So in the hydrogen biosparging foam field application, the most concerned issue is to

Experimental Results, Sg: 66%



Simulated Results, different PV surfactant solution injected:

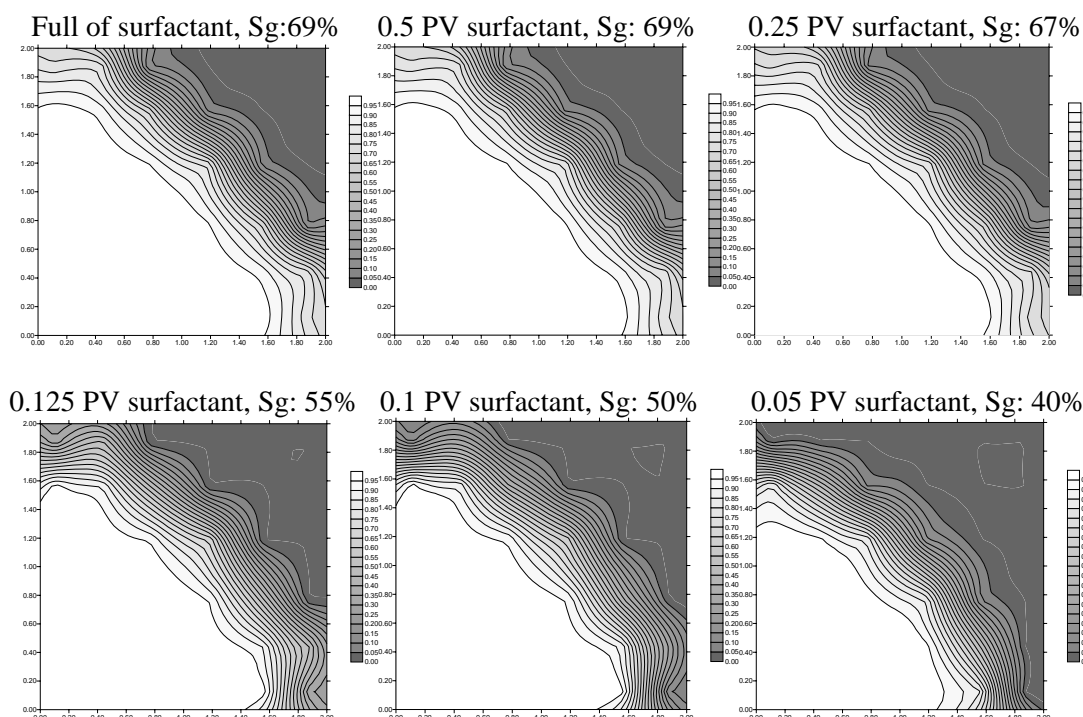


Figure 7-4 Effect of different surfactant amount on foam sweep efficiency
 Comparison based on a homogeneous 3-D sand tank foam experiment,
 0.8 psi over hydrostatic constant injection pressure, bottom sampling layer

distribute the injected hydrogen throughout the whole aquifer, especially the bottom of it. We did several simulations in our 3-D tank model and compared the gas distribution difference along the bottom sampling layer. In these simulations, different PV surfactant solution was injected prior to the gas injection and after 1 PV gas injected, the simulated bottom layer gas distribution profiles were compared with the experimental results. Figure 7-4 shows the comparison of these results. From these figures we can find that, when the injected surfactant

solution is greater than 0.25 PV, there is almost no difference on the gas sweep area of the bottom sampling layer. The total average gas saturation after 1 PV gas injected did not change also. Beginning from the 0.125 PV surfactant injection case, the gas sweep efficiency and the average gas saturation decreased with the decreasing of the injected surfactant volume. From these comparisons, we found that the threshold surfactant volume which is needed to get the same results as in the full of surfactant case is between 0.125 to 0.25 PV. Taking a conservative estimation, we choose 0.2 PV to be the minimum surfactant amount needed to be injected in a field application.

7.2.4 Scaling up in simulation--- making a connection between 1-D and 3-D

The foam simulation model has been described in Section C. The model sets a connection between 1-D foam and 3-D foam. Parameters obtained from 1-D column experiments can be applied to 3-D foam simulations and only one geometry parameter, F_g , be changed due to the difference of foam strength on 1-D and 3-D flow. We found that if the F_g value is defined as 1 in 1-D foam flow, then in the 3-D simulation, this value should be set to about 0.2 to get the best history match results. This relationship was demonstrated by two different injection pressure experiments: one is 0.8 psi over hydrostatic pressure and the other one is 0.4 psi over hydrostatic pressure. This relationship means 3-D foam is 5 times weaker than 1-D foam. We will use this 1-D and 3-D relationship in our scaling up simulations.

For heterogeneous systems when foam is present, in the discussion of Section C, besides of the $F_g=0.2$ relationship from 1-D to 3-D, we found that the C_{nf} value in the high permeability layer is about 3 times larger than its value in a homogeneous column. Table 5 of Section C shows the parameters of two best history match heterogeneous simulations in our 3-D heterogeneous tank. The tank has two layers of high permeability sand in the lower part of it. The red numbers in Table 5 shows the increase of C_{nf} value in the 3-D system, we can see that it increases about 3 times from its original value in the 1-D column. The explanation for this increase is because of foam snap-off [Falls *et al.*, 1988; Ransohoff and Radke, 1988]. The capillary pressure in the high perm region is lower than in the low perm region, when this pressure difference is large enough (usually when high perm region has a permeability which is 4 times larger than that of low permeability region), foam can be generated when it flows from low perm region to high perm region by snap-off and then the foam strength in the high perm region will be enhanced.

The other question for the scaling up simulation is how to determine the connection between a 1-D column experiment and a 3-D field application. From Table 1 we have already found that either for the 40 darcy sand or the 200 darcy sand, when the experimental overall pressure gradient is greater than some threshold value, at steady state, the generated foam strength will reach its maximum value. All the simulation parameters will remain to be about the same

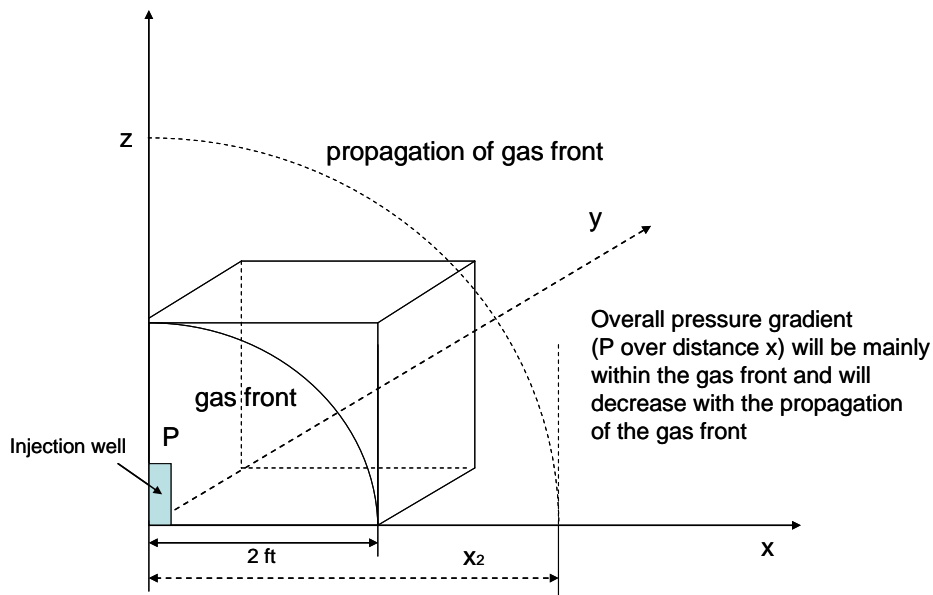


Figure 7-5 A sketch of a field injection

and do not change with the increasing of the pressure gradient. For the 40 darcy sand column, the threshold overall pressure gradient is about 0.6 psi/ft, For the 200 darcy sand, this threshold pressure gradient is about 1.5 psi/ft. When the overall pressure gradient is lower than the threshold value, the $C_{\mu f}$ value will be lower than its maximum value correspondingly.

In a 3-D field application, the generated foam strength is also depends on the value of the local pressure gradient. Let's consider a foam injection process as shown in Figure 7-5. Hydrogen is injected into the aquifer from the injection well, since the effective foam viscosity is much larger than the viscosity of water when strong foam is present, we assume the injected gas flow is like a special flow and propagates from the near well region to the further region. Here we will define a Near Well Volume (NWV) to estimate the value of the overall pressure gradient. The dimension of this volume is 2ft x 2ft x 2ft, just like the dimension of the 3-D tank in our lab. The other assumption we make is the overall pressure gradient is mainly within the propagating gas front and distribute evenly inside it. We will take the value of the overall pressure gradient when the gas front reaches the edge of the NWV as a comparison standard to the 1-D column. For example, for a 8 psi over hydrostatic pressure hydrogen injection, when the gas front propagates to the edge of the NWV, the overall pressure gradient in the NWV will be about 4 psi/ft and then we can choose the simulation parameters from corresponding 4 psi/ft 1-D experimental results.

One may ask why we choose 2ft x 2ft x 2ft as the dimension of the NWV. First of all, this dimension is large enough to approximately scale the capillary

effects. Secondly, the F_g relationship we found in our lab between 1-D and 3-D tank ($F_{g(1D)}: F_{g(3D)}=1:0.21$) is based on a similarly comparison standard: we took the overall pressure gradient along the 2 ft tank and use this value to compare to 1-D experiments. So here we will do the same simplification.

One may doubt that since the generated foam strength depends on the local pressure gradient, then no matter how low the injection pressure is, strong foam can always be generated near the injection well region because at the very beginning of the injection, when the gas front is just near the injection well, the pressure gradient within it will be always larger than the threshold pressure gradient. This imagination is not right because one should also consider the other factors which may affect the generation of foam. High pressure gradient is a necessary but not sufficient condition for foam generation. Strong foam cannot be generated as soon as the pressure gradient is above its threshold value. It will take some time for lamella to generate and accumulate. When the injection pressure is low, with the propagation of the gas front, the pressure gradient within it will drop quickly from the high value to below the threshold value. Then there will be no time for lamella to generate and accumulate under high pressure gradient and only weaker foam can be generated. This is also another reason why we choose the average overall pressure gradient in the NWV as the comparison standard: if the average pressure gradient can still be higher than the threshold value when gas front reaches the edge of NWV, then we assume the pressure gradient has been kept above the threshold value for an long enough time, strong foam can be generated in this time interval.

To estimate the region where strong foam can still be generated after foam flows beyond the NWV, let's take the 8 psi over hydrostatic pressure case as an example again. In this case, for 40 darcy sand, along the x or y direction, with the propagation of the injected gas, the overall pressure gradient within the gas front will decrease, just as shown in Figure 7-5. The maximum distance where strong foam can be generated is about 13.5 ft because at this distance the overall pressure gradient drops to about 0.6 psi/ft, which is the threshold pressure gradient. For regions within this distance, strong foam will be generated and we can choose the maximum $C_{\mu f}$ value, which is about 8000 in Table 6. In general, the distance in which strong foam can be generated is a function of the injection pressure, the higher the injection pressure is, the longer this distance will be.

For the regions more further away, in general, the pressure gradient in these regions will be lower than the threshold pressure gradient and then weaker foam will be generated. The value of $C_{\mu f}$ there should be lower than the maximum $C_{\mu f}$ value. But sometimes the situation is complex there. The generated strong foam in the near well regions may propagate into these further regions which will increase the foam strength there and make strong foam. Also, because of the shear thinning effect of foam, the local pressure gradient in the

further regions may also exceed the threshold pressure gradient and strong foam can be generated. This is a complex process and we do not have any experimental data or profiles for it. So here we will make a simplified assumption in our simulation. We will assume the $C_{\mu f}$ value in these further regions to be the same as in the near well regions, which means we can still be able to generate strong foam in these further regions.

7.2.5 Modeling the shear thinning effect between the well bore and the grid block

In the 3-D tank simulations in Section C, we modeled the shear thinning effect among grid blocks. Because in our 3-D tank, the pressure difference between the well bore and the grid block is very small, the shear thinning effect is also small between them and can be ignored. But in the field simulation, because the grid block is much bigger than the well bore, there will be a significant pressure difference between the well bore and the grid block. We need to consider the shear thinning effect between them in our field simulation and add a model for it in the simulator. Following the discussing of Bondor and Hirasaki *et al* [1972], we added a negative, rate-dependent apparent skin factor S_p in the well model to represent the non-Newtonian effects between the well bore and the gridblock. The injection rate will then be a function of this apparent skin factor due to non-Newtonian effects. We can get higher injection rate because of this non-Newtonian effects.

7.3 A hypothetical aquifer for hydrogen biosparging

7.3.1 Description

Field application of hydrogen biosparging was performed at Cape Canaveral Air Station Florida by Newell *et al* [2001]. Results from an eighteen-month low-volume pulsed hydrogen biosparging pilot test showed extensive biological dechlorination in a 30x30 ft zone located 15 to 20 ft below the water table in a sandy aquifer. In this case, hydrogen was injected about 20 ft below the water table and a 5 ft vadose zone exists above the water table. In the surfactant/foam process in Hill Air Force Base, the depth of the aquifer below the water table was also about 20 ft, the vadose on it is a few feet in depth. Air was also injected from the bottom. So, just for comparison convenience, we will also take our hypothetical aquifer to be 20 ft under water table and set the vadose zone to be 5 feet in depth above it. Hydrogen will also be injected into the aquifer from the bottom. Figure 7-6 shows the side view of the hypothetical aquifer.

Figure 7-7 shows the top view of the hypothetical aquifer. The blue circles there are the pattern of injection wells. From the figure we can see the injected gas flow should be symmetric for each injection well. So, we can just take one quarter of the adjacent area (the region in dash line in Figure 7-7) around an injection well and simulate the gas flow in this region. The outcome of the

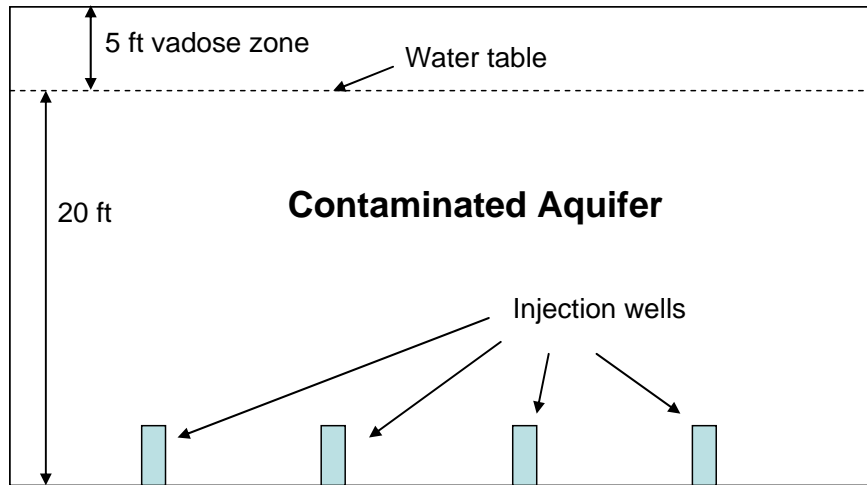


Figure 7-6 Side view of the hypothetical contaminated aquifer

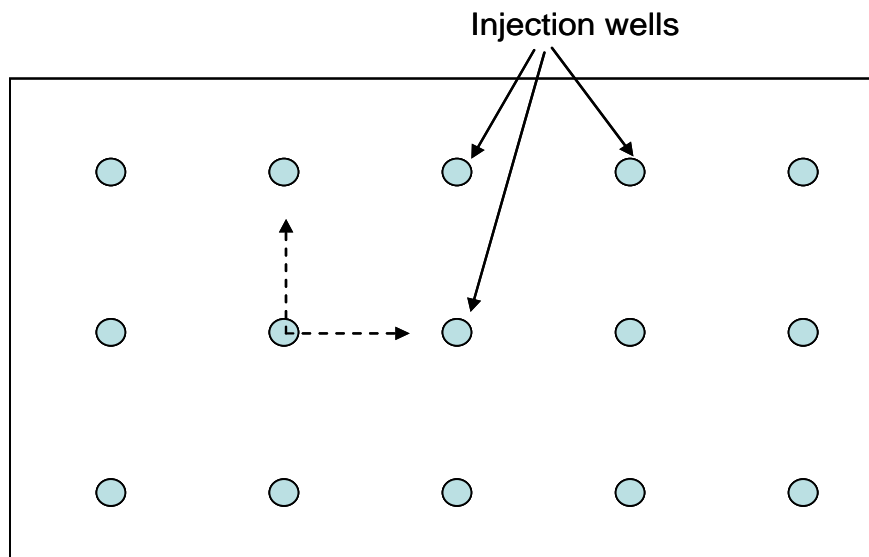


Figure 7-7 Top view of the hypothetical contaminated aquifer

simulation should confirm that a much wider well spacing than needed for sparging can be used for hydrogen foam. And with the wider well spacing, one can still completely remediating the entire aquifer between the wells, especially the base which is poorly contacted in conventional biosparging.

7.3.2 Choice of the injection pressure in a field application

In a field application, the injection pressure should be high enough to generate strong foam. A high injection pressure can provide enough driving force

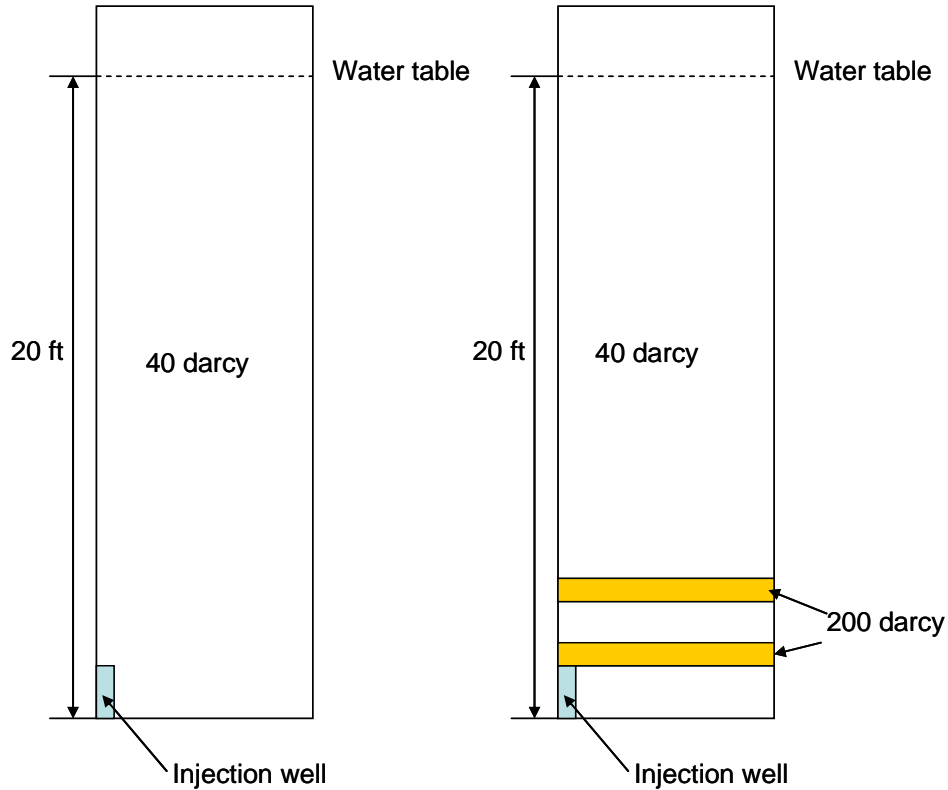


Figure 7-8 Side views of the two hypothetical aquifers

to distribute hydrogen horizontally along the bottom of the aquifer and the generated strong foam can also benefit the lateral flow of hydrogen. Taking the depth of the hypothetical aquifer to be 25 ft (including the vadose zone), the highest possible injection pressure will be about 17.5 psi, which is about 8.8 psi over the hydrostatic pressure. If the injection pressure is higher than 17.5 psi, it is possible that the sand in the aquifer be fluidized and the wells or formation of the aquifer be damaged. To be conservative, here we will take 8 psi over hydrostatic as our operation injection pressure. We will use this injection pressure in our following simulations.

7.4 Case studies of two different hypothetical aquifer formations

Two different hypothetical aquifer formations are investigated. The first one is a homogeneous sand aquifer with a permeability of 40 darcy. The second one is a heterogeneous sand aquifer with two layers of high perm sand in the lower part of it. The high perm layers are 1 ft in thickness and have a permeability of 200 darcy. One is 1.5 ft high from the bottom and the other one is 4.5 ft high from the bottom. The other part of the aquifer is still 40 darcy sand. The side views of these two aquifers are shown in Figure 7-8. We used a 6x6x6 grid block in our simulation and the dimension of each grid block is 4.2x4.2x4.2 ft. In the simulation, the four vertical boundaries are closed boundary. But since the

scale of the simulated area is quite large (25x25 ft in the horizontal cross section), before gas breakthrough, gas can always flow towards the two boundaries (boundary B1 and B2 in Figure 7-9). So in general, these two boundaries can be looked as open boundaries for the injected gas.

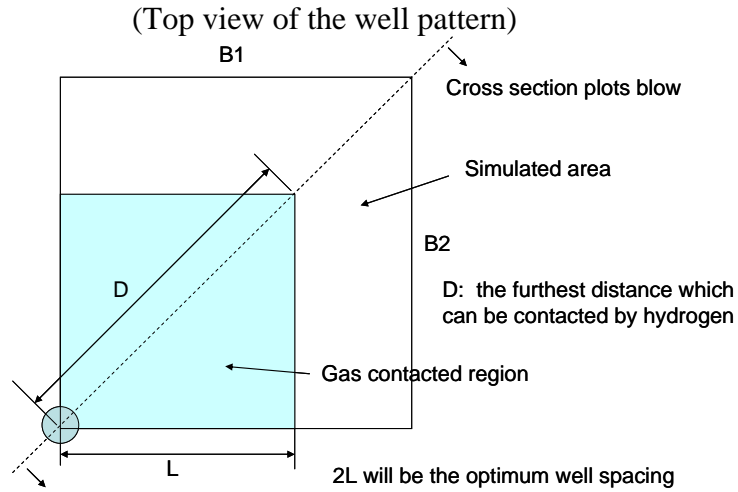
7.4.1 40 darcy homogeneous sand aquifer

A natural aquifer always has some heterogeneity, but it is always useful for us to start from a homogeneous case and make some basic comparisons and conclusions.

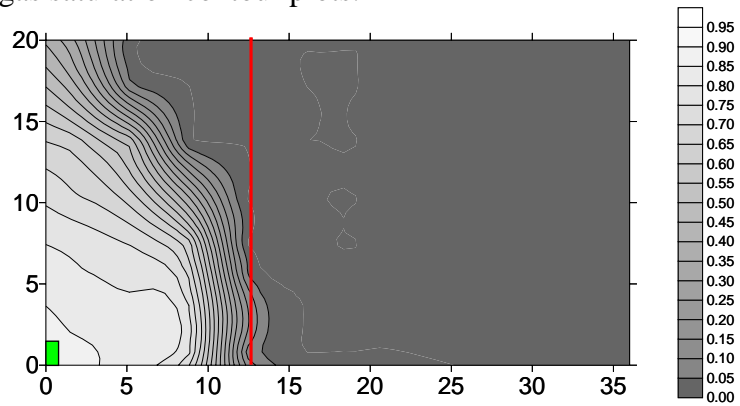
7.4.1.1 The spacing of the injection wells

The first and most important thing we are interested is the spacing of the injection wells. We are expecting to get larger well spacing and at the same time contact all the bottom of the aquifer by using foam. Since hydrogen is explosive when mixed with air, it is important to ensure that no hydrogen is leaked into the atmosphere during the sparging process. We must stop the injection as soon as hydrogen breaks through from the top of the aquifer. So our comparisons will be based on the breakthrough time of hydrogen, the simulated results will be compared at the time point of hydrogen breakthrough.

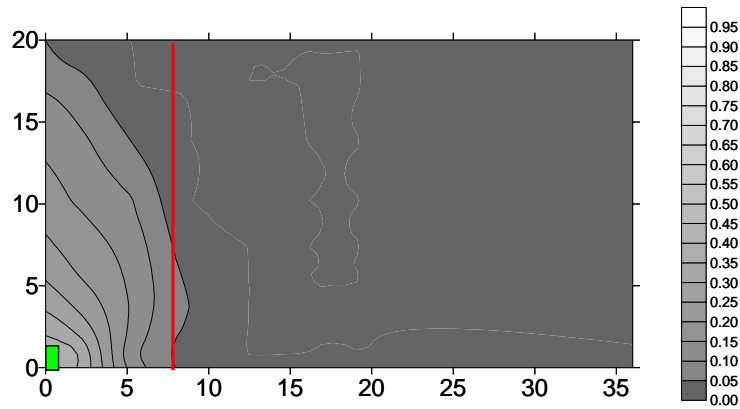
Figure 7-9A shows the simulated results of the gas saturation contour plots along the diagonal cross section of the simulated aquifer when foam is present. The gas flow is symmetric around an injection well so we just simulated one quarter of the total region. From the simulation we found that at the time of hydrogen breakthrough, the farthest distance along the diagonal direction where hydrogen can reach is about 12.5 ft, just as shown with the red line in Figure 7-9A. For the distance within this 12.5 ft, the injected hydrogen can contact almost all the bottom of the aquifer and the lower 1/2 part of the aquifer can also be fully contacted. If we convert this diagonal distance into well spacing distance, the optimum well spacing will be about 18 ft. Figure 7-9B shows the simulated results when there is no foam in the aquifer. From the comparison of 7-9A and 7-9B we can see the difference between no foam and foam results. For regular hydrogen biosparging without foam, the injected hydrogen flows upwards and breaks through from the top very quickly. The gas contacted area is smaller than in the foam case. At the time when hydrogen breaks through, the farthest distance along the diagonal direction where hydrogen can reach is only about 7.5 ft. So if one wants to contact all of the aquifer without using foam, the needed well spacing will be smaller than that when foam is present. From the figure we can see if without foam, the optimum well spacing to fully contact the aquifer is about 10 ft. Compared to when foam is present, this well spacing is much smaller. We can get more than 1.8 times larger well spacing, which is about 18 ft, when foam is present.



Cross section gas saturation contour plots:



A: With Foam



B: Without Foam

Figure 7-9 Gas saturation contour plots for with and without foam cases, homogeneous aquifer

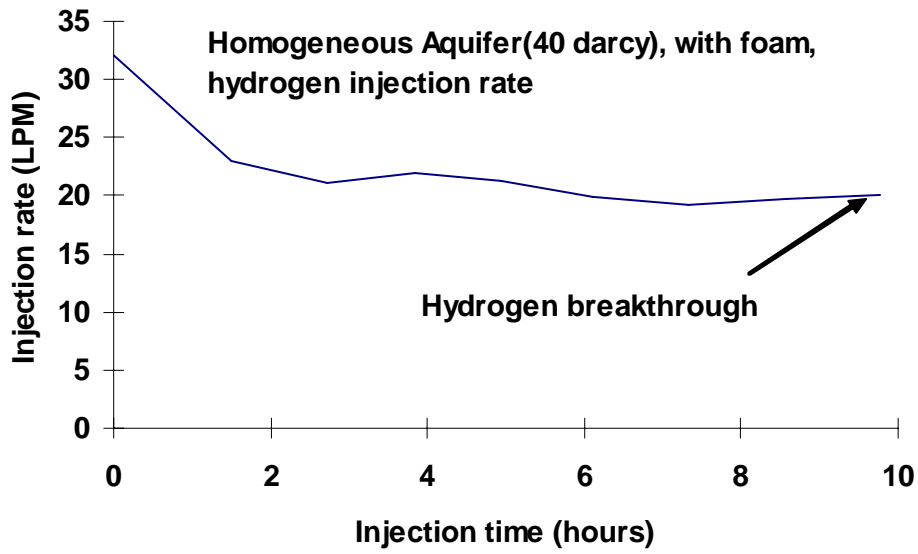


Figure 7-10 Gas injection rate, with foam in the aquifer

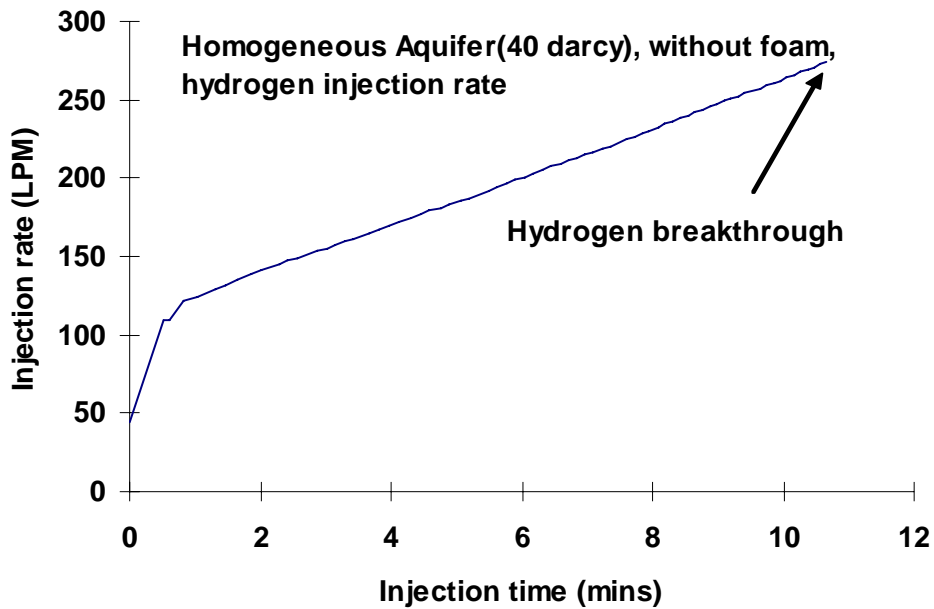


Figure 7-11 Gas injection rate, without foam in the aquifer

Also, from the plots we can see that the hydrogen saturation in the foam case is substantially larger than in the without foam case, especially in the bottom 5 ft region. In the foam case, hydrogen breaks through to the top of the aquifer after about 14,158 liter injected. When there is no foam, only about 1,841 liter hydrogen can be injected before it breaks through to the top. So by the time

of hydrogen breakthrough, the average saturation of hydrogen in foam case is about 8 times larger than in the without foam case. The high hydrogen saturation is a beneficial factor to the bioremediation process, more contaminants can be degraded because of the presents of more trapped hydrogen.

7.4.1.2 Injection rate comparison between with and without foam cases

Figure 7-10 shows the simulated injection rate for the field application when foam is present. From the simulation, it takes about 10 hours for the injected hydrogen to break through to the top of the aquifer. The injection rate is decreasing and levels off to steady state after about 1 hours of injection. At steady state the injection rate is around 20 LPM. Figure 7-11 shows the hydrogen injection rate when there is no foam. Hydrogen breaks through to the top only after about 10 mins of injection and the injection rate is much higher than in the foam case, it increases to about 250 LPM when hydrogen breaks through to the top of the aquifer.

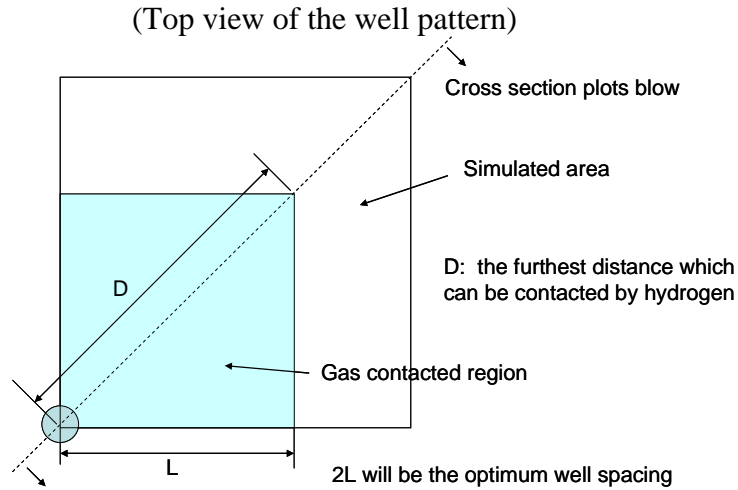
7.4.2 40 darcy and 200 darcy heterogeneous sand aquifer

The second case which is investigated is a hypothetical heterogeneous aquifer. Though foam can reduce the mobility of gas in both of the high perm and low perm regions of the porous media, it has the potential of selectively reducing the mobility more in higher permeability layers in contact with lower permeability layers. The most common explanation for this is the snap-off mechanism of foam [Falls *et al.*, 1988; Ransohoff and Radke, 1988; Tanzil, 2001]. When foam flows from low perm region to high perm region and encounters a lower capillary pressure, more lamella will be generated due to the effect of snap-off. The mobility of foam in high perm region will then be reduced more compared to in low perm region. Because of the effect of heterogeneity, we are expecting to have larger well spacing and better contact efficiency in the heterogeneous aquifer than in the homogeneous aquifer.

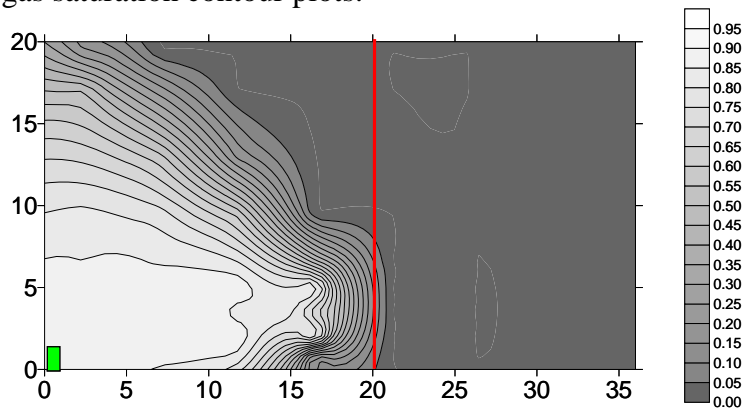
7.4.2.1 The spacing of injection wells

As in the study of the homogeneous case, the maximum possible spacing of the injection wells when foam is present is investigated by simulations. Again, the time point when hydrogen breaks through to the top of the aquifer is taken as the base of the comparison.

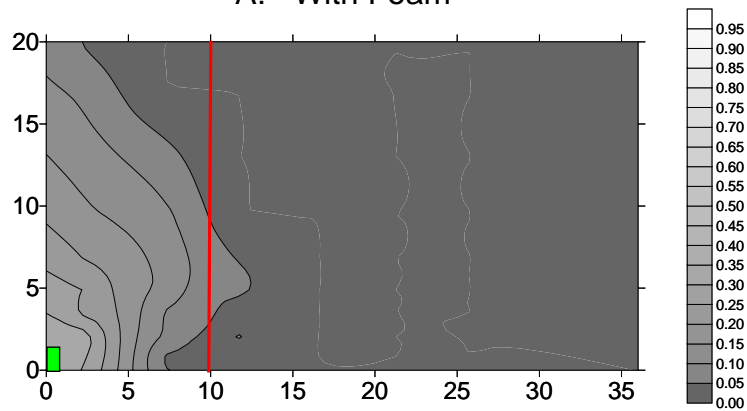
Figure 7-12A shows the simulated gas saturation contour plots along the diagonal cross section of the aquifer when foam is present. Again, because of the symmetric of the injection flow, only a quarter of the total region around the injection well was simulated. In this heterogeneous case, the furthest distance along the diagonal direction where foam can reach is about 20 ft. Hydrogen contacted almost all of the lower $\frac{1}{2}$ part of the aquifer within this 20 ft range. If we



Cross section gas saturation contour plots:



A: With Foam



B: Without Foam

Figure 7-12 Gas saturation contour plots for with and without foam cases, heterogeneous aquifer

convert this distance into well spacing, the well spacing for this heterogeneous aquifer when foam is present will be about 29 ft. Compared to the homogeneous

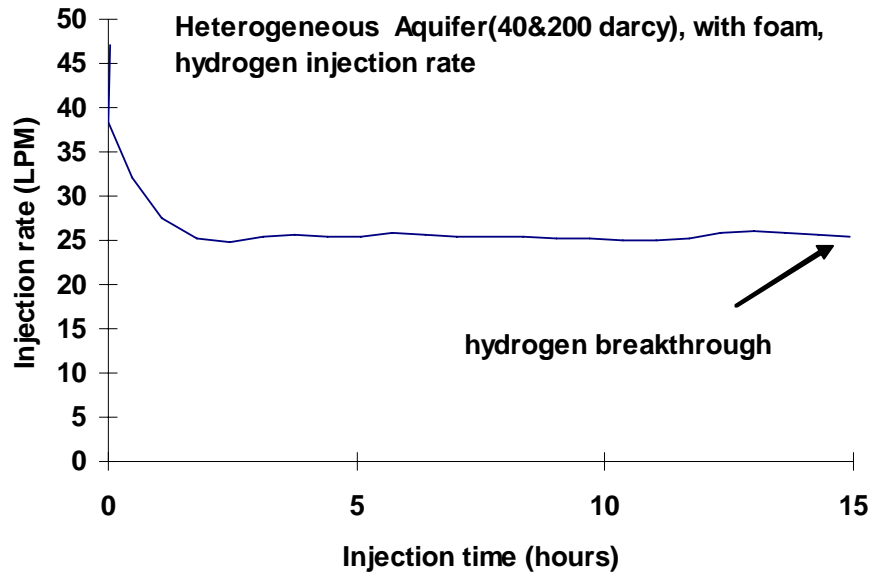


Figure 7-13 Gas injection rate, with foam in the heterogeneous aquifer

case, the well spacing we can have in this heterogeneous aquifer is much larger. In the homogeneous case, the best spacing we can have is only about 18 ft. We can see the heterogeneity greatly increases the lateral transport of hydrogen and increases the well spacing to about 1.6 times comparing to the homogenous foam case. Figure 7-12B shows the simulated results when there is no foam in the heterogeneous aquifer. Just like in the homogeneous case, the injected hydrogen breaks through to the top very fast. With the 8 psi over hydrostatic injection pressure, the furthest distance along the diagonal cross section where gas can contact is only about 7.5 ft, which corresponds to a well spacing of about 11 ft. Compared to the results when foam is present, the well spacing in the foam case can be more than 2.5 times larger.

In the heterogeneous case, the hydrogen saturation when foam is present is also much larger than in the without foam case. When foam is present, the lower ½ part of the aquifer has a high hydrogen saturation and the injected hydrogen breaks through to the top after about 24,352 liter hydrogen injected. When there is no foam, only about 2,124 liter hydrogen can be injected before breakthrough. At the point of hydrogen breakthrough, more than 10 times amount of hydrogen can be injected into the aquifer when foam is present.

7.4.2.2 Injection rate comparison between with and without foam cases

Figure 7-13 shows the hydrogen injection rate when foam is present. Hydrogen breaks through to the top of the aquifer after about 24,352 liter injected, the total injection time is about 15 hours. The injection rate levels off and reaches its steady state after about 1 hour injection and stays around 25 LPM till the breakthrough of hydrogen. Compared to the simulated injection rate

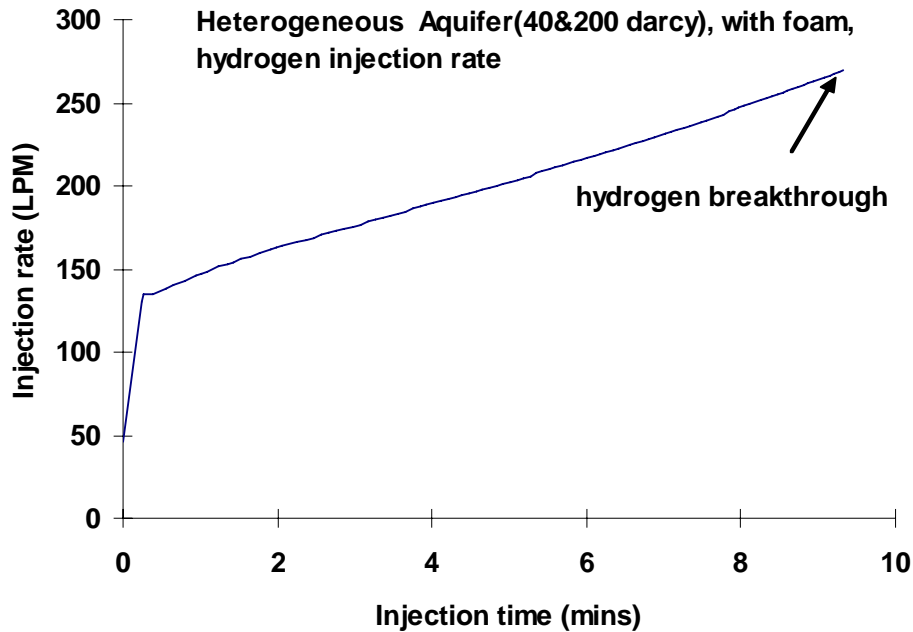


Figure 7-14 Gas injection rate, without foam in the heterogeneous aquifer

in the homogeneous case (Figure 7-10), the steady state injection rate in the heterogeneous case is a little bit higher. For the without foam case, hydrogen breakthrough to the top after about 10 mins injection and only about 1,841 liter hydrogen is injected (Figure 7-14). The injection rate when there is no foam is also much higher than in the foam case. It increases very fast and reaches about 270 LPM at the time when hydrogen breakthrough, which is about 11 times larger than the rate we get in the foam case.

7.5 Discussion and summary of Section 7

7.5.1 A comparison with the results of Cape Canaveral aquifer

We can make a rough comparison here with the results of the Cape Canaveral aquifer. Based on slug test results for 15 shallow monitoring wells, the average permeability of the aquifer was estimated to be about 34 darcy. The sand permeability there is very close to the 40 darcy sand we used in our estimation. The depth of the aquifer which is under the water table is about 20 ft, above the water table, a 5 ft high vadose zone exists. The injection pressure there was about 10 psi over hydrostatic pressure which is also close to the injection pressure we chose in our hypothetical design. So here we can roughly compare the simulated results with the Cape Canaveral results and see the benefits of foam. Figure 7-15 shows the hydrogen distribution plot after the hydrogen sparging without foam, the numbers in this plot are the dissolved gas

Cape Canaveral Hydrogen Biosparge, C. J. Newell

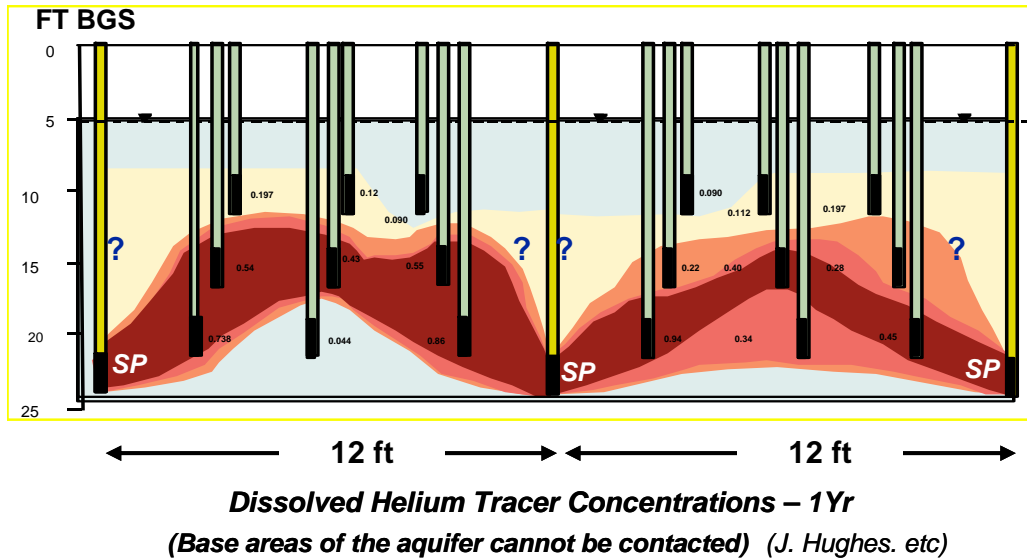


Figure 7-15 Hydrogen sparging result from Cape Canaveral aquifer

concentrations. Newell *et al* [2000] found that each sparge point appeared to deliver hydrogen concentrations in about a 5 ft radius away from the sparge point, which means there the good well spacing without foam is about 10 ft. This result consists with our homogeneous case simulation results where we also found that the best well spacing when foam is not present is about 10 ft (Figure 7-9B). Also, from Fig. 15 we can find that much of the bottom of the aquifer is not contacted by the injected gas and the dissolved gas concentration is very low there. Compared to our 40 darcy homogenous foam case study (Figure 7-9A, where we can contact the whole bottom of the aquifer using a well spacing of about 18 ft and obtain a high trapped gas saturation), it is very clear that foam can make a big improvement in the application of hydrogen biosparging.

7.5.2 Summary

In this report, we investigated several conditions which are needed to be known before a field hydrogen foam application. Also, we investigated two hypothetical aquifers and estimated the foam effect on well spacings using simulation. We can get the following conclusions:

1. The threshold surfactant concentration for the surfactant mixture we are testing is about 0.02%. When the surfactant concentration is low, it is not able to generate strong foam.
2. For the surfactant mixture we are testing, there exists a minimum overall pressure gradient to generate strong foam which is about 0.5 psi/ft. When the overall pressure gradient is lower than this value, the generated foam is not strong.

3. To get the same result as in a surfactant filled aquifer, the minimum surfactant amount needed is about 0.2 PV.
4. For a 25 ft deep, water table 5 ft lower than the ground surface, 40 darcy homogeneous aquifer, when hydrogen/foam is injected from the bottom, the optimum well spacing is about 18 ft. When there is some heterogeneity (two layers of 200 darcy sand in the lower part of the aquifer), the optimum well spacing increases to about 29 ft. This phenomena shows that the heterogeneities in aquifer can help the transport and distribution of the injected hydrogen.
5. Foam can delay the breakthrough time of hydrogen and then increase the average gas saturation in the aquifer. When there is no foam, hydrogen breaks through to the top after only about 1,900 liter hydrogen injection for both of the homogeneous and heterogeneous case. But when foam is present, one can inject much more hydrogen without breaking through to the top. For the homogeneous case, about 8 times more hydrogen can be injected before breakthrough and for the heterogeneous case, it is more than 10 times more.

References

1. Bertin, H.J., M.Y. Quintard, and L.M. Castanier. "Development of a bubble-population correlation for foam-flow modeling in porous media," *SPE J.*, December 1998b, 356-362.
2. Bertin, H.J. "Foam diversion modeling using a bubble-population correlation," paper SPE 59366 presented at the 2000 SPE/DOE Improved Oil Recovery Symposium, Tulsa, Oklahoma, 3-5 April 2000.
3. Bondor, P.L., Hirasaki, G.J., "Mathematical Simulation of Polymer Flooding in Complex Reservoirs", *SPEJ.*, October, 1972
4. Delshad, M., G.A. Pope, and K. Sepehrnoori. "A compositional simulator for modeling surfactant-enhanced aquifer remediation: 1. Formulation," *J. Contaminant Hydrology*, 23, 303-327, 1996.
5. Friedmann, F., Chen, W.H., and Gauglitz, P. "Experimental and Simulation Study of High-Temperature Foam Displacement in Porous Media," *SPERE* (February 1991) 37.
6. Hirasaki, G.J. and J.B. Lawson. "Mechanisms of foam flow in porous media: apparent viscosity in smooth capillaries," *SPE J.*, April 1985, 176-190.
7. Hirasaki, G.J., C.A. Miller, R. Szafranski, D. Tanzil, J.B. Lawson, H. Meinardus, M. Jin, J.T. Londergan, R.E. Jackson, G.A. Pope, and W.H.

- Wade. "Field demonstration of the surfactant/foam process for aquifer remediation," paper SPE 39292, presented at the 1997 SPE Ann. Tech. Conf. and Exhib., San Antonio, Texas, 5-8 October 1997b.
8. Hirasaki, G.J., C.A. Miller, R. Szafranski, D. Tanzil, J.B. Lawson, R.E. Jackson, H. Meinardus, J. Avvakoumides, V. Dwarakanath, M. Jin, L. Kennedy, P. Mariner, G.A. Pope, T. Oolman. *AATDF Surfactant/Foam Process for Aquifer Remediation*, AATDF, Rice University, Houston, TX, 1997c.
 9. Hirasaki, G.J., R.E. Jackson, M. Jin, J.B. Lawson, J. Londergan, H. Meinardus, C.A. Miller, G.A. Pope, R. Szafranski and D. Tanzil. "Field demonstration of the surfactant/foam process for remediation of a heterogeneous aquifer contaminated with DNAPL," in *NAPL Removal: Surfactants, Foams, and Microemulsion*, S. Fiorenza, C.A. Miller, C.L. Oubre and C.H. Ward (eds.), CRC Press, Boca Raton, 2000.
 10. Hirasaki, G.J., C.A. Miller, R. Szafranski, J.B. Lawson, and N. Akiya. "Surfactant/foam process for aquifer remediation," paper SPE 37257, presented at the 1997 SPE International Symposium on Oilfield Chemistry, Houston, Texas, 18-21 February 1997a.
 11. Newell, C.J., Aziz, C.E., Haas, P.E., Hughes, J.B., Khan, T.A., "Two novel methods for enhancing source zone bioremediation: direct hydrogen addition and electron acceptor diversion," presented at the Sixth International Symposium on In-Situ and On-Site Bioremediation, San Diego, California, June 4-7, 2001
 12. Newell, C.J., Haas, P.E., Hughes, J.B., Khan, T.A., "Results from two direct hydrogen delivery field tests for enhanced dechlorination," presented at the Battelle Remediation of Chlorinated and Recalcitrant Compounds Conference, Monterey, California, 2000
 13. Tanzil, D., "Foam Generation and Propagation in Heterogeneous Porous Media," Ph.D. Thesis, Rice University, Houston, TX, 2001
 14. Tanzil, D., Hirasaki, G.J., Miller, C.A., "Mobility of Foam in Heterogeneous Media: Flow Parallel and Perpendicular to Stratification," *SPE J.*, October 2000.

Action Item

In the Final Report, please respond to the following concerns related to eventual field application of the technology: ? Field implementation must take into account heterogeneous hydrogeologies, downgradient migration of DCE (i.e., away from the hydrogen), and the presence of DNAPL as thin fingering ganglia rather than as a large pool. ? Likelihood of encountering regulatory issues with injection of formaldehyde. ? Cost-competitiveness of this technology.

Response:

1. The effect of heterogeneities in the form of high permeability layers was investigated. The high permeability layers were favorable to the process as it promoted lateral migration of gas in the aquifer.
2. The dechlorination was found to stop at DCE in the presence of a concentration of surfactant needed for generating foam. This could result in downgradient migration of DCE. However, DCE may be more amiable to eventual aerobic degradation compared to PCE.
3. This process will be well suited for DNAPL as thin fingering ganglia since foam will distribute hydrogen throughout the aquifer. If DNAPL is present as a large pool, it would be better to solubilize and displace bulk of the DNAPL with a surfactant-foam process and then use hydrogen-foam bioremediation as a final polishing step.
4. Formaldehyde is not needed for the process.
5. The cost-competitiveness was not examined.

EFFECTS OF SURFACTANTS ON THE DECHLORINATION OF
CHLORINATED ETHENES

TRAVIS MCGUIRE† and JOSEPH B. HUGHES*‡

†Groundwater Services, 2211 Norfolk, Suite 1000, Houston, Texas 77098, USA

‡Rice University, Department of Civil and Environmental Engineering, George R. Brown School of Engineering, 6100 Main Street—MS 317, Houston, Texas 77005, USA

(Received 11 October 2002; Accepted 17 March 2003)

Abstract—The influence of surfactants on a perchloroethene (PCE) dechlorinating mixed culture was investigated in laboratory experiments. Surfactants (Steol CS-330, Aerosol MA 80-I, alpha olefin sulfonate 14 to 16, Neodol 25-7, Tween 80, alkyl polyglycoside, C₁₆TAB [trimethylammonium bromide], and sodium dodecyl sulfate) were evaluated for their effects on the rate and extent of PCE reductive dechlorination and their potential biodegradation by the mixed culture. Limited, if any, surfactant biodegradation was observed for the surfactants tested, and all surfactants impaired dechlorination in either the rate of PCE dechlorination or the terminal dechlorination products observed. Based on initial testing, a nonionic surfactant, Tween 80, and an anionic surfactant, Steol CS-330, were selected for additional investigation. Dechlorination of PCE to dichloroethene (DCE), vinyl chloride (VC), and ethene (ETH) occurred in all Tween 80-amended microcosms, with a depressed rate of ETH production as the only adverse effect. Steol CS-330, however, inhibited dechlorination beyond DCE at all surfactant concentrations exceeding 25 mg/L. Attempts to acclimate a culture to Steol CS-330 were unsuccessful. Inhibition of VC and ETH production was reversible on dilution of the surfactant to a concentration of 10 mg/L or less, indicating that surfactant interactions with the enzyme system responsible for reductive dechlorination of DCE may be the cause of inhibition.

Keywords—Reductive dechlorination Surfactant Perchloroethene *cis*-Dichloroethene Inhibition

INTRODUCTION

The remediation of aquifers contaminated with chlorinated solvents, particularly perchloroethene (PCE) and trichloroethene (TCE), is one of the most prevalent groundwater challenges facing environmental engineers [1,2]. The combination of low aqueous solubilities and densities greater than that of water facilitate the existence of these solvents as dense, non-aqueous-phase liquid (DNAPL) in aquifers. Dissolution of the chlorinated ethenes from the DNAPL into groundwater occurs slowly under typical aquifer conditions. Attempts to enhance dissolution through groundwater pumping have proven to be ineffective at significantly reducing the source of contamination, which may exist and contaminate groundwater for decades or even centuries [3]. Other technologies, such as enhanced dissolution/mobilization of DNAPL by surfactants [4–6] and biologically enhanced removal of chlorinated ethenes from source zones [7–9], however, may reduce the time needed for remediation.

The anaerobic process of biological reductive dechlorination through which PCE or TCE is sequentially reduced to one or more of the dichloroethene (DCE) isomers (*cis*-DCE, *trans*-DCE, and 1,1-DCE), vinyl chloride (VC), and finally to the innocuous product ethene (ETH) has been studied widely [10–14]. Though the majority of studies focus on the potential for microbial reductive dechlorination to treat the dissolved plume emanating from a DNAPL source zone, more recent laboratory investigations have demonstrated the ability of halorespiring microorganisms to carry out reductive dechlorination proximate to NAPLs and, thus, enhance the dissolution rate observed [7–9].

A key challenge in enriching the activity of dechlorinating microorganisms in DNAPL source zones at field sites is obtaining intimate contact between microorganisms, the contaminant, and the electron donor that is added. Hydrogen is a key electron donor supporting the biological reductive dechlorination of chlorinated ethenes [15]. Both direct addition of hydrogen gas and syntrophic hydrogen production via fermentation of organic substrates have been shown to support rapid and complete PCE dechlorination in laboratory studies [14]. Flow of hydrogen gas in an aquifer is governed by buoyancy caused by the low density and viscosity of hydrogen compared to water. Therefore, hydrogen gas tends to rise through the aquifer rather than being transported laterally across the formation. Results from a field demonstration investigating hydrogen biosparging of a TCE-contaminated aquifer showed dramatic decreases in chlorinated ethene concentration near the injection point; however, the reduction in concentration was less profound approximately 4.6 m from the sparge point, indicating less efficient hydrogen contacting [16].

The vertical transport of hydrogen in biosparging is a major disadvantage when considering enhancement of source-zone biological reductive dechlorination, because DNAPLs often reside at the base of the aquifer. Research on enhanced oil recovery has shown that dispersing a gas into a surfactant solution, creating a surfactant foam, increases the apparent viscosity of the gas and decreases the mobility, allowing lateral transport of the gas to occur [17]. Using hydrogen gas to generate surfactant foam has the potential to increase the residual saturation of hydrogen in a contaminated aquifer, to improve hydrogen contacting with DNAPL, and to stimulate biological reductive dechlorination. For such an approach to be feasible, however, the effects of the surfactants on the mi-

* To whom correspondence may be addressed (hughes@rice.edu).

Table 1. Properties of surfactants used in experimental studies

Surfactant ^a	Chemical class	Chemical formula ^b	Avg. MW ^c (g/mole)	CMC ^d (mg/L [mM])	COD ^e (g O ₂ /L)
Neodol 25-7	Nonionic	CH ₃ (CH ₂) ₁₁₋₁₄ O(EO) ₇ H	515	9 (0.02)	19.8 ± 0.2
APG	Nonionic	C ₈₋₁₆ polyglycoside	404	45 (0.11)	ND
Tween 80	Nonionic	C ₁₈ S ₆ (EO) ₂₀	1,308	13 (0.01)	15.6 ± 0.2
Aerosol MA 80-I	Anionic	[(C ₂ H ₅) ₂ CHCH ₂ COOCH ₂ SO ₃ Na]	388	7,100 (18.3)	15.7 ± 0.5
AOs 14-16	Anionic	CH ₃ (CH ₂) ₁₀₋₁₂ CH=CHCH ₂ SO ₃ Na	315	1,200 (3.81)	16.6 ± 0.4
Steol CS-330	Anionic	CH ₃ (CH ₂) ₁₁ (EO) ₃ OSO ₃ Na	422	449 (1.07)	16.5 ± 0.2
C ₁₆ TAB	Cationic	CH ₃ (CH ₂) ₁₅ (CH ₃) ₃ NH ₄ Br	364	361 (0.99)	ND

^a APG = alkyl polyglycoside; AOS = alpha olefin sulfonate; TAB = trimethylammonium bromide.

^b EO = ethylene oxide; S₆ = sorbitan ring.

^c MW = molecular weight.

^d CMC = critical micelle concentration (provided by manufacturer).

^e COD = chemical oxygen demand; ND = not determined. Concentrations for 1% (w/w) solution.

crobial reductive dechlorination of chlorinated ethenes must be considered.

The effects of surfactants on the anaerobic reductive dechlorination of chlorobenzenes have been investigated [18–20], and the effects of surfactants on the biotransformation of hydrophobic organic compounds have been studied quite extensively [21,22]. However, little information is available regarding the effects of surfactants on chlorinated ethene reductive dechlorination. In studies of hydrocarbon biodegradation, results have demonstrated that surfactants can increase rates of contaminant biodegradation by increasing mass transfer to the aqueous phase [18,23–25]. However, inhibition of microbial activity has also been observed in the presence of surfactants [26–28]. Toxicity of the surfactant, brought about by interaction of the surfactant with the cellular membrane or by interaction with membrane-bound proteins vital to cell function, is the most common explanation for the observed inhibition [22].

The studies presented herein focus on the effects of a range of surfactants and surfactant concentrations on the dechlorination activity of a PCE dechlorinating mixed culture. To determine the effects, whether positive or negative, both dechlorination rate and extent were monitored in the presence of surfactants. Also, studies are presented that investigate the extent to which the surfactants were degraded by the mixed anaerobic culture at high H₂ partial pressures (as would be present in a H₂-based foam). All surfactants screened in the present studies inhibited PCE dechlorination; however, the degree of inhibition varied among the surfactants. Results also demonstrated that the surfactants were not rapidly degraded by the mixed culture under the experimental conditions.

MATERIALS AND METHODS

Chemicals

The following chemicals were obtained in liquid form: Perchloroethene (PCE; >99%; Acros, Houston, TX, USA), TCE (99.5%; Acros), *cis*-DCE (97%; Acros), ethanol (200 proof; Pharmco, Brookfield, CT, USA), chloroform (99.9%; Fisher Scientific, Houston, TX, USA), and 1,2-dichloroethane (99.9%; Fisher Scientific). The following chemicals were obtained in solid form: Methylene blue chloride (Acros) and tetrabromophenolphthalein ethyl ester potassium salt (Sigma-Aldrich, St. Louis, MO, USA). Gaseous chemicals obtained from Trigas (Houston, TX, USA) included VC (8%, balance N₂) and hydrogen/CO₂ (80%/20%, v/v). Ethene (99.5%) and methane (99%) were obtained from Scott Specialty Gases

(Plumsteadville, PA, USA). The following surfactants were obtained in liquid solution: Steol CS-330 (28% active; Stepan, Northfield, IL, USA), Aerosol MA 80-I (80% active; Cytec, West Paterson, NJ, USA), alpha olefin sulfonate (AOS) 14 to 16 (39% active; Shell Chemical, Houston, TX, USA), Neodol 25-7 (100% active; Shell Chemical), Tween 80 (100% active; Sigma-Aldrich), and alkyl polyglycoside (50% active; a gift from the lab of Clarence Miller, Rice University, Houston, TX, USA). Hexadecyltrimethylammonium bromide (C₁₆TAB; Lancaster Synthesis, Pelham, NJ, USA) and sodium dodecyl sulfate (SDS; 98%; Sigma-Aldrich) were obtained as solids. All surfactants were used without purification, and a list of chemical and physical properties is given in Table 1.

Nutrient medium

The reagent-grade chemicals and concentrations used in preparation of nutrient medium were identical to those previously reported [9].

Analytical methods

Gas chromatography was used to determine the aqueous- and gas-phase concentrations of all chlorinated ethenes, ETH, and methane. For experiments in which the predominant dechlorination products were VC and ETH or in which surfactant concentrations were less than the critical micelle concentration, headspace analysis, as previously described [29], was used to determine total concentrations of chlorinated ethenes, ETH, and methane. Standards were prepared by adding *cis*-DCE, TCE, and PCE dissolved in methanol as well as VC, ETH, and methane gases, all at known volumes, to serum bottles (70 ml) containing deionized water (40 ml).

Because PCE, TCE, and *cis*-DCE partition into the hydrophobic core of surfactant micelles, a second gas chromatographic method was used to quantify aqueous-phase concentrations of these species when surfactant concentrations exceeded the critical micelle concentration. The method approximates U.S. Environmental Protection Agency Method 502.2 (<http://www.epa.gov/epahome/Standards.html>) and involves the use of a purge-and-trap apparatus coupled with a gas chromatograph. Aqueous samples (10 μl) were diluted in 40 ml of deionized water (4,000:1 v/v dilution factor) contained in 40-ml screw-top vials sealed with screw caps and Teflon®-lined silicone rubber septa. The 4,000:1 dilution factor was necessary to prevent surfactant foaming in the purge chamber of the purge-and-trap apparatus. A description of the gas chromatograph and purge-and-trap apparatus, as well as of the

operating parameters, has been given previously (see Appendix I of Fiorenza et al. [30]).

Anionic surfactant concentrations were measured via a modification of the methylene blue active substances (MBAS) method from *Standard Methods for the Examination of Water and Wastewater* [31] that included only one extraction and elimination of the backwash. Sodium dodecyl sulfate was utilized as the reference surfactant. Nonionic surfactants were measured using an extractive colorimetric method described in procedure 1 of Toei et al. [32]. Chemical oxygen demand of 1.0% (w/w, active) surfactant solutions was measured according to standard methods [31].

Culture

The suspended growth culture used in experiments was maintained as a fill-and-draw bioreactor in a glass bottle (capacity, 2.3 L; volume of liquid, 1.4 L; headspace, 0.9 L) modified with a sidearm sampling port. The inoculum for this suspended growth culture was obtained directly from the methanol/PCE enrichment culture as previously described by Carr and Hughes [14]. Twice a week, an aliquot of culture (120 ml) was removed and replaced with fresh nutrient medium (hydraulic retention time of 40.8 d). Following withdrawal of culture and addition of nutrients, the culture was purged with H₂/CO₂ (80%/20%, v/v) gas to remove dechlorination products. Electron donor (H₂/CO₂ gas) was added daily as needed via a syringe. Neat PCE (10–40 μl) was also added daily, resulting in a final aqueous concentration of 7.9 to 31.7 mg/L. The PCE added was consistently dechlorinated to VC (70–97%, molar), ETH (2–15%), and DCE (1–15%) over the period of each fill-and-draw cycle. Previous characterization of this culture suggests that at least two organisms are responsible for complete dechlorination of PCE to ETH [29].

Dechlorination experiments

Experiments investigating the effects of surfactants on the dechlorination activity of the mixed anaerobic culture were carried out in serum bottles (12 ml for short-term experiments and 70 ml for long-term experiments) with a headspace to liquid ratio of approximately 0.73. The serum bottles were sealed with Teflon-lined butyl rubber septa and aluminum crimp caps. Oxygen was evacuated from the systems by sparging with N₂ gas (ultrahigh purity at 10 psi for 10 min). The bottles were then inoculated with culture, followed by sparging with H₂/CO₂ gas (10 psi for 10 min) to remove any dissolved chlorinated ethenes, ETH, and methane remaining in the seed culture and also to provide electron donor. Electron donor was replenished daily as needed via syringe. Surfactant was added immediately following the H₂/CO₂ sparge, followed by the addition of neat PCE (0.3 μl for 12-ml bottles and 1.5 μl for 70-ml bottles, resulting in ~40 mg/L [aqueous concentration] neglecting micellar partitioning). Bottles were inverted and mixed continuously. The effect of the surfactants on the rate and extent of PCE degradation was evaluated by sampling for remaining PCE and production of lesser-chlorinated degradation products over a period of time.

Surfactant biodegradation experiment

The biodegradation of the surfactants by the mixed anaerobic culture was examined via batch microcosm experiments. Seed culture (20 ml) was added to serum bottles (38 ml) sealed with Teflon-lined butyl rubber septa and aluminum crimp caps. The bottles were sparged with N₂ gas (ultrahigh purity at 10

psi for 10 min) to remove oxygen before inoculation. The bottles were then sparged with H₂ gas (ultrahigh purity at 10 psi for 10 min), which removed any dissolved-phase methane remaining in the seed culture. The H₂ gas was replenished periodically as needed via syringe. Surfactant (1.0%, w/w, active) was added to the serum bottles as the sole externally added carbon source, with the exception of a surfactant-free reference bottle that contained no organic carbon source. Bottles were inverted and mixed continuously. Initial and final surfactant concentrations were measured. Methane production relative to the maximum theoretical amount based on measurements of chemical oxygen demand was also monitored over 70 d as an indicator of surfactant biodegradation.

Steol CS-330 acclimation culture

A bottle (620 ml) modified with a sidearm sampling port and sealed with an open-top screw cap containing a stainless-steel plug, a Viton O-ring (DuPont, Wilmington, DE, USA), and a three-way valve was sparged with N₂ gas (10 psi for 30 min) to remove oxygen from the system. Culture (300 ml) was added to the bottle along with fresh nutrient medium (70 ml). Next, the bottle was sparged with H₂/CO₂ gas (5 psi for 15 min) to supply electron donor. Electron donor was replenished daily as needed via syringe. Every fourth day, an aliquot of culture (36 ml) was removed and replaced with fresh nutrient medium containing a mass of Steol CS-330 surfactant required to attain the desired surfactant concentration in the culture. Following withdrawal of culture and addition of nutrients and surfactant, the headspace of the culture was purged with H₂/CO₂ gas to remove dechlorination products. The first 4 d of the experiment served as the surfactant-free reference period. The initial surfactant addition (day 4) resulted in a Steol CS-330 concentration of 1 mg/L. After 4 d (day 8), the surfactant concentration was increased to 5 mg/L, with this procedure being continued with the surfactant concentration being increased to 10 mg/L (day 12), 25 mg/L (day 16), and 50 mg/L (day 20). A surfactant concentration of 50 mg/L was maintained for 8 d before increasing to 100 mg/L (day 28). The surfactant concentration was held at 100 mg/L through the remainder of the experiment, or for eight additional days. At the end of the experiment (day 36), surfactant concentration was measured via the MBAS method. Neat PCE (6 μl) was added daily, with the exception of day 21, to the culture, resulting in an aqueous-phase concentration of 17.7 mg/L. The headspace of the culture was sampled daily for PCE and dechlorination metabolites.

On days 24, 28, and 36, an aliquot (4 ml) from the withdrawal was placed in a serum bottle (70 ml) containing fresh nutrient medium (36 ml) that had been evacuated of oxygen with N₂ gas and sealed with Teflon-lined butyl rubber septa and aluminum crimp caps. This dilution resulted in a 10-fold decrease in surfactant concentration. Electron donor was supplied to the bottles via sparging with H₂/CO₂ gas and was replenished via syringe as needed. Neat PCE (0.3 μl) was added to the bottles, resulting in an aqueous-phase concentration of 8 mg/L. Bottles were inverted and mixed continuously. The headspace of the bottles was sampled weekly for remaining PCE and metabolite production.

RESULTS AND DISCUSSION

Biotransformation of surfactants

The objective of this present research was to investigate the effects of surfactants on the dechlorination activity of a

Table 2. Direct measures of surfactant and methane production as indicators of surfactant biodegradation by a mixed anaerobic culture ([surfactant] = 1.0%, w/w, active; $t = 70$ d)

Surfactant ^a	Surfactant concentration ^b (%)		% Degraded	CH ₄ (mmol)		
	Initial	Final		Theoretical ^c	Actual	% Converted
None (reference)	NA ^d	NA	NA	0.16	0.05	31.2
AOS 14-16	0.93	0.86	7.2	4.9	0.11	2.2
Steol CS-330	1.02	0.94	7.6	4.9	0.08	1.6
Aerosol MA 80-I	0.95	0.96	-1.2	4.5	0.11	2.4
Neodol 25-7	1.00	0.99	1.2	5.7	0.12	2.1
Tween 80	1.05	0.67	36.9	4.5	0.09	2.0

^a AOS = alpha olefin sulfonate.

^b Anionic surfactants measured by methylene blue active substance method; nonionic surfactants measured by an extractive colorimetric method described in procedure 1 of Toei et al. [32].

^c Theoretical CH₄ based on 0.35 L CH₄ produced per g chemical oxygen demand (1 atm, 298 K).

^d NA = not applicable.

PCE-enriched mixed culture at concentrations ($\leq 1.0\%$, w/w, active) similar to what may be used in H₂-based foam injection. Surfactants were also evaluated for their biodegradability. In previous studies, a range of fermentative substrates (e.g., methanol, lactate, propionate, pyruvate, and formate) was used to support dechlorination and methane production using this culture, but none represented a complex molecule similar to the surfactants used. Because surfactant biodegradation may occur to varying extents [33], two indicators of surfactant biodegradation were utilized (surfactant remaining and methane production) after 70 d of incubation. Based on surfactant measurements, only the Tween surfactant exhibited substantial transformation over the experimental period, and methane production in all surfactant-containing microcosms accounted for only 2 to 3% of the amount theoretically resulting from complete degradation of the surfactants (Table 2). However, methane production in all surfactant-amended microcosms was greater than in the surfactant-free reference through 70 d of incubation.

From these results, it appears that acclimation of this culture to these surfactants as carbon sources would require a relatively long period of time at these concentrations. Furthermore, these results indicate that the surfactants would not likely change in concentration to an appreciable degree over the experimental periods of the present study (2-70 d). It is important to note that all of the surfactants used would most likely be degraded if given longer periods to adapt. For example, Neodol 25-7 is from a surfactant class that is known to biodegrade in mixed anaerobic cultures at low concentrations [34-36], and Tween surfactants can be biodegraded at concentrations similar to those used in studies presented herein [18-20,37]. In the case of Tween fermentation, the products formed can be used to support reductive dechlorination [20].

Effect of surfactants on PCE dechlorination activity

Representative surfactants from each surfactant class (nonionic [$n = 3$], anionic [$n = 3$], and cationic [$n = 1$]) were tested at a concentration of 1.0% (w/w, active) for their effects on dechlorination activity (i.e., rate and extent of PCE dechlorination) by the mixed anaerobic dechlorinating culture; results are presented in Table 3. After only 2 d, PCE (40 mg/L) was dechlorinated to nondetectable levels in all microcosms, with the exception of those amended with the anionic surfactant Aerosol MA 80-I and the cationic surfactant C₁₆TAB. The strong, negative effect of C₁₆TAB was not entirely unexpected, because cationic surfactants often result in

microbial toxicity [33]. However, the extent of PCE transformation within this time frame varied widely among the other surfactants assayed. The nonionic surfactant, Tween 80, had the least impact on transformation of PCE to the lesser-chlorinated species. This was the only microcosm, except for the surfactant-free control, that exhibited substantial dechlorination past DCE. Of the remaining anionic surfactants, Steol CS-330 appeared to be less inhibitory than AOS 14-16, although each exhibited TCE and DCE as the dominant products of PCE dechlorination.

Effect of surfactant concentration on PCE dechlorination activity

Because anionic surfactants and nonionic surfactants are the most commonly considered in aquifer remediation research and field demonstrations [6,38-44], one surfactant from each of these classes was selected for use in further investigations. To explore the effects of surfactant concentration on dechlorination extent, microcosms containing Tween 80 and Steol CS-330 at various concentrations (0.1%, 0.5%, and 1.0%, w/w) were monitored over a period of 15 d. As shown in Figure 1, Tween 80 exhibited no observable effect on the conversion of PCE to VC, but further reduction of VC to ETH occurred more slowly in all Tween 80-amended microcosms compared to the surfactant-free control.

Based on literature reports, it appears that other surfactants

Table 3. Two-day screening of surfactants for effect on perchloroethene (PCE) dechlorination activity presented as molar distribution of recovered products

Surfactant ^a	PCE and dechlorination metabolites recovered (% molar) ^b				
	PCE	TCE	DCE	VC	ETH
None (control)	0.0	0.0	0.6	81.3	18.1
Tween 80	0.0	0.0	1.8	91.4	6.9
Neodol 25-7	0.0	5.9	94.0	0.1	0.0
Steol CS-330	0.0	76.6	23.2	0.1	0.0
APG	0.0	88.8	11.0	0.2	0.0
AOS 14-16	0.0	96.5	2.9	0.1	0.6
Aerosol MA 80-I	87.1	12.5	0.0	0.3	0.1
CTAB	91.2	0.4	8.5	0.0	0.0

^a APG = alkyl polyglycoside; AOS = alpha olefin sulfonate; CTAB = hexadecyltrimethylammonium bromide.

^b TCE = trichloroethene; DCE = dichloroethene; VC = vinyl chloride; ETH = ethane.

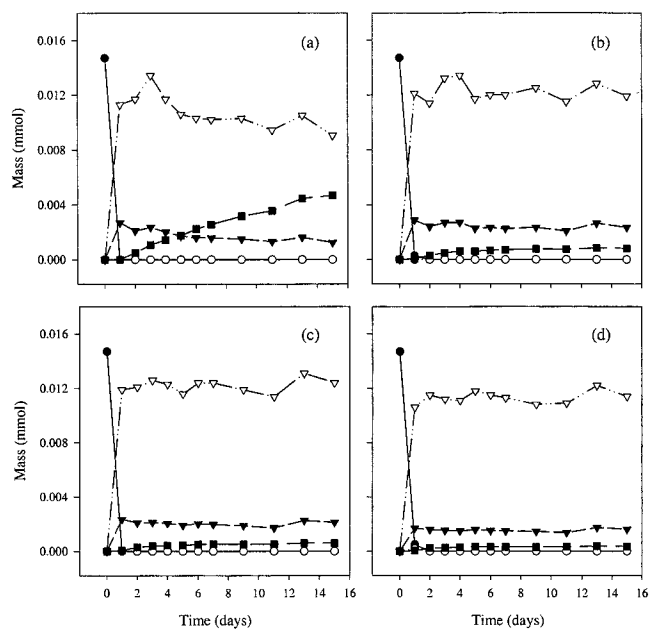


Fig. 1. Effect of Tween 80 concentration on perchloroethene (PCE) dechlorination activity. **a)** Surfactant-free control. **b)** 0.1% Tween 80. **c)** 0.5% Tween 80. **d)** 1.0% Tween 80. TCE = trichloroethene; DCE = dichloroethene; VC = vinyl chloride; ETH = ethene. ● = PCE; ○ = TCE; ▼ = DCE; ▽ = VC; ■ = ETH.

within the Tween series may have less impact than Tween 80 on dechlorination, although no others were available for studies with this culture. Yeh et al. [19] investigated the effects of a series of Tween surfactants on the reductive dechlorination activity of a mixed culture enriched with hexachlorobenzene. Hexachlorobenzene dechlorination was found to vary among microcosms amended with the Tween surfactants, and Tween 80 exhibited greater microbial inhibition than some of the other surfactants in the series.

In the Steol CS-330-amended series (Fig. 2), PCE was completely transformed in all cases within 1 d with the accumulation of TCE, which remained for variable time periods before further reduction to DCE. No production of VC or ETH occurred, as was observed with Tween 80, despite extended periods of incubation. A possible explanation for the accumulation of DCE is the sensitivity of a subset of dechlorinating strains to the surfactants. Previous work has demonstrated that the mixed culture used in the present study contains at least two populations of reductive dechlorinating microorganisms to achieve complete dechlorination [29]. The need for multiple dechlorinating strains to completely reduce PCE to ETH has been observed in other studies as well [45], and apparently, the Steol CS-330 had a strong influence at these high concentrations on the DCE-dechlorinating organism(s). Interestingly, Steol CS-330 and other surfactants also influenced methane production in the microcosms studies, because lower levels of methane were observed in the surfactant-added microcosms compared to the surfactant-free controls.

The variable length of TCE accumulation was not expected, because conversion of PCE through TCE to DCE is typically quite fast for this culture (in controls, TCE accumulation is rarely observed). A possible explanation for this observation is that TCE in surfactant micelles is less bioavailable than PCE and, by increasing the micellar phase present, the bioavailability of TCE was further reduced (all Steol CS-330 concen-

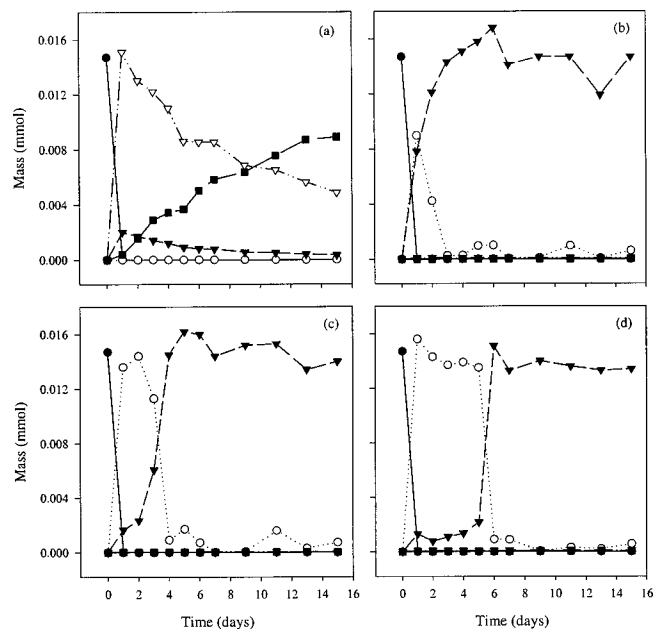


Fig. 2. Effect of Steol CS-330 concentration on perchloroethene (PCE) dechlorination activity. **a)** Surfactant-free control. **b)** 0.1% Steol CS-330. **c)** 0.5% Steol CS-330. **d)** 1.0% Steol CS-330. TCE = trichloroethene; DCE = dichloroethene; VC = vinyl chloride; ETH = ethene. ● = PCE; ○ = TCE; ▼ = DCE; ▽ = VC; ■ = ETH.

trations tested were above the critical micelle concentration [0.05%, w/w], and the increasing surfactant concentration directly correlates to an increased volume of micellar phase present). Investigators studying the bioavailability of nonchlorinated hydrophobic organic compounds partitioned into micelles have concluded that a fraction of the solubilized contaminant may not be directly available for microbial uptake [46,47]. However, further incubation of the microcosms resulted in the rapid reduction of TCE to DCE. The rapid and complete transformation of TCE to DCE after extended incubation suggests that a required acclimation to the surfactant, not reduced bioavailability, was the reason for TCE accumulation, because the latter mechanism would have likely resulted in an observable decrease in the rate of TCE transformation to DCE.

Apparently, the interaction that temporarily impairs TCE reduction is controlled by the total surfactant added (dissolved and micellar phases). Lag periods because of surfactant addition have been documented for other contaminants [18,19,27], but the mechanisms of why lag periods result are poorly understood. This process of acclimation before TCE reduction to DCE may imply that the enzymes involved in PCE conversion to TCE and in TCE conversion to DCE are distinct and regulated differently; however, other mechanisms, such as decreased substrate transport into the bacterial membrane because of the presence of the surfactant, cannot be ruled out.

To confirm that acclimation was complete after conversion of the initial PCE dose to DCE, the experiment was repeated (at surfactant concentrations of 0.5% and 1.0%), with similar results compared to those discussed previously. Instead of allowing the culture to continue to incubate with only DCE present, these microcosms were respiked with PCE. The results of this experiment are displayed in Figure 3. Rapid dechlorination to DCE without TCE accumulation was observed, confirming

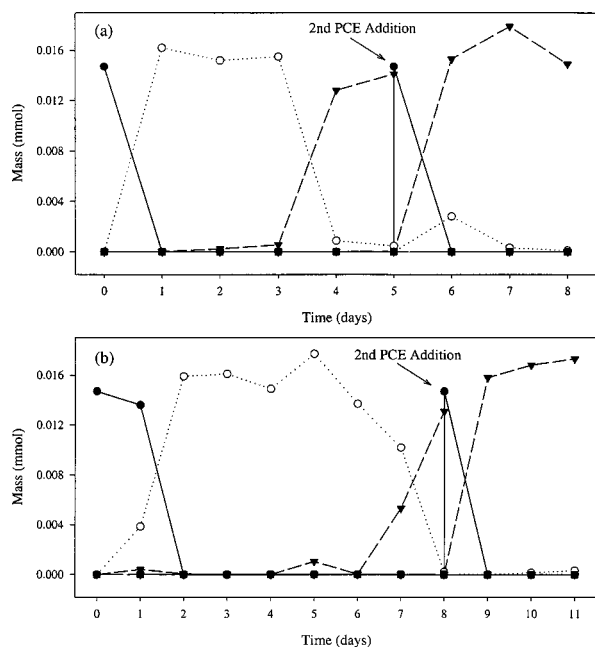


Fig. 3. Acclimation of perchloroethene (PCE) dechlorination to dichloroethene (DCE) in the presence of Steol CS-330. **a)** 0.5% Steol CS-330. **b)** 1.0% Steol CS-330. ETH = ethane. ● = PCE; ○ = TCE; ▼ = DCE; ▽ = VC; ■ = ETH.

the hypothesis that acclimation was required to achieve TCE dechlorination to DCE in the presence of Steol CS-330.

To evaluate if an acclimation period in excess of 15 d was required to achieve dechlorination of DCE to VC and ETH in the presence of Steol CS-330, an extended incubation of culture with 1% Steol CS-330 was fed only DCE and monitored for 35 d without any dechlorination being observed. Subsequent evaluations determined that VC and ETH production stopped in short-term assays (4 d) when Steol CS-330 concentrations were increased from 10 to 100 mg/L (data not shown).

Steol CS-330 acclimation culture

An experiment was conducted to determine if the microorganisms responsible for DCE dechlorination could be acclimated to Steol CS-330 by incrementally increasing the surfactant concentration over time. To determine if acclimation was possible, surfactant was initially added at a concentration (1 mg/L) that was known not to inhibit VC and ETH production. Surfactant concentration was increased periodically over a period of 36 d. Results of this experiment are shown in Figure 4. The culture contained no surfactant for the first 4 d of the experiment; this period served as the surfactant-free reference. Over the reference period, PCE (16 mg/L/d) was dechlorinated to VC and ETH. On day 4 of the experiment, an aliquot of culture (36 ml) was withdrawn and replaced with nutrient medium and Steol CS-330 at a mass sufficient to attain an active surfactant concentration of 1 mg/L. This routine was maintained, and the surfactant concentration was increased to 5, 10, 25, and 50 mg/L over 16 d. The extent of PCE dechlorination over the period of each fill-and-draw cycle actually increased slightly compared to the surfactant-free reference period with each surfactant addition up to 10 mg/L. The greatest extent of PCE reduction occurred over the 10 mg/L surfactant period. The slight enhancement of PCE dechlorination observed with each surfactant addition up to 10 mg/L could

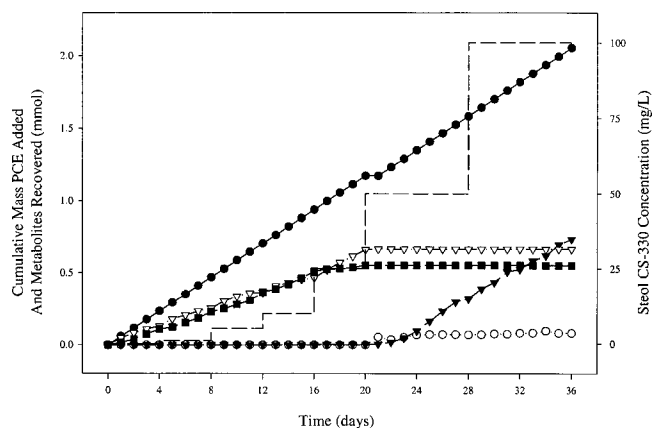


Fig. 4. Effect of incrementally increasing Steol CS-330 concentration on perchloroethene (PCE) dechlorination activity in a mixed culture: Cumulative PCE addition and metabolite production. PCE = perchloroethene; TCE = trichloroethene; DCE = dichloroethene; VC = vinyl chloride; ETH = ethane; TCE = trichloroethene; DCE = dichloroethene; VC = vinyl chloride; ETH = ethane. ● = PCE; ○ = TCE; ▼ = DCE; ▽ = VC; ■ = ETH; dashed line = Steol CS-330.

not be explained, although researchers have observed enhanced polycyclic aromatic hydrocarbon degradation rates at extremely low surfactant concentrations [23].

A decrease in ETH production was observed on increase of Steol CS-330 to 25 mg/L, and a further increase of surfactant to 50 mg/L resulted in complete loss of VC and ETH production. The initial PCE addition at a surfactant concentration of 50 mg/L was dechlorinated almost entirely to TCE, despite the fact that no previous TCE production had been observed. Thus, an acclimation period for PCE reduction to DCE was evident even at a very low surfactant concentration in a culture that had been exposed to surfactant for more than two weeks. Subsequent PCE additions during this fill-and-draw cycle resulted in increased concentrations of DCE and decreasing amounts of TCE. By day 25, PCE was completely reduced to only DCE, and this trend continued throughout the remainder of the experiment. Conversely, the organisms responsible for reduction of DCE to VC and ETH exhibited no acclimation to the surfactant. Also, it appears that the fermentative community did not respond to the surfactant as a carbon source when fed at lower levels, because the surfactant concentration measured at the end of the experiment verified that no degradation of the surfactant had occurred.

Surfactant interactions with proteins, especially membrane-bound enzymes such as those involved in respiratory processes, are a known mechanism of surfactant toxicity toward microorganisms [21]. In some cases, enzymes have been shown to regain activity on removal of the surfactant-enzyme complex [33]. To evaluate if this mechanism could be contributing to the results obtained, aliquots of surfactant-amended culture were removed and diluted (1:10 v/v) into fresh nutrient medium on days 24, 28, and 36 of the Steol CS-330 acclimation culture experiment and spiked with PCE. Results of this experiment are shown in Table 4. Monitoring of these microcosms demonstrated that production of VC and ETH was regained on dilution of the surfactant below the threshold concentration, further suggesting that the interaction of Steol CS-330 monomers with the dehalogenase enzyme system of the population of microorganisms responsible for DCE and VC reduction may be the cause for the observed inhibition.

Table 4. Extent of perchloroethene (PCE) dechlorination in microcosms developed from the Steol CS-330 acclimation culture with surfactant concentrations diluted below the dichloroethene (DCE) dechlorination threshold concentration

Steol CS-330 acclimation culture		Microcosms			PCE and dechlorination metabolites recovered (% molar) ^a				
Time (d)	CS-330 concentration (mg/L)	Diluted CS-330 concentration (mg/L)	Sample time (d)	PCE	TCE	DCE	VC	ETH	
24	50	5	7	0.0	20.7	56.2	23.0	0.2	
			14	0.0	0.0	12.8	84.3	2.9	
			21	0.0	0.0	10.4	83.2	6.3	
28	50	5	7	0.0	1.6	46.0	52.4	0.0	
			14	0.0	0.0	13.2	85.2	1.6	
			21	0.0	0.0	12.3	84.0	3.7	
36	100	10	7	0.0	0.0	94.8	5.2	0.0	
			14	0.0	0.0	76.2	23.8	0.0	
			21	0.0	0.0	8.9	89.7	1.4	

^a TCE = trichloroethene; DCE = dichloroethene; VC = vinyl chloride; ETH = ethene.

Effect of surfactants similar in structure to Steol CS-330 on PCE dechlorination activity

Relationships between surfactant properties and microbial toxicity likely exist, but quantification of the correlations is difficult, especially when utilizing a mixed culture [37]. To probe interactions of surfactant characteristics on dechlorination by this culture, surfactants containing hydrophobic groups similar to Steol CS-330, but with differing hydrophiles, were compared to Steol CS-330 in the extent of dechlorination achieved. Specifically, Neodol 25-7, containing a C₁₂₋₁₅ hydrophobe and an ethoxylated nonionic hydrophile, along with the anionic surfactant, SDS, void of ethoxy groups but containing a C₁₂ hydrophobe and a sulfate hydrophile, were used.

Microcosms were amended with Neodol 25-7 or SDS at concentrations of 0.1%, 0.5%, and 1.0% (w/w), and PCE dechlorination was monitored after 3 and 7 d of incubation and compared to the results obtained for Steol CS-330 at the same concentrations and time. Results of this experiment are shown in Table 5. Sodium dodecyl sulfate was found to completely inhibit the PCE reductive dechlorination process, because PCE was the only chlorinated ethene detected. In microcosms amended with Neodol 25-7, however, PCE was almost entirely reduced to DCE after 3 d, which remained the dominant dechlorination product through the incubation.

From this observation, it appears that the anionic sulfate group of Steol CS-330 is not responsible for inhibition of DCE reduction, because Neodol 25-7, a surfactant with a similar

structure that lacks a sulfate group, exhibited a very similar dechlorination extent to that of Steol CS-330. However, the microorganisms that dechlorinate TCE to DCE do not appear to require a similar acclimation period in the presence of Neodol 25-7 as that necessary in the presence of Steol CS-330. This result is likely accounted for by the fact that Neodol 25-7 contains an average of four more ethylene oxide (EO) groups compared to Steol CS-330, and microbial toxicity trends among similar surfactants imply that an increasing number of EO groups relates to decreasing toxicity [33]. A similar argument can be made to explain the observed toxicity of SDS compared to Steol CS-330. The only structural difference in the two surfactants is the presence of an EO chain in the hydrophilic portion of Steol CS-330. The results suggest that hydrophobic interactions with the microorganisms may be contributing to inhibition to a greater degree than hydrophilic interactions. Previous observations of loss of DCE degradation by this culture in the presence of tridecane support this supposition [7,9].

The most evident surfactant property appearing to affect PCE transformation in the present study is the presence and number of EO groups in the surfactant molecule. Sodium dodecyl sulfate (C₁₂SO₄⁻) completely inhibited PCE reduction. However, Steol CS-330 (C₁₂EO₃SO₄⁻) had no effect on the initial PCE reduction step, and a lag in PCE reduction to DCE was overcome by a short acclimation period. Increasing the degree of ethoxylation to an average of seven EO groups (Neo-

Table 5. Comparison of rate and extent of perchloroethane (PCE) dechlorination in microcosms amended with surfactants similar in structure to Steol CS-330

Surfactant ^a	Concentration (%)	Dechlorination products (% t = 3 d) ^b					Dechlorination products (% t = 7 d) ^b				
		PCE	TCE	DCE	VC	ETH	PCE	TCE	DCE	VC	ETH
SDS	1.0	100	0	0	0	0	100	0	0	0	0
	0.5	100	0	0	0	0	100	0	0	0	0
	0.1	100	0	0	0	0	100	0	0	0	0
	1.0	0	91.9	7.3	0.5	0.2	0	6.1	93.1	0.5	0.2
	0.5	0	64.9	34.8	0.2	0.1	0	0.2	99.5	0.2	0.1
Steol CS-330	0.1	0	1.8	97.6	0.6	0	0	0.3	99.1	0.6	0
	1.0	0	3.7	96.3	0	0	0	2.6	97.3	0	0.1
	0.5	0	1.8	98.1	0	0.1	0	1.5	98.4	0	0.1
Neodol 25-7	0.1	0	0.3	99.7	0	0.1	0	0.2	99.7	0	0.1

^a SDS = sodium dodecyl sulfate.

^b TCE = trichloroethene; DCE = dichloroethene; VC = vinyl chloride; ETH = ethene.

dol 25-7, C₁₂₋₁₅EO₇H) effected rapid reduction of PCE to DCE without the need for acclimation. Moreover, the surfactant containing the most EO groups, Tween 80, which has an average of 20 EO groups distributed throughout the hydrophilic portion of the molecule, was the only surfactant screened that exhibited dechlorination beyond DCE and VC. The decreased toxicity caused by the presence and number of EO groups could result from increased distribution of electronegativity and steric hindrance, allowing for decreased interaction of the molecule with the bacterial membrane and/or membrane-bound proteins.

The inhibiting activity of surfactants toward microbial transformation processes is usually accounted for via one or a combination of three mechanisms: decreased bioavailability of the contaminant because of micellar solubilization [48], uptake of the surfactant as a preferential substrate over the contaminant [25,49], or interaction of the surfactant with vital components of the microorganism [27,50,51]. Experiments investigating the effect of Steol CS-330 concentration demonstrated that both PCE and TCE in a micellar solution are rapidly degraded, indicating that decreased bioavailability did not limit dechlorination. Preferential degradation of the surfactant was excluded based on results of the surfactant biodegradation study and the Steol CS-330 acclimation culture experiment. The only remaining explanation for the observed effects of Steol CS-330 on the reductive dechlorination process is surfactant-microorganism interaction. Developing a better understanding of these interactions will be required to achieve complete dechlorination in aquifers after surfactant injection. Interestingly, it appears that certain surfactants will not appreciably impair initial steps of dechlorination after short acclimation periods.

Acknowledgement—We would like to acknowledge support from the Strategic Environmental Research and Development Program (SERDP).

REFERENCES

- U.S. Environmental Protection Agency. 1993. Evaluation of the Likelihood of DNAPL Presence at NPL Sites, National Results. EPA 540-R-93-073. Office of Solid Waste and Emergency Response, Washington, DC.
- Pankow JF, Cherry JA. 1996. *Dense Chlorinated Solvents and Other DNAPLs in Groundwater*. Waterloo Press, Portland, OR, USA.
- Johnson RL, Pankow JF. 1992. Dissolution of dense chlorinated solvents into groundwater. 2. Source functions for pools of solvent. *Environ Sci Technol* 26:896–901.
- West CC, Harwell JH. 1992. Surfactants and subsurface remediation. *Environ Sci Technol* 26:2324–2330.
- Sabatini DA, Knox RC, Harwell JH, eds. 1995. *Surfactant-Enhanced Subsurface Remediation: Emerging Technologies*. American Chemical Society, Washington, DC.
- Hirasaki GJ, Jackson RE, Jin M, Lawson JB, Londergan J, Meinardu H, Miller CA, Pope GA, Szafranski R, Tanzil D. 2001. Field demonstration of the surfactant/foam process for remediation of a heterogeneous aquifer contaminated with DNAPL. In Fiorenza S, Miller CA, Oubre CL, Ward CH, eds. *NAPL Removal: Surfactants, Foams, and Microemulsions*. Lewis, Boca Raton, FL, USA, pp 7–166.
- Carr CS, Garg S, Hughes JB. 2000. Effect of dechlorinating bacteria on the longevity and composition of PCE-containing non-aqueous phase liquids under equilibrium dissolution conditions. *Environ Sci Technol* 34:1088–1094.
- Yang Y, McCarty PL. 2000. Biologically enhanced dissolution of tetrachloroethene DNAPL. *Environ Sci Technol* 34:2979–2984.
- Cope N, Hughes JB. 2001. Biologically enhanced removal of PCE from NAPL source zones. *Environ Sci Technol* 35:2014–2021.
- Bouwer EJ, McCarty PL. 1983. Transformations of 1- and 2-carbon halogenated aliphatic organic compounds under methanogenic conditions. *Appl Environ Microbiol* 45:1286–1294.
- Vogel T, McCarty P. 1985. Biotransformation of tetrachloroethylene to trichloroethylene, dichloroethylene, vinyl chloride, and carbon dioxide under methanogenic conditions. *Appl Environ Microbiol* 49:1080–1083.
- Freedman DL, Gossett JM. 1989. Biological reductive dechlorination of tetrachloroethylene and trichloroethylene to ethylene under methanogenic conditions. *Appl Environ Microbiol* 55:2144–2151.
- DiStefano TD, Gossett JM, Zinder SH. 1992. Hydrogen as an electron donor for dechlorination of tetrachloroethene by an anaerobic mixed culture. *Appl Environ Microbiol* 58:3622–3629.
- Carr CS, Hughes JB. 1998. Enrichment of high-rate PCE dechlorination and comparative study of lactate, methanol, and hydrogen as electron donors to sustain activity. *Environ Sci Technol* 32:1817–1824.
- Middeldorp PJM, Luijten MLGC, van de Pas BA, van Eekert MHA, Kengen SWM, Schraa G, Stams AJM. 1999. Anaerobic microbial reductive dehalogenation of chlorinated ethenes. *Bioremediation J* 3:151–169.
- Newell CJ, Haas PE, Hughes JB, Khan TA. 2001. Two novel methods for enhancing source zone bioremediation: Direct hydrogen addition and electron acceptor diversion. In Magar VS, Fennell DE, Morse JJ, Alleman BC, Leeson A, eds. *Anaerobic Degradation of Chlorinated Solvents*. Battelle, Columbus, OH, USA, pp 19–26.
- Hirasaki GJ. 1989. The steam-foam process. *Journal of Petroleum Engineering* May:449–556.
- Van Hoof PL, Jafvert CT. 1996. Reductive dechlorination of chlorobenzenes in surfactant-amended sediment slurries. *Environ Toxicol Chem* 15:1914–1924.
- Yeh DH, Pennell KD, Pavlostathis SG. 1999. Effect of Tween surfactants on methanogenesis and microbial reductive dechlorination of hexachlorobenzene. *Environ Toxicol Chem* 18:1408–1416.
- Yeh DH, Pavlostathis SG. 2001. Development of hexachlorobenzene-dechlorinating mixed cultures using polysorbate surfactants as a carbon source. *Water Sci Technol* 43:43–50.
- Rouse JD, Sabatini DA, Suflita JM, Harwell JH. 1994. Influence of surfactants on microbial degradation of organic compounds. *Crit Rev Environ Sci Technol* 24:325–370.
- Volkering FM, Breure AM, Rulkens WH. 1998. Microbiological aspects of surfactant use for biological soil remediation. *Biodegradation* 8:401–417.
- Aronstein BN, Calvillo YM, Alexander M. 1991. Effect of surfactants at low concentrations on the desorption and biodegradation of sorbed aromatic compounds in soil. *Environ Sci Technol* 25:1728–1731.
- Bury SJ, Miller CA. 1993. Effect of micellar solubilization on biodegradation rates of hydrocarbons. *Environ Sci Technol* 27:104–110.
- Tiehm A, Stieber M, Werner P, Frimmel FH. 1997. Surfactant-enhanced mobilization and biodegradation of polycyclic aromatic hydrocarbons in manufactured gas plant soil. *Environ Sci Technol* 31:2570–2576.
- Laha S, Luthy RG. 1991. Inhibition of phenanthrene mineralization by nonionic surfactants in soil-water systems. *Environ Sci Technol* 25:1920–1930.
- Tsomides HJ, Hughes JB, Thomas JM, Ward CH. 1995. Effect of surfactant addition on phenanthrene biodegradation in sediments. *Environ Toxicol Chem* 14:953–959.
- Cort T, Bielefeldt A. 2000. Effects of surfactants and temperature on PCP biodegradation. *J Environ Eng* 126:635–643.
- Zheng D, Carr CS, Hughes JB. 2001. Influence of hydraulic retention time on extent of PCE dechlorination and preliminary characterization of the enrichment culture. *Bioremediation J* 5:159–168.
- Fiorenza S, Miller CA, Oubre CL, Ward CH, eds. 2000. *NAPL Removal: Surfactants, Foams, and Microemulsions*. Lewis, Boca Raton, FL, USA.
- American Public Health Association, American Water Works Association, Water Pollution Control Federation. 1992. *Standard Methods for the Examination of Water and Wastewater*, 18th ed. American Public Health Association, Washington, DC.
- Toei K, Motomizu S, Umamo T. 1982. Extractive spectrophotometric determination of nonionic surfactants in water. *Talanta* 29:103–106.

33. Swisher RD. 1987. *Surfactant Biodegradation*, Vol 18. Marcel Dekker, New York, NY, USA.
34. Wagener S, Schink B. 1988. Fermentative degradation of nonionic surfactants and polyethylene glycol by enrichment cultures and by pure cultures of homoacetogenic and propionate-forming bacteria. *Appl Environ Microbiol* 54:561–565.
35. Federle TW, Schwab BS. 1992. Mineralization of surfactants in anaerobic sediments of a laundromat wastewater pond. *Water Res* 26:123–127.
36. Huber M, Meyer U, Rys P. 2000. Biodegradation mechanisms of linear alcohol ethoxylates under anaerobic conditions. *Environ Sci Technol* 34:1737–1741.
37. Yeh DH, Pennell KD, Pavlostathis SG. 1998. Toxicity and biodegradability screening of nonionic surfactants using sediment-derived methanogenic consortia. *Water Sci Technol* 38:55–62.
38. Fountain JC, Starr RC, Middleton T, Beikirch M, Taylor C, Hodge D. 1996. A controlled field test of surfactant-enhanced aquifer remediation. *Ground Water* 34:910–916.
39. Pennell KD, Pope GA, Abriola LM. 1996. Influence of viscous and buoyancy forces on the mobilization of residual tetrachloroethylene during surfactant flushing. *Environ Sci Technol* 30:1328–1335.
40. Shiau BJ, Sabatini DA, Harwell JH. 1995. Properties of food grade (edible) surfactants affecting subsurface remediation of chlorinated solvents. *Environ Sci Technol* 29:2929–2935.
41. Johnson JC, Sun S, Jaffe PR. 1999. Surfactant enhanced perchloroethylene dissolution in porous media: The effect on mass transfer rate coefficients. *Environ Sci Technol* 33:1286–1292.
42. Mayer AS, Zhong L, Pope GA. 1999. Measurement of mass-transfer rates for surfactant-enhanced solubilization of nonaqueous phase liquids. *Environ Sci Technol* 33:2965–2972.
43. Jeong SW, Corapcioglu MY, Roosevelt SE. 2000. Micromodel study of surfactant foam remediation of residual trichloroethylene. *Environ Sci Technol* 34:3456–3461.
44. Zhou M, Rhue RD. 2000. Screening commercial surfactants for remediating DNAPL source zones by solubilization. *Environ Sci Technol* 34:1985–1990.
45. Rosner BM, McCarty PL, Spormann AM. 1997. In vitro studies on reductive vinyl chloride dehalogenation by an anaerobic mixed culture. *Appl Environ Microbiol* 63:4139–4144.
46. Guha S, Jaffe PR. 1996. Biodegradation kinetics of phenanthrene partitioned into the micellar phase of nonionic surfactants. *Environ Sci Technol* 30:605–611.
47. Guha S, Jaffe PR. 1996. Bioavailability of hydrophobic compounds partitioned into the micellar phase of nonionic surfactants. *Environ Sci Technol* 30:1382–1391.
48. Macur RE, Inskeep WP. 1999. Effects of a nonionic surfactant on biodegradation of phenanthrene and hexadecane in soil. *Environ Toxicol Chem* 18:1927–1931.
49. Tiehm A. 1994. Degradation of polycyclic aromatic hydrocarbons in the presence of synthetic surfactants. *Appl Environ Microbiol* 60:258–263.
50. Laha S, Luthy RG. 1992. Effects of nonionic surfactants on the solubilization and mineralization of phenanthrene in soil-water systems. *Biotechnol Bioeng* 40:1367–1380.
51. Rouse JD, Sabatini DA, Harwell JH. 1995. Influence of anionic surfactants on bioremediation of hydrocarbons. In Sabatini DA, Knox RC, Harwell JH, eds, *Surfactant-Enhanced Subsurface Remediation: Emerging Technologies*. American Chemical Society, Washington, DC, pp 124–140.